DSPACE

https://dspace.org/

Effect of time on the tensile strength of several Bushveld Complex rock types

Nyungu, David

2013-07-15
http://hdl.handle.net/10539/12834

Downloaded from a DSpace repository. https://dspace.org/

EFFECT OF TIME ON THE TENSILE STRENGTH OF SEVERAL BUSHVELD COMPLEX ROCK TYPES

David Nyungu

A Dissertation submitted to the Faculty of Engineering and the Built Environment, University of the Witwatersrand, in fulfilment of the requirements of the degree of Master of Science in Engineering.

Johannesburg 2013

DECLARATION

I declare that this dissertation is my own unaided work. It is being submitted for the degree of Master of Science in Engineering to the University of Witwatersrand, Johannesburg. It has not been submitted before for any degree or examination to any other University.

.....

(Signature of Candidate)

.....day of.....year.....

day *month* *year*

DEDICATION

“A Rock Engineer falls at least once in his life because he is expected to look up more than down”, (Anonymous). I am gratified to have family and acquaintances in my life to pick me up whenever I fall.

ACKNOWLEDGEMENTS

Mr Henry Chiwaye, for his assistance with the numerical models used in this research.

Abstract

Despite observations of spalling and damage of Bushveld Complex (BC) mine excavation wall rock over the passage of time, there have been very few time-dependent or creep tests carried out in South Africa on rock, particularly on BC rock types. The research detailed in this dissertation deals with the investigation of stress and strain conditions influencing spalling of wall rock in BC mine excavations, and the influence of time on the tensile strength of several BC rock types. The research includes a review of the BC mining environment; a review of literature relevant to time-dependent behaviour of rock; laboratory testing of BC rocks in uniaxial compression and in indirect tension; time-dependent laboratory testing in indirect tension; and elastic numerical modelling of typical BC mine excavations. The results show that the magnitude of the tensile strength of BC rock types is approximately 5% of their uniaxial compressive strength magnitudes. The long term uniaxial compressive strength of the BC rocks, interpreted from the axial stress-volumetric strain graphs in the UCS test is on average 78MPa, which is 56% of the UCS value. The tensile strength of the BC rock types was found to be time-dependent. However, ultimate minimum long term tensile strength values could not be determined in this research owing to limited testing machine availability. Although the individual test specimen failure times showed large variations, logarithmic time-to-failure trends of the nine test categories in the research showed a general time-dependent behaviour. The long term tensile strength is shown to be less than 70% of the normal tensile strength. Extension strains at tensile strength failure ranged between 1.6×10^{-4} and 2.1×10^{-4}. Values corresponding with the long term tensile strength are less than 70% of this range, namely, less than 1.1×10^{-4} to 1.5×10^{-4}. The time-dependent data presented in the dissertation represent new knowledge, since such rock testing and analysis does not appear to have been carried out before on BC rock types.

The compressive stresses determined in the numerical models were found to be an order of magnitude lower than the compressive strength of the rock. Tensile stresses in the models were of comparable magnitude to the tensile strength of the BC rock types investigated in this research. The numerical models showed that large zones of extension strain can occur around BC excavations, and that the magnitudes of the extension strain can substantially exceed the critical values

determined from the laboratory testing. There is no conclusive prerequisite for tensile conditions to exist, to induce critical extension strain. The implication of this is that there are substantial zones surrounding BC mine excavations that will be prone to spalling conditions and perhaps more significant failure.

Table of contents

DECLARATION ii

DEDICATION iii

ACKNOWLEDGEMENTS iii

Abstract iv

List of Figures ix

List of Tables xvi

List of Symbols xvii

CHAPTER 1 1

INTRODUCTION 1

1.1 Background 1

1.2 Definition of the problem 3

1.3 Research objectives 5

1.4 Research methodology 6

1.5 Content of the dissertation 7

CHAPTER 2 8

CHARACTERISTICS AND ANALYSIS OF THE BUSHVELD COMPLEX MINING ENVIRONMENT 8

2.1 Introduction 8

2.1.1 Geology of the Bushveld Complex 8

2.1.2 Stratigraphy of the Bushveld Complex 10

2.1.3 The Bushveld Complex rock types 13

2.2 Behaviour of rock under stress 15

2.2.1 In-situ stress conditions of the Bushveld Complex 15

2.2.2 Behaviour of intact rock under stress 17

2.2.3 Characteristics of rock failure 26

2.3 Time-dependent characteristics of rock 28

2.3.1 Time-dependent behaviour in rock 28
2.4 Summary and conclusions 34
CHAPTER 3 36
STRESS AND STRAIN ANALYSIS 36
3.1 Introduction 36
3.1.1 Mining methods used in the Bushveld Complex 36
3.2 Characteristic geometries of Bushveld Complex mine excavations 39
3.2.1 Geometries of an in-stope pillar 39
3.2.2 Geometries of a mining stope 40
3.2.3 Geometries of an incline shaft 41
3.3 Numerical and analytical methods 41
3.3.1 Review of numerical methods in mining 42
3.3.2 Stress-strain analysis objectives 43
3.3.3 Methodology for stress and extension strain analysis 44
3.4 Stress and extension strain analysis 44
3.4.1 Analysis of results - in-stope pillar model 45
3.5 Conclusion 56
CHAPTER 4 57
LABORATORY TESTS ON BUSHVELD COMPLEX ROCKS 57
4.1 Introduction 57
4.1.1 Testing objectives 57
4.1.2 Testing methodology 58
4.1.3 Spatial location of core samples 58
4.1.4 Distribution of test specimens 59
4.1.5 Preparation of test specimens 61
4.2 The UCS test set up 62
4.3 Analysis of UCS test results 63

4.3.1 Processing of UCS test results 63
4.3.2 Deformation properties 65
4.3.3 Analysis of volumetric strain 66
4.3.4 UCS test results summary 67
4.4 Brazilian Indirect Tensile (BIT) strength test 68
4.4.1 Normal Brazilian Indirect Tensile (BIT) strength test 69
4.4.2 Time-dependent Brazilian Indirect Tensile (BIT) strength test 72
4.4.3 Time-dependent BIT test results 75
4.5 Conclusions 78
CHAPTER 5 80
DISCUSSION OF STRESS-STRAIN ANALYSIS RESULTS 80
5.1 Introduction 80
5.2 Results of laboratory testing 80
5.3 Results of the numerical analyses 81
5.3 Implications from the numerical analyses and the laboratory testing 84
CHAPTER 6 85
CONCLUSIONS AND RECOMMENDATIONS 85
REFERENCES 88
APPENDICES 99
Appendix A: Geological log sheet for drill hole BH6082 99
Appendix B: Laboratory rock strength test results 107
B1 UCS test results and long term strength analysis 107
B2 Normal Brazilian Indirect Tensile (BIT) strength test results 117
B3 Time-dependent Brazilian Indirect Tensile (BIT) Strength test results 118
Appendix C: Numerical modelling results (Stress and strain analysis) 126
C1 Stress and strain analysis: Incline shaft 126
C2 Stress and strain analysis: mining stope 132

List of Figures

Figure 1-1: Spalling in a haulage observed in a platinum mine located in the western limb of the Bushveld Complex 2

Figure 1-2: Advance Strike Gully (ASG) stress induced fractures in a deep gold mine 3

Figure 1-3: Spalling in a strike orientated pillar in a platinum mine 4

Figure 1-4: Excavation wall damage and fracture extension observed in BC mines 4

Figure 2-1: Geology map of the Bushveld Complex (after Viljoen and Schürmann, 1998) 9

Figure 2–2: Typical stratigraphy of the Bushveld Complex 10

Figure 2-3: Lithographic representation of the Bushveld Complex (Rangasamy, 2010) 11

Figure 2-4: Schematic cross-section of the upper portion of the Upper Critical Zone of the Rustenburg Layered Suite, at Northam Platinum Mine (Smith and Basson, 2006) 13

Figure 2-5: Ratio of the principal horizontal stress to the principal vertical stress for South African mines, (after Stacey and Wesseloo, 2004). 16

Figure 2-6: Stress induced failure in the roof of a dip oriented tunnel in a platinum mine, (Stacey and Wesseloo, 2004) 17

Figure 2-7: Failure modes in compression (Ashby and Hallam, 1986) 18

Figure 2-8: Crack branching mode under compressive loading (Halm and Dragon, 1998) 20

Figure 2-9: Mechanism of brittle fracture under multi-axial compression, Bieniawski, (1967) 21

Figure 2-10: Tensile strength testing set up, a) The dog bone shaped specimen used in direct tensile strength tests (Ryder and

Jager, 2002) and b) Brazilian disc set up used in indirect tensile strength tests 24

Figure 2-11: Creep curve showing different stages of deformation of rocks (Dubey and Gairola, 2008) 30

Figure 2-12: Principle of operation of the CSIR creep testing machine (Drescher and Handley, 2003) 30

Figure 2-13: Extension fracturing in an unsupported clay tunnel (Blumling et al, 2007) 33

Figure 2-14: Time-dependent stope creep closure (Malan et al, 2007) 34

Figure 2-15: Continuous stope closure after blasting and the definition of closure terms, (Malan et al, 2007) 34

Figure 3-1: Conventional breast mining layout in the UG2 reef. After (Egerton, 2004) 37

Figure 3-2: A typical room and pillar mining layout. After (Egerton, 2004) 38

Figure 3-4: Modelling geometries of a 29 m by 1.8 m high stope 40

Figure 3-5: Modelling geometry of a 7 m wide by 4 m high incline shaft 41

Figure 3-6: Extension of damaged zone for different time progressions in a section located 6 m behind the tunnel face (Bonini et al, 2009) 42

Figure 3-7: Distribution of Major Principal Stress (σ_1) at a depth of 500m with a k-ratio = 1 45

Figure 3-8: Distribution of Major Principal Stress (σ_1) at a depth of 500m with a k-ratio = 2 46

Figure 3-9: Distribution of Major Principal Stress (σ_1) at a depth of 1000m with a k-ratio = 1 46

Figure 3-10: Distribution of Major Principal Stress (σ_1) at a depth of 1000m with a k-ratio = 2 47

Figure 3-11: Distribution of Minor Principal Stress (σ_3) at a depth of 500m with a k-ratio = 1 48

Figure 3-12: Distribution of Minor Principal Stress (σ_3) at a depth of 500m with a k-ratio = 2 48

Figure 3-13: Distribution of Minor Principal Stress (σ_3) at a depth of 1000m with a k-ratio = 1 49

Figure 3-14: Distribution of Minor Principal Stress (σ_3) at a depth of 1000m with a k-ratio = 2 49

Figure 3-15: Distribution of extension strain at a depth of 500m with a k-ratio = 1..... 51

Figure 3-16: Distribution of extension strain at a depth of 500m with a k-ratio = 2..... 51

Figure 3-17: Distribution of extension strain at a depth of 1000m with a k-ratio = 1..... 52

Figure 3-18: Distribution of extension strain at a depth of 1000m with a k-ratio = 2..... 52

Figure 3-19: Distribution of Critical Extension strain at a depth of 500 m and k = 2..... 53

Figure 3-20: De-lamination of hanging wall strata 54

Figure 3-21: Hanging wall damage under tensile stresses in a stope 55

Figure 3-22: Spalling parallel to the haulage walls induced by extension strain observed in a FW haulage mined in anorthositic norite 55

Figure 4-1: Graphical presentation of the distribution of test specimen..... 61

Figure 4-2: Rock specimens for UCS and BIT test shapes 62

Figure 4-3: The Amsler testing machine..... 62

Figure 4-5: Stress-Strain graph for mottled anorthosite specimen UCA7..... 65

Figure 4-6: Failure mode observed in specimen tested in uniaxial compression, (a) before the test and (b) after the test..... 65

Figure 4-7: Determination of the “long term strength” for specimen (UCA7) 66

Figure 4-8: The MTS 815 rock testing machine used to load BIT discs 68

Figure 4-9: Curved platens used in the BIT test set up, (a) before the test and (b) after the test 68

Figure 4-10: Normal BIT load-time plot 69

Figure 4-11: Specimen failure in the BIT test 71

Figure 4-12: Calculated strains at various load levels for the nine test categories 73

Figure 4-13: Time-dependent Load-Time plot 74

Figure 4-14: Time-dependent BIT Load-Time plot 74

Figure 4-15: Time-to-failure plot for test category B (Rock type: spotted anorthositic norite) 76

Figure 4-16: Load-Time plot for averages of all the test results 77

Figure 4-17: Percentage load-Time plot for averages of all test results 77

Figure 4-18: Strain-Time plot for averages of all test results 78

Figure 5-1: Distribution of extension strain around an in-stope pillar 82

Figure 5-2: Illustration of the zone in a stope sidewall prone to fracture propagation 83

Figure 5-3: Illustration of zones in the stope hanging wall prone to fracture propagation 83

Figure B1-1: Stress-strain graph for spotted anorthositic norite (S.A.N.) rock type specimen UCB6 108

Figure B1-2: Stress-strain graph for pyroxenite (P.) rock type specimen UCC8 108

Figure B1-3: Stress-strain graph for mottled anorthosite (M.A.) rock type specimen UCD10 109

Figure B1-4: Stress-strain graph for norite (N.) rock type specimen UCE7 109

Figure B1-5: Stress-strain graph for spotted anorthositic norite (S.A.N.) rock type specimen UCF6 110

Figure B1-6: Stress-strain graph for anorthositic norite (A.N.) rock type specimen UCG7 110

Figure B1-7: Stress-strain graph for spotted anorthosite (S.A.) rock type specimen UCH7..... 111

Figure B1-8: Stress-strain graph for mottled anorthosite (M.A.) rock type specimen UCI9 111

Figure B1-9: Rate of change of volumetric strain with respect to stress (UCB6)..... 112

Figure B1-10: Rate of change of volumetric strain with respect to stress (UCC8) 113

Figure B1-11: Rate of change of volumetric strain with respect to stress (UCD10) 113

Figure B1-12: Rate of change of volumetric strain with respect to stress (UCE7)..... 114

Figure B1-13: Rate of change of volumetric strain with respect to stress (UCF6)..... 114

Figure B1-14: Rate of change of volumetric strain with respect to stress (UCG7) 115

Figure B1-15: Rate of change of volumetric strain with respect to stress (UCH10) 115

B1-16: Rate of change of volumetric strain with respect to stress (UCI9) 116

Figure B3-1: Time-to-failure plots: (mottled anorthosite) 121

Figure B3-2: Time-to-failure plots: (spotted anorthositic norite)..... 122

Figure B3-3: Time-to-failure plots: (pyroxenite) 122

Figure B3-4: Time-to-failure plots: (mottled anorthosite) 123

Figure B3-5: Time-to-failure plots: (norite)..... 123

Figure B3-6: Time-to-failure plots: (spotted anorthositic norite)..... 124

Figure B3-7: Time-to-failure plots: (anorthositic norite) 124

Figure B3-8: Time-to-failure plots: (spotted anorthosite) 125

Figure B3-9: Time-to-failure plots: (mottled anorthosite) 125

Figure C1-1: Major Principal Stress at a depth of 500m with k-ratio = 1 126

Figure C1-2: Major Principal Stress at a depth of 500m with k-ratio = 2 127

Figure C1-3: Major Principal Stress at a depth of 1000m with k-ratio = 1 127

Figure C1-4: Major Principal Stress at a depth of 1000m with k-ratio = 2 128

Figure C1-5: Minor Principal Stress at a depth of 500m with k-ratio = 1 128

Figure C1-6: Minor Principal Stress at a depth of 500m with k-ratio = 2. The depth of influence of low compressive and tensile stresses is indicated 129

Figure C1-7: Minor Principal Stress at a depth of 1000m with k-ratio = 1 129

Figure C1-8: Minor Principal Stress at a depth of 1000m with k-ratio = 2 130

Figure C1-9: Extension strain at a depth of 500m with k-ratio = 1..... 130

Figure C1-10: Extension strain at a depth of 500m with k-ratio = 2..... 131

Figure C1-11: Extension strain at a depth of 1000m with k-ratio = 1..... 131

Figure C1-12: Extension strain at a depth of 1000m with k-ratio = 2..... 132

Figure C2-1: Major Principal Stress at a depth of 500m with k-ratio = 1 133

Figure C2-2: Major Principal Stress at a depth of 500m with k-ratio = 2 133

Figure C2-3: Major Principal Stress at a depth of 1000m with k-ratio = 1 134

Figure C2-4: Major Principal Stress at a depth of 1000m with k-ratio = 2 134

Figure C2-5: Minor Principal Stress at a depth of 500m with k-ratio = 1 135

Figure C2-6: Minor Principal Stress at a depth of 500m with k-ratio = 2 135

Figure C2-7: Minor Principal Stress at a depth of 1000m with k-ratio = 1 136

Figure C2-8: Minor Principal Stress at a depth of 1000m with k-ratio = 2 136

Figure C2-9: Extension strain at a depth of 500m with k-ratio = 1..... 137

Figure C2-10: Extension strain at a depth of 500m with k-ratio = 2..... 137

Figure C2-11: Extension strain at a depth of 1000m with k-ratio = 1..... 138

Figure C2-12: Extension strain at a depth of 1000m with k-ratio = 2..... 138

List of Tables

Table 4-1: Exploration drill hole coordinates 58

Table 4-2: Specimen nomenclature..... 59

Table 4-3: Distribution of test specimens 60

Table 4-4: Recorded UCS test values for specimen UCA7 64

Table 4-5: Summaries of UCS test results (average values are presented here) 67

Table 4-6: Summaries of Normal Brazilian Indirect Tensile BIT strength test results 70

Table 4-7: Comparison of UCS and BIT strength test 70

Table 4-8: Time-dependent BIT test loads 72

Table 4-9: Time-dependent test results..... 75

Table B1-1: Uniaxial compressive strength test results..... 107

Table B2-2: Normal Brazilian Indirect Tensile (BIT) strength test results 117

Table B3-3: Time-dependent Brazilian Indirect Tensile (BIT) strength test results 118

List of Symbols

2-D	2-Dimensional numerical modelling
AE	Acoustic Emission
ASG	Advance Strike Gully
BC	Bushveld Complex
BIT	Brazilian Indirect Tensile strength test
BRC	Bottom Reef Contact
Cr/Fe	Chrome to iron ratio
Cr_2O_3	Chromite
D	Diameter of a rock drill core sample
FW	Footwall
HW	Hangingwall
ISRM	International Society of Rock Mechanics
km	kilometre(s)
km^2	Square kilometre(s)
kPa	kilo Pascal(s)
L/D	length to diameter ratio of a cylindrical rock specimen
LG	Lower Group
m	metre(s)
m^2	Square metre(s)
Ma	Megaannum
MG	Middle Group
mm	millimetre(s)
MPa	Mega Pascal(s)
MR	Merensky Reef
MTS	Multiple Testing System
NBA - NBI	Normal Brazilian tensile strength test samples
P	Load at failure in the Brazilian Indirect Tensile strength test
PGE	Platinum Group Elements
PGMs	Platinum Group Metals

Phase 2	An elastic 2-D numerical modelling software
r.t.p.	Room temperature pressure
R	Radius of the Brazilian test disc
SEM	Scanning Electron Microscope
SW	Sidewall
t/D	thickness to diameter ratio of a Brazilian Disc Specimen
T(s)	Time in seconds
TRC	Top Reef Contact
TB%A - TB%I	Time-dependent Brazilian tensile strength test samples
UG	Upper Group
UG2	PGE bearing reef type called the Upper Group 2
UCA - UCI	Uniaxial Compressive strength test samples
E	Young's Elastic Modulus
σ_1, σ_2 and σ_3	Major, Intermediate and Minor Principal Stress
σ_t	Direct or indirect tensile strength
σ_c	Uniaxial Compressive Strength
°	Angular measurement in Degrees
k	k-ratio = horizontal stress/vertical stress
ε_1, ε_2 and ε_3	Major, Intermediate and Minor Principal strain
ε_r, ε_a	Radial strain and axial strain
v	Poisson's ratio
π	Pi = 3.14 to two decimal places

CHAPTER 1

INTRODUCTION

1.1 Background

South Africa is a key metals mining and minerals processing power house of the world and is host to a wide range of the world's largest mineral resources. Precious metal resources in South Africa occur mainly in the Witwatersrand Basin (gold, uranium) (Namakando, 2006) and the Bushveld Complex (PGMs, chrome ore). The nation is a major producer of gold and base metals and hosts most of the world's mineral reserves of Platinum Group Metals (PGMs) – 89% (about 75% and 50% of the world's reserves of platinum and palladium respectively (Hilliard, 1996; Cawthorn, 1999; and Chamber of Mines, 2010). The same amount of reserves of PGMs and gold are found at deep levels, currently being slowly exploited, but with future production potential estimated to last more than a hundred years. Cawthorn (1999) suggests that, since mining of PGMs in the Bushveld Complex (BC) has only progressed to an average of 2000m below surface, the proven reserves may easily double with increases in mining depth. Underground mines contribute the bulk of PGMs and gold production in South Africa (Internet: Hilliard, 1997). In underground operations, primary and secondary excavations are mined to access the mineral reserves and these have to remain open and stable for the life of mine.

The bulk of the PGM ore is mined at depths between 500m and 2000m below surface. At shallow depth high horizontal stress conditions prevail, due possibly to tectonics, with horizontal to vertical stress ratios ranging between 0.8 and 4.5 (Stacey, 2002). These stress conditions can induce spalling fractures in tunnel hanging walls (Ryder and Jager, 2002). Spalling refers to a failure process involving extensional splitting cracks (Fairhurst and Cook, 1966). Figure 1-1 illustrates the propensity for excavation walls to experience spalling at a depth approximately 400m below surface observed in a Bushveld Complex platinum mine. The walls of the

haulage were observed to scale from the exposed outside wall surfaces inwards into the rock mass with the passage of time. Without the confinement provided by shotcrete, mesh and lacing, loss of wall rock material through fall out of slabs of wall rock leads to loss of confinement, with subsequent exposure of fresh rock surfaces susceptible to the same damage.



Figure 1-1: Spalling in a haulage observed in a platinum mine located in the western limb of the Bushveld Complex

In contrast, pronounced and predictable stress-induced fractures are observed in excavation walls in deep level gold mines, (Figure 1-2) with a shorter onset time (days to weeks) than is observed in shallow Bushveld Complex mines, where fractures develop months to years after excavation.



Figure 1-2: Advance Strike Gully (ASG) stress induced fractures in a deep gold mine

In shallow BC mines (average 500 m below surface), the rock compressive strength (UCS) is usually greater than the compressive stress in the excavation walls. In these stress conditions surface fractures take months to years to appear and propagate at very slow rates.

1.2 Definition of the problem

Time-dependent spalling of excavation wall rock material has been observed in the BC mines, occurring months to years after excavation due to fracture initiation and propagation in intact rock, (Figure 1-1) and (Figure 1-3). According to Ryder and Jager (2002), the creep rate in rock is dependent on the magnitude of the deviatoric stress (σ_1 - σ_3) and not the individual magnitudes of σ_1 and σ_3, where σ_1 and σ_3 are the major and minor principal stresses respectively. Creep activity is therefore more pronounced close to the exposed excavation walls (i.e. the sidewall and the hanging wall) where the deviatoric stresses are large and confining stresses are low.



Figure 1-3: Spalling in a strike orientated pillar in a platinum mine

Damage in excavation walls in the BC mines is exacerbated by the intersection of fractures with naturally-occurring, shallow dipping discontinuities and layered rock, resulting in the formation of blocks of rock with high fall out and unravelling potential, as sketched in Figure 1-4.

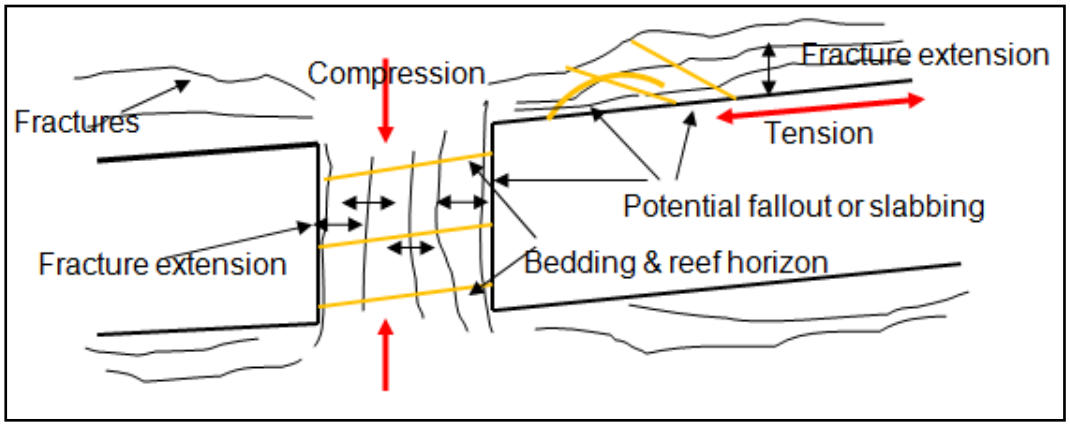


Figure 1-4: Excavation wall damage and fracture extension observed in BC mines

The minimum principal stress in the wall rock in BC mine excavations is low compressive and occasionally tensile, usually lower than the respective compressive and tensile strengths of the host rock material. However, in such conditions, significant magnitudes of extension strain may occur. An analysis of the stress conditions, together with an assessment of the mechanisms of excavation wall rock damage in typical BC mine excavations, is therefore very important in the design of life of mine excavations. Despite the importance of the current discussion, there have been very few studies on time-dependent and tensile creep in rock (Zhao, 2011), more so on BC rock types. Extension characteristics and the effect of time on the tensile strengths of several BC rock types are the focus of the research presented in this dissertation.

1.3 Research objectives

This research investigates the phenomenon of stress induced fracturing in, and time-dependent tensile strength characteristics of BC mine excavation wall rocks. The following objectives are highlighted:

- Provide a background to the characteristics of the BC mining environment and the associated excavation wall stability problems.
- Explore the distributions of stresses around BC mine excavations.
- Evaluate the compressive and tensile strength and deformation characteristics of several BC rock types, assessing the implications of these results to mining in the Bushveld Complex.
- Investigate extension strain distributions around typical BC mine excavations, contrasting the magnitudes of the strain values calculated in numerical analyses with the strain values at failure from laboratory tests.
- Investigate the time-dependent characteristics of the tensile strength of several BC rock types subjected to constant indirect tensile stresses lower than their tensile strengths.

The methodology followed in conducting this research follows.

1.4 Research methodology

The methodology adopted for this research includes:

- Review of the BC mining environment focusing on the following:
  - Relating the BC geology and characteristics of the BC rock types,
  - Outlining the mining methods amenable to mining the BC PGM ore reserves, and typical excavation types used in the BC mines, and
  - Investigating in-situ stress characteristics in the BC Mines
- Review of failure of rock under stress, focusing on:
  - Investigating fracture mechanisms in rock under low normal stress levels and the associated failure mode, and
  - Outlining laboratory compressive, tensile and time-dependent (creep) rock testing methods
- Review the application of numerical modelling in time-dependent (rheological) rock masses
- Carry out numerical analysis of stress and strain around models of typical BC excavations, using rock properties derived from laboratory test results, to investigate the zones of critical extension strain (zones of potential fracture initiation)
- Conducting laboratory uniaxial compressive strength (UCS) and Brazilian indirect tensile (BIT) strength tests to establish the intact rock strengths and elastic properties of several BC rock types.
- Conducting time-dependent BIT strength tests on several BC rock types, establishing their time-to-failure under predetermined constant stress levels derived as fractions of the tensile strength of the respective rock types (0.7; 0.75; 0.8; 0.85 and 0.9 x σ_t).

A comparison is made between strain values calculated from laboratory tests and magnitudes of extension strain values obtained from numerical models, and the resulting implications on the stability of the excavations are discussed. Time-to-

failure values from time-dependent tensile creep tests are recorded and analysed, to investigate time-dependent trends in the tensile strength of several BC rock types.

1.5 Content of the dissertation

Chapter 2 gives the characteristics of the Bushveld Complex (BC) mining environment, and a review of the laboratory test methods and the behaviour of rock under various stress conditions. Characteristic mine excavations prescribed by the BC mining environment, and stress-strain analysis conducted on model excavations based on the BC mining set up, are presented in Chapter 3. Chapter 4 reports results of laboratory tests on several BC rock types aimed at investigating their elastic properties, long term strength and time-dependent characteristics under indirect tension. Discussions of the findings, and comparison of stress-strain analysis results and laboratory test results, are covered in Chapter 5. The final chapter gives the conclusions and recommendations from the research.

CHAPTER 2

CHARACTERISTICS AND ANALYSIS OF THE BUSHVELD COMPLEX MINING ENVIRONMENT

2.1 Introduction

The Bushveld Complex (BC) is host to the world's most important Platinum Group Metals (PGMs) reserves. As such it is imperative to understand the structural properties of the PGMs ore reefs and hosting environment that prescribe the current choice of mining methods utilised in the BC mines. This entails outlining the characteristic BC geology, in-situ and induced stress conditions and mechanical properties of the rock types hosting the BC mine excavations. With this aim numerical stress analyses and laboratory rock strength tests have been carried out.

2.1.1 Geology of the Bushveld Complex

Drill core from Impala Platinum Mines' surface exploration drilling projects in its Rustenburg division was used in this research to investigate the strength and deformational characteristics of several BC rock types. The spatial location in the BC and a typical lithographic description of the test drill core used in this research are provided here. Different hypotheses have been raised regarding the possible formation and genesis of the Bushveld Complex mineralization by Cawthorn (1999), Mitchell and Manthree (2002), Seabrook et al (2002), Brown (2005), Cawthorn et al (2006), Simmat et al (2006), Smith and Basson (2006), Wilson and Chunnett (2006), Perrit and Roberts (2007), and Naldrett et al (2009), but these are not debated in detail here. Simplistically "the Bushveld Complex formed by the repeated injections of lava (or magma) into a sub-volcanic, shallow-level chamber. With differential cooling different sub-horizontal mineral accumulations were formed starting from the base of the depositional chamber now commonly known as the Bushveld Complex (BC). Subsequent feeding of molten magma into this chamber resulted in intervals of repeated mineral accumulations with important concentrations of minor minerals like chromicise and vanadium" (Cawthorn, 1999). Figure 2-1 shows a geological map of

the Bushveld Complex giving the locations of some of the operations of Impala Platinum Mines.

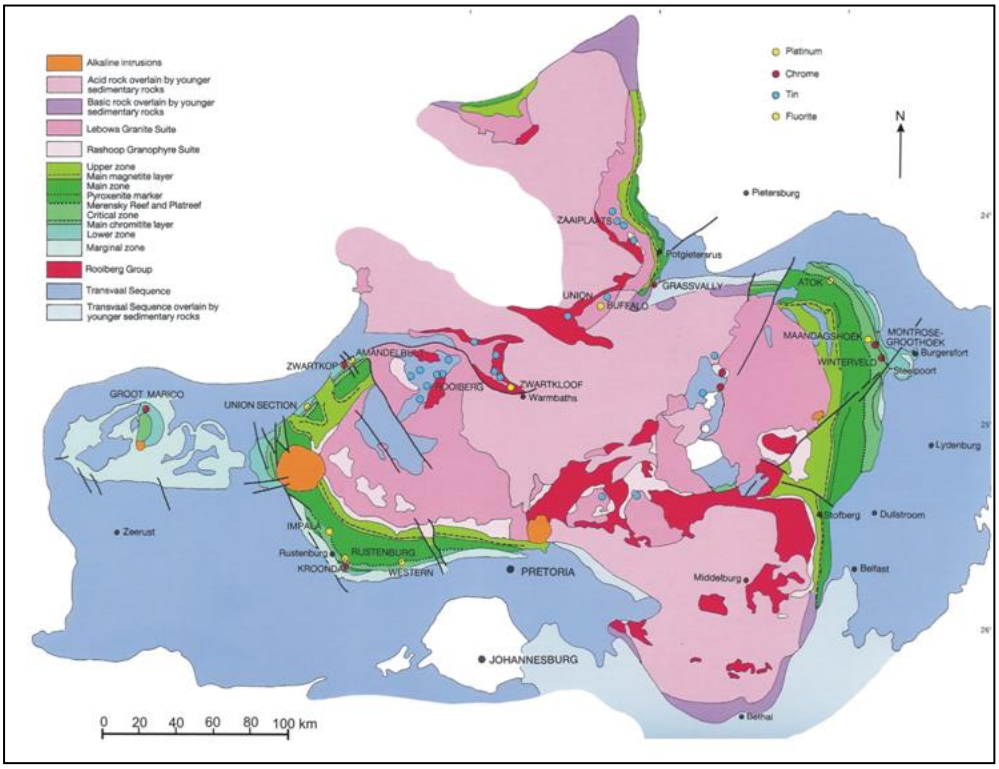


Figure 2-1: Geology map of the Bushveld Complex (after Viljoen and Schürmann, 1998)

The 2060 Ma old (BC) is an irregular, saucer shaped massive layered igneous intrusion, with outcrop extremities of ~450 km east–west and ~300 km north–south (Simmat et al, 2006). “The (BC) platinum reserves consist of three different reefs; the Merensky reef (MR), the Upper Group 2 (UG2) chromicise reef, both of these can be traced on surface for about 300 kilometres in two separate horizons, and the Platreef which extends for 30 kilometres” (Cawthorn, 1999; 2006). Below these reef horizons lies the Upper Group 1 (UG1) reef, the platinum content of which has not yet been widely proven to be economically viable. The down-dip continuity of these reefs has been confirmed at just more than 3000m below surface for the Merensky and UG2 reefs (Cawthorn, 1999).

2.1.2 Stratigraphy of the Bushveld Complex

A typical stratigraphic section through the BC given by Cawthorn (2006) is shown in Figure 2-2. The mineralisation of interest with regard to platinum reserves is contained in the Upper Critical zone of the BC.

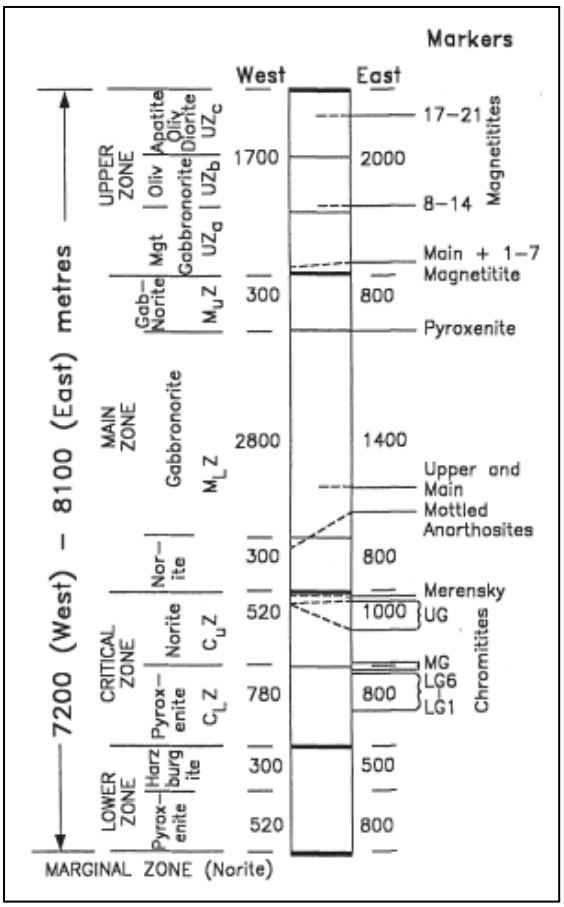


Figure 2–2: Typical stratigraphy of the Bushveld Complex

The following extract from an unpublished report describes the mineral composition of the Lower, Middle and Upper Groups of the BC. “Locally up to 25 chromicise seams have been recorded, but 13 are regionally persistent. These are shown in Figure 2-3 and are subdivided into Lower (LG), Middle (MG) and Upper (UG) groups. The main Cr production in both the eastern and western Bushveld comes from the LG6 seam, which averages about 1 m in thickness but can widen to 2.5 m. The LG6A seam, 0.3 m thick, occurs in the hanging wall and is separated from the LG6 by a 0.8 m pyroxenite layer with disseminated chromites. As a result of the good parting at the contacts of the LG6A and the weak friable nature of the pyroxenite in places, the two reefs sometimes have to be mined together to a mining width of

approximately 1.8m. The LG6 seam typically comprises 97% chromite with an average Cr/Fe ratio of 1.6 and Cr_2O_3 content of 46%, the quality being slightly better in the Eastern Bushveld. The Middle Group comprises four horizons but each horizon may consist of more than one seam. They occur within a stratigraphic interval of 30 m to 50 m in both the eastern and western Bushveld. The lower two seams (MG1 and MG2) occur in pyroxenite (Lower Critical Zone) host rocks, while the MG3 and MG4 accumulated within norites and anorthosites which places them in the Upper Critical Zone" (Rangasamy, 2010).

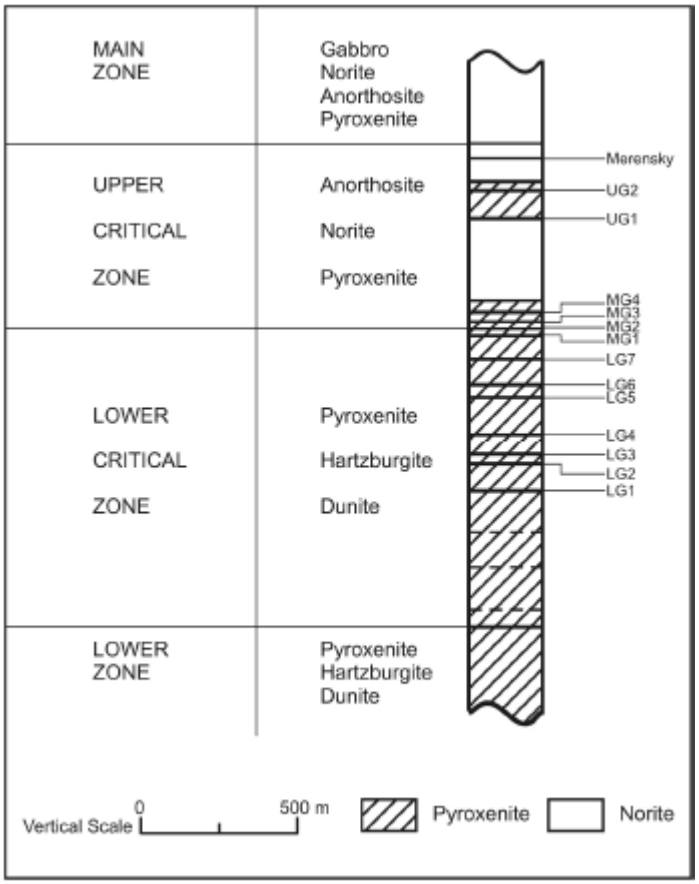


Figure 2-3: Lithographic representation of the Bushveld Complex (Rangasamy, 2010)

The Bushveld Complex is made up of several zones; the most important of which is the Critical zone. "The Upper Group comprises two chromicise seams. The lower UG1 seam, although up to a metre in thickness, has never been mined. The upper UG2 seam is extensively mined for its platinum group element (PGE) content. The quality of the chromite did not until recently allow its exploitation as a by-product. The

Merensky reef is the basal layer of a classic cyclic unit, which grades upwards from pyroxenite to an anorthosite. Overlying the anorthosite is the Bastard reef, which also forms the base of a cyclic unit terminating in the 'giant mottled anorthosite', which is taken as the top of the Critical Zone. The reef can, from its normal stratigraphic position where it conformably overlies the full succession of FW strata in an area, abruptly or gradually transgress its FW to form local 'potholes' commonly 100 m^2 to 30000 m^2 in area, or even regions of pothole reef several km^2 in extent. Potholes interrupt the reef, appear unexpectedly and unpredictably and range in size from 1 m to greater than 500 m in diameter" (Lomberg et al, 1999). Based on regional changes in geological characteristics, the Merensky reef is divided into two facies: the Rustenburg facies to the south of the Pilanesberg intrusion and the Swartklip facies to the north. "The reef in its most common form is a pegmatoidal (coarse-grained) feldspathic pyroxenite generally bounded by thin (approx. 20 mm) chromicise layers. The immediate hanging wall is pyroxenite, 1 - 5 m thick which grades upwards through norites to anorthosites. The FW generally comprises various types of norite and anorthosite, and less commonly feldspathic pyroxenite or harzburgite, which however often forms the immediate FW of pothole reefs" (Rangasamy, 2010).

Egerton (2004) gives the middling between the Merensky reef and the UG2 reef ranging between 12 m and 400 m, with sections of the BC where the two reefs merge and can be mined together, the most common scenario being multiple reef extraction. According to a study of Impala Platinum Mines' 18 Shaft project contained in an unpublished geotechnical report by Rangasamy (2010), "The average depths of intersection below natural ground level for the reefs are 1391 m for the Merensky (MR) bottom reef contact (BRC) and 1448 m for the UG2 top reef contact (TRC). The shallowest reef contacts are 1048 m for the MR and 1093 m for the UG2 reef". The deepest reef contacts were given as 1881 m and 1964 m, for the MR and UG2 respectively in that particular project set up. The separation between the two mining horizons was reported as 20.56 m (minimum) and 105.64 m (maximum), with an average of 60 m. A gentle reef dip of 9 - 14˚ prevailed in the area covered in the report. A schematic cross section of the upper portion of the Upper Critical Zone of the Rustenburg Layered Complex, at Northam Platinum Mine, is shown in (Figure 2-4).

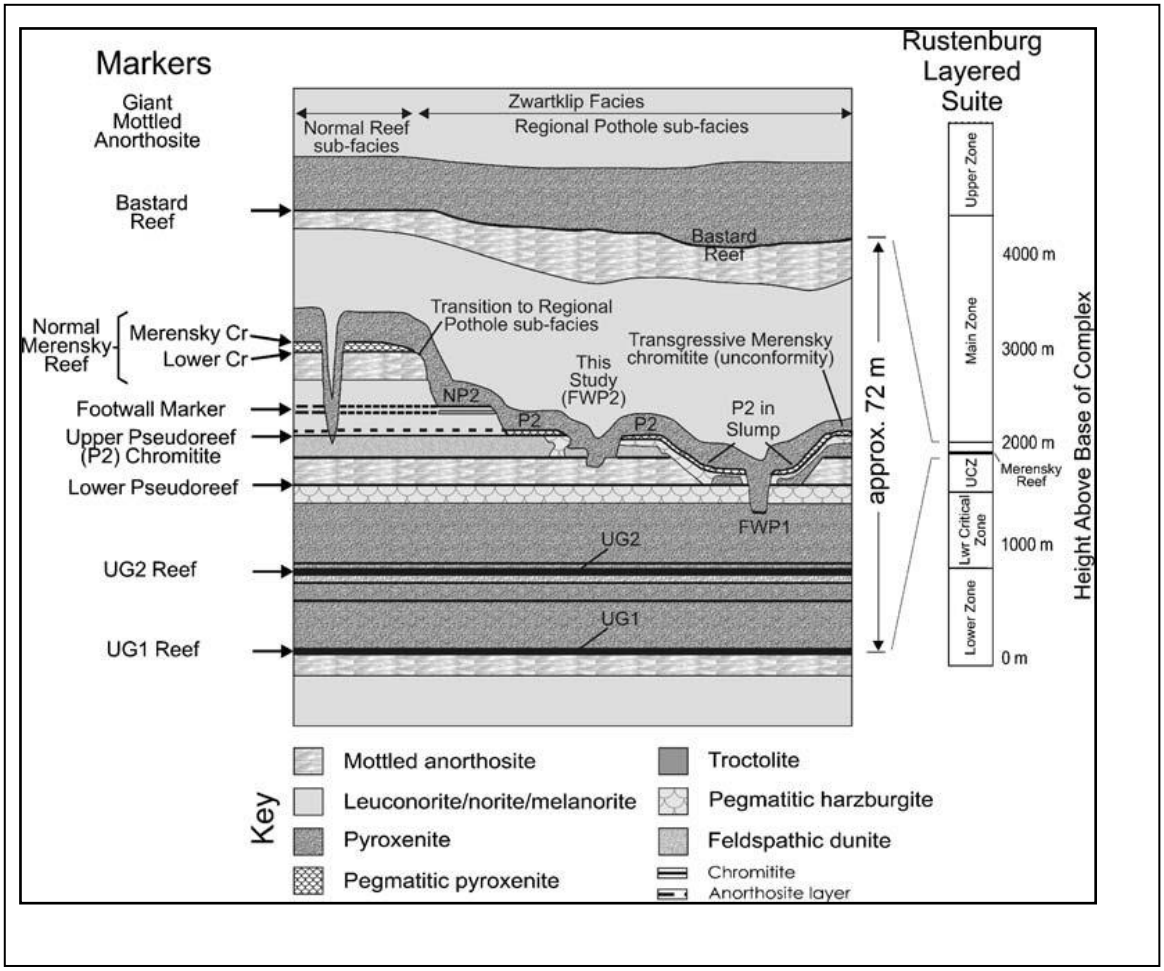


Figure 2-4: Schematic cross-section of the upper portion of the Upper Critical Zone of the Rustenburg Layered Suite, at Northam Platinum Mine (Smith and Basson, 2006)

Occurrences of potholes, faults and dykes in the Merensky and Upper Group 2 reefs disrupt the otherwise uniform dipping, shallow dipping and narrow tabular reef characteristics peculiar to the Bushveld Complex mines. Geological losses of between 20 and 25% have been reported by Egerton (2004) as a result of faults and dykes intersected in the reef horizon.

2.1.3 The Bushveld Complex rock types

“Characteristics of the Critical Zone are: chromicise seams; repeated cyclic units comprising a lowermost pyroxenite layer usually with a basal chromicise layer grading upwards through norites (melanorite, leuconorite into anorthosite and very well developed layering” (Cameron and Desborough, 1964). “The uppermost unit of the Upper Critical Zone is an anorthosite with large inter-cumulus pyroxene mottles.”

(Mitchell and Manthree, 2002). The focus of this discussion is a chemical and physical description of anorthositic rock types which make up the bulk of the host rock for the platinum reserves in the BC.

2.1.3.1 Anorthositic rock types in the Bushveld Complex

Rocks are different to metals in that they are non-homogeneous due to their granular make-up (Mercer, 2006), comprising "...an aggregate of crystals and sometimes amorphous particles of mineral or organic matter, with sizes in the range of millimetres to centimetres. ... They are held together with various amounts of cement. The grains can consist of different kinds of minerals with different mechanical behaviour. On a larger scale rocks are mostly continuous and homogeneous, but quite often joints, faults, bedding planes, or different strata appear. The result is rocks do not behave homogeneously as metals usually do" (Critescu and Hunsche, 1998).

Anorthosite rock type is predominant in the Bushveld Complex and platinum bearing formations the world over (Barnes and Maier, 2002). "Most anorthosite rock type is dated between 3200 Ma and 2500 Ma. It is considerably less abundant than either basalt or granite, but the complexes in which it occurs are often immense. Anorthosite rock is a type of igneous rock composed predominantly of calcium-rich feldspar. Anorthosite consists of plagioclase and feldspar grains cemented together. This aggregate makes anorthosite a brittle rock. The rock consists of 90% or more of cumulus plagioclase, together with small amounts of ortho-pyroxene and/or augite. Mottled anorthosite refers to anorthosite in which large areas of inter-cumulus ortho-pyroxene and/or augite (from 10 mm diameter up to the diameter of tennis balls) form dark mottles in a matrix of pure white or pale grey anorthosite. Spotted anorthosite is anorthosite in which a small percentage of cumulus ortho-pyroxene gives the effects of dark spots in the pale anorthosite matrix. All anorthosites found on the earth consist of coarse crystals, but some from the moon are finely crystalline" (Barnes and Maier, 2002). It is generally accepted that crystalline rocks are brittle, therefore stronger under compression than they are under tensile stress, as witnessed by tensile strength values that are a magnitude of up to 20% lower than the corresponding compressive strength values.

2.2 Behaviour of rock under stress

In-situ or virgin stress determines the stress redistribution observed when excavations are mined in rock (Mercer, 2006). It is important therefore to carry out in-situ stress measurements and use the data in mine planning and design to help predict the behaviour of wall rock in planned excavations. However, in-situ stress measurements are both difficult and expensive to conduct, hence relatively few data have been collected the world over.

2.2.1 In-situ stress conditions of the Bushveld Complex

Around the world different authors have provided in-situ stress data from their investigations carried out in the field during projects. Stacey and Wesseloo (2004) collected a database of in-situ stress measurements across South Africa and results of this investigation relevant to the BC are summarised in Figure 2-5. Generally high principal stress k-ratios (2.5 – 4) are experienced in the BC mines at shallow depth levels. At greater depths of about 1000 m, the stress ratios are lower, in the region of (1 - 1.5).

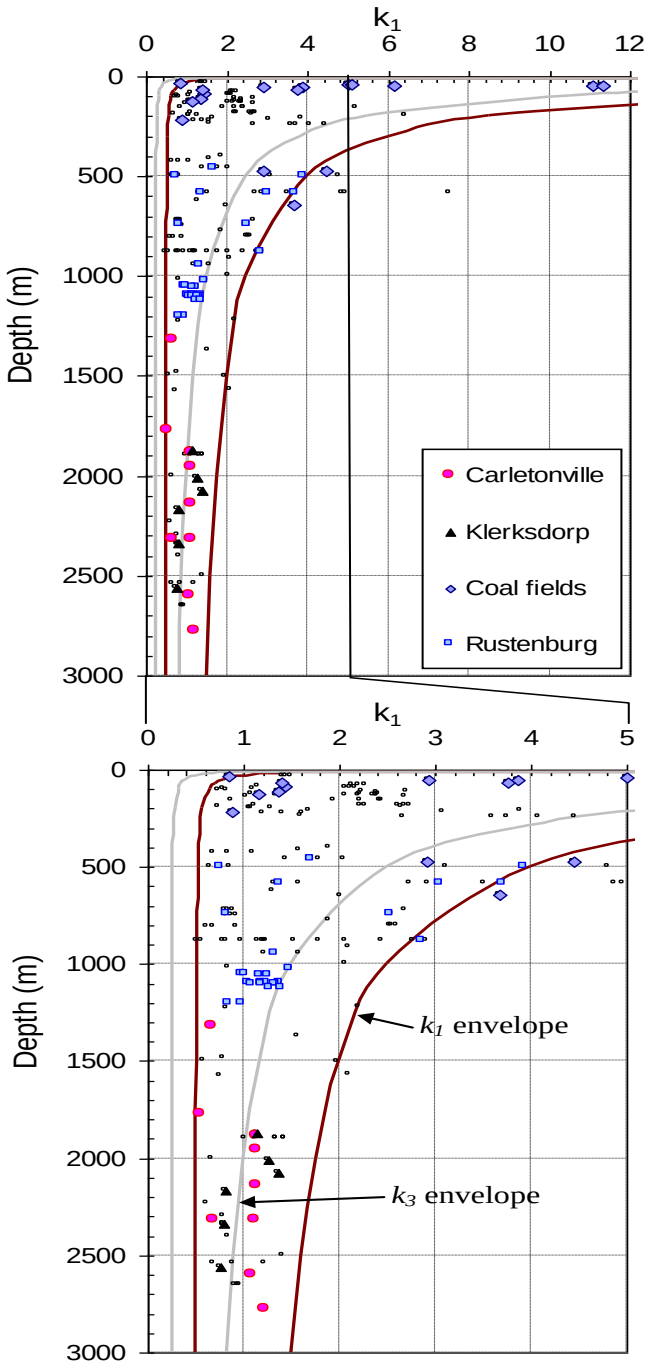


Figure 2-5: Ratio of the principal horizontal stress to the principal vertical stress for South African mines, (after Stacey and Wesseloo, 2004).

Instability problems in inclined shafts and in dip oriented tunnels have resulted in the Rustenburg mining environment due to the unique stress conditions as demonstrated in Figure 2-6.



Figure 2-6: Stress induced failure in the roof of a dip oriented tunnel in a platinum mine, (Stacey and Wesseloo, 2004)

The platinum and chrome mines in the Bushveld Complex (BC) have a high horizontal stress in the “strike” direction as evidenced by observed “gothic arches” in tunnels and haulages oriented on dip. Sidewall and hanging wall slabbing has however been observed in platinum mine excavations in orientations free of the major horizontal principal stress influence. The mechanism of fracture propagation therefore has to be investigated at shallow depth in BC mines.

2.2.2 Behaviour of intact rock under stress

Laboratory tests are usually low cost and quick methods widely used to investigate the modes and mechanisms of failure of rock specimens under different loading conditions. Various modes of failure and mechanisms of failure under stress have been explored (Stacey and Yathavan, 2003). Fracture propagation in low stress, shallow depth mining environments is investigated to explain the observations made in wall rock of BC mine excavations.

2.2.2.1 Behaviour of rock under compression

Different failure mechanisms are observed in rock prescribed by the stress conditions and the inherent strength (and deformities) of the rock type under investigation. Research has been carried out on the behaviour of rock under compression (Bieniawski, 1967; 1969; 1970; Ashby and Hallam, 1986; Halm and Dragon, 1998; Betournay and Mitri, 2003; Drescher and Handley, 2003; Szwedzicki, 2006; and Li et al, 2010). Various modes of failure were proposed and are briefly discussed here.

Failure modes in rock specimens

Ashby and Hallam (1986) gave failure models for a rock specimen under compression, as shown in Figure 2-7. According to Ashby and Hallam (1986) and as depicted in Figure 2-7, (a) and (d) show slabbing when one or few cracks propagate parallel to the principal compression, (b) depicts failure by aggregation of cracks to form a shear zone and (c) presents near homogeneous deformations by distributed micro-cracking. There are many possible crack orientations and therefore no two rock specimens from the same rock type are likely to fracture in the exact same manner.

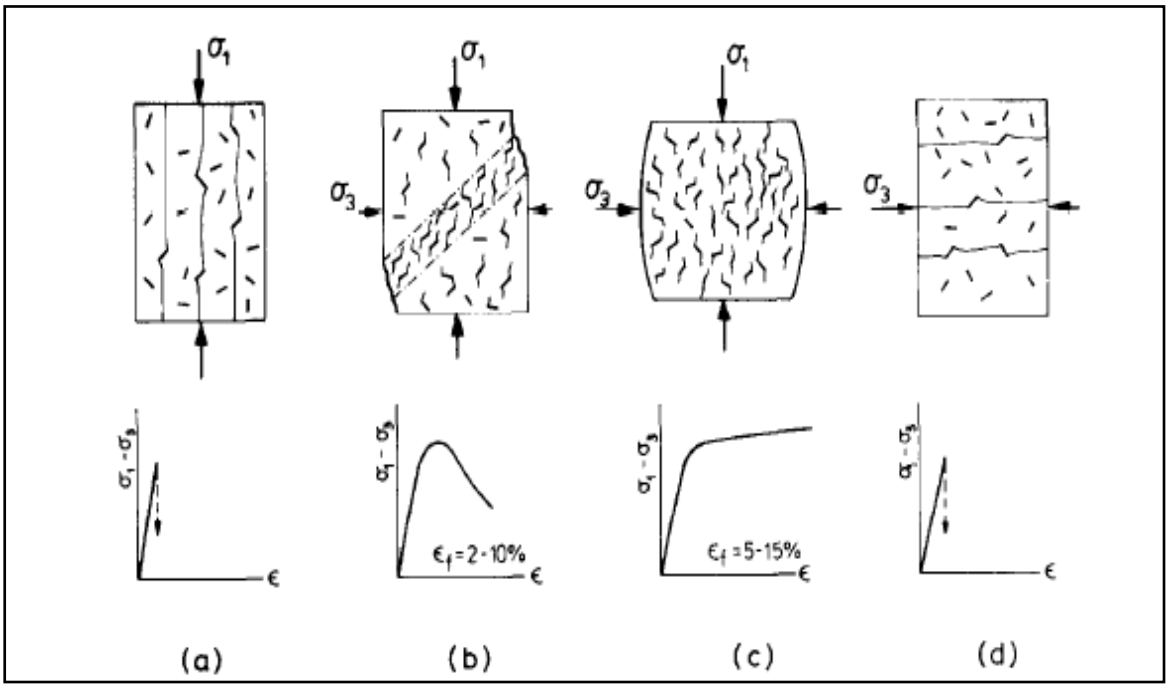


Figure 2-7: Failure modes in compression (Ashby and Hallam, 1986)

Ashby and Hallam (1986) described the failure process in rock as consisting of “the growth of single cracks in a stable way up to a stage where the interaction of cracks increases the stress intensity driving crack growth and leads to instability and final failure”. Betournay and Mitri (2003) observed that samples tested uniaxially exhibited nearly equal spalling from all sides prior to the shear failure of the centre portion. A varying degree of rock spalling (which can be attributed to extension fractures) parallel to the free face was observed in the biaxial tested samples. Szwedzicki (2006) stated that under compression a rock specimen can fail under tension or compression, or a combination of both. He suggested that in uniaxial compression tests on cylindrical specimens, the highest value of UCS is found for a specimen that fails under extension. This postulation should however not be taken to suggest that wherever high UCS values are observed extension is involved, or vice versa, but it is a sign of fracture propagation in the direction of principal stress.

Crack initiation and propagation in rock specimens

The Griffith theory on crack initiation and growth in rock explains extension of cracks when energy higher than the granular molecular bond in the rock is supplied to a crack tip (Bieniawski, 1967a). Griffith’s theory explains the existence of cracks and initiation of fractures in rock, but does not explain the rate of propagation and extension of fractures; neither does it predict the occurrence of fracture failure, (Hoek and Bieniawski, 1965). Ashby and Hallam (1986) discovered that a critical stress was required to initiate crack growth, dependent on the initial crack length and orientation, the coefficient of friction and the stress state. Bieniawski (1967b) tested the behaviour of a crack in a glass sample and showed that fracture initiation will start once the shear movement of the crack faces results in stable extension of the crack tip close to the initial crack. The condition of the crack surfaces with regard to shear movements therefore plays a big role in the initiation of fracturing in a glass specimen. Halm and Dragon (1998) postulated a meso-crack theory for crack growth as shown in Figure 2-8. This illustrates the tendency of fracturing in rock parallel to the direction of the applied stress.

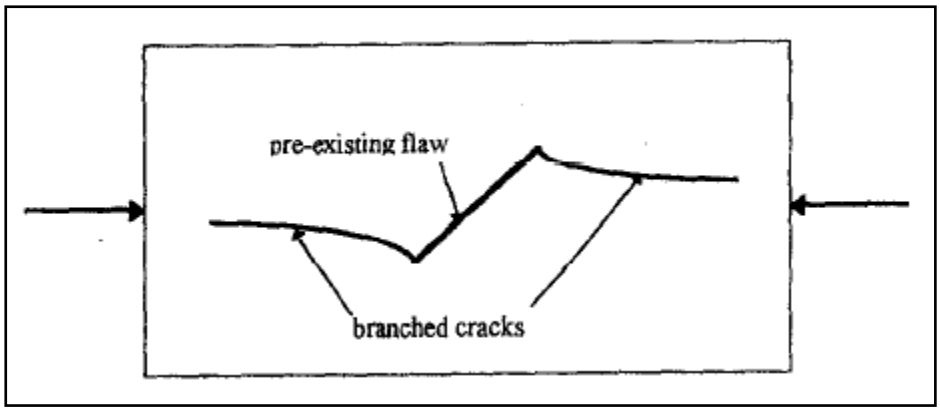


Figure 2-8: Crack branching mode under compressive loading (Halm and Dragon, 1998)

Krausz *et al* (1988) proposed an energy based fracture kinetics of crack growth for all materials. This concept, which deals with inter-atomic bond energies, is more suitable to homogeneous material unlike rock, which is largely heterogeneous. Bieniawski (1967a; 1969; 1970) investigated fracture mechanisms in rock extensively. Bieniawski (1967a) stated that a direct relationship existed between the stress applied and the extension of crack length in rock. This process is irreversible, hence permanent or plastic behaviour is dominant in rock compared with the small elastic portion represented in stress-strain plots.

Long term strength in rock

Bieniawski (1967a) gave four stages of fracture development in rock starting from fracture initiation and culminating in failure. These can be stated as:

- I crack closure (closing of cracks),
- II fracture initiation (linear elastic deformation),
- III critical energy release (stable fracture propagation)
- IV strength failure when maximum strength is achieved (unstable fracture propagation) and
- V rupture (coalescence of cracks) [failure of the rock].

The transition point between stable fracture propagation and unstable fracture propagation marks the “long term strength” of the rock specimen, Figure 2-9.

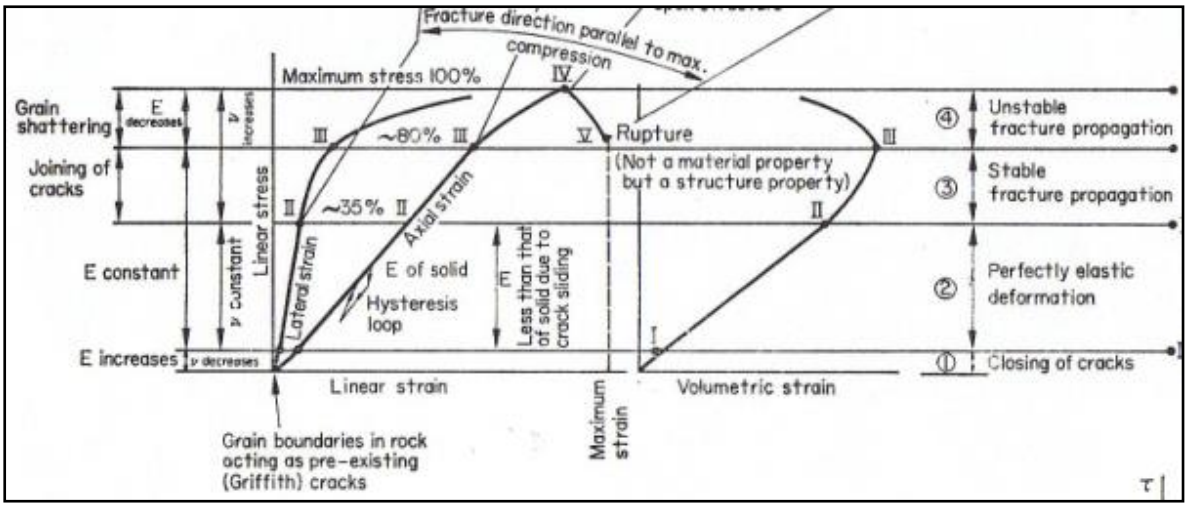


Figure 2-9: Mechanism of brittle fracture under multi-axial compression, Bieniawski, (1967a)

Volumetric strain is given as the sum of the three orthogonal principal strains;

Volumetric strain = $(\varepsilon_1 + \varepsilon_2 + \varepsilon_3) = (\varepsilon_1 + 2 \times \varepsilon_3)$ since $\varepsilon_2 = \varepsilon_3$ in a triaxial test,

where ε_1, ε_2 and ε_3 are the major, intermediate and minor principal strain respectively.

Of interest is the volumetric strain-stress plot whose turning point showed the “long term strength” of a rock specimen in Bieniawski’s analysis. This point was depicted by Bieniawski (1969) to be about 80% of the UCS of the specimen and could be checked by plotting the volumetric strain-stress curve for the specimen tested under uniaxial compression. The same stress level was observed within tests of the same rock type and is attributed to the onset of unstable fracture propagation. At this point, if the stress applied is kept constant, eventual rupture of the specimen will occur with the passage of time. In both the volumetric strain vs axial stress and lateral strain vs axial stress the departure from linearity marks the point of fracture initiation in the rock specimen. However, this point is not the same for axial strain vs axial stress plot.

Hooke's constitutive laws

Rock under uniaxial compression follows the Hooke's law constitutive behaviour given by:

$$E = \sigma/\varepsilon$$

Where E = elastic or Young's modulus, σ = stress and ε = strain.

In three dimensions, Hooke's law is given by the following equations in strain-stress terms:

$$\varepsilon_1 = [\sigma_1 - v(\sigma_2 + \sigma_3)]/E$$
$$\varepsilon_2 = [\sigma_2 - v(\sigma_1 + \sigma_3)]/E$$
$$\varepsilon_3 = [\sigma_3 - v(\sigma_1 + \sigma_2)]/E$$

where σ_1, σ_2 and σ_3 are major, intermédiate and minor principal stress respectively, E is the Elastic modulus and v is Poisson's ratio.

The elastic modulus determines how much a rock specimen can deform under load before failure occurs, or within the rock's elastic range. The elastic modulus of rock is therefore a consistent property for the rock type and for linear elastic behaviour can be used to calculate typical failure strain values from stresses recorded at failure.

Effect of shape and size on the strength of rock specimens

The shape and size of rock specimen influences its strength and deformation behaviour. The influence of the height-to-width ratio on the failure mode of rectangular hard rock prisms loaded under uniaxial compression was studied by Li et al (2010). They investigated the surface parallel slabbing observed in deep hard rock mines by investigating the stress conditions required to initiate slabbing in hard granite rock surfaces using rectangular specimens with a range of width-height ratios. They found out that at a height-to-width ratio of 0.5 the failure mode in the specimen changed from shear to slabbing. They gave a slabbing strength of 60% of the uniaxial compressive strength for Iddefjord granite from Norway. This indicates that when tangential stresses calculated in excavation boundaries exceed the slabbing or spalling threshold then fracture of excavation walls may be expected.

2.2.2.2 Behaviour of rock under tension

Goodman (1989), Bieniawski (1989) and Okubo and Fukui (1996) carried out extensive direct tensile strength tests on several rock types and made a comparison of the behaviour of rock under compression and under tension. They found that "crack extension occurs in tension, whereas in compression, consolidation and crack extension simultaneously occur". Diederichs (2002; 2007) and Diederichs et al (2004) carried out research into tensile slabbing in hard rock. They compared the long term strength curves from laboratory tests to the in-situ strength of hard rock. Their conclusion was that the in-situ strength of hard rock was less than the long term strength of laboratory samples at low confinement, and therefore slabbing may occur under such stress conditions.

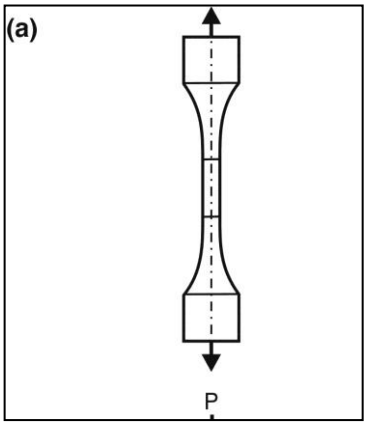
Bieniawski (1967c) investigated fracture mechanisms and long term strength in rock under tension. He found that the fracture process of rock under compression and direct tension were virtually the same except that, under tension, there is an absence of crack closure, and durations of stable and unstable crack propagation processes are shorter. From Bieniawski's results for norite under compression, fracture initiation occurred at 35% of the maximum load while in tension it occurred at 94.5% of the maximum load. It was also shown that unstable fracture propagation occurred in compression at 73% of the maximum load, while in tension it occurred at 96.5% of the maximum load.

The Brazilian Indirect Tensile (BIT) strength test

Tensile strength can be measured through direct or indirect methods. In the early stages, a cylindrical dog-bone shaped specimen was suggested for use in minimizing the effects of gripping of ends (Brace, 1964; Brace and Tapponier, 1976 and Hoek, 1964) as shown in Figure 2-10a. However, such specimens are difficult and expensive to prepare in rock. The preparation of these shaped specimens is not suitable for all rocks, especially for laminated soft rocks or very brittle hard rocks, which usually fail during specimen preparation. The Brazilian Indirect Tensile (BIT) strength test set up was hence developed to overcome this difficulty.

The Brazilian Indirect Tensile (BIT) strength test set up is shown in Figure 2-10b. This test involves using a cylindrical specimen of radius R and length *l,* where,

preferably, R>25 mm and *l* = R (ISRM, 1981). The specimen is aligned with its axis horizontal and compressed to failure between two concave steel platens by a load P.



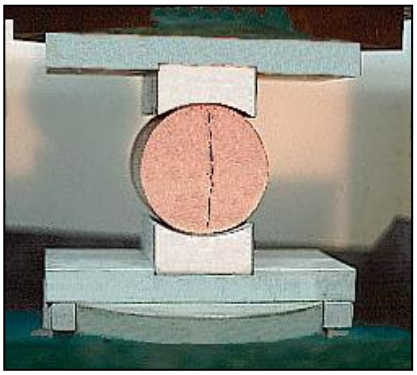
(b) 

Figure 2-10: Tensile strength testing set up, a) The dog bone shaped specimen used in direct tensile strength tests (Ryder and Jager, 2002) and b) Brazilian disc set up used in indirect tensile strength tests

In the test an induced indirect tensile stress field acts across the loaded diameter tending to split the loaded disc apart. The value of the induced indirect tensile stress at failure can be calculated from:

$$\sigma_3 = -\frac{P}{(\pi R l)} = -\sigma_t$$

Where P = load applied across test specimen, R = radius of test specimen and *l* = the thickness of the test specimen (Jaeger and Cook, 1979).

Mellor and Hawkes (1971) explain that while the Brazilian test, carried out on solid rock discs, is particularly appealing because of its simplicity in specimen preparation, it produces failure in a biaxial, rather than a uniaxial, stress field. However, the

results from BIT tests have been widely found to be comparable to typical tensile strength values, and therefore the test is widely used to establish tensile strength values in rock (Ryder and Jager, 2002). The Brazilian test has been used in numerous applications in the past. The test has been used to test the elastic properties of concrete by Hondros (1959), thin spray-on liner products (TSLs) and shotcrete by Yilmaz (2010), the tensile strength of coal by Berenbaum and Brodie (1959) and Evans (1961), and that of rocks by Berenbaum and Brodie (1959); Hobbs (1964); Hudson et al (1972); Chen and Hsu (2001) and Wang et al (2004). Hondros (1959) developed a method to measure the elastic modulus and Poisson's ratio using the Brazilian test, but Wang et al (2004) found that in this process additional strain gauge measurements must be implemented for improved accuracy, making the procedure tedious.

Tests carried out on anisotropic rock specimens have shown the Brazilian tensile strength to be dependent on the angle between the planes of rock anisotropy and the loading direction (Chen and Hsu, 2001). The rock types tested in the current research showed no anisotropy or lamination as they are largely igneous, isotropic and homogeneous, therefore anisotropy effects have been ignored here. Hudson et al (1972) observed that when carrying out the Brazilian test it was imperative to concentrate the stress at the centre of the specimen so that crack initiation was not at the circumferential contacts of the loading platens. They discovered this when they used flat platens on granite, Solenhofen limestone and Tennessee marble discs and rings. During the unloading tests Hudson et al (1972) found out that failure always initiated at the loading points for flat platens and at the boundary of the hole on the loaded diameter when a load distributing device was employed. Jaeger and Hoskins (1966) had suggested a 15° loading arc on marble specimens to correct the situation encountered by Hudson et al (1972) and gave a true value of the tensile strength of the rock disc. They unloaded the specimen at the first sign of failure and observed that cracks initiated in the interior of the sample 'as an extension fracture' which propagated to the surface. For validity of Brazilian test results Wang et al (2004) emphasised the need for crack initiation from the centre of the specimen and not from the specimen periphery in the Brazilian test. They suggested that a loading angle corresponding to the flat end width must be greater than a critical value of

(2α ≥ 20°). Curved platens were used in the current research following this argument to ensure crack initiation at the disc centre.

2.2.3 Characteristics of rock failure

Rock naturally fails when the applied stress exceeds the strength of the rock. Despite this fact, rock specimens have been observed to fracture or fail at stress levels lower than their Uniaxial Compressive Strength (UCS) values. In dry conditions, under uniaxial stress, minerals generally fail by fracture at some value of stress without prior internal rearrangement of their atomic structure (Duncan, 1969). Lockner et al (1992) stated that "when rock is subjected to low stress levels, geometrically sharp cracks concentrate stress at their tips to such a degree that local failure can occur at modest applied stress". This geometrical enhancement of stress is a fundamental notion in fracture mechanics and has been successfully used to analyze the strength of materials. Brace (1964), Hoek and Beniawski (1964) and Bieniawski (1967; 1969; 1970) proved that Griffith's theory is a good basis for the study of the fracture of hard rock. Griffith's theory indicates that, even if low stress loading conditions prevail, as long as the energy generated on cracks exceeds the molecular bond energy, propagation will result, leading to eventual widespread failure. As a result Griffith's fracture criterion is expressed in terms of the uniaxial tensile strength of the material, since the molecular cohesive strength is difficult to determine by direct measurement.

2.2.3.1 Fracture development in rock at low stress

Stacey and Yathavan (2003) studied the initiation of fractures at low stress levels in rock. Studies and data on tunnel fracturing due to induced stress provided by Grimstad and Bhasin (1997) supported by findings of Myrvang et al (2000) showed that stress induced failure occurs even when the maximum induced stresses are as low as a quarter to half of the rock strength. Ortlepp (1997) observed rock bursts in a sandstone roof of a shallow coal mine with a low horizontal stress of 2 to 3 MPa and a k–ratio of between 3 and 4. These findings further support the existence of low stress fracturing in underground mining and construction and point to the fact that, "the understanding of the mechanism of fracture initiation is essential for the correct design of underground excavations" (Bieniawski, 1967). Brace and Tapponier (1976)

observed new trans-granular cracks to form in Westerly granite specimens loaded under biaxial compression at about 75% of the peak stress. These cracks started at high angle interfaces of dissimilar minerals and rarely at inclined pre-existing shear cracks. The nucleation of cracks theory is further supported by Reches and Lockner (1994) in their Acoustic Emission (AE) testing of crack propagation in Westerly granite. Investigating the time it takes for these phenomena to manifest themselves under low stress loading in rock is important to giving more information on the time-dependent tensile strength of rock.

2.2.3.2 The extension strain criterion

Several authors have observed face parallel slabbing or spalling at low confining stress and pointed towards extension fracturing as a fracturing mechanism. An extension strain criterion was proposed by Stacey (1981) to describe the fracture process existing in excavation walls at low stress levels. Stacey commented that the existence of tensile conditions in rock is not a pre-requisite for the existence of extension strain, since extension may occur with all three principal stresses being compressive. According to Stacey (1981), fracture of brittle rock will initiate when the total extension strain in the rock exceeds a critical value which is characteristic of that rock type. Expressed simply, fracture initiates when:

$$\varepsilon_3 \geq \varepsilon_{cr}$$

where ε_{cr} is the critical value of extension strain and ε_3 is the minimum principal (extension) strain.

Fractures were observed to form in planes normal to the direction of extension strain which corresponds with the direction of minimum principal stress (the least compressive principal stress). Stacey (1981) wrote an equation for this behaviour for linear material based on their strength properties as follows:

$$\varepsilon_3 = \frac{1}{E} [\, \sigma_3 - \nu\, (\sigma_1 + \sigma_2)]$$

where ε_3 is minimum principal strain, σ_1, σ_2 and σ_3 are the principal stresses, E is the Elastic modulus and ν is the Poisson's ratio.

From this argument it was shown that if

$$\nu\,(\sigma_3 + \sigma_2) > \sigma_3$$

then the strain induced will be an extension strain, possibly leading to fracture. The negative values of extension strain, and the zones under this influence, can easily be identified in numerical models representing typical excavations. A comparison of the magnitude of critical extension values observed here with actual laboratory test derived strains, obtained at tensile failure, may be used to confirm if fracture initiation and propagation may be expected in the excavation wall material.

2.3 Time-dependent characteristics of rock

Stress fields in in-situ rock change due to various mining activities (Mercer, 2006). When an excavation is mined, stress redistribution occurs around the opening resulting in compression, (major principal stress, σ_1) and sometimes tension (minor principal stress, σ_3) concentration in the rock. A change in the stress field can result in significant deformations in a rock mass occurring over a relatively long period of time, especially as a result of creep, both within the intact rock and on the structures making up the rock mass as a whole. The long term strength of the rock mass is therefore partly controlled by the time-dependent weakening of intact rock (Lajtai, 1990).

2.3.1 Time-dependent behaviour in rock

Studies were conducted of time-dependent behaviour of clay based rock intended for use as underground repositories for waste and toxic chemicals, galleries and access tunnels by D'Elia (1991), Bernier et al (2004), Blumling et al (2007) and Bonini (2009), rock salt caverns by Brouard (1988), Hunsche (1988), Charpentier (1988) and Bérest et al (2005), hard solid rock in compression by Bieniawski (1967c; 1970), Kovács (1971), Drescher (2002), Drescher and Handley (2003), Li et al (2010) and Zhao et al (2011), granular material by Wang (2011) and rock masses in slopes for open pit operations by Mercer (2006). Brittle materials are known to show the effect of delayed fracture or static fatigue, which is defined as "a fracture, which occurs after the elapse of time under a constant stress" (Salganik et al, 1994). These cover diverse aspects of time-dependent behaviour in rock. An attempt is made here to

distinguish between creep behaviour in intact rock specimens and rheological behaviour in rock masses.

2.3.1.1 Creep behaviour in intact rock

Creep is defined as increasing strain while the stress is held constant (Rinne, 2008). Bieniawski (1970) states three basic time-dependent cases that can be investigated namely:

(i) gradually increasing compression at different but constant rates of deformation,
(ii) gradually increasing compression at varying rates of deformation and
(iii) constant load application for various time durations.

Creep is observed mainly in soft rocks like salt, coal and more or less in all other rocks. However all types of hard rock also exhibit creep characteristics with long enough time intervals (Critescu and Hunsche, 1998). Creep consists of three stages according to Yu (1998) "... the first stage is instantaneous elastic strain when a constant load is applied. If the load is sustained longer or the stress level increases, then primary (transient) creep or attenuating creep occurs. At high stress, secondary creep or steady state creep occurs. If the applied stress approaches or passes the yield limit or the material strength, the strain will increase rapidly and a tertiary creep or accelerating creep will appear and lead to eventual failure of the specimen." The tertiary stage always terminates in fracture and establishes the link with the phenomenon of time-dependent failure (Wawersik, 1972). Figure 2-11 shows the stages of creep in rock.

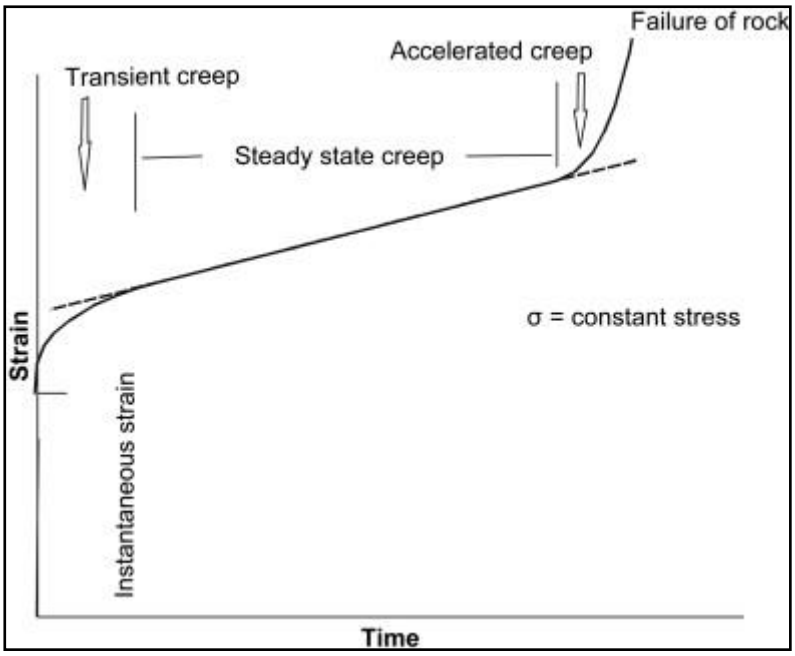


Figure 2-11: Creep curve showing different stages of deformation of rocks (Dubey and Gairola, 2008)

Drescher and Handley (2003) also observed the same creep stages when they carried out uniaxial compression creep tests on Ventersdorp lava and Elsburg Quartzite. They used the CSIR creep testing machine schematically illustrated in Figure 2-12.

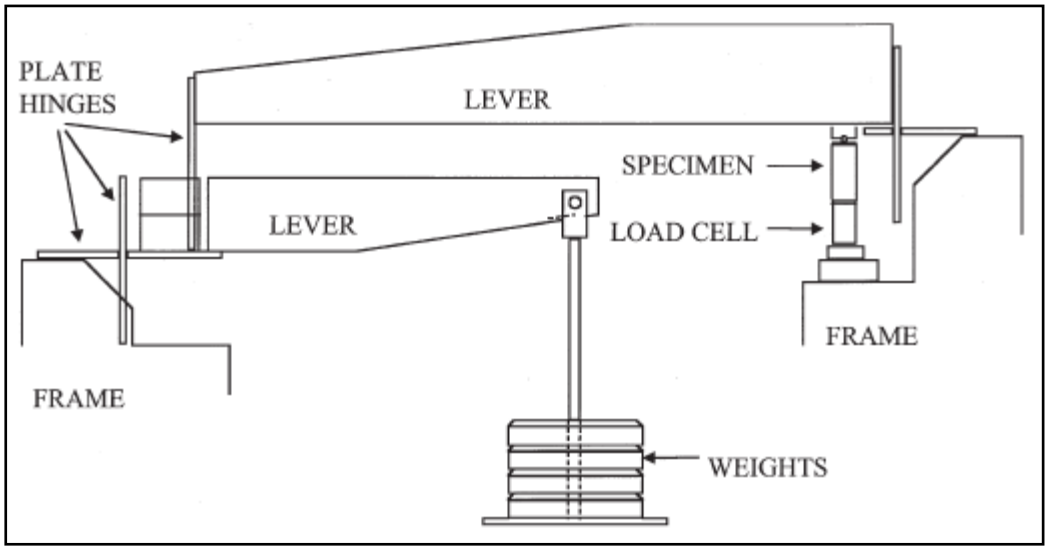


Figure 2-12: Principle of operation of the CSIR creep testing machine (Drescher and Handley, 2003)

Zhao et al (2011) carried out creep tests on red sandstone under uniaxial compression and tension. They observed that under low stress levels the creep

curve of sandstone consisted of decay and steady state creep while the accelerated creep stage typical of brittle fracturing was observed under high stress levels.

Long term creep tests done by servo-controlled testing machines have been found to be expensive and prone to loading history effects (Li and Xia, 1999). A creep test on potash salt rocks from Saskatchewan lasted from 2 to 8 months at a given load, with most tests conducted over a 4-month period (Duncan and Lajtai, 1993). Watson et al (2009) conducted creep tests on an anorthosite rock specimen with the Wits MTS machine using triaxial loading with an axial loading of 72 MPa and a confining stress of 1 MPa and the test lasted 3 hours. This explains the scarcity of research data from creep tests especially on BC rock types.

Kranz (1976) investigated crack growth in loaded granite using an SEM (Scanning Electron Microscope) and concluded that new cracks developed continuously under constant load. Schimdtke and Lajtai (1985) observed time-to-fracture for granite and anorthosite rock types through load-hold tests, with the result that stresses as low as 50% of the short-term strength (standard laboratory determinations) almost certainly caused time-dependent stress corrosion cracking in brittle rocks severe enough to cause delayed failure. Fabre and Pellet (2006) conducted strain creep tests on clayey Tournemire argillite rock in France. Strain or deformation characteristics were plotted against time, showing a linear behaviour with time on all strain levels. These findings point towards the importance of including time-dependent behaviour in the design of excavations in rock.

Creep is primarily influenced by stress level, temperature, humidity and chemical action or environment (Jaeger and Cook, 1979; Malan, 1998 and Bérest et al, 2005). Bérest et al (2005) used small dead weights (equivalent to a stress $\sigma \approx 0.02$ - 3 MPa) on top of rock salt in tests in an effort to keep “the applied stress as constant as possible”, and the tests lasted “several hundreds of days” (650 days for rock salt samples and 150 to 200 days for argillite samples). In these tests there was great concern regarding the influence of the local environment over time. They observed that “the behaviour of salt under small stress ($\sigma \approx 0.1$ MPa) exhibits the same general features as observed under larger stresses ($\sigma \approx 5$ - 20 MPa).

Secondary creep has been proved to lead to failure for stresses as much as 30% below the tested laboratory strengths, i.e. the long term strength of rock can be as low as 70% of the Unconfined Compressive Strength (UCS) (Ryder and Jager, 2002). Dubey and Gairola (2008) used uniaxial compression (UCS) tests to test the effects of anisotropy on rocksalt. They used constant stress loading levels of (30%, 40%, 50%, 60%, 70%, 72%, 75% and 80%) of the rocksalt's uniaxial compressive strength (failure stress or peak stress) to conduct creep tests. They also found out that at higher stress loading levels structural anisotropy was insignificant to the creep results.

2.3.1.2 Rheological characteristics of rock masses

Rheological behaviour in rock comprises of the effects of discontinuities like faults and joints together with the time-dependent deterioration of intact rock. Closure observed in the backs of stopes in deep mines can be easily attributed to rheological behaviour of the rock mass. In less competent rock, time-dependent processes have the benefit of dissipating strain energy in a non-violent fashion, whereas highly stressed mining areas in competent rock are prone to strata bursting due to little time-dependent behaviour (Brady and Brown, 1985).

Fakhimi and Fairhurst (1994) indicated that excavation "stand-up time" may run typically between "minutes to years" depending on the rock mass involved. They developed a mechanistic model for intact rock which incorporates time-dependent deterioration of the rock strength with time for prediction of stand-up time of rock structures. Excavations made in rock often assume "pseudo-stability" immediately after mining and may stand for years to several decades before failure occurs due to time-dependent deformation (Blumling et al, 2007 and Pellet et al, 2009). Figure 2-13 shows extension fracturing in an unsupported clay tunnel studied by Blumling et al (2007). They studied the extension of the excavation damage zone (EDZ) in a tunnel left unsupported after excavation.

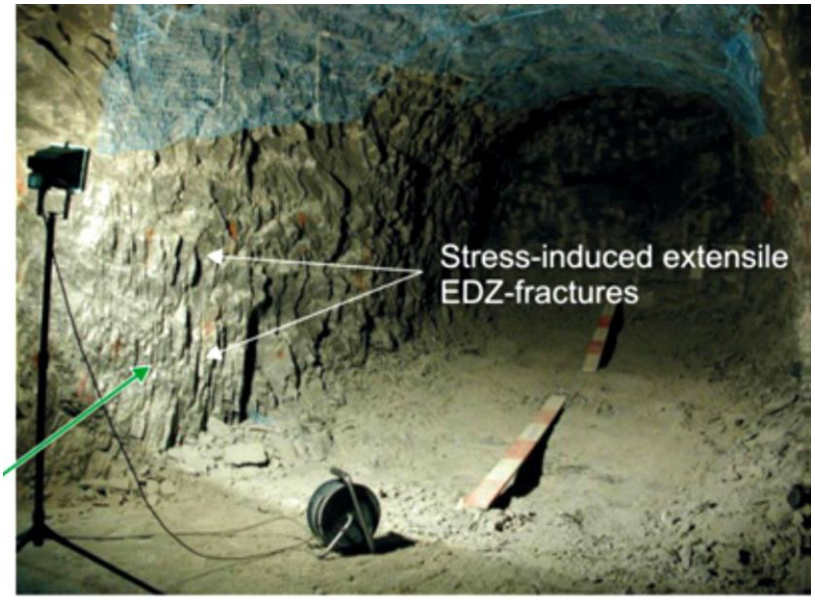


Figure 2-13: Extension fracturing in an unsupported clay tunnel (Blumling et al, 2007)

Similar conditions are extrapolated to exist in hard rock types with the passage of longer periods of time than is observed in the softer rock types investigated by Blumling et al (2007). The argument here is that if excavations, especially ones in soft rock, are left to stand for long enough periods of time, creep effects will lead to integrity loss and eventual failure due to strength decay. Malan et al (2007) investigated stope closure in an intermediate depth Merensky Reef stope 1400 m below surface. Despite the mine being in brittle hard rock they observed time-dependent creep behaviour as illustrated in Figures 2-14 and 2-15. The data was recorded by a closure station at a fixed location in a panel and, with time, the face moved away from the measurement point due to regular blasting. Interpretation is difficult since the curves include both changes in face position and the time-dependent deformation of the rock.

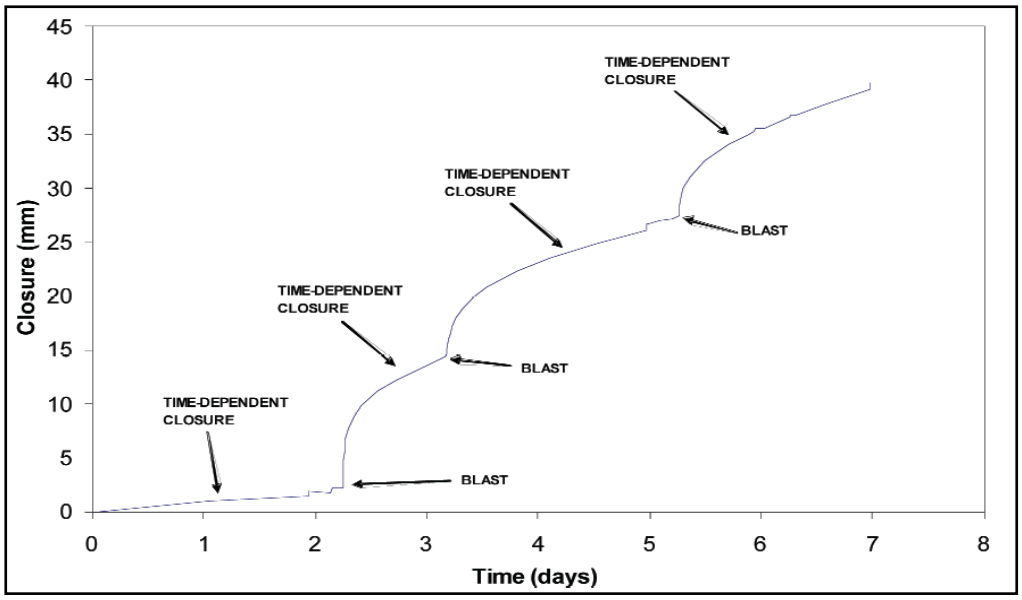


Figure 2-14: Time-dependent stope creep closure (Malan et al, 2007)

In between blasting times the steady time-dependent closure cycles were clearly repeated during the recordings. These observations illustrated the combination of time-dependent behaviour in the intact rock forming the rock mass and rheological behaviour of the rock mass.

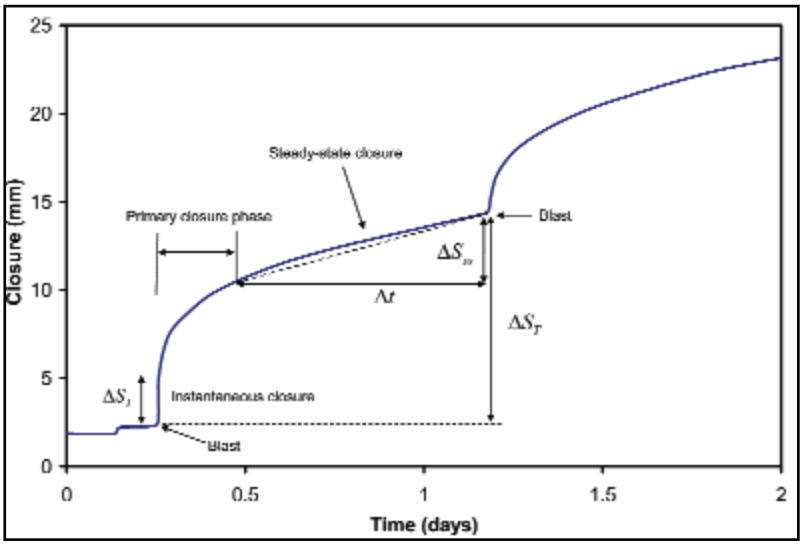


Figure 2-15: Continuous stope closure after blasting and the definition of closure terms, (Malan et al, 2007)

2.4 Summary and conclusions

The literature survey has shown the BC mining environment as consisting largely of narrow tabular, uniform and shallow dipping reefs occasionally disturbed by

geological structures such as faults, dykes and potholes. High k-ratios prevail in the BC with higher horizontal stresses than vertical stresses oriented along the strike of BC rock strata. In these stress conditions excavation walls are often under low compressive stresses and sometimes under tensile stresses. More importantly, the brittle nature of BC rock types, particularly anorthositic rock types, was revealed.

Several modes of failure and fracture stages in brittle rock were discussed, with a common fact that rock has inherent discontinuities (flaws) that extend and coalesce when the energy from applied stress exceeds the molecular bond between rock grains and surrounding matrix resulting in accelerated fracture propagation and failure. The extension strain criterion was reviewed as a methodology adopted in this research to investigate the onset of fracturing in rock. A study of brittle fracture propagation at low stress revealed the time-dependent nature of rock under stress. Creep activities were found by Jager and Ryder (2002) to be more pronounced close to the exposed excavation walls, where the deviatoric stresses are large, coupled with low confining stresses. Overall the review of literature illustrates that there have not been many long term or creep strength tests in rock around the world, as the methods are time consuming and therefore expensive. In South Africa, there have been very few such tests carried out, the work by Drescher (2002) and Kovács (1971) being notable exceptions.

Laboratory rock strength test methods were reviewed, with the UCS, normal and time-dependent BIT strength tests being adopted for this research. The analysis of volumetric strain to establish the long term strength of rock, used by Bieniawski (1967; 1969; 1970), was adopted in this research with UCS tests. The long term compressive strength of rock has been found from the current review to range between 60% and 80% of the UCS of the rock type. Fracture propagation in rock was shown to lead to deterioration of excavation walls with potential damage to life of mine excavations. Fracture propagation in norite rock types has been shown to initiate at 35% of the peak compressive load and 94% of the peak tensile load. A background is thus set for the investigation of deformational characteristics of several BC rock types.

CHAPTER 3

STRESS AND STRAIN ANALYSIS

3.1 Introduction

The Bushveld Complex (BC) mining environment, in-situ stress data, laboratory strength test methods and deformational characteristics of rock under different stress conditions were reviewed in the previous chapter. A brief description of the mining methods used to exploit the narrow tabular PGM-rich reefs of the BC and the analysis of stress and strain around typical excavations follows. The objective of this chapter is to illustrate stress and extension strain scenarios that might be conducive to the initiation and propagation of fractures around openings, using generic models based on the characteristic BC mining geometry. Implications for the behaviour of BC rock types hosting life of mine excavations under tensile stress or low compressive stress (i.e., stress conditions that are prevalent in the BC mining environment) are discussed here.

3.1.1 Mining methods used in the Bushveld Complex

Depending on the depth of operation and geology, conventional and/or mechanised methods are utilised to exploit narrow reef ores of the Bushveld Complex. Conventional mining methods commonly, but not exclusively, use track bound equipment, while trackless equipment is largely, but not exclusively utilised in mechanised mining operations. With reference to Chapter 2, where the BC geology was discussed, the reefs from which PGM ores are mined are largely of uniform width and constant gradient, disturbed occasionally by the intersection of dykes and by reef rolls caused by the intersection of potholes.

3.1.1.1 Conventional mining methods

Conventional mining methods are commonly used to extract narrow tabular reefs like the Merensky, UG2 and several gold bearing reefs of the Witwatersrand basin. The reef is extracted from uniform width stopes using handheld jack hammers to drill

charge holes, and panel faces are subsequently blasted. Broken ore is transported out of the stopes by scraper winches acting down dip at the stope face, and then along strike oriented gullies in the reef footwall (FW) waste. Complete reef extraction is not possible since in-stope and regional stability pillars are left in-situ to maintain the excavations open and reduce the size of exposed hanging wall (HW) span, thus decreasing the height of the tensile zone. A typical conventional breast mining layout described by Egerton (2004) is shown in Figure 3-1. Up-dip and down-dip mining are variations of the conventional mining method with different mining advance directions.

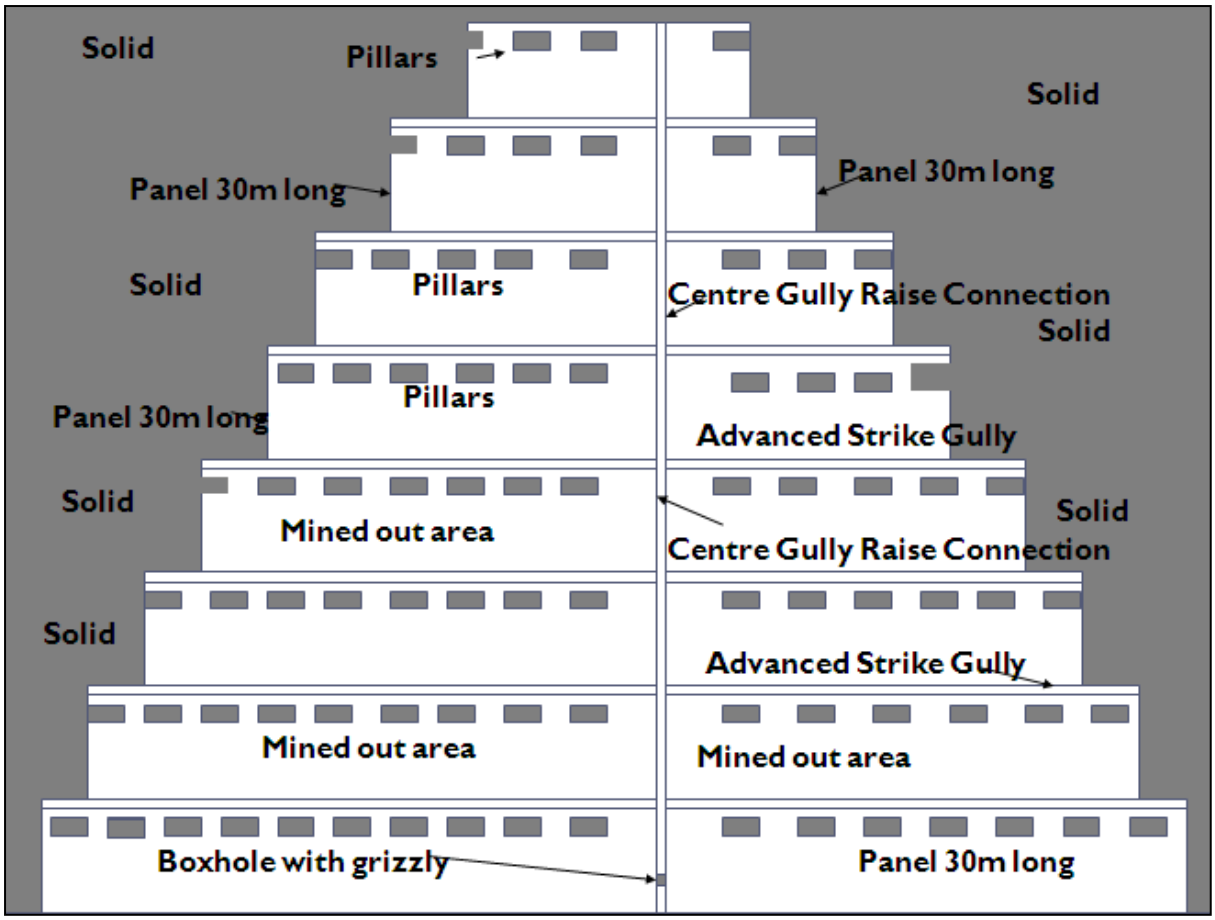


Figure 3-1: Conventional breast mining layout in the UG2 reef (after Egerton, 2004)

Smith and Basson (2006) refer to the existence of potholes left in-situ as pillars in the Merensky reef mining stopes. Potholes may not be mined because they are often associated with heavy jointing in the rock mass, and the resultant footwall horizon is not amenable with ore cleaning operations using scraper winches. Pillars left in the

Merensky reef horizon may induce elevated stresses on the footwall excavations, including the UG2 mining stopes at deeper levels beneath the Merensky reef.

3.1.1.2 Mechanised mining methods

Room and pillar mining layouts are used to mine uniform shallow-dip, continuous reef at shallow depth using mechanised equipment. Most development is on reef with roadways and split holings made between pillars to afford access to machinery and equipment. The split holings also serve for ventilation purposes. Room and pillar mining methods have become equally popular in the Bushveld Complex mines as conventional mining methods, particularly at shallow mining depth. Hybrid room and pillar mining methods have also been tried in the BC platinum mines. A typical room and pillar operation is shown in Figure 3-2.

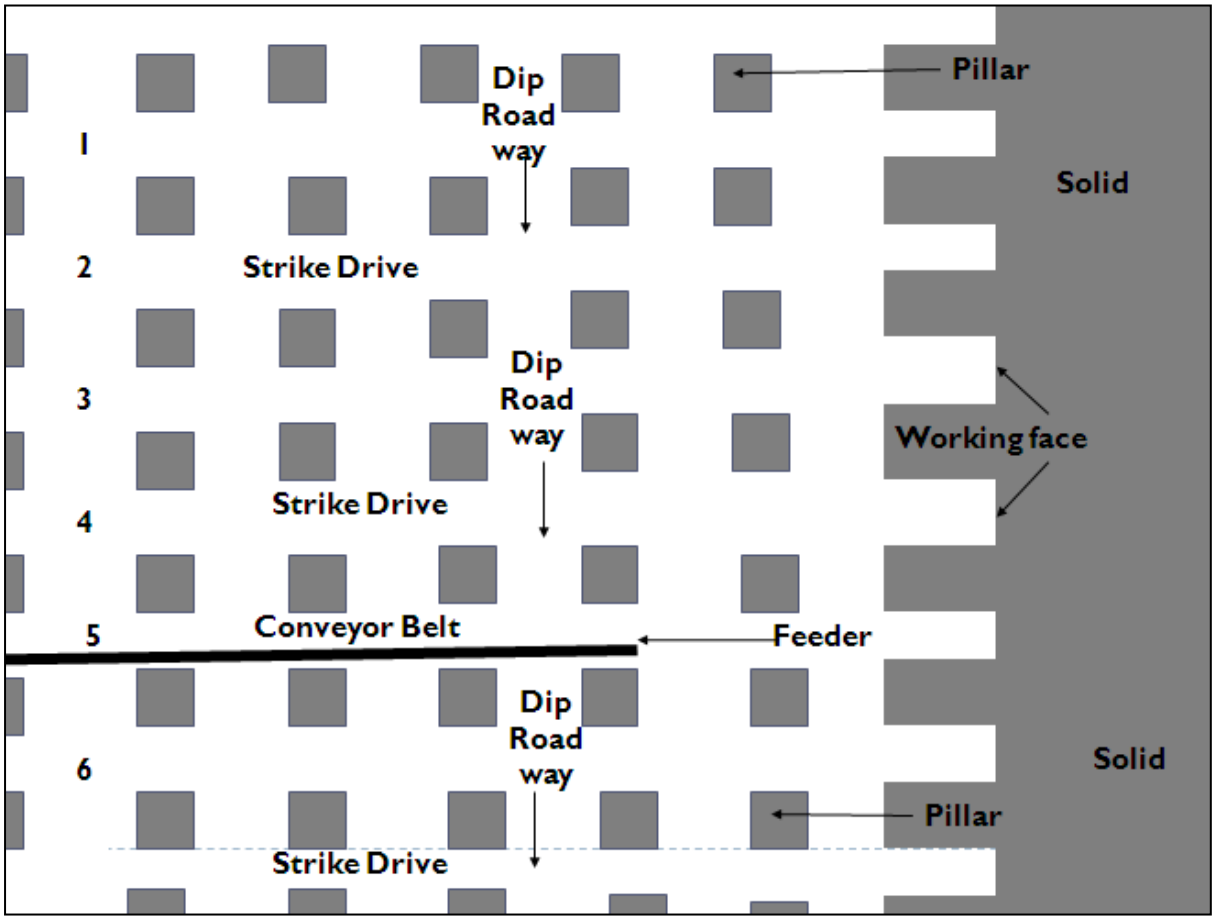


Figure 3-2: A typical room and pillar mining layout (after Egerton, 2004)

Roof bolters install mechanical bolts and/ or resin bolts in the hanging wall in the rooms. There are several variations to the mechanised room and pillar mining

method, as described by Egerton (2004). Pillars in this mining set up are often square and cut to remain stable within their elastic limit. The geometry common to conventional and mechanised mining methods is the creation of shallow dipping uniform height excavations with pillars left in-situ. The life of mine access excavations and pillars mined in these mining methods have been observed to be subject to time-dependent deformations.

3.2 Characteristic geometries of Bushveld Complex mine excavations

Theoretical mining geometries based on typical BC mine excavations were used in this research and are briefly discussed here. Generic models were used to analyse stress and extension strain using a 2-D (2-Dimensional) commercial software package (Phase2) for the purposes of illustrating characteristic stress distributions and illustrate susceptibility to the initiation of fractures around modelled excavations.

3.2.1 Geometries of an in-stope pillar

2-D analyses were used as they suffice to indicate the stress and strain distributions expected around the excavation assuming uniformity and continuity in the out of plane direction with the resulting model shown in Figure 3-3.

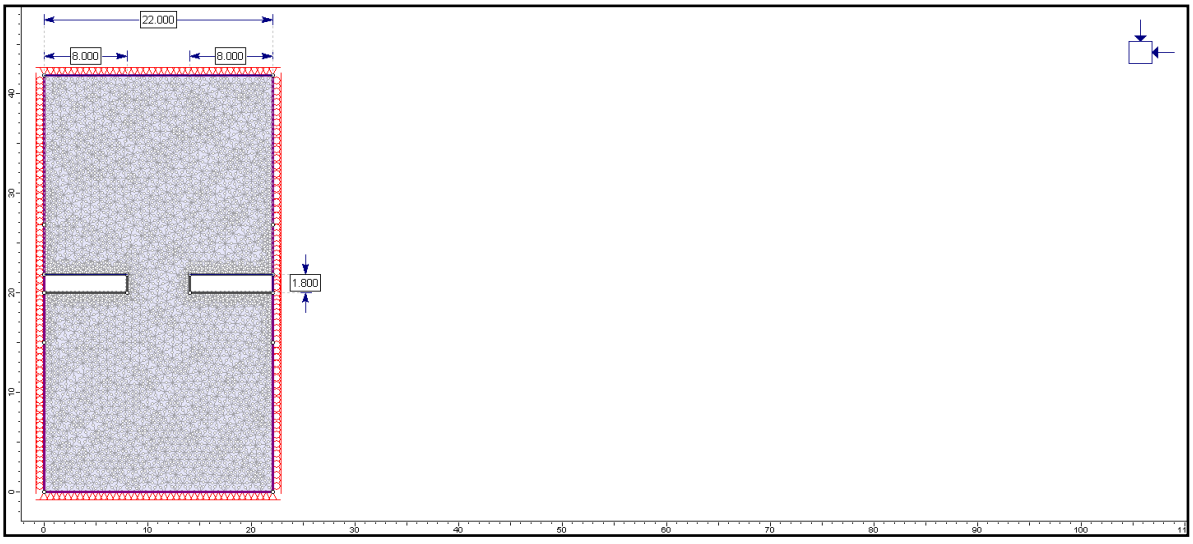


Figure 3-3: Modelling geometry of a 6 m wide by 1.8 m high in-stope pillar

In conventional mining methods, in-stope strike pillars are designed to crush on cutting and to operate in their post peak state utilising their residual strength. The

criterion based on a width to height ratio not exceeding 3 and a Factor of Safety (FOS) < 1. Width to height ratios are typically 2 – 2.5 and in stoping widths of 1.2 - 1.75 m, typical crush pillars are 2.4 – 3.5 m wide. These pillars can be dip or strike oriented. Panel spans here are determined by the height of the tensile zone, mining depth or the use of the elastic beam theory to determine stable spans between pillars. In room and pillar mining elastic pillars loaded below their peak strength with a Factor of Safety (FOS) > 1.5 are cut in a uniform array, often based on square shaped pillars. The width to height ratio for these pillars must be greater than 5. The aim is to achieve profitable extraction ratios from several combinations of pillar and room sizes complying with the requirements of the pillar geometry and strength criterion applied. Characteristic pillar sizes in room and pillar mining are 5 -10 m with 6 – 12 m rooms.

3.2.2 Geometries of a mining stope

Panel spans are typically 15 – 40 m long where conventional mining methods are used whilst 6 – 12 m is the room span typically mined in room and pillar mining methods, with pillars cut on a systematic array. The geometry of a 29 m long panel with a 1.8 m stope width is depicted in Figure 3-4.

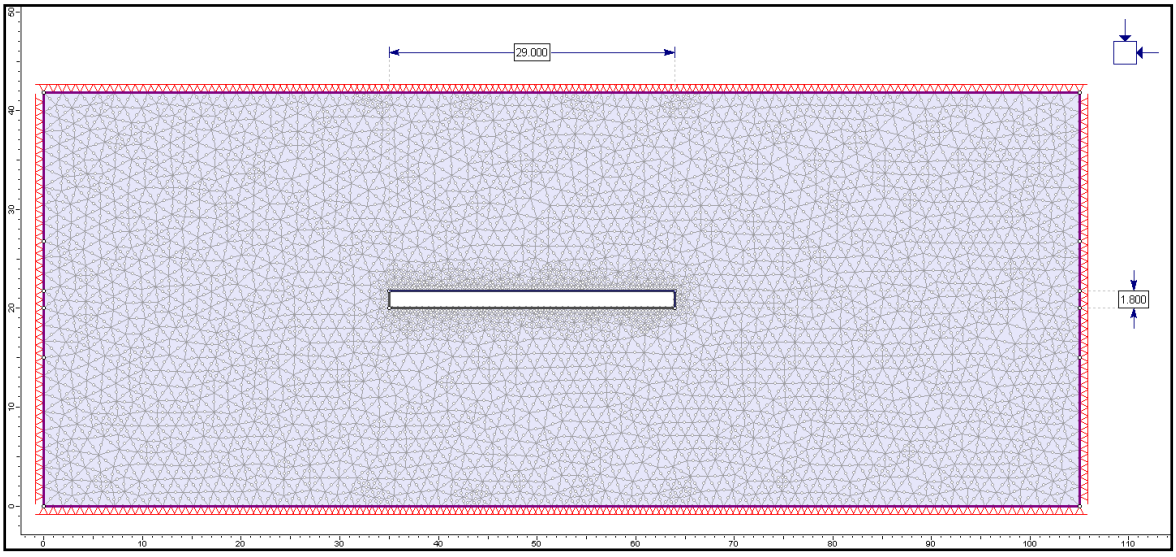


Figure 3-4: Modelling geometries of a 29 m by 1.8 m high stope

3.2.3 Geometries of an incline shaft

Roadways and declines are typically 3 – 8 m wide and 1.8 – 4 m high. A 7 m wide by 4 m high shallow dipping incline is represented in Figure 3-5.

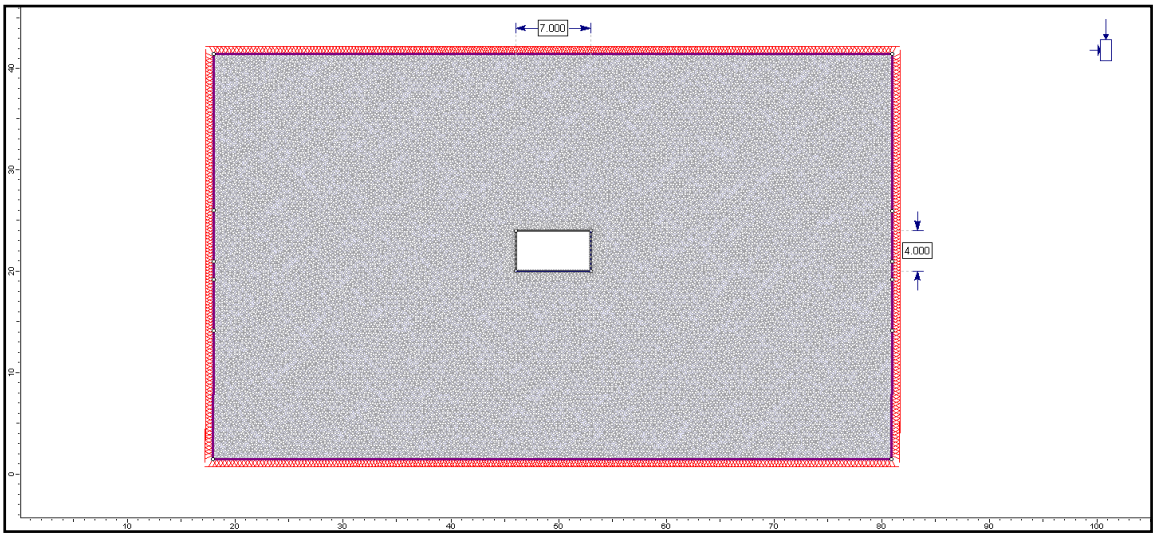


Figure 3-5: Modelling geometry of a 7 m wide by 4 m high incline shaft

Continuum and elastic assumptions were made, and analyses were carried out using the assumption of plane strain conditions where the out of plane strain is assumed to be zero or very negligible. A uniform geometry of the models is assumed to continue infinitely in the out of plane direction. The dimensions of the excavations represented in the models are indicated in Figures 3-3 to 3-5. Note that the models discussed here represent typical excavations mined in BC mines.

3.3 Numerical and analytical methods

Direct methods of investigating in-situ behaviour of rock are not always available or practical and as a result researchers turn to numerical methods and laboratory tests on rock to determine trends and behaviour of rock masses under different stress conditions. The use of numerical modelling to analyse the time-dependent behaviour of rock under different loading conditions in excavations made in soft and hard rock is reviewed here.

3.3.1 Review of numerical methods in mining

Numerical modelling can be used to investigate the behaviour of rock around excavations otherwise difficult to measure in-situ to put observed and laboratory test results into the practical context of typical mine excavations. Time-dependent numerical modelling for underground excavations has been performed by Boidy et al (2002), Bonini et al (2009) and Pellet et al (2009). Boidy et al *(*2002) used Lemaitre's visco-plastic model to simulate the time-dependent behaviour of a tunnel in Switzerland. Confirmation of propagation of the damage zone with the progression of time through numerical analysis was illustrated by the work done by Bonini et al (2009). They proved that clay shales exhibited time-dependent behaviour both at laboratory and tunnel level, Figure 3-6.

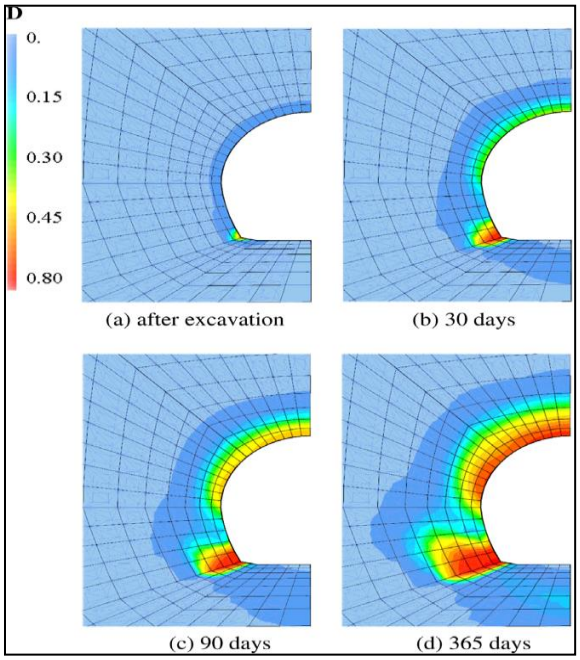


Figure 3-6: Extension of damaged zone for different time progressions in a section located 6 m behind the tunnel face (Bonini et al, 2009)

In conclusion of their studies on clay shale, Bonini et al (2009) found that parameters determined from laboratory tests could not always be directly used for appropriate prediction of tunnel behaviour. This was mainly because of the complications introduced by water content, swelling or squeezing, fracturing and jointing, effects

which might not be present in a laboratory size specimen. Pellet et al (2009) used the Lemaitre visco-elastic damageable model to calculate strains with respect to time as well as time to failure. They confirmed the extension of the damage zone inwards from the excavation walls with the passage of time. They showed that it is possible to assess the time-dependent changes in the extension of the Excavation Damage Zone (EDZ) induced in front of the work face.

In the current research, 2-D numerical analysis was used to determine stress and strain distributions around typical BC mine excavations and to illustrate zones around the excavations where the extension strains occur.

3.3.2 Stress-strain analysis objectives

Anderson (1951) indicated that establishing in-situ stress conditions in underground mining is difficult. According to Anderson's concept in ideal 'standard state' conditions the lateral stress state should equal the vertical stress as depth increases. It is also difficult and expensive to establish induced stress conditions by direct measurement. The behaviour of rock under stress is therefore determined through monitoring other physical quantities like strain, or through numerical modelling of excavations (Pollard et al, 2005). Elastic plane strain, 2-Dimensional numerical modelling was used to investigate the distribution of stress and strain around typical Bushveld Complex mine excavations. The objectives of the numerical analysis are:

- To illustrate the distribution of elastic stress (compressive major σ_1 and minor σ_3 principal stresses) around three typical Bushveld Complex excavations;
- To illustrate characteristic distributions of extension strains around typical Bushveld Complex mine excavations, and to compare their magnitudes with typical strain values obtained at tensile failure in laboratory indirect tensile strength tests, and;
- To interpret the results from the numerical analyses in relation to the observed underground behaviour of the rock surrounding the excavations.

The geological characterisation and description of typical mining geometries given in preceding sections was used as a basis for the models used here.

3.3.3 Methodology for stress and extension strain analysis

Numerical analysis was achieved by:

- Investigating the distribution of stress (major principal stress, σ_1 and minor principal stress, σ_3) around the following excavation models (see also section 3.2);
  - A 6 m wide in-stope dip pillar in a 1.8 m high stope width, Figure 3-3;
  - A typical 29 m long stope in a 1.8 m high stope width, Figure 3-4 and
  - A 7 m x 4 m decline shaft, Figure 3-5.
- Illustrating the distribution of extension strain around the modeled excavations with emphasis on:
  - Depicting the characteristic magnitudes and orientations of extension strains in the excavation peripheries and at various locations around the excavations.
  - Depicting the zones around the model excavations where potential initiation of fractures might occur (i.e. zones of critical extension strain).
  - Comparing the calculated extension strain values with the strain values observed at tensile failure in the laboratory tests conducted on several BC rock types.
  - Drawing potential parallels between the modeling results and the observed failure behaviour in BC mine excavation wall rock and characteristic failure modes observed in compressive and indirect tensile strength tests.

Average properties of the several anorthositic rock types (reported in Chapter 4) were used to assign rock strength and deformational properties to the models.

3.4 Stress and extension strain analysis

Stress and extension strain were determined at different depths for two k-ratios: a k-ratio of 2, characteristic of the shallow BC mining environment (Stacey and Wesseloo, 2004), and a k-ratio of 1 representing theoretical hydrostatic loading conditions more typical of the deeper mines. The models were analysed for two depths of 500m and 1000m below surface. The overburden unit weight was taken as

29 kN/m^3, derived from the average density of several Bushveld Complex rock types determined in laboratory testing (see Chapter 4). The further aim of the analyses was to illustrate the locations of high stresses, and the extents of tensile zones and zones of extension strain around typical BC mine excavations that could promote fracture initiation, fracture propagation and spalling in anorthositic rock types.

3.4.1 Analysis of results - in-stope pillar model

Results of the computation of the major principal stress (σ_1), minor principal stress (σ_3) and extension strain around a typical in-stope pillar model are depicted in Figure 3-7 to Figure 3-12.

3.4.1.1 Major Principal Stress

The major principal stress distribution around an in-stope pillar model is depicted in Figures 3-7 to 3-10 for two different loading conditions and two different depths below surface.

σ_1 contours: Depth = 500 m and k = 1

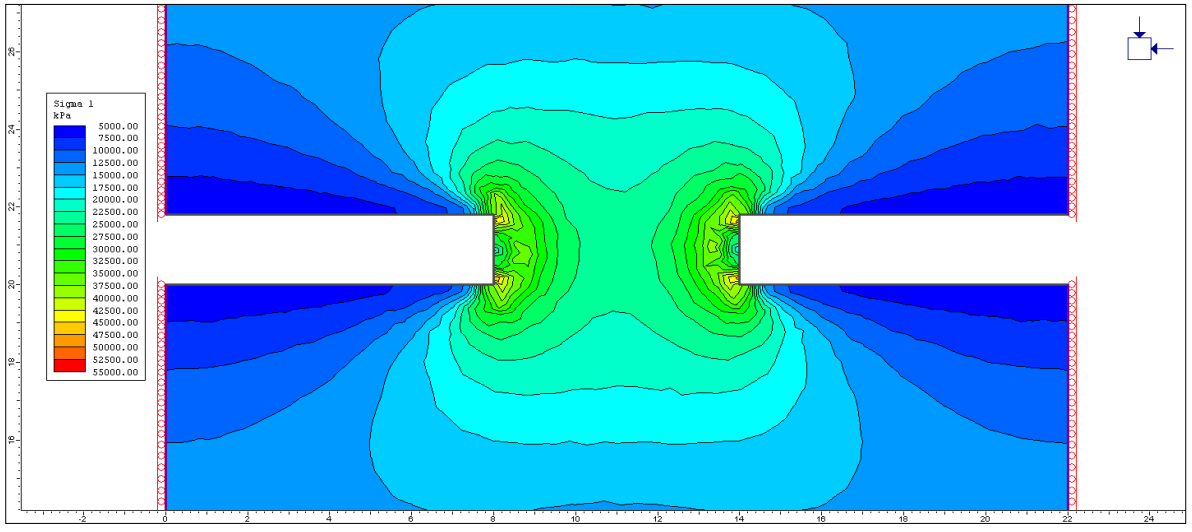


Figure 3-7: Distribution of Major Principal Stress (σ_1) at a depth of 500m with a k-ratio = 1

σ_1 contours: Depth = 500 m and k = 2

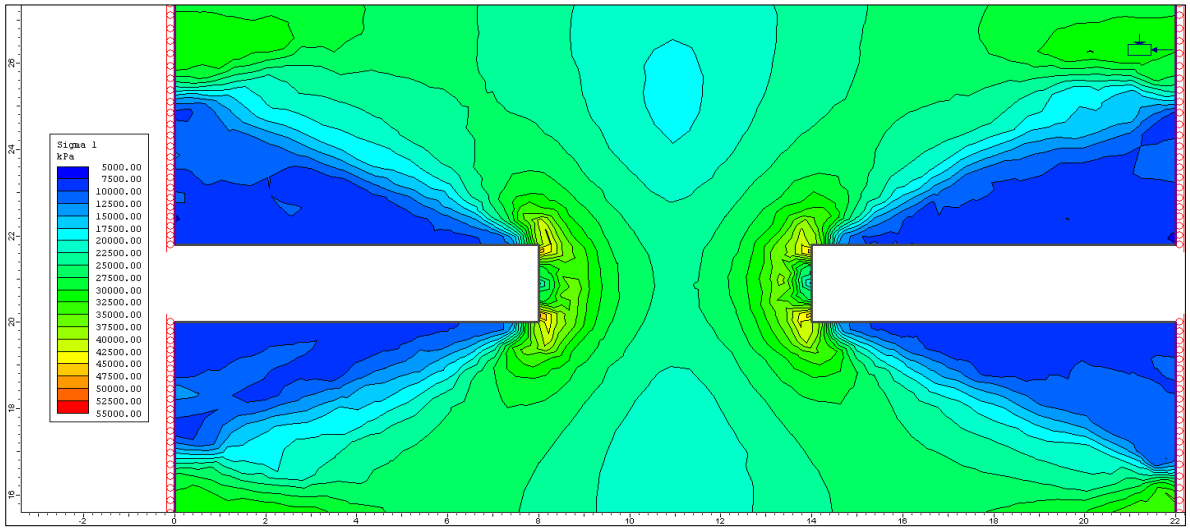


Figure 3-8: Distribution of Major Principal Stress (σ_1) at a depth of 500m with a k-ratio = 2

σ_1 contours: Depth = 1000 m and k = 1

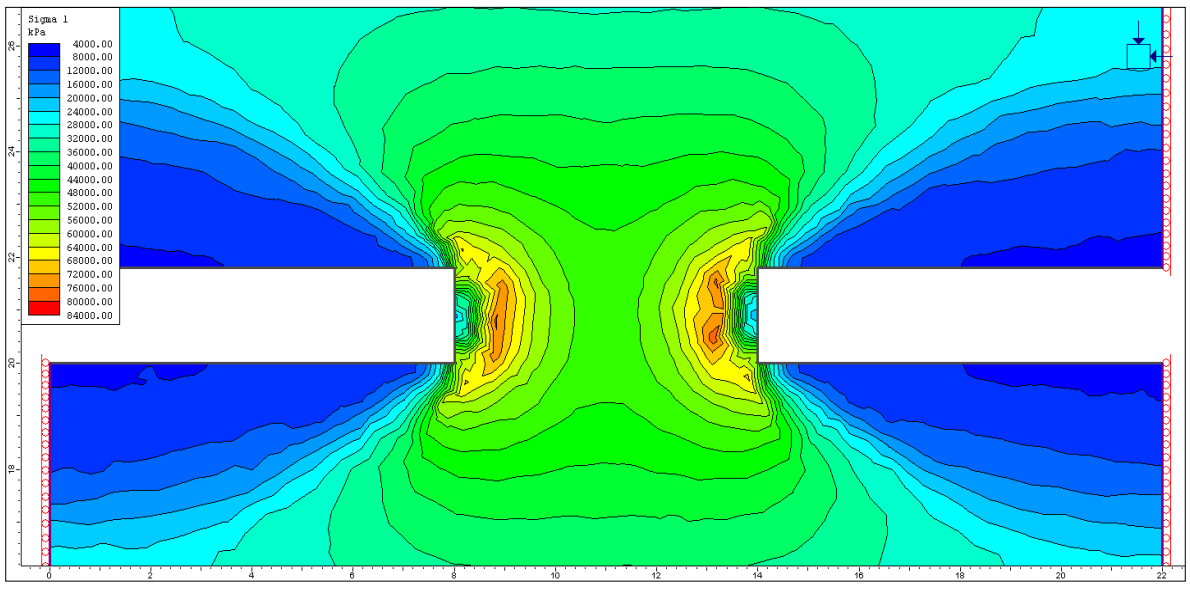


Figure 3-9: Distribution of Major Principal Stress (σ_1) at a depth of 1000m with a k-ratio = 1

σ_1 contours: Depth = 1000 m and k = 2

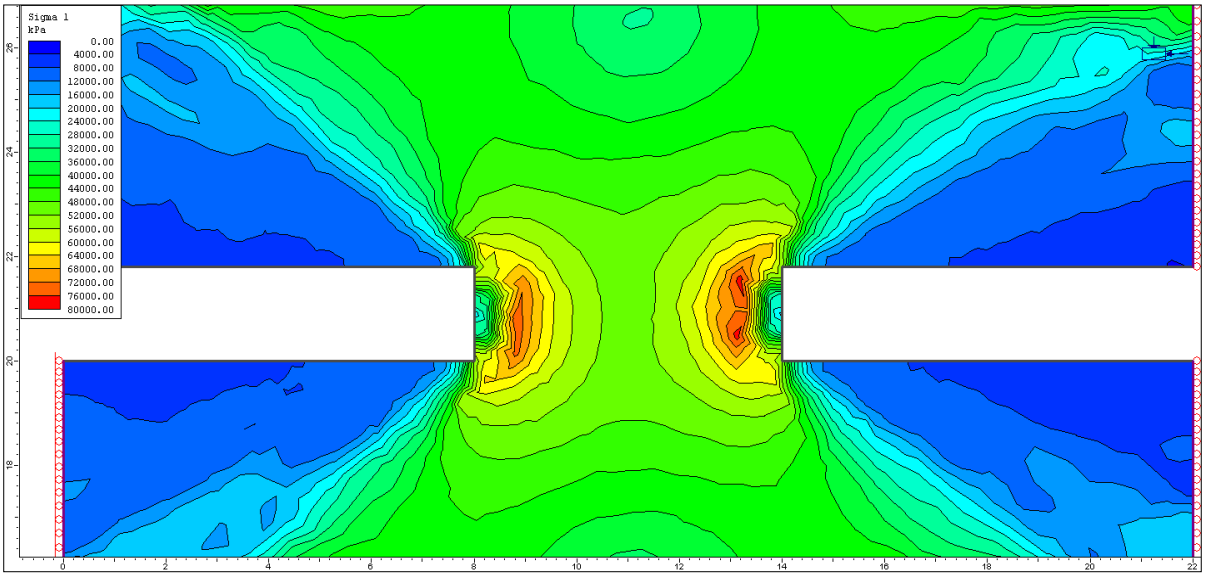


Figure 3-10: Distribution of Major Principal Stress (σ_1) at a depth of 1000m with a k-ratio = 2

The results of the analysis of major principal stress show that at a depth of 500 m for both k-ratios 1 and 2 low compressive stresses (5 – 7.5 MPa) are observed in the HW and parts of the pillar sidewall (blue to light blue in the models). At the pillar apexes stress concentrations, illustrated by elevated stresses (25 – 35 MPa), are observed. At a simulated depth of 1000 m and k-ratio = 2, lower major principal stress values (0 – 4 MPa) are observed in the hanging wall of the excavation. At the pillar cores intermediate stress conditions (27.5 – 44 MPa) are observed. The orientation of the major principal stress contours in all cases is parallel to the excavation walls (hanging, foot and sidewalls – HW, FW and SW). The major principal compressive stress values observed in the immediate walls of the excavation are up to 10 times lower than the compressive strengths of the BC rock types. The compressive strength of the BC rock types are discussed in Chapter 4.

3.4.1.2 Minor Principal Stress

The minor principal stress (σ_3) was computed and its distribution around the modelled excavation is presented in Figures 3-11 to 3-14.

σ_3 contours: Depth = 500m and k = 1

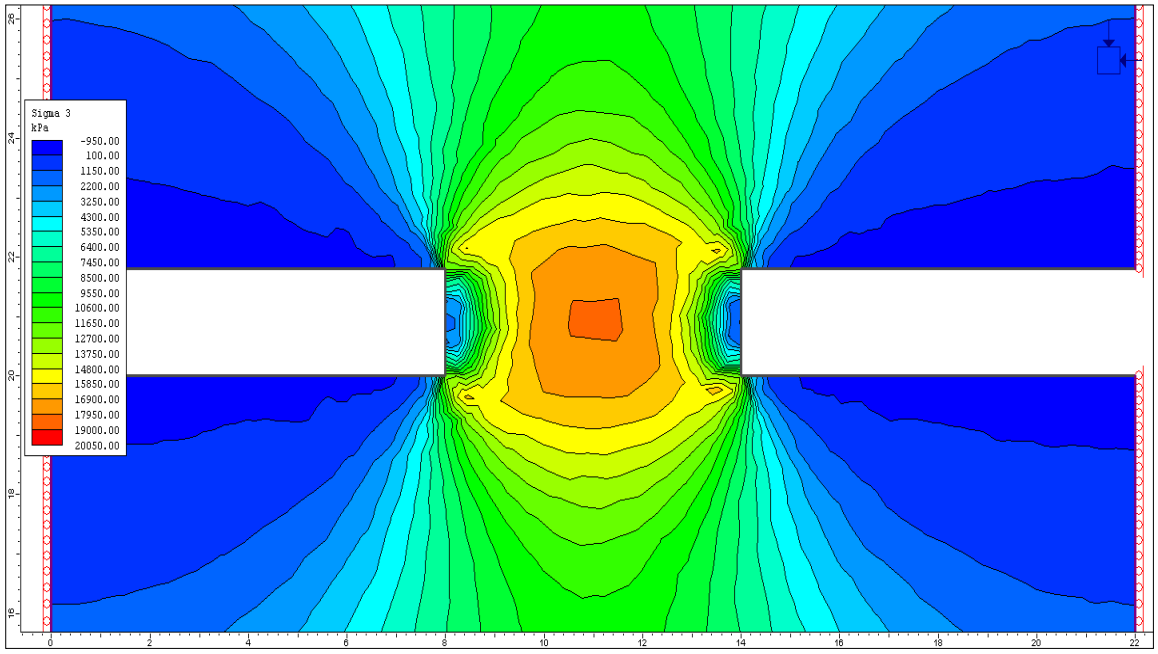


Figure 3-11: Distribution of Minor Principal Stress (σ_3) at a depth of 500m with a k-ratio = 1

σ_3 contours: Depth = 500m and k = 2

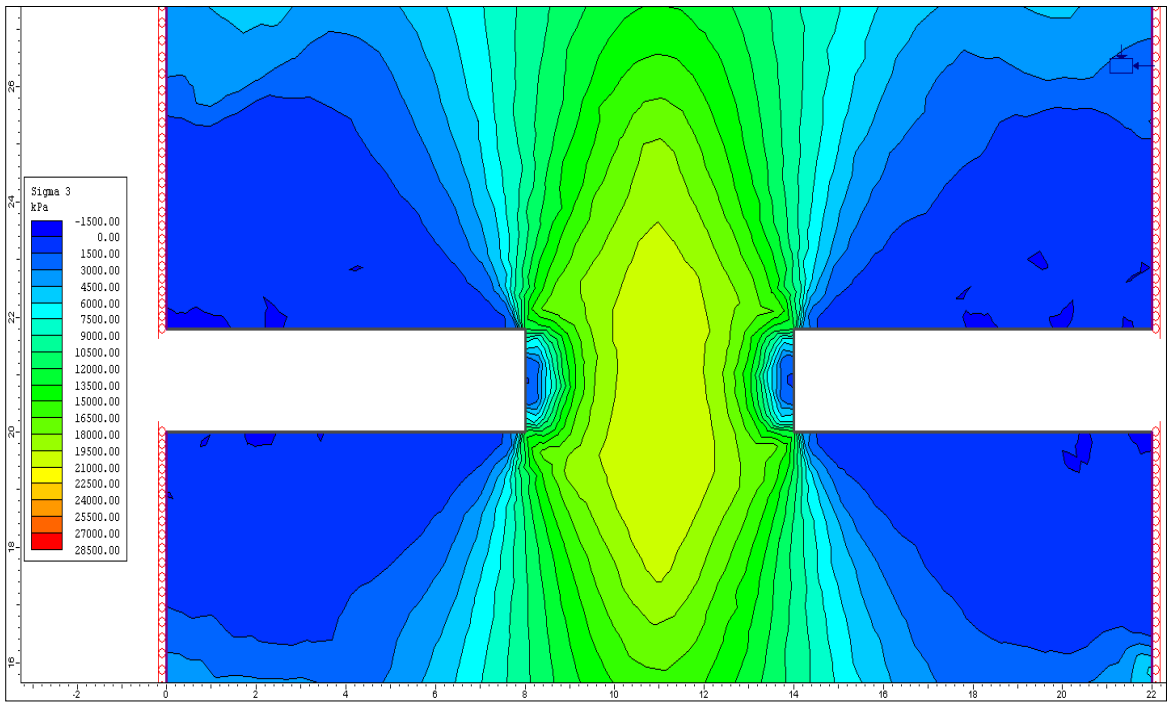


Figure 3-12: Distribution of Minor Principal Stress (σ_3) at a depth of 500m with a k-ratio = 2

σ_3 contours: Depth = 1000m and k = 1

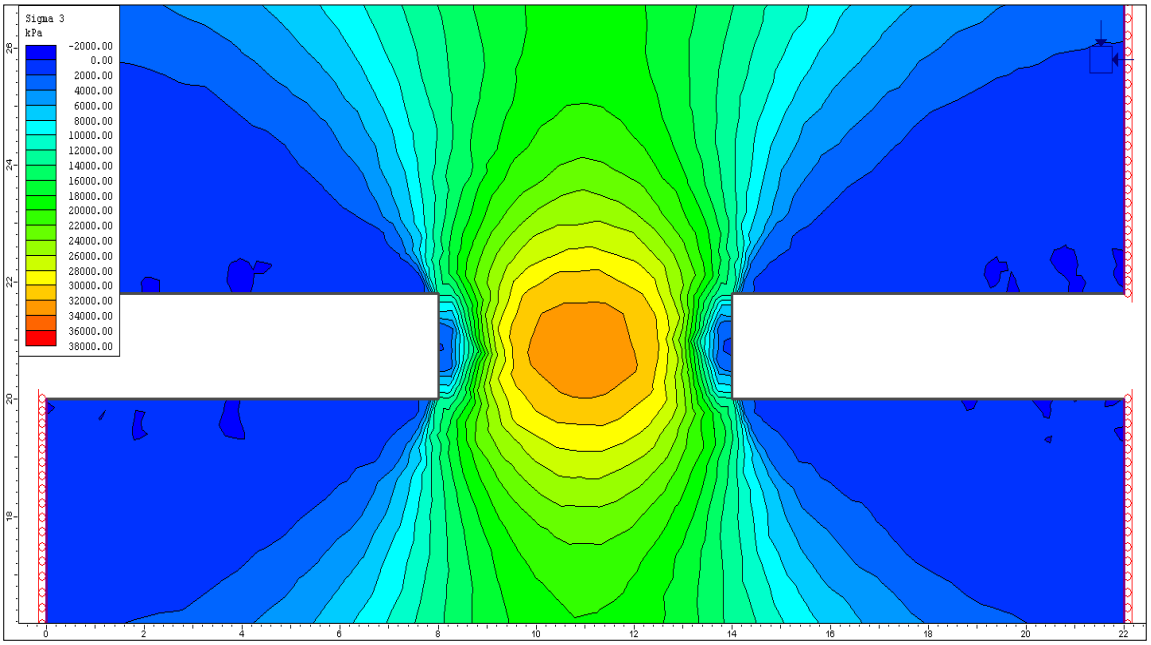


Figure 3-13: Distribution of Minor Principal Stress (σ_3) at a depth of 1000m with a k-ratio = 1

σ_3 contours: Depth = 1000m and k = 2

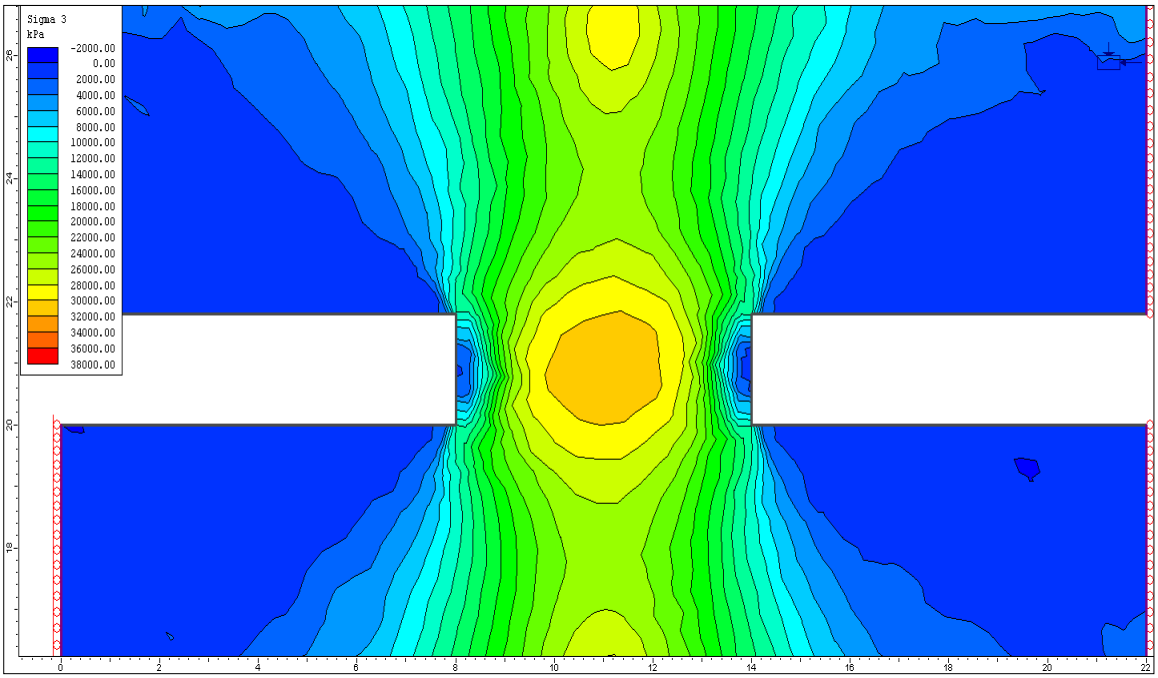


Figure 3-14: Distribution of Minor Principal Stress (σ_3) at a depth of 1000m with a k-ratio = 2

Very low stress (0 to 2 MPa) and negative minor principal stress (0 to -2 MPa) values are observed in the immediate excavation walls (light blue to dark blue), implying very low confinement to possibly tensile excavation wall conditions. The pillar core is under moderate stress (23 – 27 MPa) implying moderate confining stress. Minor principal stress depicted in Figure 3-12 ranges from (-1.5 to 3 MPa), much lower in magnitude than the tensile strengths of Bushveld Complex rock types which have an average tensile strength of 7.2 MPa. The orientation of minor principal stress contours is parallel to the excavation wall surfaces in the HW and pillar SW and resembles the orientations of fracture planes observed in the wall rock.

3.4.1.3 Extension strains

The evaluation of extension strains that follows was carried out to allow application of the extension strain criterion proposed by Stacey (1981), see also section 2.2.3.2. The strain equation

$$e_3 = \frac{1}{E} [\, \sigma_3 - \nu\, (\sigma_1 + \sigma_2)]$$

was inserted into the user defined data analysis in the Phase2 programme to compute the distribution of minimum principal strain around the modelled excavations. Extension strains that exceed a critical extension strain value indicate the initiation of fracturing in rock. It is to be noted that the value of σ_2 used in the analyses results from the plane strain assumption, and thus the calculated extension strains are not completely correct. Nevertheless, they are adequate to indicate the approximate magnitudes of extension strain in the rock surrounding typical BC excavations. The distribution of extension strain around the pillar model is given in Figure 3-15 and Figure 3-18.

The extension strain values depicted in Figure 3-15 range from -1.6 x 10^{-3} to 2.45 x 10^{-3} (blue to dark green) starting from the excavation wall surface to the interior core of the pillar. In all four cases, the immediate peripheries of the excavations are shown to experience negative extension strains, which indicate the potential initiation of fracture in the rock.

Extension strain contours: Depth = 500m and k = 1

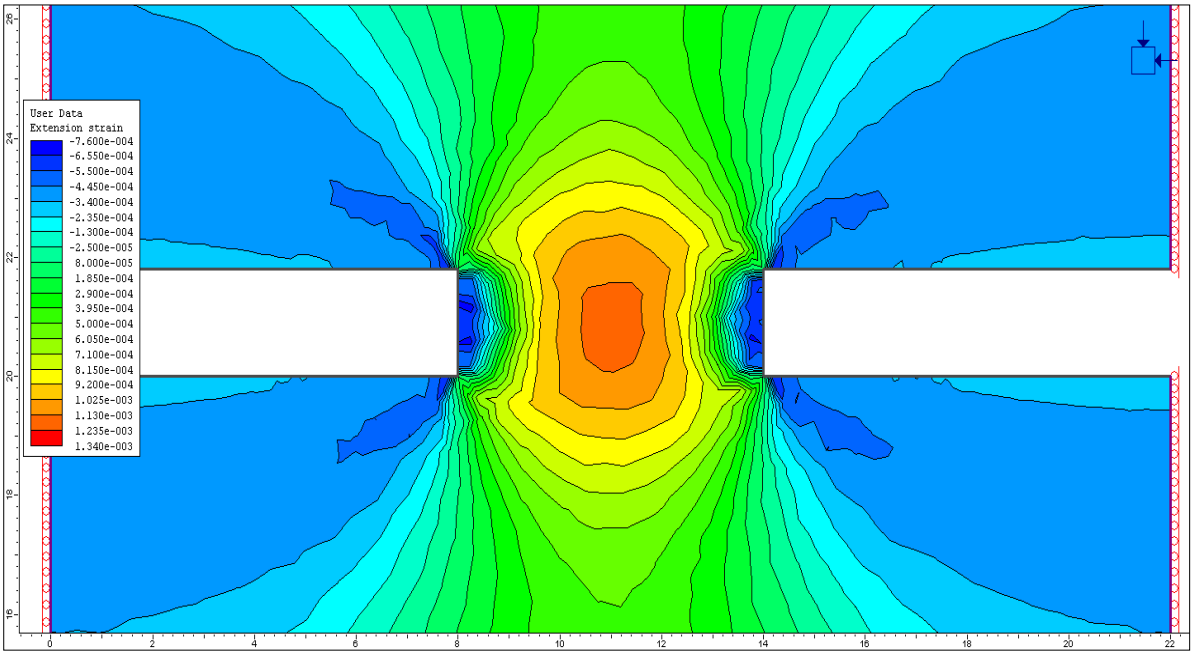


Figure 3-15: Distribution of extension strain at a depth of 500m with a k-ratio = 1

Extension strain contours: Depth = 500m and k = 2

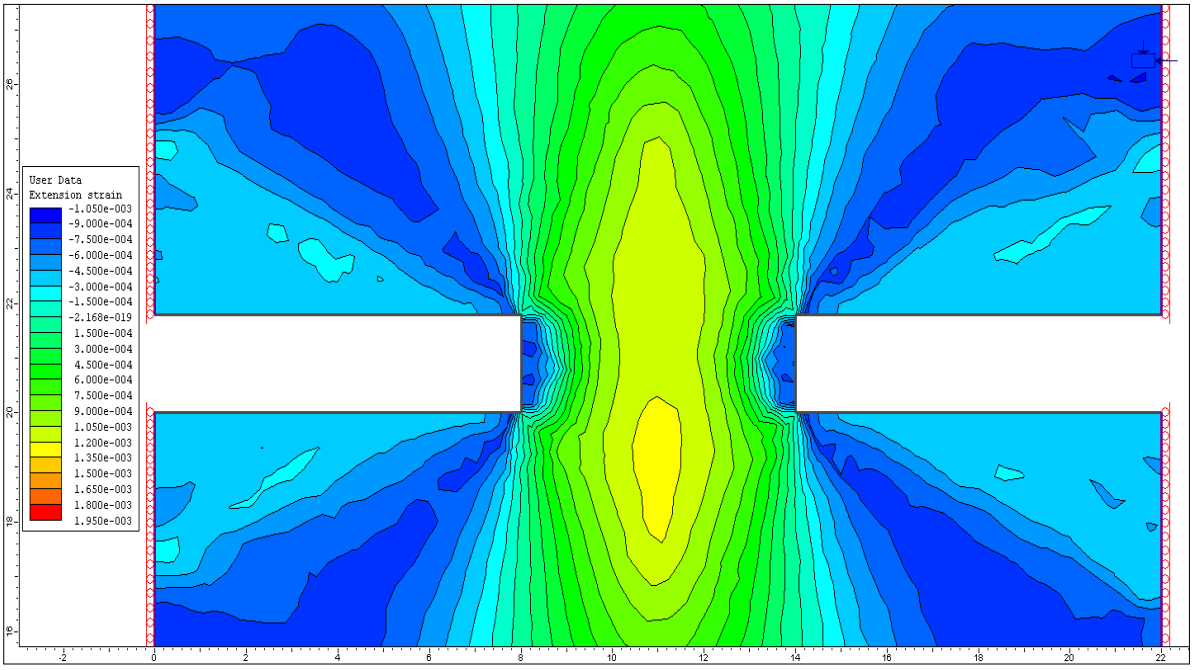


Figure 3-16: Distribution of extension strain at a depth of 500m with a k-ratio = 2

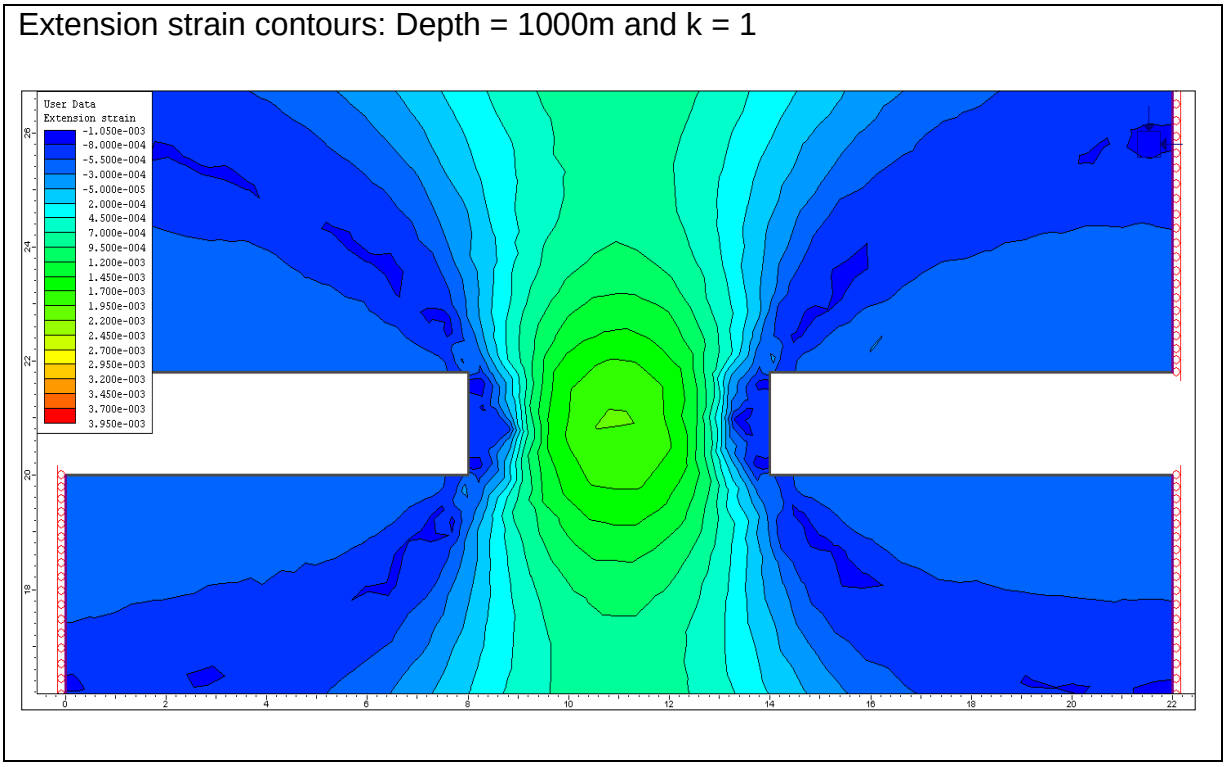


Figure 3-17: Distribution of extension strain at a depth of 1000m with a k-ratio = 1

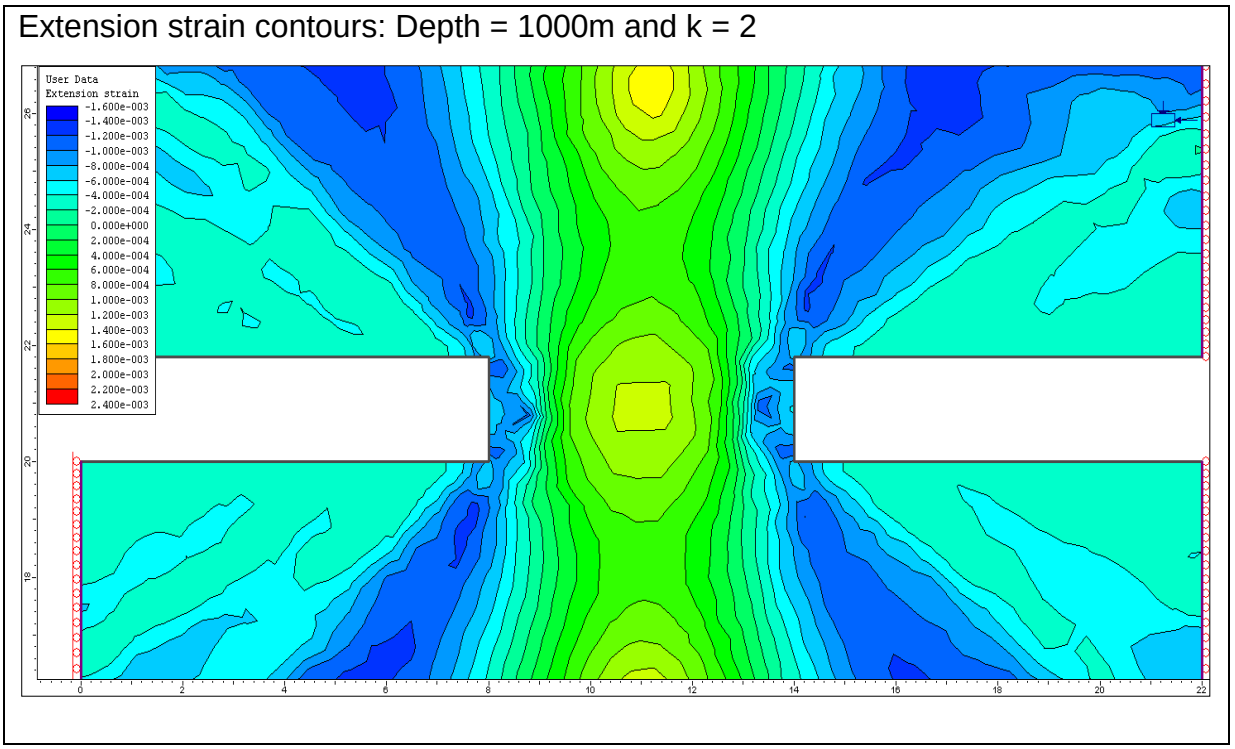


Figure 3-18: Distribution of extension strain at a depth of 1000m with a k-ratio = 2

An annotated picture of extension strain modelling is given in Figure 3-19 depicting the zone of influence of critical extension strain with similar values to laboratory tensile strains at failure.

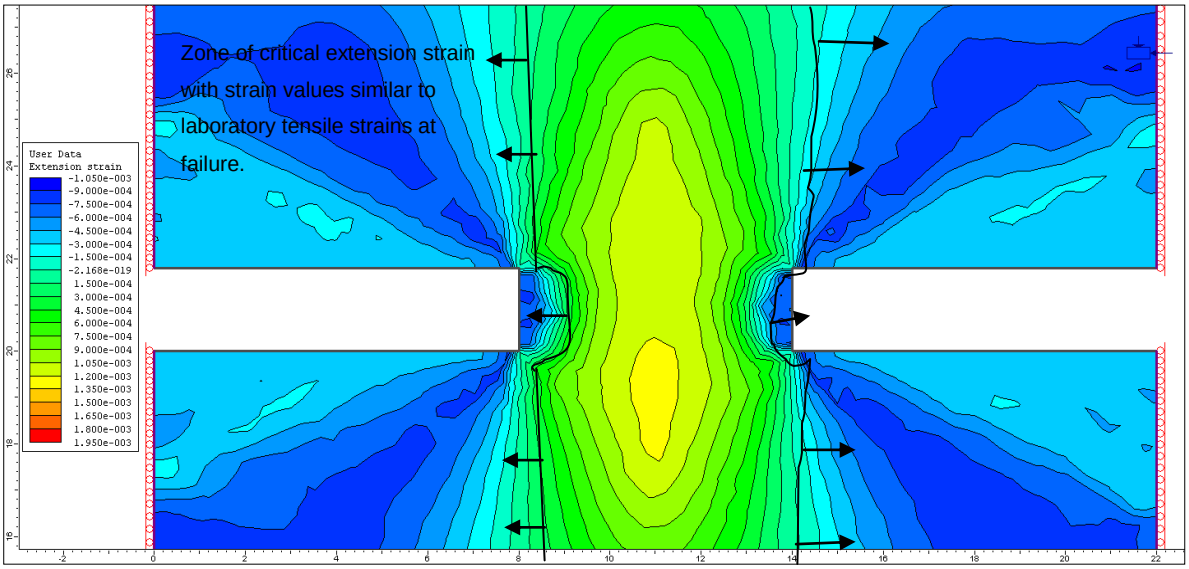


Figure 3-19: Distribution of Critical Extension strain at a depth of 500 m and k = 2

Stacey (1981) stated that each rock type has a critical extension strain value at which fracture propagation initiates. Depending on the stress loading conditions, the critical strain value may be exceeded at some location on the boundary of the excavation resulting in spalling of the rock material in that zone. With little confinement at the rock wall surface and the intersection of natural geological discontinuities, slabs of rock may fall out with time. The zones around the excavation periphery where fractures could be expected to initiate are demarcated with arrows in Figure 3-19. The magnitudes of extension strain depicted here are in the order of 1.05×10^{-3} and less, exceeding the calculated strain values at failure obtained from laboratory indirect tensile strength test results of some 1.6×10^{-4}, see chapter 4.

3.4.1.4 Excavation wall spalling observed underground

In the BC, in-stope pillars are cut in reef rock types which contain low strength and brittle chrome seams alternating with pyroxenite and anorthositic rock type layers. Failure in in-stope pillars may therefore manifest through the weak chrome seam exacerbated by the layered nature of the Merensky and UG2 reefs. Although observed hanging wall de-lamination has arguably been attributed to the layered

nature of the BC rocks, the direct effect of low confinement or tensile stress conditions augmenting dilation or extension of the laminated HW is evident. The models depicted zones of critical extension strain and principal stress contours with orientations that are compatible with the spalling observed in the excavation wall rock. Without quantifying the extent of fracturing or the depth of the fractured zones around in-stope pillars, observations were made on pillars cut in the UG2 reef horizon of a platinum mine.

The photographs that follow in Figures 3-20 to 3-22 were taken in platinum mine stopes that had been standing for at least 6 months. The laminated beam in the hanging wall of the stope de-laminated due to tensile dilation under the weight of the beam. Face parallel fractures with the same orientation as the modelled principal stress contours developed slowly at stresses lower than the compressive or tensile strengths of the host rock types, Figure 3-21. Loose blocks form when the fractures propagate and intersect natural discontinuities, resulting in unravelling around support. Installed support in these conditions curbs the propagation of fractures, and slows down the manifestation of excavation wall damage.



Figure 3-20: De-lamination of hanging wall strata



Figure 3-21: Hanging wall damage under tensile stresses in a stope

Spalling of the wall rock was also observed in a platinum mine haulage, Figure 3-22. Annotations on the picture were made to illustrate spalling and the profile of the haulage as the walls had been white-washed, obscuring the spalling.

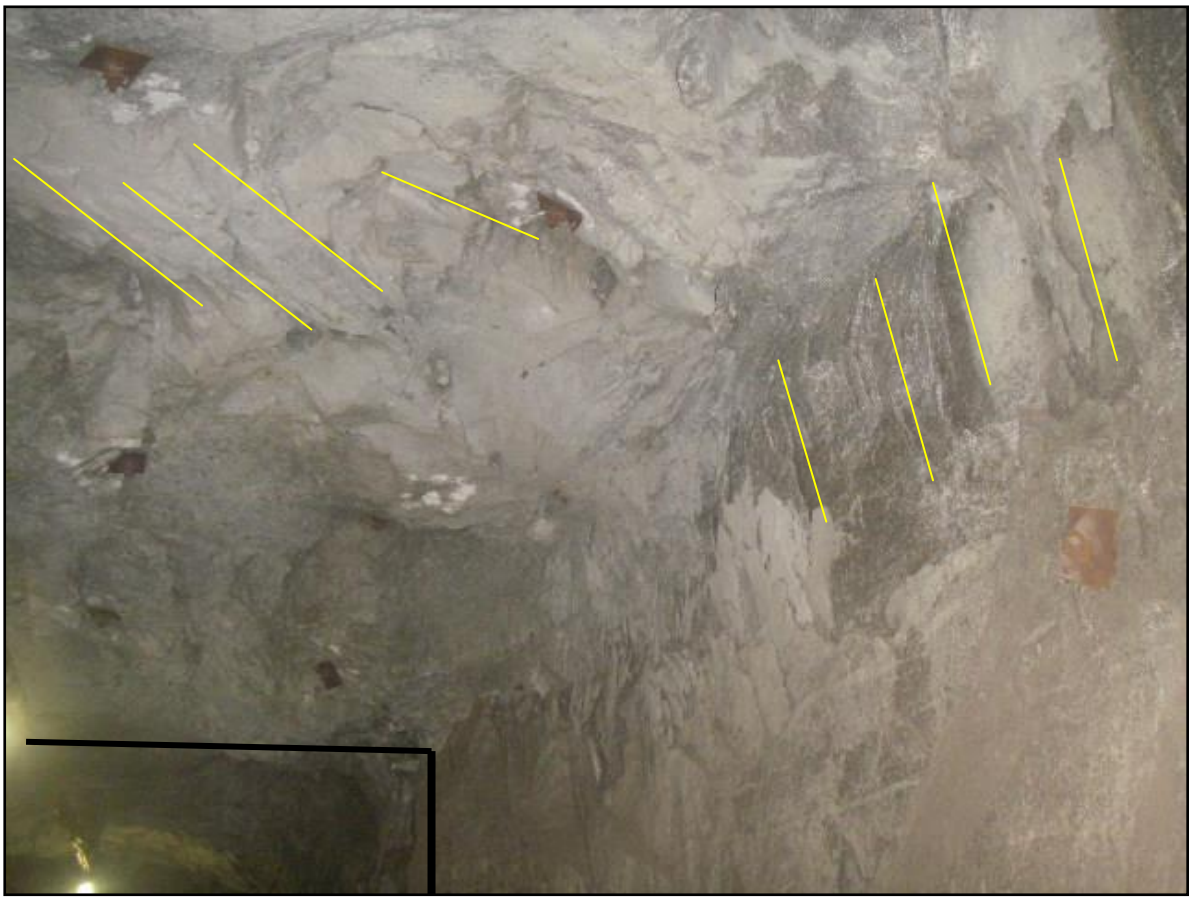


Figure 3-22: Spalling parallel to the haulage walls induced by extension strain observed in a FW haulage mined in anorthositic norite

Modelling results for a stope and an incline shaft excavation are presented in Appendix C and direct reference to these is made in the main content of this research. To bring this analysis into the context of characteristic strains observed in actual rock, a laboratory rock testing programme was conducted and the results are presented in the next chapter. A comparison can therefore be made between strain values observed in rock specimens at failure and modelled critical extension strains.

3.5 Conclusion

Fracture initiation and propagation mechanisms were investigated in Chapter 2, showing that fracture propagation may take place even at low compressive stresses, and even more so under tensile stress, with fractures often aligned parallel to the direction of the principal stress contours. The potential for fracture development was investigated through numerical modelling reported in Chapter 3. The models showed that low confinement, and in some instances, tensile stress conditions, around excavation peripheries may promote fracturing, slabbing and dilation of the excavation walls. The results of the analyses demonstrated that very substantial zones of extension strains, of significant magnitudes, occur around the boundaries of BC excavations. The propagation of fractures commonly observed in excavations is sub-parallel to the orientation of the excavation walls. In addition, fractures may intersect pre-existing natural discontinuities, resulting in the formation of key blocks with a potential to fall out from the excavation walls. Thus, investigation of the effect of time on the behaviour of BC rock types under tensile stress and extension strain is very important with regard to the long term stability of excavations in these rocks.

CHAPTER 4

LABORATORY TESTS ON BUSHVELD COMPLEX ROCKS

4.1 Introduction

The preceding chapters provided a background on the Bushveld Complex (BC) mining environment, the characteristic mining methods used in the BC, the behaviour of rock under different stress conditions and stress-strain analysis around typical BC excavations. Laboratory rock strength tests have been carried out to provide data for comparison with the behaviour of several BC rock types under stress loading conditions in typical BC mine excavations presented in the previous chapter. The current chapter reports the results of Uniaxial Compressive Strength (UCS), and normal and time-dependent Brazilian Indirect Tensile (BIT) strength tests.

4.1.1 Testing objectives

Laboratory rock strength tests were carried out on several Bushveld Complex (BC) rock types to establish the following characteristics of the rock types under compressive stress:

- Elastic properties and failure characteristics under uniaxial compression (UCS), the results of which were used as input for the numerical analysis of stress-strain presented in the previous chapter.
- Long term strength and stress-strain values observed at failure.
- Indirect tensile strength characteristics and
- Time-dependent behaviour under indirect tension.

These objectives were achieved using the methodology outlined in the following section. All rock specimen preparation and testing was carried out in the Genmin Rock Testing Laboratory at the University of the Witwatersrand.

4.1.2 Testing methodology

The following methodology was used to achieve the investigative objectives outlined above:

- Conducting:
  - UCS tests on cylindrical specimens of several BC rock types prepared from different depth sections along a single, vertical drill hole core;
  - Normal BIT tests on Brazilian discs of several BC rock types, and
  - Time-dependent constant hold-load BIT tests on Brazilian discs of several BC rock types stressed to pre-determined hold-load levels (90%, 85%, 80%, 75% and 70%) of the average tensile strength (σ_t) of the rock type, i.e. load at failure from the normal BIT test. The times-to-failure for the different test categories at constant load were recorded for time-dependent analysis.
- Processing, representing and analysing the recorded results.

4.1.3 Spatial location of core samples

The UCS and BIT test specimens were prepared from core of a single exploration drill hole BH6082. The spatial location of the drill hole is given in Table 4-1.

Table 4-1: Exploration drill hole coordinates

Borehole Identification	Co-ordinates		
	X	**Y**	**Collar Z-value**
BH6082	2823730.32	-28219.79	1122.51m AMSL

A full geological log sheet can be found in Table A1-1 in Appendix A. The vertical borehole gives a good cross-sectional representation of the Bushveld Complex stratigraphy. Drill hole core samples were taken from a depth up to 10m above and below the hanging wall (HW) and footwall (FW) contacts of the Merensky (MR), Upper Group 1 (UG1) and Upper Group 2 (UG2) reef horizons.

4.1.4 Distribution of test specimens

Several rock types were identified from the drill core which was used in the preparation of cylindrical specimens for Uniaxial Compressive Strength (UCS) tests and discs for Brazilian Indirect Tensile (BIT) strength tests.

The test specimens were given sample identities for easy referencing according to rock type, lithographic placement (depth) and the test type carried out as shown in Table 4-2.

Table 4-2: Specimen nomenclature

Rock type	Lithographic zone depth/ From-To (m)	Rock type ID code	UCS sample ID code	Normal BIT sample ID code	Time-dependent BIT sample ID code
Mottled Anorthosite	(1637.54 – 1645.27)	A	UCA	NBA	TB%A
Spotted Anorthositic Norite	(1615.64 – 1627.50)	B	UCB	NBB	TB%B
Pyroxenite	(1603.85 – 1610.05)	C	UCC	NBC	TB%C
Mottled Anorthosite	(1600.07 – 1602.37)	D	UCD	NBD	TB%D
Norite	(1564.79 – 1566.92)	E	UCE	NBE	TB%E
Spotted Anorthositic Norite	(1561.45 - 1564.70)	F	UCF	NBF	TB%F
Anorthositic Norite	(1557.30 - 1558.45)	G	UCG	NBG	TB%G
Spotted Anorthosite	(1550.51 – 1557.30)	H	UCH	NBH	TB%H
Mottled Anorhtosite	(1546.38 – 1550.51)	I	UCI	NBI	TB%I

Nine test specimen categories were identified using this methodology and were given alphabetical codes (A to I), starting from the deepest level hosting the Upper Group 1 (UG1) rock types to the shallowest level hosting the Merensky (MR) rock types. The nomenclature was completed by assigning short prefixes (UC, NB and TB) representing uniaxial compression, normal Brazilian and time-dependent Brazilian strength tests respectively. The rock types represented in the nine test specimen categories are: spotted and mottled anorthosite, pyroxenite, norite,

anorthositic norite and spotted anothositic norite. UCS and BIT test specimens were cut alternately from the core to give an unbiased sample representation for the two test methods. No two test specimens for the same test method were cut adjacent to each other. The distribution of prepared test specimens for the different test specimen categories is given in Table 4-3.

Table 4-3: Distribution of test specimens

Reef profile	Rock type	Depth	Identity code	No. of specimen tested in UCS test	No. of specimen tested in Normal BIT test	No. of specimen tested in Time-dependent BIT test	No. of specimen per rock type
		From - To (m)					
UG1 FW	Mottled Anorthosite (M.A.)	(1637.54 – 1643.27)m	A	5	6	32	**43**
UG2 FW	Spotted Anorthositic Norite (S.A.N.)	(1615.64 – 1627.50)m	B	5	8	44	**57**
UG2 HW	Pyroxenite (P.)	(1603.85 – 1610.05)m	C	5	9	17	**31**
UG2 HW	Mottled Anorthosite (M.A.)	(1600.07 - 1602.37)m	D	5	7	24	**36**
MR FW	Norite (N)	(1564.79 – 1566.92)m	E	5	7	11	**23**
MR FW	Spotted Anorthositic Norite (S.A.N.)	(1561.45 – 1564.70)m	F	5	7	17	**29**
MR HW	Anorthositic Norite (A.N.)	(1557.30 – 1558.45)m	G	5	8	14	**27**
MR HW	Spotted Anorthosite (S.A.)	(1550.51 – 1557.30)m	H	5	8	35	**48**
MR HW	Mottled Anorthosite (M.A.)	(1546.38 – 1550.51)m	I	5	7	28	**40**
Total no. of specimens				**45**	**67**	**222**	**334**

The distribution of the test specimens is presented graphically in Figure 4-1.

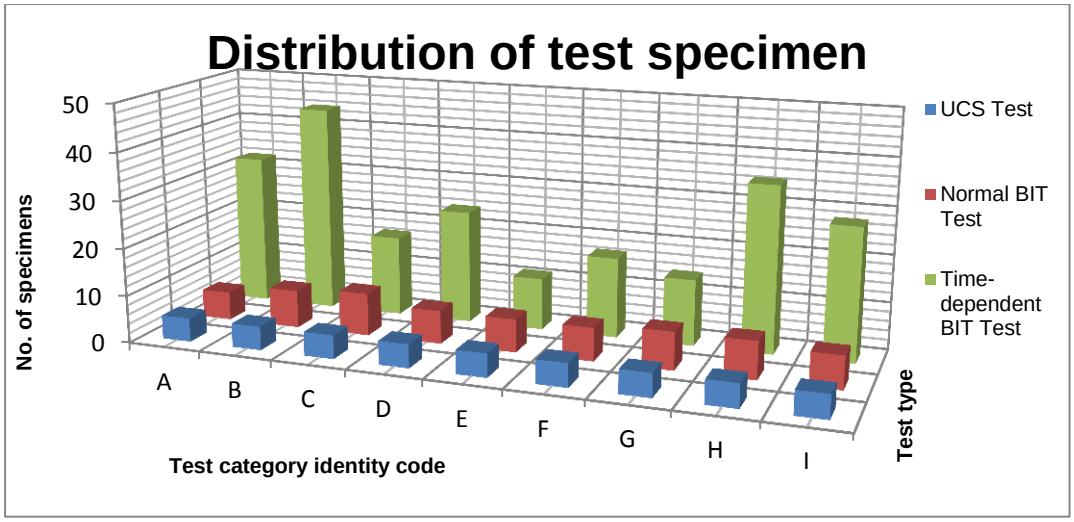


Figure 4-1: Graphical presentation of the distribution of test specimen

The greatest numbers of test specimens were prepared for the BIT test, and most of these were used in the time-dependent tests. For each test type, the numbers of specimens that were tested successfully and gave valid results varied.

4.1.5 Preparation of test specimens

All specimens were prepared and tested according to the ISRM Suggested Methods for rock testing (ISRM, 1981; 2007). The drill core samples were largely undisturbed, intact and showed no signs of stress relief induced “discing” or high stress fracturing, hence the test specimens were considered not to have visible pre-existing deformities. All tests covered in this research were carried out in anhydrous conditions at room temperature and pressure (r.t.p.). The sample width, height, diameter and weight were measured and recorded after the samples were left to dry naturally, to avoid the influence of moisture from the water used during specimen cutting. The cores were BQ size with a diameter, D = 36.3 mm and were prepared to yield specimens with a length-to-diameter ratio, L/D, of 2.2 – 3.0 for the UCS tests, and a thickness-to-diameter ratio, t/D, of 0.4 - 0.6 for the Brazilian tests, Table 4-4. An average width to height ratio of 2.2 and 0.5 for the UCS and BIT test specimens respectively was achieved. Two shapes of specimen were used, as illustrated in Figure 4-2.



Figure 4-2: Rock specimens for UCS and BIT test shapes

The specimens were cut parallel, ground and polished flat to remove all asperities and undulations which could introduce non-uniform loading.

4.2 The UCS test set up

The Amsler conventional compression rock testing machine was used to carry out UCS tests, Figure 4-3.

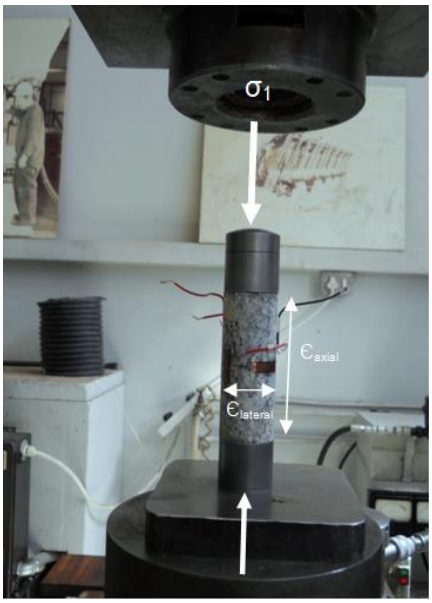


Figure 4-3: The Amsler testing machine

Strain gauges were attached in circumferential and axial directions on the UCS test specimens to measure strain during the test. Lead wires from the gauges, and the output from a load cell, were connected to a data recording and processing computer to give strain and stress values, which were used to analyse the compressive behaviour of the various rock types. The Amsler testing machine is a conventional loading machine, and despite non-violent failure of many specimens on reaching peak strength, not much information could be salvaged from the post-peak period of the tests due to the recording limitations of the recording system and rupture of strain gauges at specimen failure.

4.3 Analysis of UCS test results

A comprehensive UCS testing programme was conducted. Only a summary of the UCS test results together with the long term strength analysis is presented here to keep the write-up small and the analysis focused. The salient trends from the results are presented here, and the full set of all results is contained in Appendix B1.

4.3.1 Processing of UCS test results

Detailed processing of one UCA test category is presented here together with stress-strain plots. A full set of the UCS results for all the test categories, and representative stress-strain plots, are contained in Appendix B1. Recorded test values for mottled anorthosite specimen UCA7 are presented in Table 4-4 as an example of the results obtained.

Table 4-4: Recorded UCS test values for specimen UCA7

MOTTLED ANORTHOSITE UG1 F/W DEPTH (1637.54-1643.27)m UCA7									
Load, (kN)	**Stress, (MPa)**	**Axial strain, εa x 10^{-3}**	**Radial strain, εr x 10^{-3}**	**Volumetric strain, εv x 10^{-3}**	**Load, (kN)**	**Stress, (MPa)**	**Axial strain, εa x 10^{-3}**	**Radial strain, εr x 10^{-3}**	**Volumetric strain, εv x 10^{-3}**
0	0	0	0	0	115.247	111.359	1988	-481	1026
5.096	4.924	167	-6	155	120.735	116.662	2038	-519	1000
10.192	9.848	376	-13	350	125.047	120.829	2081	-545	991
15.288	14.772	527	-25	477	130.143	125.753	2131	-583	965
20.384	19.696	681	-38	605	135.239	130.677	2187	-615	957
25.088	24.242	811	-57	697	140.335	135.601	2230	-659	912
30.184	29.166	948	-82	784	145.431	140.525	2280	-697	886
35.672	34.469	1053	-101	851	150.526	145.448	2335	-748	839
40.376	39.014	1146	-120	906	155.622	150.372	2385	-798	789
45.08	43.559	1220	-139	942	160.326	154.918	2434	-855	724
50.175	48.482	1295	-158	979	165.03	159.463	2478	-906	666
55.271	53.407	1357	-184	989	170.126	164.387	2533	-982	569
60.367	58.331	1412	-203	1006	175.222	169.311	2577	-1064	449
65.071	62.876	1462	-222	1018	180.318	174.235	2633	-1191	251
70.167	67.800	1518	-247	1024	185.414	179.159	2682	-1343	-4
75.263	72.724	1573	-272	1029	190.118	183.705	2732	-1577	-422
80.359	77.648	1629	-298	1033	195.214	188.629	2800	-2300	-1800
85.063	82.194	1679	-317	1045	219	211.612	2800	-2300	-1800
90.159	87.118	1728	-342	1044					
95.255	92.042	1784	-367	1050					
100.351	96.966	1834	-393	1048	219kN load @ failure				
105.055	101.511	1883	-424	1035					
110.151	106.435	1939	-450	1039					

The data from the test results was processed and used to plot stress-strain curves as a visual aid, Figure 4-5. The average values of elastic properties of mottled anorthosite (A) are indicated on the plot. The plot shows largely linear behaviour up to the peak strength for the specimen, a trend largely repeated in the other four specimens in the rock type test category (A), see Appendix B1.

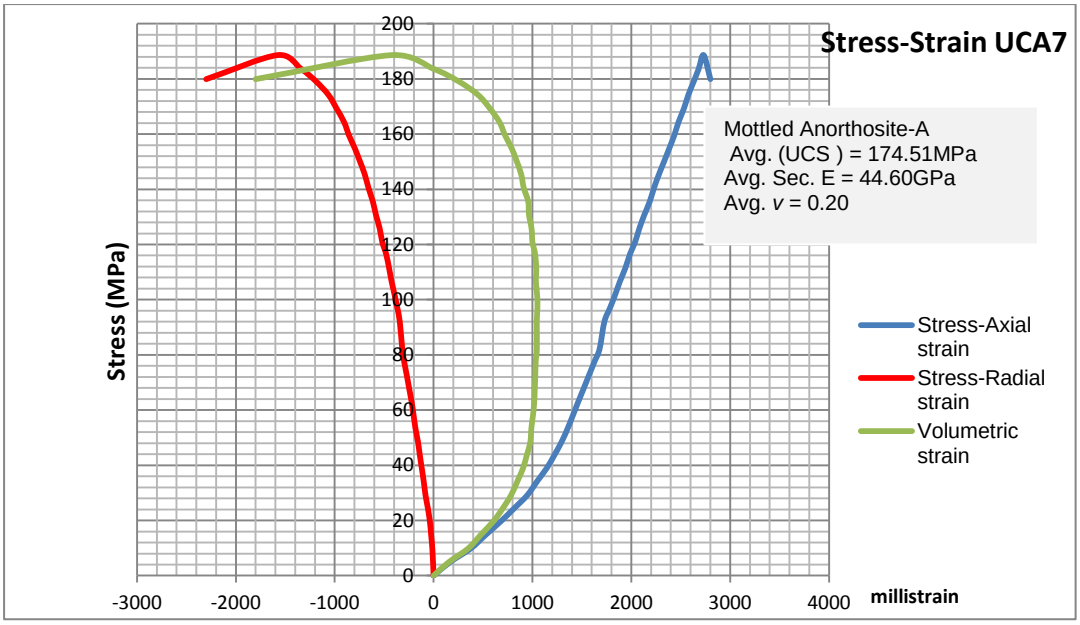
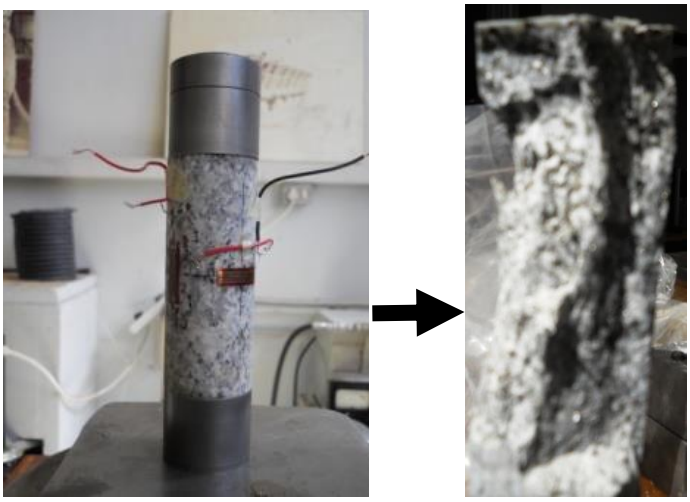


Figure 4-5: Stress-Strain graph for mottled anorthosite specimen UCA7

4.3.2 Deformation properties

The specimens failed in a combined extension and shear fashion resulting in some cases of conical shaped end pieces and a completely fractured or crushed middle portion, Figure 4-6.



(a) (b)

Figure 4-6: Failure mode observed in specimen tested in uniaxial compression, (a) before the test and (b) after the test

Crack propagation parallel to the axis of the specimens was clearly visible in the specimens tested indicating dilation in a direction perpendicular to the loading

direction. Dilation that occurred in the test specimens can be quantified through volumetric strain analysis presented in the following section.

4.3.3 Analysis of volumetric strain

Based on Bieniawski (1967a)'s long term strength analysis, axial stress-volumetric strain plots were used to evaluate the long term strength of the test specimens. According to Bieniawski (1967a) the point of departure from linearity or the point of inflexion of the stress-volumetric strain plot marks the "long term strength" of the specimen. The rate of change of the stress-volumetric strain plot, as shown in Figure 4-7, was used to investigate the long term strength of the specimens as the inflexion point was not clearly visible from the stress-strain plots.

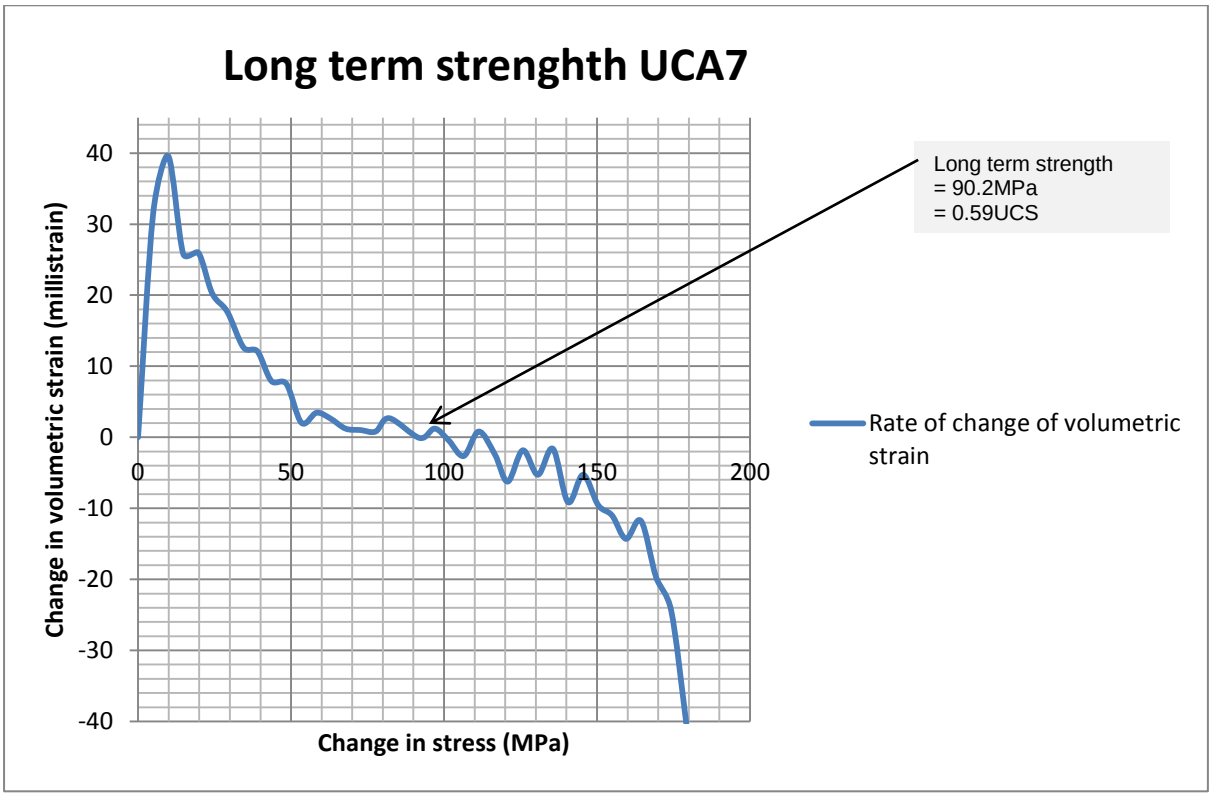


Figure 4-7: Determination of the "long term strength" for specimen (UCA7)

Long term strengths were processed for each test category and average values calculated. The significant variation shown in the test results can be attributed to specimen inherent variability and defects and inconsistent strain gauge feedback. Average long term strength values are presented here to investigate trends from the nine test categories. The rate of volumetric strain-stress plots were expanded when

necessary to identify the long term strength value. For test specimen UCA7 the long term strength was determined as 90.2MPa (~0.59 x UCS). A summary of the UCS test results together with the long term strength values is given in the following section (Table 4-5).

4.3.4 UCS test results summary

A summary of the average UCS test results is given in Table 4-5, and the detailed set of test results is contained in Appendix B1. Further plots of representative samples are presented in Appendix B. There do not appear to be any trends related to the depth of placement of the rock specimens as the results showed a random distribution along the length of the test core.

Table 4-5: Summaries of UCS test results (average values are presented here)

Rock type/ Code	M. A. (A)	S. A.N. (B)	P. (C)	M. A. (D)	N. (E)	S. A. N. (F)	A. N. (G)	S. A. (H)	M. A. (I)
Sample diameter, D (mm)	36.30	36.30	36.30	36.30	36.30	36.30	36.30	36.30	36.30
Sample length, L (mm)	80.74	84.79	81.66	81.13	83.71	82.87	80.99	81.03	80.98
L/D ratio	2.23	2.34	2.25	2.24	2.29	2.28	2.23	2.23	2.23
Sample mass, M (g)	231.41	254.20	270.30	230.93	261.32	248.10	253.48	237.80	232.32
Sample density, ρ (kg/m^3)	2769.46	2898.71	3198.41	2750.49	3016.40	2892.39	2990.22	2835.12	2772.17
Failure load, (kN)	180.60	139.40	129.80	140.50	96.00	154.60	114.00	159.60	182.20
UCS, σ_c (MPa)	174.51	134.70	125.42	135.76	92.76	149.38	110.15	154.22	176.05
Elastic Modulus, E (GPa)	44.60	33.32	35.49	39.01	30.90	40.65	37.90	42.64	45.31
Poisson's ratio, *v*	0.20	0.21	0.17	0.28	0.19	0.21	0.15	0.22	0.19
Long term strength (MPa)	90.2	61.8	56.5	59.75	53.5	75.6	83.6	103.33	125.75
% of UCS	57	46	44	44	57	51.4	72.4	67	68.75

The average value of the "long term strength" for the nine categories of rock types was 78MPa which is 56.39% of the UCS (0.56 x average UCS) value of the rock types tested. The lowest "long term strength" values were recorded for pyroxenite and mottled anorthosite rock types at 44% of their respective UCS values.

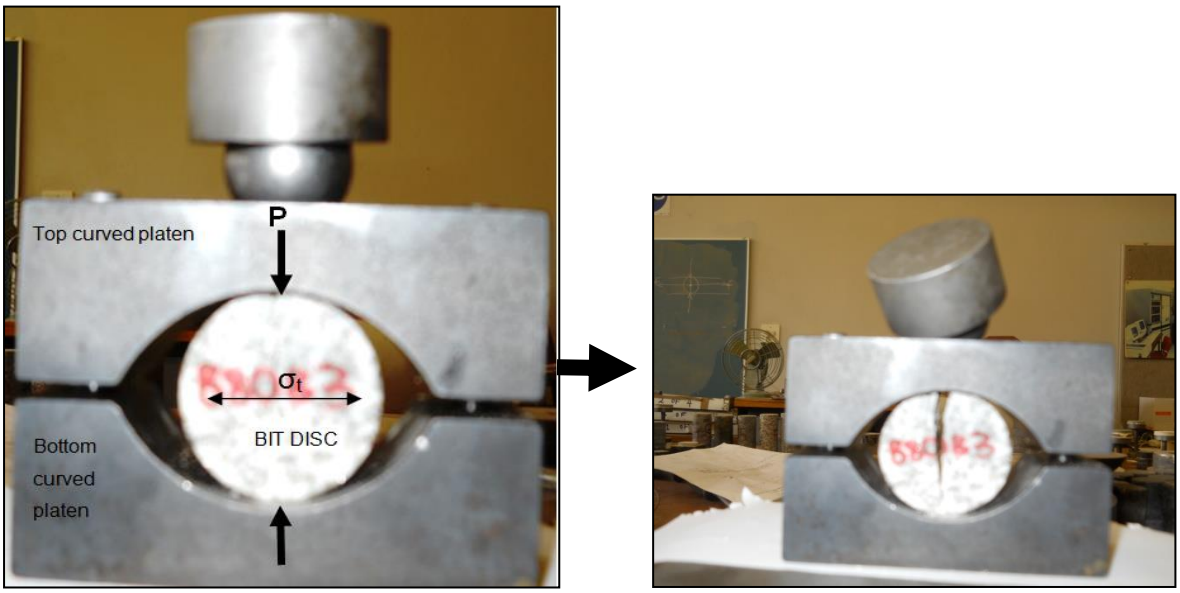
4.4 Brazilian Indirect Tensile (BIT) strength test

The (Multiple Testing System) MTS 815 servo-controlled machine was used to carry out normal and time-dependent Brazilian Indirect Tensile (BIT) strength tests. The MTS 815 rock testing machine together with its accessories is shown in Figure 4-8.



Figure 4-8: The MTS 815 rock testing machine used to load BIT discs

Curved platens (Figure 4-9) were used to ensure that tensile failure would initiate at the centre of the BIT test discs (Hudson et al, 1972; Wang et al, 2004) and not at the two contacts with the platens.



(a) (b)

Figure 4-9: Curved platens used in the BIT test set up, (a) before the test and (b) after the test

The spherical steel ball above the top platen helped align the applied stress through the diameter of the rock disc specimens. The platens had a system of pegs and guide holes to prevent non-uniform loading, as can be seen in Figure 4-9.

4.4.1 Normal Brazilian Indirect Tensile (BIT) strength test

A constant loading rate of 2kN/min was used to load specimens, targeted to fail in 3 to 4 minutes depending on their tensile strength. An example of a load-time plot, for specimen NBA1, is shown in Figure 4-10.

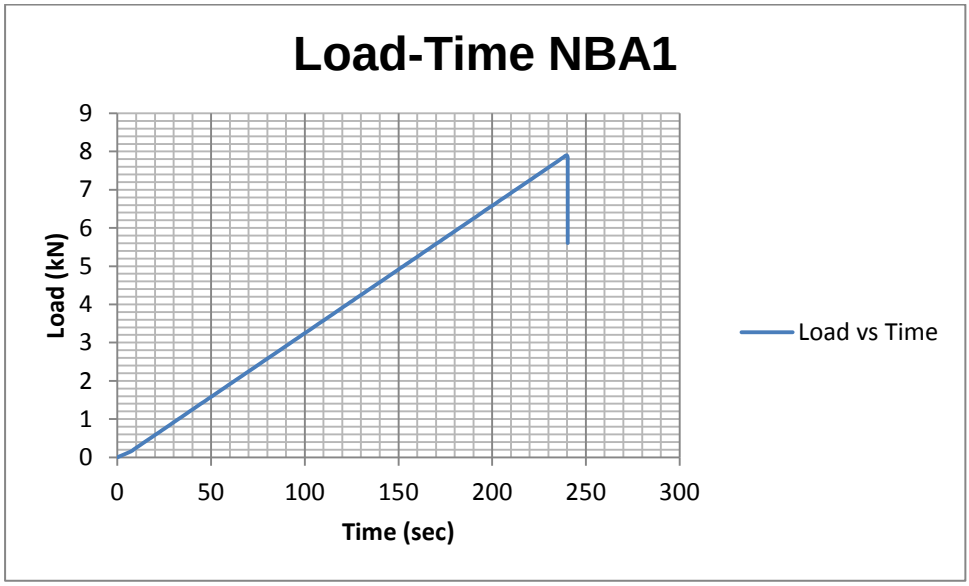


Figure 4-10: Normal BIT load-time plot

The load drop trigger on the MTS machine was consistent with the initial appearance of the tensile split of the Brazilian disc samples. The load at failure for each test specimen was recorded and used to calculate the average tensile strength for the different test categories. A summary of the results of the normal Brazilian tensile strength tests is presented in Table 4-6 (elastic modulus values are those obtained from the UCS tests).

Table 4-6: Summaries of Normal Brazilian Indirect Tensile BIT strength test results

Rock type	Sample ID	Sample diameter, D (mm)	Sample thickness, t (mm)	t/D ratio	Sample mass, M (g)	Average load at failure, P (kN)	Average BIT strength, σ_t (MPa)	Average Elastic modulus, E (GPa)	Average strain at failure, (millistrain)	Average Time-to-failure (sec)
Mottled Anorthosite (A)	DBA	36.30	19.27	0.53	54.26	8.19	7.46	46.72	0.16	220.71
Spotted Anorthositic Norite (B)	DBB	36.30	18.88	0.52	55.46	6.84	6.35	33.32	0.19	205.72
Pyroxenite (C)	DBC	36.30	18.97	0.52	62.67	7.43	6.89	35.40	0.19	206.77
Mottled Anorthosite (D)	DBD	36.30	18.77	0.52	53.84	6.83	6.38	39.01	0.16	138.02
Norite (E)	DBE	36.30	18.36	0.51	57.67	6.92	6.62	30.90	0.21	160.35
Spotted Anorthositic Norite (F)	DBF	36.30	18.61	0.51	55.24	8.27	7.76	40.65	0.19	138.17
Anorthositic Norite (G)	DBG	36.30	17.65	0.49	56.31	7.71	7.65	37.90	0.20	203.85
Spotted Anorthosite (H)	DBH	36.30	17.59	0.48	51.29	7.11	7.10	42.64	0.17	213.83
Mottled Anorthosite (I)	DBI	36.30	17.06	0.47	48.93	6.82	7.04	45.31	0.16	214.03

A comparison between UCS and BIT strength values is presented in Table 4-7.

Table 4-7: Comparison of UCS and BIT strength test

Test category	BIT (MPa)	UCS (MPa)	BIT/UCS	UCS/BIT
A	7.91	174.51	0.05	22.05
B	6.61	134.7	0.05	20.38
C	7.18	125.42	0.06	17.47
D	6.60	135.76	0.05	20.57
E	6.69	92.76	0.07	13.87
F	7.99	149.38	0.05	18.69
G	7.45	110.15	0.07	14.79
H	6.87	154.22	0.04	22.45
I	6.59	176.05	0.04	26.71
Average	7.10	139.22	0.05	19.67

On average the BIT strength was found to be averagely 20 times lower than the UCS of the same rock type. Typical strain values at failure were calculated based on the elastic modulus for the rock type test category. The full set of the normal BIT test results is contained in Appendix B3. Typical strain values at tensile failure ranged $1.6x10^{-1}$ to $2.1x10^{-1}$ millistrain, with an average value of 1.8×10^{-1} millistrain, well within range of the magnitudes of the extension strain values determined, from the

numerical modelling, in the immediate walls of BC excavations, as reported in Chapter 3.

4.4.1.1 Deformation characteristics

All valid test results had a clearly visible diametrical split observed in the direction of loading, caused by induced tensile stress, as indicated by the samples of failed discs, Figure 4-11.



Figure 4-11: Specimen failure in the BIT test

A few specimens, with suspected inherent defects, showed failure in more than one place and in more than the diametrical direction, with a shorter time-to-failure and/or smaller load at failure than expected. This was particularly observed in the pyroxenite rock type, test category C. Some of the test specimens crushed where they made contact with the top and bottom platens.

With the long term compressive strength and tensile characteristics of several BC rock types established, including the typical extension strain at failure, it was imperative to investigate the influence of time on the tensile strength of these rock types.

4.4.2 Time-dependent Brazilian Indirect Tensile (BIT) strength test

Pre-determined load levels, derived from the tensile strength values recorded in the normal BIT test results, were used in the time-dependent BIT strength tests. The load levels were a percentage of those corresponding with the tensile strength values for the respective rock test categories. Test sets, consisting of five specimens per hold-load level for each test category, were conducted.

Constant hold-load level = X% of normal BIT load capacity

where X = 70; 75; 80; 85 and 90 representing 5% intervals.

Owing to limited availability of the MTS machine the longest time-dependent tests were tested at 70% of tensile capacity, limiting the longest test runs to not more than three days. The calculated load levels and corresponding expected strain values based on the application of the elastic law are given in Table 4-8.

Table 4-8: Time-dependent BIT test loads

Rock type/ Specimen I.D.	Mean load at failure, P_{mean} (kN)	Elastic Modulus, *E* (Gpa)	Static BIT test load, Phold = $X_{\%}$ of P_{mean} (kN)									
			90% Phold, (kN)	(0.9 x ε) x 10^{-3}	85% Phold, (kN)	(0.85 x ε) x 10^{-3}	80% Phold, (kN)	(0.8 x ε) x 10^{-3}	75% Phold, (kN)	(0.75 x ε) x 10^{-3}	70% Phold, (kN)	(0.7 x ε) x 10^{-3}
SB%A	8.19	46.72	7.37	0.14	6.96	0.14	6.55	0.13	6.14	0.12	5.73	0.11
SB%B	6.84	33.32	6.16	0.17	5.81	0.16	5.47	0.15	5.13	0.14	4.79	0.13
SB%C	7.43	35.40	6.69	0.18	6.32	0.17	5.94	0.16	5.57	0.15	5.20	0.14
SB%D	6.83	39.01	6.15	0.15	5.81	0.14	5.46	0.13	5.12	0.12	4.78	0.11
SB%E	6.92	30.90	6.23	0.19	5.88	0.18	5.54	0.17	5.19	0.16	4.84	0.15
SB%F	8.27	40.65	7.44	0.17	7.03	0.16	6.62	0.15	6.20	0.14	5.79	0.13
SB%G	7.71	37.90	6.94	0.18	6.55	0.17	6.17	0.16	5.78	0.15	5.40	0.14
SB%H	7.11	42.64	6.40	0.15	6.04	0.14	5.69	0.13	5.33	0.12	4.98	0.12
SB%I	6.82	45.31	6.14	0.14	5.80	0.13	5.46	0.12	5.12	0.12	4.77	0.11

A theoretical stress-strain plot at the various load levels for the various rock types test categories is shown in Figure 4-12. Included in the plot is the strain sustained in a specimen at tensile failure shown at the peak of each individual plot. This graph depicts typical strains calculated at different load levels under indirect or induced tension.

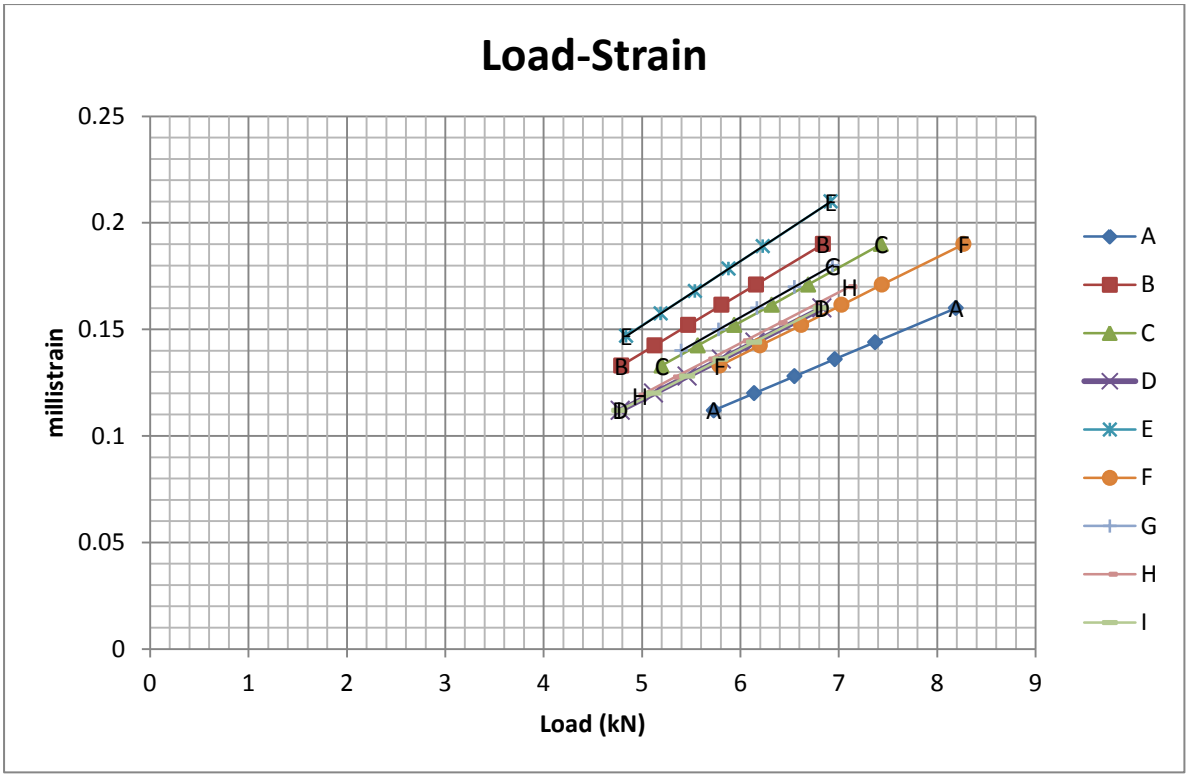


Figure 4-12: Calculated strains at various load levels for the nine test categories

Loads on each test specimen were increased at a rate of 2kN/min up to a constant load corresponding to the required percentage of the load capacity. The time-to-failure, T(s), the time from the onset of the constant load stage up to test specimen failure, was recorded for complete test runs where specimen failure was observed. Some of the test runs, particularly ones at 90% of tensile load, failed during the load application stage, before reaching the constant load phase. Other test runs with similar premature failure results were attributed to variability and inherent defects in the test specimens, resulting in rapid failure and lower strength. An example of this is given for sample SB90A1, whose constant time-dependent test load would have been 7.33kN but failure occurred on reaching 7.3kN during the loading stage, Figure 4-13.

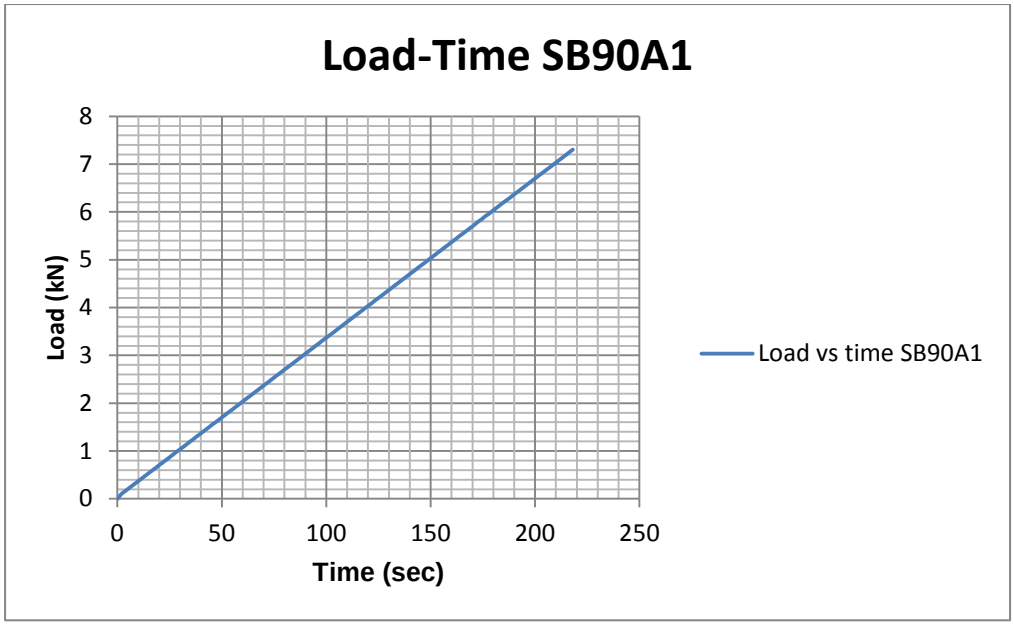


Figure 4-13: Time-dependent Load-Time plot

The variation in t/D ratio for the test specimens was so negligible that specimen shape and size was ruled out as influencing the strength of the samples. A load-time plot where the specimen loaded at constant load until the specimen failed in tension is presented in Figure 4-14.

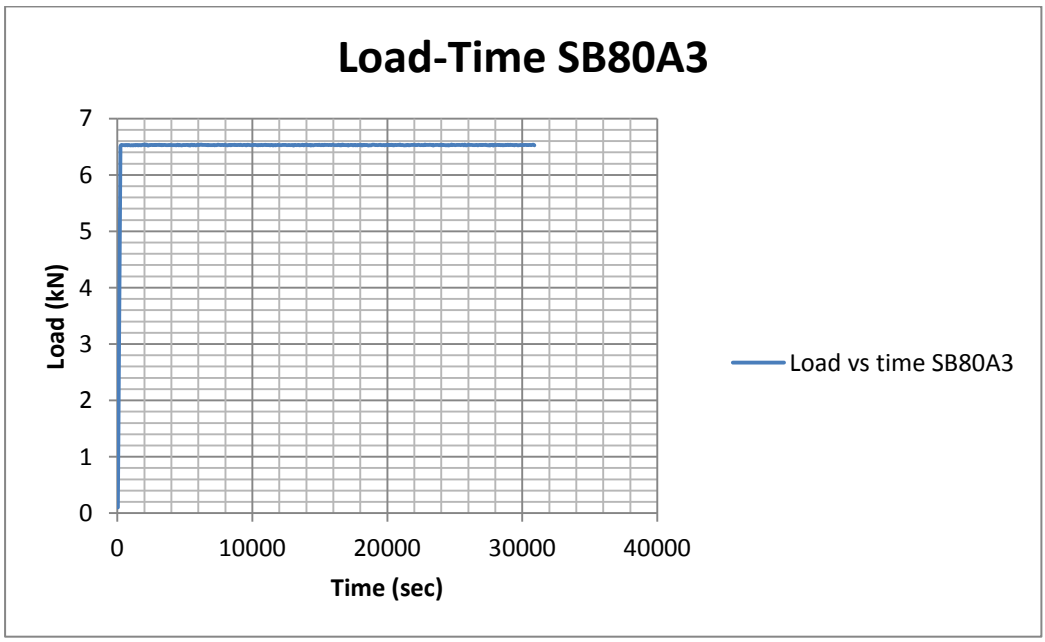


Figure 4-14: Time-dependent BIT Load-Time plot

In a few test runs, particularly in the low load tests at 70%, failure did not occur within three days, and in other cases the MTS machine tripped due to overheating. In cases in which times to failure were expected to be longer, tests at those particular load levels were aimed to run over weekends in an attempt to achieve valid times-to-failure. Valid test results were therefore only recorded if the initial loading build-up was completed to the hold stage, if the MTS machine did not trigger the stop command due to external vibrations or overheating, and if the test was completed within three days.

4.4.3 Time-dependent BIT test results

Each set of test specimens tested in this research used a single constant load. The time-dependent test results for the nine specimen categories are summarised in Table 4-9.

Table 4-9: Time-dependent test results

Rock type/ Specimen I.D.	Mean BIT strength, P_{mean} (kN)	Static BIT test load, $X_{\%}$ of P_{mean} (kN) and Time-to-failure, T (s)									
		90%	Time, T (s)	85%	Time, T (s)	80%	Time, T (s)	75%	Time, T (s)	70%	Time, T (s)
SB%A	8.19	7.37	268	6.96	972	6.55	11658	6.14	39831	5.73	111480
SB%B	6.84	6.16	1587	5.81	2200	5.47	4578	5.13	19837	4.79	62226
SB%C	7.43	6.69	16830	6.32	38695	5.94	33705	5.57	207423	5.20	23605
SB%D	6.83	6.15	229	5.81	16328	5.46	82700	5.12	36306	4.78	151889
SB%E	6.92	6.23	1652	5.88	375	5.54	10327	5.19	1679	4.84	60706
SB%F	8.27	7.44	-	7.03	375	6.62	1705	6.20	2698	5.79	60709
SB%G	7.71	6.94	643	6.55	147	6.17	-	5.78	2483	5.40	805
SB%H	7.11	6.40	4214	6.04	12291	5.69	8168	5.33	67109	4.98	62350
SB%I	6.82	6.14	6213	5.80	45191	5.46	33038	5.12	38993	4.77	39151

The individual creep test results show a random scatter in the time-to-failure, and hence it was decided to use a logarithmic trend line to investigate the time-dependent trends. The trend line of the time-to-failure starts off with a steep gradient which flattens, with time, to a strength value below which specimen failure may not be expected over an infinite period of time. This value may be taken as the long term tensile strength of the rock type. The limitation in determining the long term tensile strength of BC rocks in this way is the limited range of test loads and the limited number of creep tests available to define a smooth curve of load vs time-to-failure.

Ideally creep test loads at intervals ranging up to 90% of the tensile strength should be used to investigate time-dependent trends of the rock types. In addition, large numbers of tests would be required to take the rock variability satisfactorily into account. The results for test category B shown in Figure 4-15 illustrate the scatter in the results and the trend in the time-dependent results.

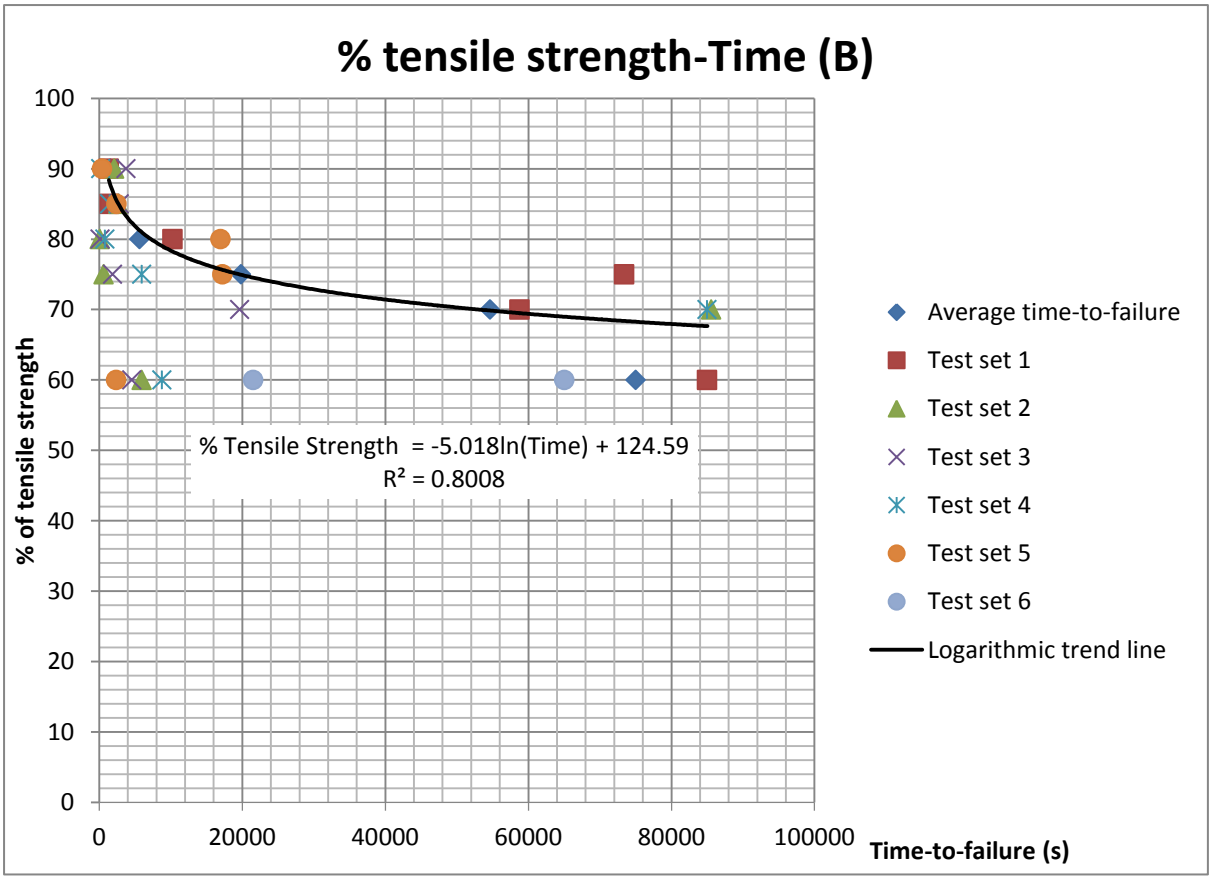


Figure 4-15: Time-to-failure plot for test category B (Rock type: spotted anorthositic norite)

In test category B, minimum creep loads of 60% of the normal tensile strength were applied, while the other eight test categories the minimum was 70% of tensile strength. A theory that the long term tensile strength of a rock type is expected to be lower than its compressive long term strength established via UCS tests is mooted here. Plots of load against average time-to-failure for all nine test categories are presented in Figures 4-16 and Figure 4-17. A full set of the time-dependent results and plots for the nine test categories is presented in Appendix B3.

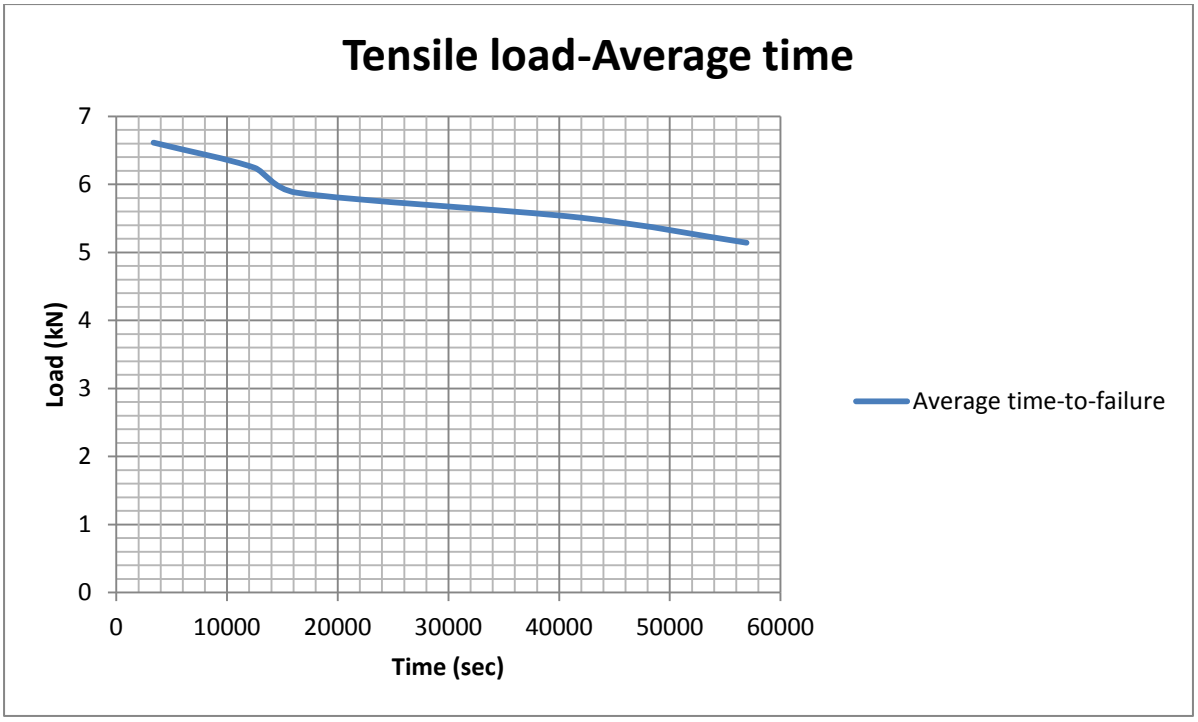


Figure 4-16: Load-Time plot for averages of all the test results

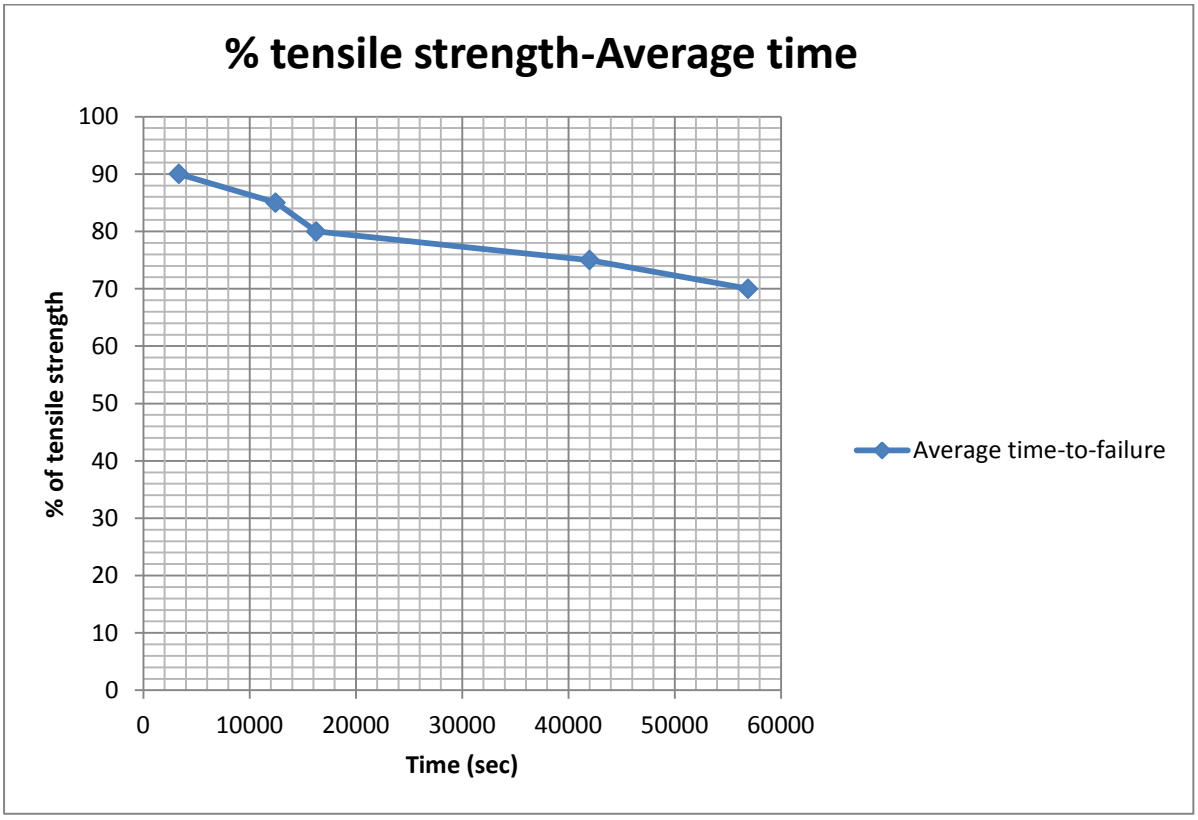


Figure 4-17: Percentage load-Time plot for averages of all test results

Extension strains were calculated from the tensile strength test results, making use of the elastic moduli. From these data a plot of strain-time is shown in Figure 4-18,

giving an indication of times for rock to attain strains at which extension strain failure may occur according to the analyses presented in Chapter 3.

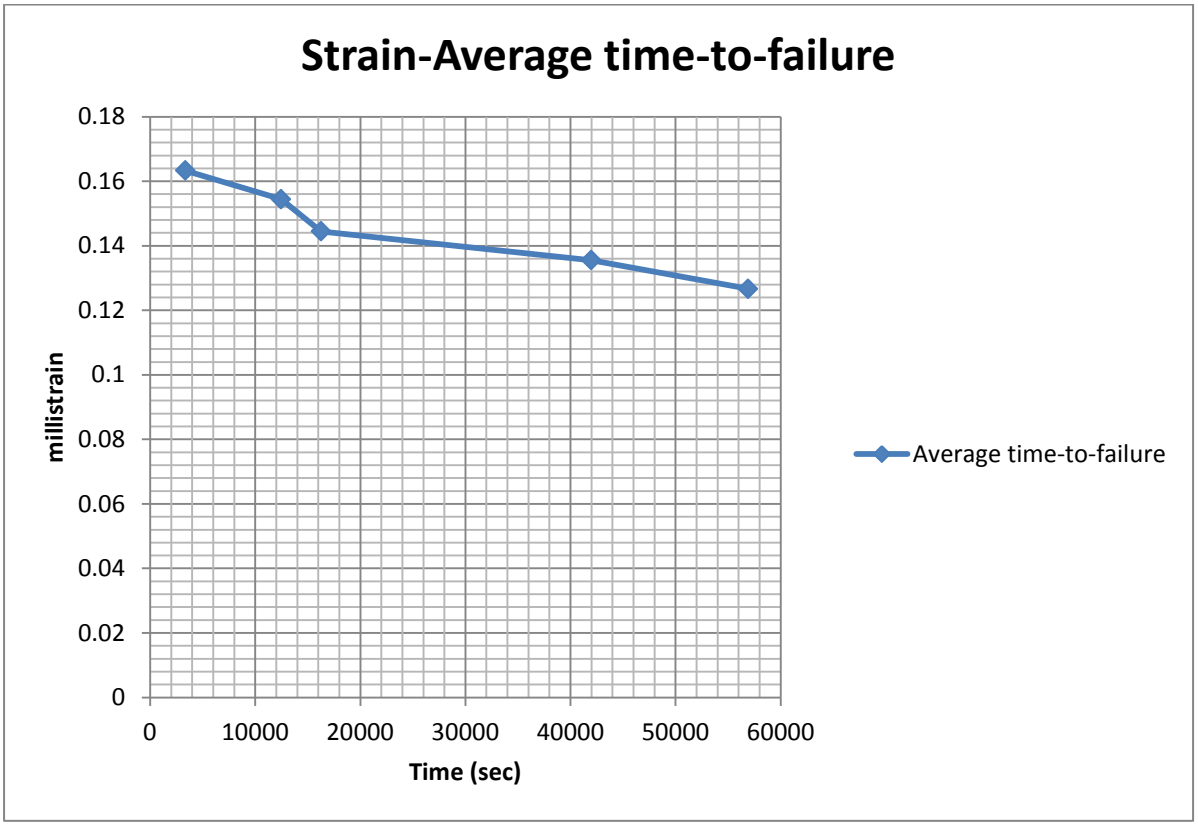


Figure 4-18: Strain-Time plot for averages of all test results

The main limitation of the test load ranges applied in these creep tests is that the time-to-failure results were influenced by test machine availability, and test loads lower than at least 50% should ideally have been used. However, the results provide some data when none existed before, and are conclusive in showing the time-dependency of the tensile strength of several BC rock types.

4.5 Conclusions

Elastic properties of several BC rock types, and their interpreted long term compressive strengths, were established through the UCS test. Tensile properties for these rock types were established under normal and time-dependent indirect tension. The following points were highlighted:

- The average “long term strength” of the rock types calculated from the UCS tests was 78 MPa which is equivalent to 56.5% of the average UCS for the rock types.
- Tensile strengths (σ_t) of BC rock types were on average 5% of the corresponding UCS strength (σ_c).
- Using the elastic properties of the BC rock types and Hooke’s constitutive laws of elasticity in rock, typical extension strain values at tensile failure were calculated giving maximum and minimum average strain values of 1.8×10^{-4} and 1.2×10^{-4} respectively.
- Generally the tensile strength of the BC rocks showed time-dependency although individual results showed a lot of variance in the time to failure.
- The time for the time-dependent tests was limited by machine availability to not more than three days, thus preventing the investigation of a full range of creep test loads (0 – 90% of the tensile strength).
- The average time-to-failure plots showed increasing creep failure time with decreasing creep load. However, owing to the limited creep test periods, the ultimate long term tensile strength, if it existed, could not be concluded from the research. Nevertheless, the results showed that the long term tensile strength is less than 70% of the normal tensile strength.

CHAPTER 5

DISCUSSION OF STRESS-STRAIN ANALYSIS RESULTS

5.1 Introduction

Evaluation of the stress and strain distributions in the Bushveld Complex (BC) mining environment was conducted using numerical analyses, and laboratory strength testing was used to evaluate the strength characteristics of BC rock types. Chapter 3 presented the results of numerical analyses of the distribution of stress and strain around modelled excavations in BC rock masses. Laboratory rock strength test results were reported in Chapter 4, including a comprehensive characterisation of the deformational behaviour of several BC rock types loaded in compression and indirect tension. The current chapter correlates findings from numerical analyses with laboratory rock strength test results to establish the implications of the effect of time on the stability of mining excavations in the BC.

5.2 Results of laboratory testing

From the compressive and tensile strength tests carried out, the following key outputs may be summarised:

1. Average UCS values obtained for the BC rocks varied between 93MPa and 176MPa, with an average value of 138MPa.
2. The average long term strength of the rocks, interpreted from the volumetric strain curves in the UCS tests, was 78MPa, which is 56% of the UCS. The lowest long term strength value obtained was 44% of the corresponding UCS value.
3. Tensile strength magnitudes of the rocks were found to be between 4% and 7% of the UCS magnitudes (the tensile strength magnitude is about 20 times lower than the UCS magnitude).
4. The minimum long term tensile strengths of the rocks could not be determined owing to testing machine availability, but are certainly less than 70% of their normal tensile strengths.

5. Extension strain magnitudes at strength failure interpreted from the normal tensile strength tests indicate a range of between 1.6 x 10^{-4} and 2.1 x 10^{-4}. Values corresponding with the long term tensile strength would therefore be less than 70% of this range, or less than 1.1 x 10^{-4} to 1.5 x 10^{-4}.

5.3 Results of the numerical analyses

The following points stand out from the numerical analyses of stress-strain distribution:

1. Numerical models gave higher ranges of stress (25 to 37 MPa) in the pillar core than in the outer walls consisting of the immediate stope hanging walls and sidewalls with stresses of 5 to 15MPa.
2. The models illustrated that the outer wall rock of mine excavations may well have low compressive and in some instances tensile conditions.
3. The stress conditions expected in the excavation walls of the models are lower than the UCS, but are within range of the tensile strengths of the rock types investigated in this research.
4. The magnitudes of extension strains determined from the modelling (Figure 5-1) are as large as 1.05 x 10^{-3}, well exceeding the extension strain magnitudes at tensile failure obtained from laboratory indirect tensile strength test results, summarized in Section 5.2 above.

Note that observations made in actual BC mine excavations revealed that fracturing of intact rock occurs over a protracted time period; possibly due to the extension of fractures, and that the manifestation of such fracturing was curbed by installed support.

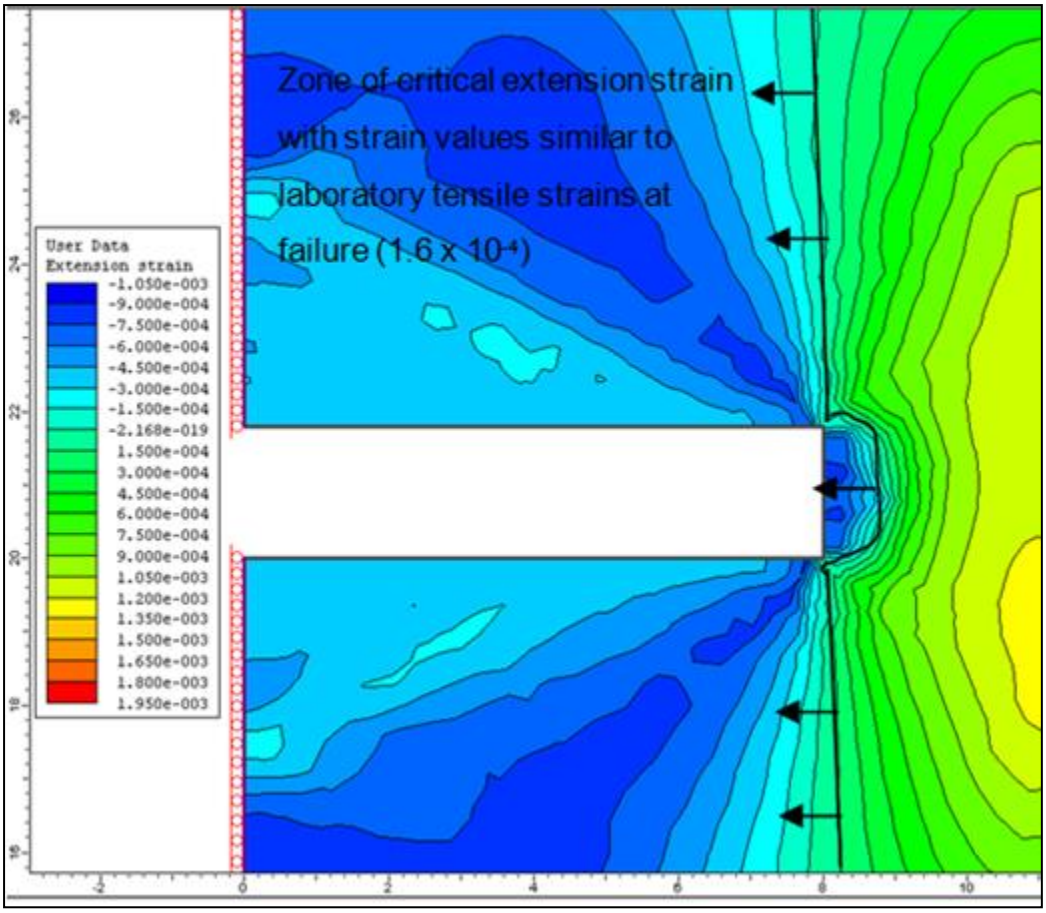


Figure 5-1: Distribution of extension strain around an in-stope pillar

Figures 5-2 and 5-3 illustrate the theoretical magnitudes of the extent of the influence of critical extension strain at which fracture propagation is anticipated. These magnitudes may be modified and reduced by the presence of parting planes and other weakness planes in the rock mass. The main purpose of the analyses was to demonstrate the potential occurrence of large zones of extension in underground excavations in the BC mines.

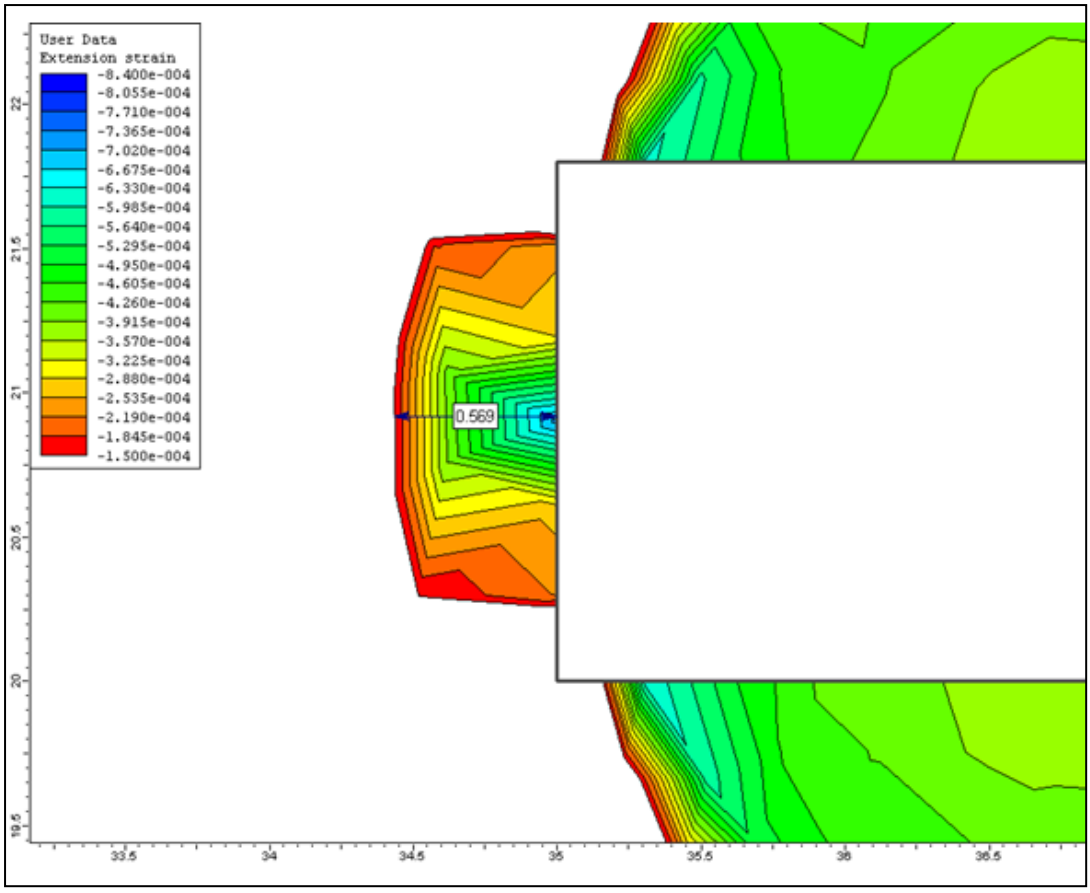


Figure 5-2: Illustration of the zone in a stope sidewall prone to fracture propagation

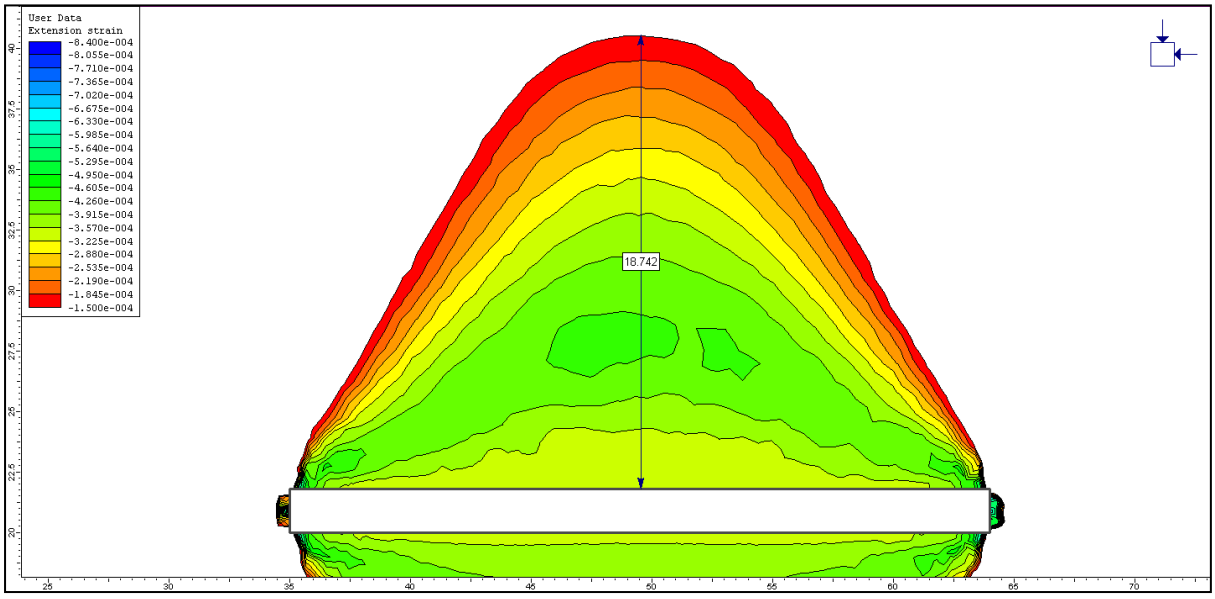


Figure 5-3: Illustration of zones in the stope hanging wall prone to fracture propagation

5.3 Implications from the numerical analyses and the laboratory testing

At the surface of excavations walls, rock is subjected to low confinement normal to the surface, whilst subjected to high compressive stresses in the plane of the surface. Under such conditions fractures may develop due possibly to the induced tensile stress and extension strain sustained in the excavation wall rock. The walls of most Bushveld Complex mine excavations are exposed to these conditions for periods of time varying from months to years. The research has shown that these excavations may be susceptible to stress induced fracturing under such conditions, particularly when time-dependency is taken into account.

Images of zones around modelled excavation walls prone to fracture propagation, according to this discussion are depicted in Figures 5-2 to 5-3. Note that only extension strain values (negative strains) were contoured in both images. In these illustrations, the estimated depth of extension strain, representative of the magnitude of extension strain at tensile failure, is read off as 0.5m into the pillar sidewall and 18.7m into the stope hanging wall. However these values are theoretical and do not consider the presence of parting planes and other weakness planes which may modify the magnitudes of the zones depicted here.

The research results have thus helped to explain some of the observed failure in intact rock forming the rock mass hosting mines in the BC.

CHAPTER 6

CONCLUSIONS AND RECOMMENDATIONS

The research detailed in this dissertation has dealt with the investigation of stress and strain conditions influencing spalling of wall rock in Bushveld Complex mine excavations. This involved a review of the Bushveld Complex mining environment, a review of literature relevant to time-dependent behaviour of rock, laboratory testing of Bushveld Complex rocks in uniaxial compression and in indirect tension, including time-dependent indirect tension, and elastic numerical modelling of typical mine excavations. The following are the conclusions from the research:

- There have been very few time-dependent or creep tests carried out in South Africa on rock, particularly on Bushveld Complex rock types. The laboratory testing carried out for the research described in this dissertation has now provided some data in this regard, which represents a contribution of new knowledge.
- The Brazilian test does not appear to have been used before in time-dependent tests, and the new data provided from this research again represent a contribution of new knowledge. The BIT creep tests proved to be quick and effective for establishing time-dependent behaviour of rock under (indirect) tension.
- The magnitude of the tensile strength of BC rock types was equal to approximately 5% of their compressive strength magnitudes.
- The long term uniaxial compressive strength of the BC rocks, interpreted from the axial stress-volumetric strain graph from the UCS test, is, on average, 78MPa, 56% of the UCS value.
- The tensile strength of the BC rock types was found to be time-dependent. However, the minimum long term tensile strength value could not be determined in this research owing to limited testing machine availability. Although the logarithmic time-to-failure of the nine test categories in the research showed a general time-dependent trend, the individual test specimen failure times showed a large variation.

- Extension strains at tensile strength failure ranged between 1.6×10^{-4} and 2.1×10^{-4}. Values corresponding with the long term tensile strength are less than 70% of this range, namely, less than 1.1×10^{-4} to 1.5×10^{-4}.
- Numerical analysis of BC excavations was carried out using elastic models and assuming homogeneity of material based on average elastic properties of several BC rock types. The compressive stresses determined in the models were found to be an order of magnitude lower than the compressive strength of the rock. Tensile stresses were of comparable magnitude to the tensile strength of the BC rock types investigated in this research.
- The numerical models showed that large zones of extension strain can occur around BC excavations, and that the magnitudes of the extension strain exceed the critical values determined from the laboratory testing.
- Observations made in actual BC mine excavations revealed that fracturing of intact rock occurs over a protracted time period, and that its manifestation is curbed by installed support.
- There is no conclusive prerequisite for tensile conditions to exist, to induce critical extension strain. Both compressive and tensile stress conditions were observed to generate critical (negative) extension strain.

The research that has been described has focused on the tensile and extension behaviour of Bushveld Complex rocks. This research could not conclusively establish the long term tensile strengths, but managed to establish the time-dependent behaviour of several BC rock types. What has been established is that the long term tensile strength is less than 70% of the normal tensile strength, and probably less than 60% of this value. Numerical modelling has established that substantial zones of extension strain occur around BC mining excavations, and that the magnitudes of these strains exceed the strain magnitudes corresponding with tensile strength failure. The implication of this is that there are substantial zones surrounding BC mine excavations that will be prone to spalling conditions and perhaps more significant failure.

The main conclusion from the research is that tensile and extension behaviour is very important and should be given more attention. It is recommended that further

programmes of time-dependent testing of BC rocks should be carried out in the future.

REFERENCES

Anderson, E. M. (1951). The Dynamics of Faulting (2nd. Ed.). Oliver & Boyd, Edinburgh, 208p.

Ashby, M. F. and Hallam, S. D. (1986). The failure of brittle solids containing small cracks under compressive stress states. *Acta metall***,** Vol. 34, No. 3, pp. 497-510.

Barnes, S-J. and Maier, W. D. (2002). Platinum-Group Element Distribution in the Rustenberg Layered Suite of the Bushveld Complex South Africa. *The Geology, Geochemistry, Mineralogy and Mineral Beneficiation of Platinum-Group Elements,* Ottawa, Ontario, Can. Inst. Min. and Met. Spec. Vol. 54, pp431-458.

Berenbaum, R. and Brodie, I. (1959). Measurement of the tensile strength of brittle materials. *Britain Journal of Applied Physics* 10, pp282-287.

Bérest, P., Blum, P. A., Charpentier, J. P., Gharbi, H. and Valès, F. (2005). Very slow creep tests on rock samples. *Int. J. Rock Mech. & Min. Sci.,* 42, pp 569 -576.

Bernier, F., Sillen, X. and Marivoet, J. (2004). Lessons learned with respect to (Excavtion Damage Zone) EDZ in Plastic Clays, Luxemburg, 3–5 November 2003, European Commission Report EUR 21028 EN.

Bétournay, M. C. and Mitri, H. S. (2003). Laboratory simulation of the behaviour of highly stressed mining fronts. *ISRM 2003-Technology roadmap for rock mechanics, South African Institute of Mining Metallurgy.*

Bieniawski, Z. T. (1967a). The Mechanism of Brittle Fracture of Rock. *International Journal of Rock Mechanics and Mining Sciences,* Vol. 4, pp. 396–435.

Bieniawski, Z. T. (1967b). Mechanism of Brittle of Rock, Part 2. *South African Council for Scientific and Industrial Research (CSIR) Institute – Technology and Engineering*, pg. 452.

Bieniawski, Z. T. (1967c). Mechanism of Brittle of Rock, Part 3. *South African Council for Scientific and Industrial Research (CSIR) Institute – Technology and Engineering*, pg. 452.

Bieniawski, Z. T. (1969). Brittle Failure of Rock Materials: The results and Constitutive models. *CSIR.*

Bieniawski, Z. T., Denkhaus, H. G. and Vogler, U. W. (1969). Failure of fractured rock. *International Journal of Rock Mechanics, Mineral Science and Geomechanics.* Abtsr., vol. 6, 323-341, 197.

Bieniawski, Z. T. (1970). Time-dependent behaviour of brittle rock. *CSIR.*

Bieniawski, Z. T. (1989). Engineering rock mass classifications. Wiley, New York, 251p.

Blümling, P., Bernier, F., Lebon, P. and Derek Martin, C. (2007). The excavation damaged zone in clay formations - time-dependent behaviour and influence on performance assessment. *Physics and Chemistry of the Earth* 32, pp 588–599.

Boidy, E., Bouvard A. and Pellet F. (2002). Back analysis of time-dependent behaviour of a test gallery in claystone. *International Journal of Tunneling and Underground Space Technology* 17, pp415–424.

Bonini, M., Debernardi, D., Barla, M. and Barla, G. (2009). The mechanical behaviour of clay shales and implications on the design of tunnels. *Rock Mechanics and Rock Engineering Journal,* vol. 42 (2), pp361-388.

Brace, W. F. (1964). State of stress in the earth's crust. Ed. Judd, American Elsevier Publishing Co. New York, pp111 – 180.

Brace, W. F. and Tapponier, P. (1976). Development of stress induced micro-cracks in Westerly granite. *Int. J. Rock Mech. Min. Sci.& Geomech., Abstr.* Vol. 13, pp 103 – 122, Pergamon Press, Great Britain.

Brady, B. H. G. and Brown, E. T. (1985). Rock Mechanics for Underground Mining, London, Boston: Allen & Unwin.

Brouard, B. (1988). On the behaviour of solution mined caverns. PhD. thesis, Ecole Polytechnique, France.

Brown, R. (2005). The PGE Reefs of the Bushveld Complex and the Great Dyke. *Unpublished AngloPlatinum Exploration Geology Report.*

Cameron, E. N. and Desborough, G. A. (1964). Origin of certain magnetite bearing pegmatite in the eastern part of the Bushveld Complex South Africa. *Economics of Geology,* 59 (1964), pp 197–225.

Cawthorn, R.G. (1999). The Platinum and Palladium resources of the Bushveld Complex, *South African Journal of Science*, 95, Nov. 1999.

Cawthorn, R.G. and Boerst, K. (2006). Origin of the Pegmatite Pyroxenite in the Merensky Unit, Bushveld Complex South Africa. *Journal of Petrology,* Vol. 47, No. 8, pp1509-1510.

Charpentier, J.P. (1988). Creep of rock salt at elevated temperature. In: *Proceedings of second conference on the mechanical behaviour of salt.* Clausthal-Zellerfeld, Germany: Transactions of Technical Publishers, pp 131 – 136.

Chen, C.S. and Hsu, S. C. (2001). Measurement of indirect tensile strength of anisotrpic rocks by the ring test. *Journal of Rock Mechanics and Rock Engineering,* Vol. 34, Iss. 4 pp 293-321.

Critescu, N. D. and Hunsche, U. (1998). Time effects in rock mechanics, Series in materials modeling and computation, Wiley, Chi Chester, U.K., ISBN 0471 955175.

D' Elia, B. (1991). Deformation problems in the Italian structurally complex clay soils. In: *Proc. 10th Europ. Conf. on Soil Mech. and Found. Eng.*, Vol. 4, pp 1159–1170.

Diederichs, M.S. (2002). Stress induced damage accumulation and implications for hard rock engineering. In: Hammah, R., Bawden, W., Curran, J., Telesnicki, M., (eds.) Mining and Tunneling innovation and opportunity. Proceedings of the 5th North American Rock Mechanism Symposium and the 17th tunneling Association of the Canada Conference, Toronto 1: 3-12. Univ. Toronto *Press*, Toronto.

Diederichs, M. S., Kaiser, P. K. and Eberhardt, E. (2004). Damage initiation and propagation in hard rock during tunneling and the influence of near face stress rotation. *Int. J. rock Mech. Min. Sci.* 41: pp785-812.

Diederichs, M.S. (2007). The Canadian Geotechnical Colloquim: Mechanistic interpretation and practical application of damage and spalling prediction criteria for deep tunneling. Can. Geotech. J. 44: pp1082-1116.

Drescher, K. (2002). An investigation into the mechanics of time-dependent deformation of hard rocks. MSc. Faculty of Engineering, University of Pretoria, Pretoria.

Drescher, K. and Handley, M. F. (2003). Aspects of time-dependent deformation in hard rock at great depth. *Journal of the South African Institute of Mining and Metallurgy*, Vol. 103, No. 5, pp 325.

Dubey, R. K. and Gariola, V. K. (2008). Influence of structural anisotropy on creep of rocksalt from Simla Himalaya, India: An experimental approach. *Journal of Structural Geology*, 30 (6), pp710-718.

Duncan, N., (1969). Engineering Geology and Rock Mechanics, Leonard Hill, London.

Duncan, E. J. S. and Lajtai, E. Z. (1993). The Creep of Potash salt from Saskatchewan. *Geotechnical and Geological Engineering Journal*, Vol. 11, No. 3.

Egerton, F.M.G. (2004). Presidential Address: The mechanics of UG2 mining in the Bushveld Complex. *SAIMM*.

Evans, I. (1961). The tensile strength of coal. *Colliery Eng*., Vol 38, pp 428–434.

Fabre, G. and Pellet, F. (2006). Creep and time-dependent damage in argillaceous rocks. *Int. J. of Rock Mech. and Min. Sci.*, Vol. 43, Iss. 6, pp 950-960.

Fairhurst, C. and Cook, N. G. W. (1966). The phenomenon of rock splitting parallel to the direction of maximum compression in the neighbourhood of a surface. In: *Proceedings of the First Congress on the International Society of Rock Mechanics*, Lisbon, pp 687-692.

Goodman, R. E. (1989): Introduction to rock mechanics, 2nd ed. Wiley, New York, pp 562.

Grimstad, E. and Bhasin, R. (1997). Rock support in hard rock tunnels under high stress. *Proc. Int. Symp. Rock Support – applied solutions for underground structures*, Lillehammer, Norway, ed. Broch, Myrvang, Stjern, Norwegian Society of Chartered Engineers, pp 504-513.

Halm, D. and Dragon, A. (1998). An anisotropic model of damage and frictional sliding for brittle materials. *European Journal of Mechanics, A/Solids.* Vol. 17, No. 3, pp. 439 – 460.

Hobbs, D. W. (1964). An assessment of a technique for determining the tensile strength of rock. *Brit. J. Appl. Phys*. Vol. 16.

Hoek, E. and Bieniawski, Z. T. (1965). Brittle rock fracture propagation in rock under compression. *Int. J. Fracture Mech.* 1, 137 -155.

Hondros, G. (1959). Evaluation of Poisson's ratio and the modulus of materials of low tensile resistance by the Brazilian (indirect tensile) test with particular references to concrete. *Australian Journal of Applied Science,* 10 (3) pp. 243–268.

Hudson, J. A., Brown, E. T. and Rummel, F. (1972). The controlled failure of rock discs and rings loaded in diametral compression. *Int. J. Rock Mech.Min. Sci.* Vol. 9, pp. 241-248.

Hunsche, U. (1988). Measurement of creep in rock salt at small strain rates. In: *Proceedings of second conference on the mechanical behaviour of salt.* Clausthal-Zellerfeld, Germany: Transactions of Technical Publishers, pp.187–196.

ISRM (1981). Suggested methods for rock characterisation, testing and monitoring.

ISRM (2007). The complete ISRM Suggested Methods for Rock Characterisation, Testing and Monitoring: 1974-2006. *Editors:* Ulisay, R. & Hudson, J. A.

Jaeger, J. C. and Cook, N. G. (1979). Fundamentals of rock Mechanics. Chapman and Hill Ltd. and Science Paperbacks.

Jaeger, J. C. and Hoskins, E. R. (1966). Rock failure under the confined Brazilian test. *J. Geophys. Res.* 71, pp. 2651–2659.

Kovács, I. K. A. (1971). An investigation of the time-dependent behaviour of solid rock in uniaxial compression. *National Mechanical Engineering Research Institute, Council for Scientific and Industrial Research Report,* MEG 1032, Pretoria, South Africa.

Kranz, R. L. (1976). Crack growth and development during creep of Barre granite. *Int. J. Rock Mech. Min. Sci. & Geomech*. Abstr. 16, pp. 23-35.

Krausz, A. S. and Krausz, K. (1988). Fracture kinetics of crack growth. Kluwer Academic Publishers, Dordrecht, The Netherlands.

Lajtai, E. Z. (1990). Time-dependent behaviour of the rock mass. *Journal of Geotechnical and Geological Engineering*, Pages 109-124.

Li, D., Li, C. C. and Li, X. (2010). Influence of sample height-to-width ratios on failure mode for rectangular prism samples of hard rock loaded in Uniaxial compression. *Rock Mech. Rock Eng., 44: 255-267.*

Li, Y. and Xia, C. (1999). Time-dependent tests on intact rocks in uniaxial compression. *Int. J. Rock Mech. and Mining Sciences*, Vol. 37, Issue 3, pp. 467-475.

Lockner, D. A., Moore, D. E. and Reches, Z. (1992). Micro-crack interaction leading to shear fracture. *The 33rd Symposium on Rock Mechanics (USRMS).* A. A. Balkaema, Rotterdam.

Lomberg, K. G., Martin, E. S., Patterson, M. A. and Venter, J. E. (1999). The morphology of potholes in the UG2 chromicise layer and Merensky Reef (pothole reef facies) at Union Section, Rustenburg Platinum Mines. *South African Journal of Geology,* Vol. 102 pp. 209–220.

Malan, D. F. (1998). An investigation into the identification and modeling of time-dependent behaviour of deep level excavation in hard rock. PhD. thesis University of the Witwatersrand, JHB, 1998.

Malan, D. F., Napier, J. A. L. and Van Janse Rensburg, A. L. (2007). Stope deformation measurements as a diagnostic measure of rock behaviour: A decade of research. *Journal of The South African Institute of Mining and Metallurgy,* 107 (11), pp. 743 – 765.

Mellor, M. and Hawkes, I. (1971). Measurement of tensile strength by diametrical compression. *Engineering Geology,* Vol. 5, pp. 173 – 225.

Mercer, K. G. (2006)**.** Investigation into the time dependent deformation behaviour and failure mechanisms of unsupported rock slopes based on the interpretation of observed deformation behaviour. PhD. Thesis University of the Witwatersrand, Johannesburg.

Mitchell, A. A. and Manthree, R. (2002). The Giant Mottled Anorthosite: a transitional sequence at the top of the Upper Critical Zone of the Bushveld Complex. *South African Journal of Geology,* Vol. 105, No. 1, pp. 15 – 24.

Myrvang, A. M., Alnaes, L., Hansen, S. E. and Davik, K. I. (2000). Heavy spalling problems in road tunnels in Norway – long time stability and performance of sprayed concrete as rock support. *Proc. Int. Symp. Rock Support – applied solutions for underground structures*, Lillehammer, Norway, ed. Broch, Myrvang, Stjern, Norwegian Society of Chartered Engineers, pp 751-764.

Naldrett, A. J., Wilson, A., Kinnaird, J. and Chunnett, G. (2009). PGE Tenor and Metal Ratios within and below the Merensky reef, Bushveld Complex: Implications for its genesis. *Journal of Petrology,* egp015v1.

Okubo, S. and Fukui, K. (1996). Complete stress strain curves for various rock types in uniaxial tension. *Int. J. Rock Mech. Min. Sci. & Geomech. Abstr.* Vol. 33. No. 6. pp 549 – 556.

Ortlepp, W. D. (1997). Rock fracture and rockbursts – an illustrative study. *J. S. Afr. Inst. Min. Metall.,* pp 255.

Pellet, F., Roosefid, M. and Deleruyelle, F. (2009). On the 3-D numerical modelling of the time-dependent development of the damage zone around underground galleries during and after excavation. *Journal of Tunnelling and Underground Space Technology,* Vol. 24, Iss. 6, pp 665-674.

Perrit, S. and Roberts, M. (2007). Flexural-slip structures in the Bushveld Complex, South Africa? *Journal of Structural Geology, 29, Johannesburg, South Africa.*

Pollard, D. D. and Fletcher, R. C. (2005). Fundamentals of structural geology. *Cambridge University Press,* pp. 228.

Rangasamy, T. R. (2010). IMP03: Geotechnical report, Impala 18#. Unpublished company report, Middindi Consulting Pty. (Ltd.).

Reches, Z. and Lockner, D. A. (1994). The nucleation and growth of faults in brittle rocks. *J. Geophys. Res., 99,* 18,159-18,174.

Rinne, M. (2008). Fracture mechanics and subcritical crack growth approach to model time-dependent failure in brittle rock. PhD. Thesis, Faculty of Engineering and Architecture, Dep. Of Civil and Environmental Engineering, Helsinki University of Technology, Helsinki.

Ryder, J. A. and Jager, A. J. (2002). A textbook on rock mechanics for tabular hard rock mines. *The Safety in Mines Research Advisory Committee (SIMRAC), Johannesburg.*

Salganik., R., L., Rapoport, I., and Gotlib, V. A. (1994). Delayed fracture in brittle wear: an approach. *Int. J. of Fracture,* Vol.68*,* pp. 65-72.

Schmidtke, R. H. and Lajtai, E. Z. (1985). The long-term strength of Lac du Bennet granite. *Int. J. Rock Mech. Min Sci. Geomech. Abstr,* 22, pp. 461-465.

Seabrook, C. L., Cawthorn, G. and Kruger, F. J. (2002). The Merensky reef, Bushveld Complex: Mixing of minerals not mixing of magmas. *Econ. Geo.,* Vol. 100, No. 6, pp. 1191 - 1206.

Simmat, C. M., Herselman, P., Le R., R¨utschlin, M., Mason, I.M. and Cloete, J.H. (2006). Remotely sensing the thickness of the Bushveld Complex UG2 platinum reef using borehole radar. *Journal of Geophysics and Engineering,* Vol. 3, pp. 43 – 49.

Smith, D. S. and Basson, I. J. (2006). Shape and distribution analysis of Merensky Reef potholing, Northam Platinum mine, western Bushveld Complex: Implications for pothole formation and growth. *Minerallium Deposita April 2006,1-15.*

Stacey, T. R. (1981). A simple extension strain criterion for fracture of brittle rock. *Int. J. Rock Mech. Min. Sci. Geomech.* Abstr., Volume 18:6, pp 469-474.

Stacey, T. R. (2002). Best practice rock engineering for other mines. *The Safety in Mines Research Advisory Committee (SIMRAC), Johannesburg.*

Stacey, T. R. and Yathavan, K. (2003). Examples of fracturing of rock at very low stress levels. *ISRM – Technology roadmap for rock mechanics, South African Institute of Mining and Metallurgy*.

Stacey, T. R. and Wesseloo, J. (2004). Updated stress database for South Africa. *In-situ Rock Stress, Lu, Li and Dalde (eds.) Taylor and Francis, pp. 461 – 471.*

Stacey, T. R. and Yathavan, K. (2004). Laboratory observations relevant to fracture initiation at low stress levels. *Abstr: The miner's guide through the earth's crust, South African National Institute of Rock Engineers.*

Szwedzicki, T. (2006). A hypothesis on mode of failure of rock samples tested in uniaxial compression. *Journal of Rock Mechanics and Rock Engineering*. Vol. 40, No. 1, pp. 97-104.

Viljoen, M. J. and Schürmann, L. W. (1998). Platinum-Group Metals. In: Wilson, M.G.S. & Anhaeusser, C. R. (eds.)*, The Mineral Resources of South Africa, Council for Geoscience,* 532-568*.*

Wang, Q. Z., Jia, X. M., Kou, S. Q., Zhang, Z. X. and Lindqvist, P–A. (2004). The flattened Brazilian disc specimen used for testing elastic modulus, tensile strength and fracture toughness of brittle rocks: analytical and numerical results. *Int. J. Rock Mech. & Min. Sci.,* 41, pp. 245 – 253.

Wang, Z., Wong, R. C. K. and Qiao, L. (2011). Investigation on relations between grain crushing amounts and void ratio change of granular materials in one-dimensional compression and creep tests. *J. Rock Mech. And Geotech. Eng., 3 (Supp.) 415 – 420.*

Watson, B. P., Kuipers, J. S., Henry G., Palmer, C. E. and Ryder J. A. (2009), Nonlinear rock behaviour and its implications for deeper level platinum mining. *SAIMM,* Vol. 108, Refereed Paper, pp 5-9.

Wawersik, W. R. (1972). Time-dependent rock behaviour in uniaxial compression. *Proc. 14th Symp. On Rock Mech, ASCE,* pp. 85 – 106.

Wilson, A. and Chunnett, G. (2006). Trace element and Platinum Group element distributions and the genesis of the Merensky Reef, Western Bushveld Complex, South Africa. *Journal of Petrology,* Vol. 47, No. 12, pp 2369-2403.

Yilmaz, H. (2010). Tensile strength testing of thin spray-on liner products (TSLs) and shotcrete. *Journal of The Southern African Institute of Mining and Metallurgy,* vol. 110, No. 10, pp 559.

Zhao, B., Liu, D. and Dong, Q. (2011). Experimental research on creep behaviours of sandstone under uniaxial compressive and tensile stress. *Journal of Rock Mechanics and Geotechnical Engineering, 3 (Supp.): 438 - 444.*

***Internet sources*:**

1. Namakando, M. (2006). Chief Editor esnet: Mining in South Africa. INTERNET.http://es.net.oneworld.net/sections/mining-in-south-africa/ Cited 9 May 2012.

2. Hilliard, H. E. (1996). Platinum Group Metals. INTERNET.http://minerals.usgs.gov/minerals/pubs/commodity/platinum/550496.pdf Cited 9 May 2012.

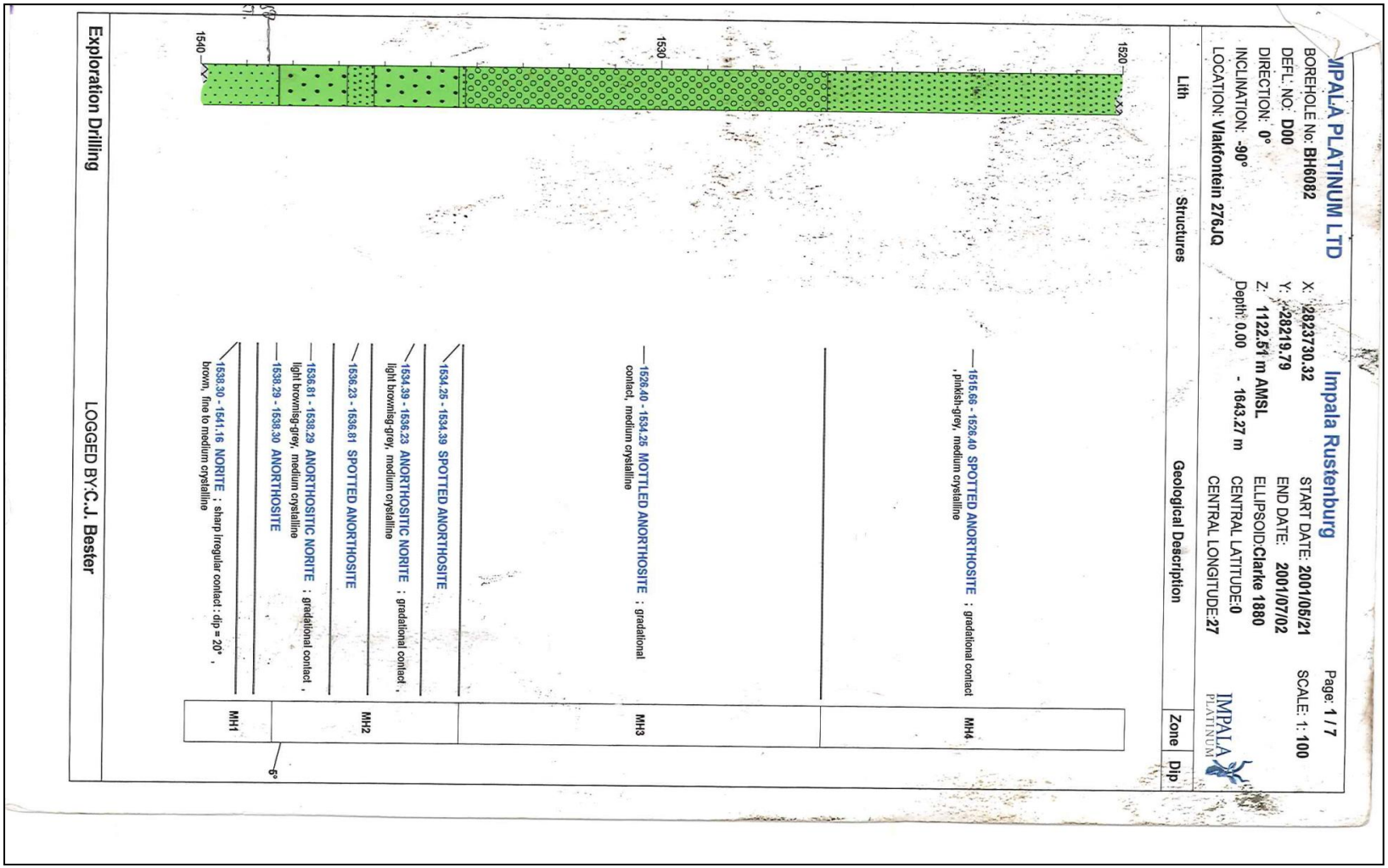
3. Chamber of Mines (2010). South African Mining Industry snapshot 2009.INTERNET.http://www.bullion.org.za/ Cited 9 May 2012.

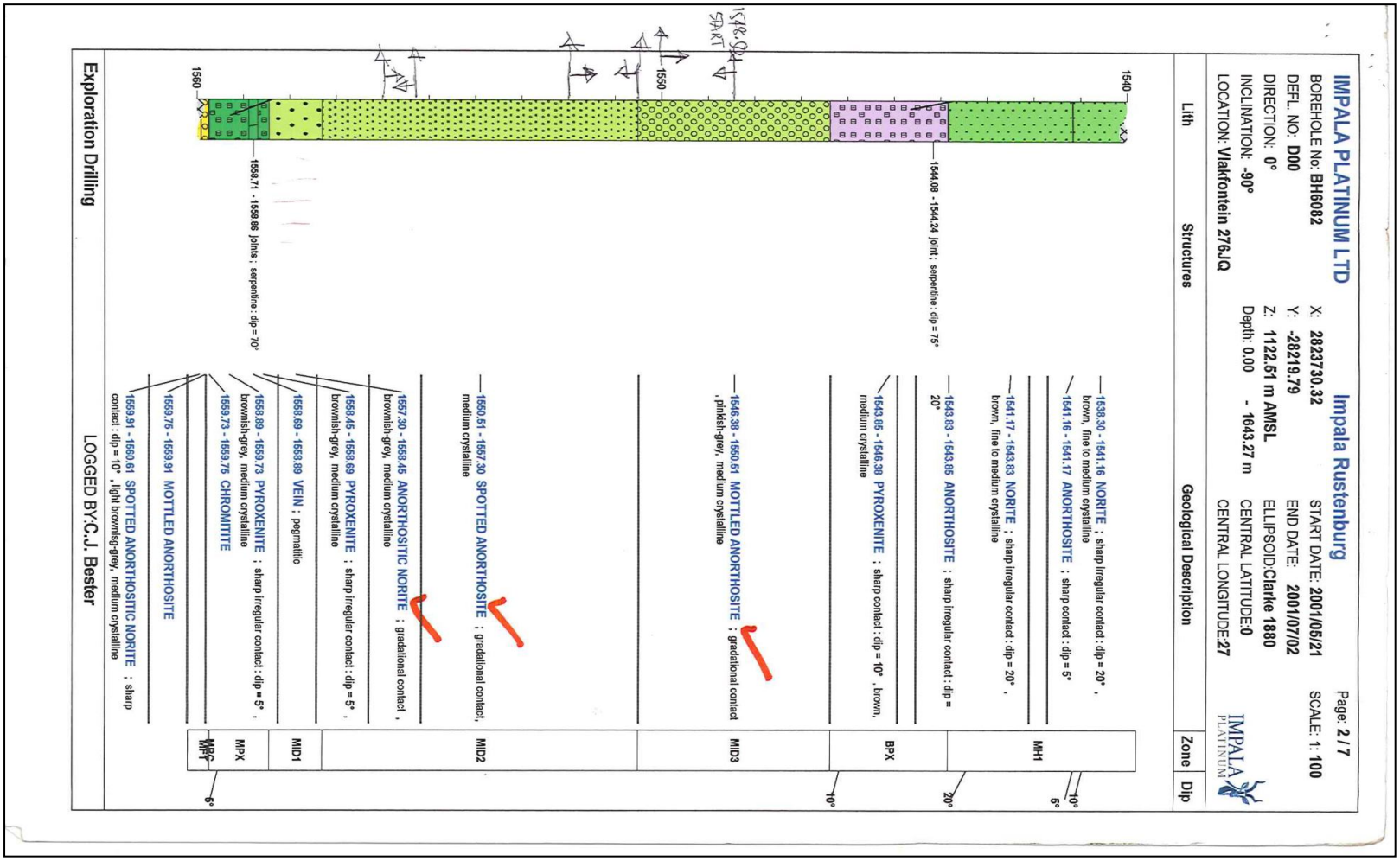
APPENDICES

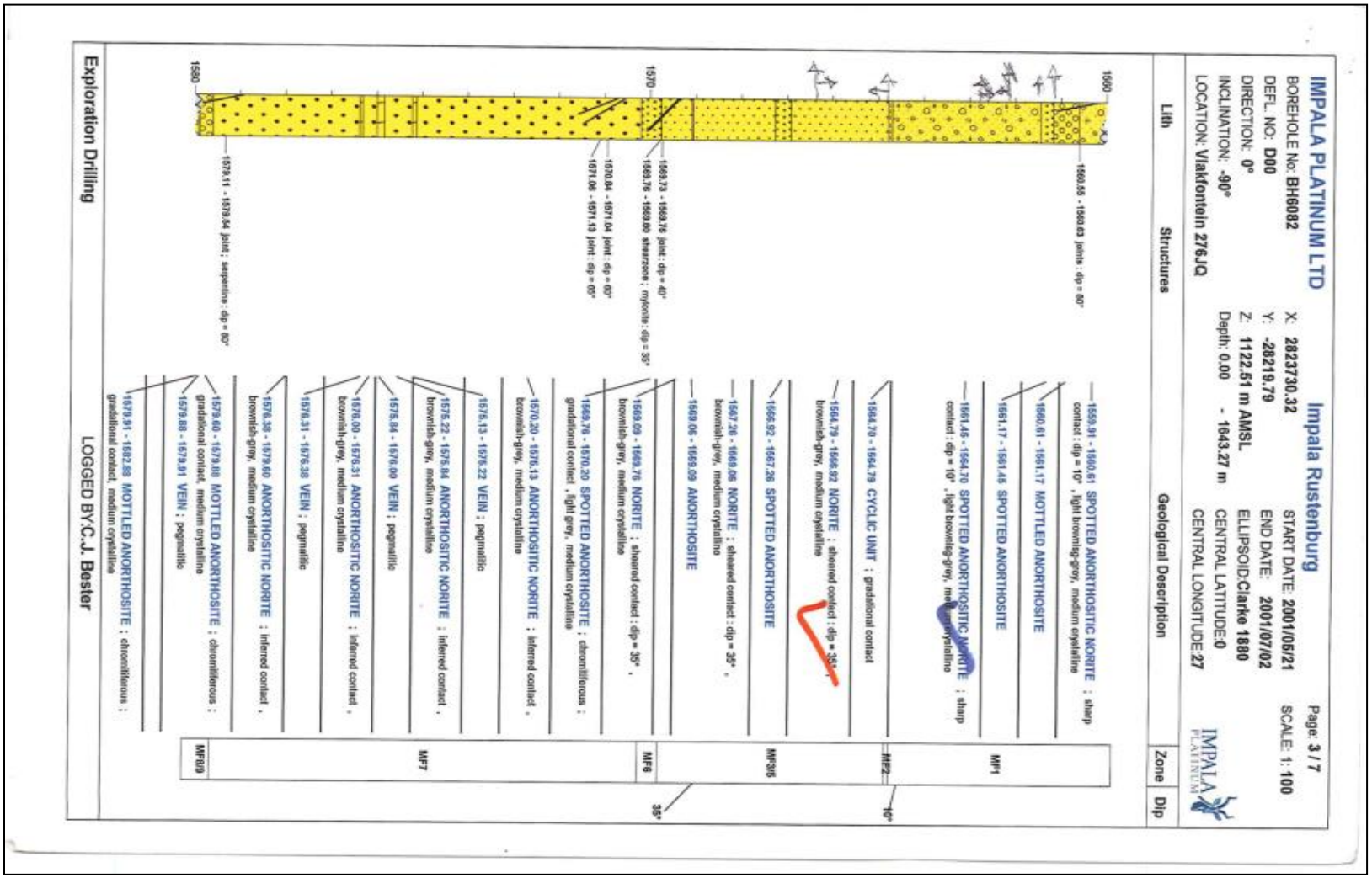
Appendix A: Geological log sheet for drill hole BH6082

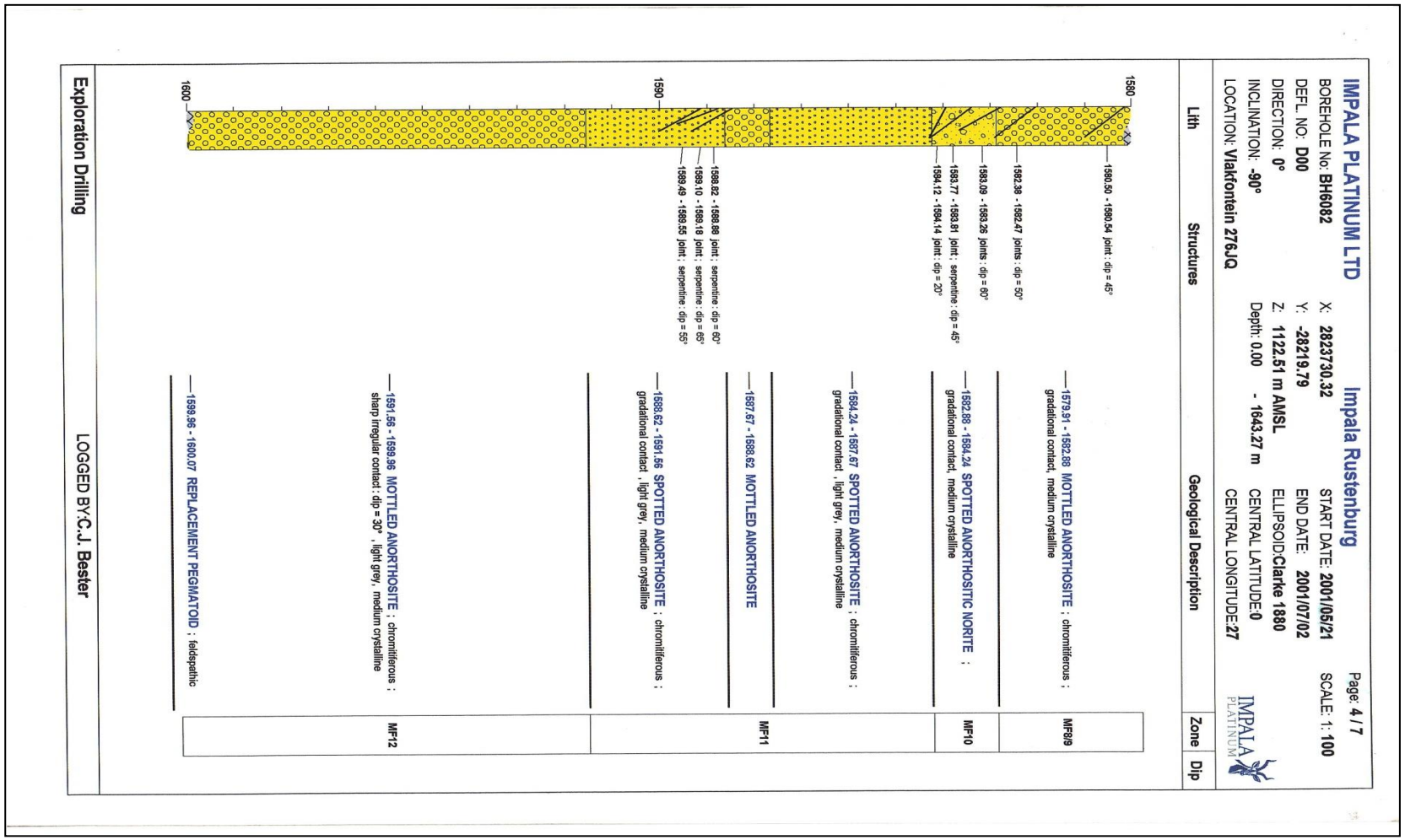
Borehole BH6082 was used to prepare laboratory test specimens in this research and the log sheet is given in Table A1-1. The drill hole was part of Impala Platinum's Rustenburg surface exploration drilling in the Rustenburg Layered Suite. The markings on the log sheet were made during the preparation of samples.

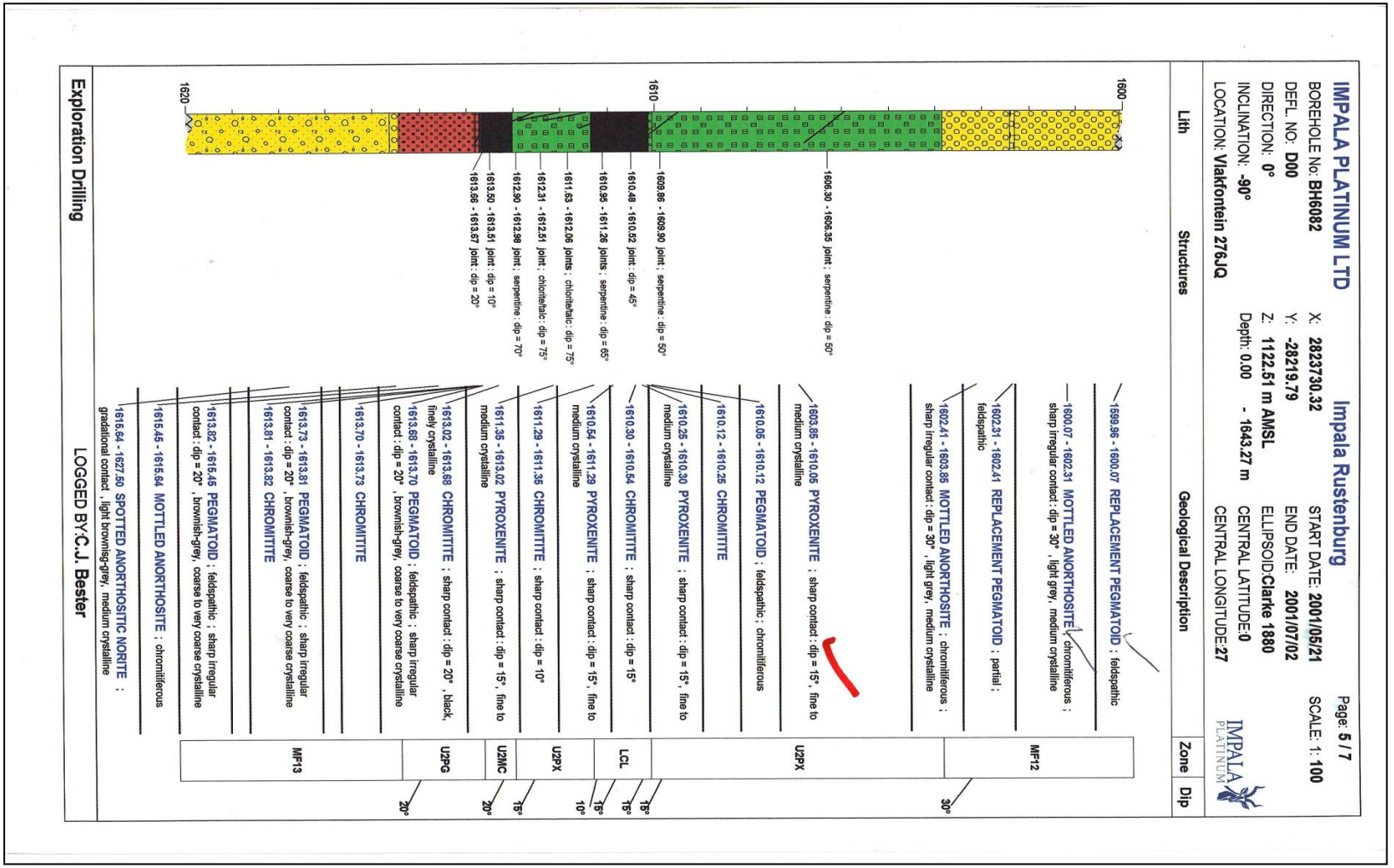
Appendix A1-1: Geological log sheet for borehole BH6082

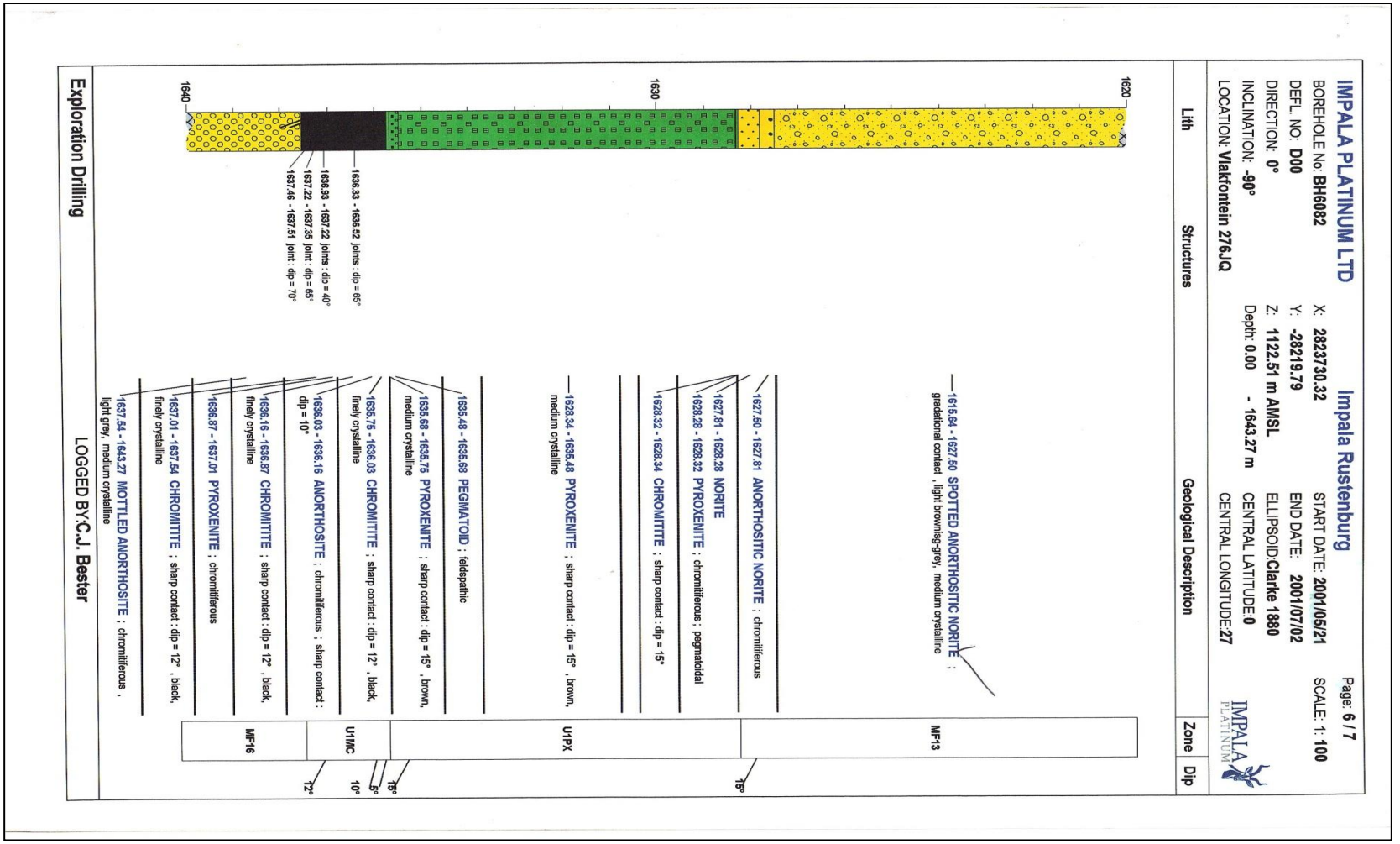

IMPALA PLATINUM LTD
Impala Rustenburg
BOREHOLE No: BH6082
DEFL: NO: D00
DIRECTION: 0°
INCLINATION: -90°
LOCATION: Vlakfontein 276JQ
X: 2823730.32
Y: 28219.79
Z: 1122.51 m AMSL
Depth: 0.00 - 1643.27 m
START DATE: 2001/05/21
END DATE: 2001/07/02
ELLIPSOID:Clarke 1880
CENTRAL LATITUDE:0
CENTRAL LONGITUDE:27
Page: 1 / 7
SCALE: 1: 100
Lith
Structures
Geological Description
Zone
Dip
1520
1530
1540
1515.66 - 1526.40 SPOTTED ANORTHOSITE ; gradational contact , pinkish-grey, medium crystalline
MH4
1526.40 - 1534.25 MOTTLED ANORTHOSITE ; gradational contact, medium crystalline
MH3
1534.25 - 1534.39 SPOTTED ANORTHOSITE
1534.39 - 1536.23 ANORTHOSITIC NORITE ; gradational contact , light brownisg-grey, medium crystalline
1536.23 - 1536.81 SPOTTED ANORTHOSITE
MH2
1536.81 - 1538.29 ANORTHOSITIC NORITE ; gradational contact , light brownisg-grey, medium crystalline
1538.29 - 1538.30 ANORTHOSITE
1538.30 - 1541.16 NORITE ; sharp irregular contact : dip = 20° , brown, fine to medium crystalline
MH1
8°
Exploration Drilling
LOGGED BY:C.J. Bester


IMPALA PLATINUM LTD
Impala Rustenburg
BOREHOLE No: BH6082
DEFL. NO: D00
DIRECTION: 0°
INCLINATION: -90°
LOCATION: Vlakfontein 276JQ
X: 2823730.32
Y: -28219.79
Z: 1122.51 m AMSL
Depth: 0.00 - 1643.27 m
START DATE: 2001/05/21
END DATE: 2001/07/02
ELLIPSOID:Clarke 1880
CENTRAL LATITUDE:0
CENTRAL LONGITUDE:27
Page: 2 / 7
SCALE: 1: 100
IMPALA PLATINUM
Lith
Structures
Geological Description
Zone
Dip
1540
1550
1560
1544.08 - 1544.24 joint ; serpentine ; dip = 75°
1558.71 - 1558.88 joints ; serpentine ; dip = 70°
1538.30 - 1541.16 NORITE ; sharp irregular contact : dip = 20° , brown, fine to medium crystalline
1541.16 - 1541.17 ANORTHOSITE ; sharp contact : dip = 5°
1541.17 - 1543.83 NORITE ; sharp irregular contact : dip = 20° , brown, fine to medium crystalline
1543.83 - 1543.85 ANORTHOSITE ; sharp irregular contact : dip = 20°
1543.85 - 1546.38 PYROXENITE ; sharp contact : dip = 10° , brown, medium crystalline
1546.38 - 1550.51 MOTTLED ANORTHOSITE ; gradational contact , pinkish-grey, medium crystalline
1550.51 - 1557.30 SPOTTED ANORTHOSITE ; gradational contact, medium crystalline
1557.30 - 1558.45 ANORTHOSITIC NORITE ; gradational contact , brownish-grey, medium crystalline
1558.45 - 1558.69 PYROXENITE ; sharp irregular contact : dip = 5° , brownish-grey, medium crystalline
1558.69 - 1558.89 VEIN ; pegmatitic
1558.89 - 1559.73 PYROXENITE ; sharp irregular contact : dip = 5° , brownish-grey, medium crystalline
1559.73 - 1559.75 CHROMITITE
1559.75 - 1559.91 MOTTLED ANORTHOSITE
1559.91 - 1560.61 SPOTTED ANORTHOSITIC NORITE ; sharp contact : dip = 10° , light brownish-grey, medium crystalline
MH1
BPX
MID3
MID2
MID1
MPX
MPC
10°
5°
20°
10°
5°
Exploration Drilling
LOGGED BY:C.J. Bester


IMPALA PLATINUM LTD
Impala Rustenburg
BOREHOLE No: BH6082
DEFL. NO: D00
DIRECTION: 0°
INCLINATION: -90°
LOCATION: Vlakfontein 276JQ
X: 2823730.32
Y: -28219.79
Z: 1122.51 m AMSL
Depth: 0.00 - 1643.27 m
START DATE: 2001/05/21
END DATE: 2001/07/02
ELLIPSOID:Clarke 1880
CENTRAL LATITUDE:0
CENTRAL LONGITUDE:27
Page: 3 / 7
SCALE: 1: 100
Lith
Structures
Geological Description
Zone
Dip
1560
1570
1580
1560.55 - 1560.63 joints : dip = 60°
1559.91 - 1560.61 SPOTTED ANORTHOSITIC NORITE ; sharp contact : dip = 10° , light brownish-grey, medium crystalline
1560.61 - 1561.17 MOTTLED ANORTHOSITE
1561.17 - 1561.45 SPOTTED ANORTHOSITE
MF1
1561.45 - 1564.70 SPOTTED ANORTHOSITIC NORITE ; sharp contact : dip = 10° , light brownish-grey, medium crystalline
1564.70 - 1564.79 CYCLIC UNIT ; gradational contact
MF2
10°
1564.79 - 1568.92 NORITE ; sheared contact : dip = 35° , brownish-grey, medium crystalline
1568.92 - 1567.26 SPOTTED ANORTHOSITE
MF3/5
1567.26 - 1569.06 NORITE ; sheared contact : dip = 35° , brownish-grey, medium crystalline
1569.06 - 1569.09 ANORTHOSITE
1569.09 - 1569.76 NORITE ; sheared contact : dip = 35° , brownish-grey, medium crystalline
MF6
35°
1569.76 - 1570.20 SPOTTED ANORTHOSITE ; chromitiferous ; gradational contact , light grey, medium crystalline
1570.20 - 1576.13 ANORTHOSITIC NORITE ; inferred contact , brownish-grey, medium crystalline
1576.13 - 1576.22 VEIN ; pegmatitic
1576.22 - 1576.84 ANORTHOSITIC NORITE ; inferred contact , brownish-grey, medium crystalline
MF7
1576.84 - 1576.00 VEIN ; pegmatitic
1576.00 - 1576.31 ANORTHOSITIC NORITE ; inferred contact , brownish-grey, medium crystalline
1576.31 - 1576.38 VEIN ; pegmatitic
1576.38 - 1579.60 ANORTHOSITIC NORITE ; inferred contact , brownish-grey, medium crystalline
1579.60 - 1579.88 MOTTLED ANORTHOSITE ; chromitiferous ; gradational contact, medium crystalline
MF8/9
1579.88 - 1579.91 VEIN ; pegmatitic
1579.91 - 1582.88 MOTTLED ANORTHOSITE ; chromitiferous ; gradational contact, medium crystalline
1578.11 - 1579.54 joint ; serpentine : dip = 80°
Exploration Drilling
LOGGED BY:C.J. Bester


IMPALA PLATINUM LTD
Impala Rustenburg
BOREHOLE No: BH6082
DEFL. NO: D00
DIRECTION: 0°
INCLINATION: -90°
LOCATION: Vlakfontein 276JQ
X: 2823730.32
Y: -28219.79
Z: 1122.51 m AMSL
Depth: 0.00 - 1643.27 m
START DATE: 2001/05/21
END DATE: 2001/07/02
ELLIPSOID:Clarke 1880
CENTRAL LATITUDE:0
CENTRAL LONGITUDE:27
Page: 4 / 7
SCALE: 1: 100
Lith
Structures
Geological Description
Zone
Dip
1580
1590
1600
1580.50 - 1580.54 joint : dip = 45°
1582.38 - 1582.47 joints : dip = 50°
1583.09 - 1583.28 joints : dip = 60°
1583.77 - 1583.81 joint : serpentine : dip = 45°
1584.12 - 1584.14 joint : dip = 20°
1588.82 - 1588.88 joint : serpentine : dip = 60°
1589.10 - 1589.18 joint : serpentine : dip = 65°
1589.49 - 1589.55 joint : serpentine : dip = 55°
1579.91 - 1582.88 MOTTLED ANORTHOSITE ; chromitiferous ; gradational contact, medium crystalline
1582.88 - 1584.24 SPOTTED ANORTHOSITIC NORITE ; gradational contact, medium crystalline
MF8/9
MF10
1584.24 - 1587.67 SPOTTED ANORTHOSITE ; chromitiferous ; gradational contact , light grey, medium crystalline
1587.67 - 1588.82 MOTTLED ANORTHOSITE
MF11
1588.82 - 1591.56 SPOTTED ANORTHOSITE ; chromitiferous ; gradational contact , light grey, medium crystalline
1591.56 - 1599.96 MOTTLED ANORTHOSITE ; chromitiferous ; sharp irregular contact ; dip = 30° , light grey, medium crystalline
MF12
1599.96 - 1600.07 REPLACEMENT PEGMATOID ; feldspathic
Exploration Drilling
LOGGED BY:C.J. Bester


IMPALA PLATINUM LTD
Impala Rustenburg
Page: 5 / 7
BOREHOLE No: BH6082
X: 2823730.32
START DATE: 2001/05/21
SCALE: 1: 100
DEFL. NO: D00
Y: -28219.79
END DATE: 2001/07/02
DIRECTION: 0°
Z: 1122.51 m AMSL
ELLIPSOID:Clarke 1880
INCLINATION: -90°
Depth: 0.00 - 1643.27 m
CENTRAL LATITUDE:0
LOCATION: Vlakfontein 276JQ
CENTRAL LONGITUDE:27
IMPALA PLATINUM
Lith
Structures
Geological Description
Zone
Dip
1600
1610
1620
1599.96 - 1600.07 REPLACEMENT PEGMATOID ; feldspathic
1600.07 - 1602.31 MOTTLED ANORTHOSITE ; chromitiferous ; sharp irregular contact : dip = 30° , light grey, medium crystalline
1602.31 - 1602.41 REPLACEMENT PEGMATOID ; partial ; feldspathic
1602.41 - 1603.85 MOTTLED ANORTHOSITE ; chromitiferous ; sharp irregular contact : dip = 30° , light grey, medium crystalline
MF12
30°
1603.85 - 1610.05 PYROXENITE ; sharp contact : dip = 15° , fine to medium crystalline
1610.05 - 1610.12 PEGMATOID ; feldspathic ; chromitiferous
1610.12 - 1610.25 CHROMITITE
1610.25 - 1610.30 PYROXENITE ; sharp contact : dip = 15° , fine to medium crystalline
1610.30 - 1610.54 CHROMITITE ; sharp contact : dip = 15°
1610.54 - 1611.29 PYROXENITE ; sharp contact : dip = 15° , fine to medium crystalline
1611.29 - 1611.35 CHROMITITE ; sharp contact : dip = 10°
1611.35 - 1613.02 PYROXENITE ; sharp contact : dip = 15° , fine to medium crystalline
U2PX
U2MC
U2PG
LCL
15°
10°
20°
1606.30 - 1606.35 joint ; serpentine : dip = 50°
1609.86 - 1609.90 joint ; serpentine : dip = 50°
1610.48 - 1610.52 joint : dip = 45°
1610.95 - 1611.26 joints ; serpentine : dip = 65°
1611.53 - 1612.06 joints ; chloritehalo : dip = 75°
1612.31 - 1612.51 joint ; chloritehalo : dip = 75°
1612.90 - 1612.98 joint ; serpentine : dip = 70°
1613.50 - 1613.51 joint : dip = 10°
1613.66 - 1613.67 joint : dip = 20°
1613.02 - 1613.68 CHROMITITE ; sharp contact : dip = 20° , black, finely crystalline
1613.68 - 1613.70 PEGMATOID ; feldspathic ; sharp irregular contact : dip = 20° , brownish-grey, coarse to very coarse crystalline
1613.70 - 1613.73 CHROMITITE
1613.73 - 1613.81 PEGMATOID ; feldspathic ; sharp irregular contact : dip = 20° , brownish-grey, coarse to very coarse crystalline
1613.81 - 1613.82 CHROMITITE
1613.82 - 1615.45 PEGMATOID ; feldspathic ; sharp irregular contact : dip = 20° , brownish-grey, coarse to very coarse crystalline
1615.45 - 1615.64 MOTTLED ANORTHOSITE ; chromitiferous
1615.64 - 1627.50 SPOTTED ANORTHOSITIC NORITE ; gradational contact , light brownisg-grey, medium crystalline
MF13
Exploration Drilling
LOGGED BY:C.J. Bester


IMPALA PLATINUM LTD
Impala Rustenburg
BOREHOLE No: BH6082
DEFL. NO: D00
DIRECTION: 0°
INCLINATION: -90°
LOCATION: Vlakfontein 276JQ
X: 2823730.32
Y: -28219.79
Z: 1122.51 m AMSL
Depth: 0.00 - 1643.27 m
START DATE: 2001/05/21
END DATE: 2001/07/02
ELLIPSOID:Clarke 1880
CENTRAL LATITUDE:0
CENTRAL LONGITUDE:27
Page: 6 / 7
SCALE: 1: 100
Lith
Structures
Geological Description
Zone
Dip
1620
1630
1640
1636.33 - 1636.52 joints : dip = 65°
1636.33 - 1637.22 joints : dip = 40°
1637.22 - 1637.35 joint : dip = 65°
1637.46 - 1637.51 joint : dip = 70°
1615.64 - 1627.50 SPOTTED ANORTHOSITIC NORITE ; gradational contact , light brownish-grey, medium crystalline
1627.50 - 1627.81 ANORTHOSITIC NORITE ; chromitiferous
1627.81 - 1628.28 NORITE
1628.28 - 1628.32 PYROXENITE ; chromitiferous ; pegmatoidal
1628.32 - 1628.34 CHROMITITE ; sharp contact : dip = 15°
1628.34 - 1635.48 PYROXENITE ; sharp contact : dip = 15° , brown, medium crystalline
1635.48 - 1635.68 PEGMATOID ; feldspathic
1635.68 - 1635.75 PYROXENITE ; sharp contact : dip = 15° , brown, medium crystalline
1635.75 - 1636.03 CHROMITITE ; sharp contact : dip = 12° , black, finely crystalline
1636.03 - 1636.16 ANORTHOSITE ; chromitiferous ; sharp contact : dip = 10°
1636.16 - 1636.87 CHROMITITE ; sharp contact : dip = 12° , black, finely crystalline
1636.87 - 1637.01 PYROXENITE ; chromitiferous
1637.01 - 1637.54 CHROMITITE ; sharp contact : dip = 12° , black, finely crystalline
1637.54 - 1643.27 MOTTLED ANORTHOSITE ; chromitiferous , light grey, medium crystalline
MF13
UtPX
UtMC
MF16
15°
15°
5°
10°
12°
Exploration Drilling
LOGGED BY:C.J. Bester

IMPALA PLATINUM LTD — **Impala Rustenburg** — Page: **7 / 7**

BOREHOLE No: **BH6082** — X: **2823730.32** — START DATE: **2001/05/21** — SCALE: 1: **100**

DEFL. NO: **D00** — Y: **-28219.79** — END DATE: **2001/07/02**

DIRECTION: **0°** — Z: **1122.51 m AMSL** — ELLIPSOID:**Clarke 1880**

INCLINATION: **-90°** — Depth: **0.00 - 1643.27 m** — CENTRAL LATITUDE:**0**

LOCATION: **Vlakfontein 276JQ** — CENTRAL LONGITUDE:**27**

IMPALA PLATINUM

Lith	Structures	Geological Description	Zone	Dip
1640		1637.54 - 1643.27 **MOTTLED ANORTHOSITE** ; chromitiferous , light grey, medium crystalline	MF16	

Exploration Drilling — LOGGED BY:**C.J. Bester**

Appendix B: Laboratory rock strength test results

B1 UCS test results and long term strength analysis

Uniaxial compressive strength UCS results were presented briefly in Chapter 4. For space and organisation of the thesis the full set of results and graph plots of the nine test categories are given in this section to give a full picture of the UCS test results, Table B1-1.

Table B1-1: Uniaxial compressive strength test results

Rock type/ Code	Sample ID	Sample diameter, D (mm)	Sample length, L (mm)	L/D ratio	Sample mass, M (g)	Sample density, ρ (kg/m^3)	Failure load (kN)	UCS, σ_c (MPa)	Elastic Modulus, E (GPa)	Poisson's ratio, v	Long term strength, L-T, (MPa)	(LT/UCS) %
Mottled	*UCA6*	30.30	82.35	2.27	234.40	2750.00	159.00	153.67	42.34	0.10	111.00	72
Anorthosite A	UCA7	36.30	83.60	2.30	233.40	2755.50	219.00	211.61	54.89	0.23	91.00	72
	UCA8	36.30	83.65	2.30	237.40	2750.37	184.00	177.79	44.36	0.11	111.00	63
	UCA9	36.30	82.50	2.27	234.30	2746.54	181.00	174.89	49.00	0.30	51.00	29
	UCA10	36.30	83.35	2.30	237.80	2741.07	178.00	172.00	43.00	0.19	87.00	51
Average		**36.30**	**83.09**	**2.29**	**235.46**	**2748.70**	**184.20**	**177.99**	**46.72**	**0.19**	**90.20**	**57**
Spotted	UCB6	36.30	84.80	2.34	253.70	2890.82	142.00	137.21	33.47	0.23	60.00	43
Anorthositic	UCB7	36.30	84.60	2.33	255.00	2912.57	142.00	137.21	34.31	0.20	77.00	56
Norite B	UCB8	36.30	84.85	2.34	254.20	2903.92	141.00	136.24	32.67	0.22	60.00	44
	UCB9	36.30	85.00	2.34	253.50	2881.75	135.00	130.45	30.94	0.18	58.00	44
	UCB10	36.30	84.70	2.33	254.60	2904.50	137.00	132.38	35.20	0.20	54.00	41
Average		**36.30**	**84.79**	**2.34**	**254.20**	**2898.71**	**139.40**	**134.70**	**33.32**	**0.21**	**61.80**	**46**
Pyroxenite C	UCC6	36.30	81.80	2.25	271.90	3211.83	103.00	99.53	33.72	0.01	-	-
	UCC7	36.30	81.40	2.24	268.60	3188.44	178.00	172.00	39.17	0.42	54.00	32
	UCC8	36.30	81.70	2.25	271.40	3209.85	108.00	104.36	32.29	0.18	49.00	47
	UCC9	36.30	82.00	2.26	269.70	3178.07	129.00	124.65	36.32	0.11	64.00	51
	UCC10	36.30	81.40	2.24	269.90	3203.87	131.00	126.58	35.95	0.14	59.00	46
Average		**36.30**	**81.66**	**2.25**	**270.30**	**3198.41**	**129.80**	**125.42**	**35.49**	**0.17**	**56.50**	**44**
Mottled	UCD6	36.30	81.30	2.23	233.00	2769.25	145.00	140.11	38.54	0.48	43.00	31
Anorthosite D	UCD7	36.30	81.20	2.24	231.70	2757.19	139.00	134.31	-	-	-	-
	UCD8	36.30	81.30	2.24	232.50	2763.31	140.00	135.28	36.73	0.14	103.00	76
	UCD9	36.30	81.00	2.23	230.70	2752.07	140.00	135.28	42.70	0.41	44.00	32
	UCD10	36.30	81.00	2.23	228.80	2729.40	143.00	138.18	37.61	0.30	46.00	34
Average		**36.30**	**81.13**	**2.24**	**230.93**	**2750.49**	**140.50**	**135.76**	**39.01**	**0.28**	**59.75**	**44**
Norite E	UCE6	36.30	83.35	2.23	260.30	3017.63	90.00	86.96	30.31	0.17	64.00	74
	UCE7	36.30	84.00	2.31	266.00	3059.84	104.00	100.49	32.60	0.24	46.50	46
	UCE8	36.30	83.60	2.30	260.20	3007.45	100.00	96.63	30.10	0.16	53.00	55
	UCE9	36.30	83.80	2.31	259.10	2987.59	97.00	93.73	31.26	0.20	49.00	51
	UCE10	36.30	83.80	2.31	261.00	3009.49	89.00	86.00	30.25	0.18	55.00	57
Average		**36.30**	**83.71**	**2.29**	**261.32**	**3016.40**	**96.00**	**92.76**	**30.90**	**0.19**	**53.50**	**57**
Spotted	UCF6	36.30	84.00	2.31	250.50	2881.54	161.00	155.57	40.44	0.18	80.00	51
Anorthositic	UCF7	36.30	83.70	2.31	250.20	2888.41	152.00	146.87	40.35	0.21	77.00	52
Norite F	UCF8	36.30	83.85	2.31	253.90	2925.88	161.00	155.57	40.98	0.23	77.00	49
	UCF9	36.30	83.80	2.31	252.70	2913.79	142.00	137.21	40.24	0.20	67.00	49
	UCF10	36.30	79.00	2.18	233.20	2852.32	157.00	151.70	41.25	0.23	71.00	56
Average		**36.30**	**82.87**	**2.28**	**248.10**	**2892.39**	**154.60**	**149.38**	**40.65**	**0.21**	**75.60**	**51.4**
Anorthositic	UCG6	36.30	82.15	2.26	256.40	3015.83	93.00	89.86	34.14	0.13	81.00	76
Norite G	UCG7	36.30	82.00	2.26	260.80	3073.20	120.00	115.95	47.58	0.17	80.00	69
	UCG8	36.30	80.50	2.22	242.70	2913.20	126.00	121.75	32.52	0.14	105.00	86
	UCG9	36.30	79.80	2.20	239..5	2900.01	114.00	110.15	40.87	0.16	81.00	70
	UCG10	36.30	80.50	2.22	254.00	3048.84	117.00	113.05	34.40	0.15	71.00	61
Average		**36.30**	**80.99**	**2.23**	**253.48**	**2990.22**	**114.00**	**110.15**	**37.90**	**0.15**	**83.60**	**72.4**
Spotted	UCH6	36.30	79.10	2.18	231.10	2823.06	159.00	153.64	40.70	0.16	118.00	77
Anorthosite H	UCH7	36.30	80.90	2.23	235.80	2816.39	181.00	174.89	48.53	0.22	90.00	51
	UCH8	36.30	82.40	2.27	239.80	2812.02	145.00	140.11	39.27	0.31	-	-
	UCH9	36.30	79.55	2.19	230.50	2799.80	162.00	156.54	42.16	0.22	-	-
	UCH10	36.30	83.20	2.29	251.80	2924.35	151.00	145.91	42.54	0.17	102.00	73
Average		**36.30**	**81.03**	**2.23**	**237.80**	**2835.12**	**159.60**	**154.22**	**42.64**	**0.22**	**103.33**	**67**
Mottled	UCI6	36.30	79.80	2.20	229.20	2775.29	196.00	189.39	49.22	0.19	139.00	74
Anorthosite I	UCI7	36.30	81.80	2.25	235.30	2779.49	197.00	190.35	44.51	0.18	155.00	82
	UCI8	36.30	79.00	2.18	227.10	2777.71	156.00	150.74	42.88	0.17	-	-
	UCI9	36.30	83.80	2.31	239.50	2761.59	183.00	176.83	46.06	0.22	101.00	57
	UCI10	36.30	80.50	2.22	230.50	2766.76	179.00	172.96	43.89	0.21	108.00	62
Average		**36.30**	**80.98**	**2.23**	**232.32**	**2772.17**	**182.20**	**176.05**	**45.31**	**0.19**	**125.75**	**68.8**

Representative stress-strain plots from the UCS are given in Figures B1-1 to B1-8.

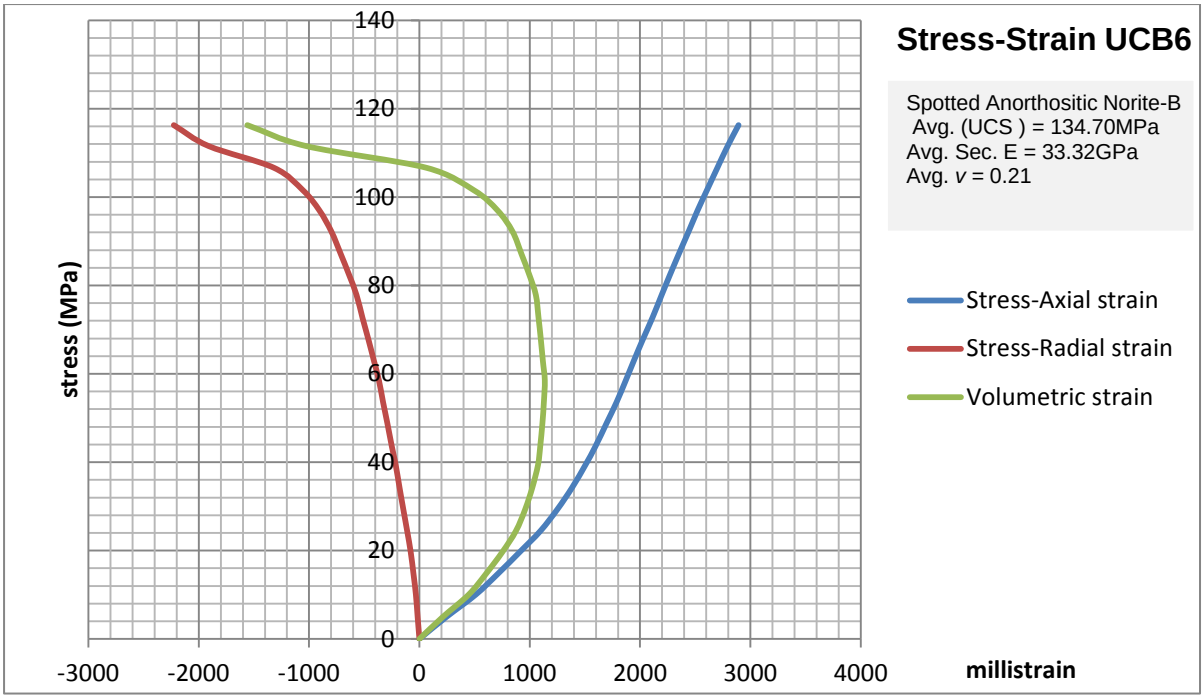


Figure B1-1: Stress-strain graph for spotted anorthositic norite (S.A.N.) rock type specimen UCB6

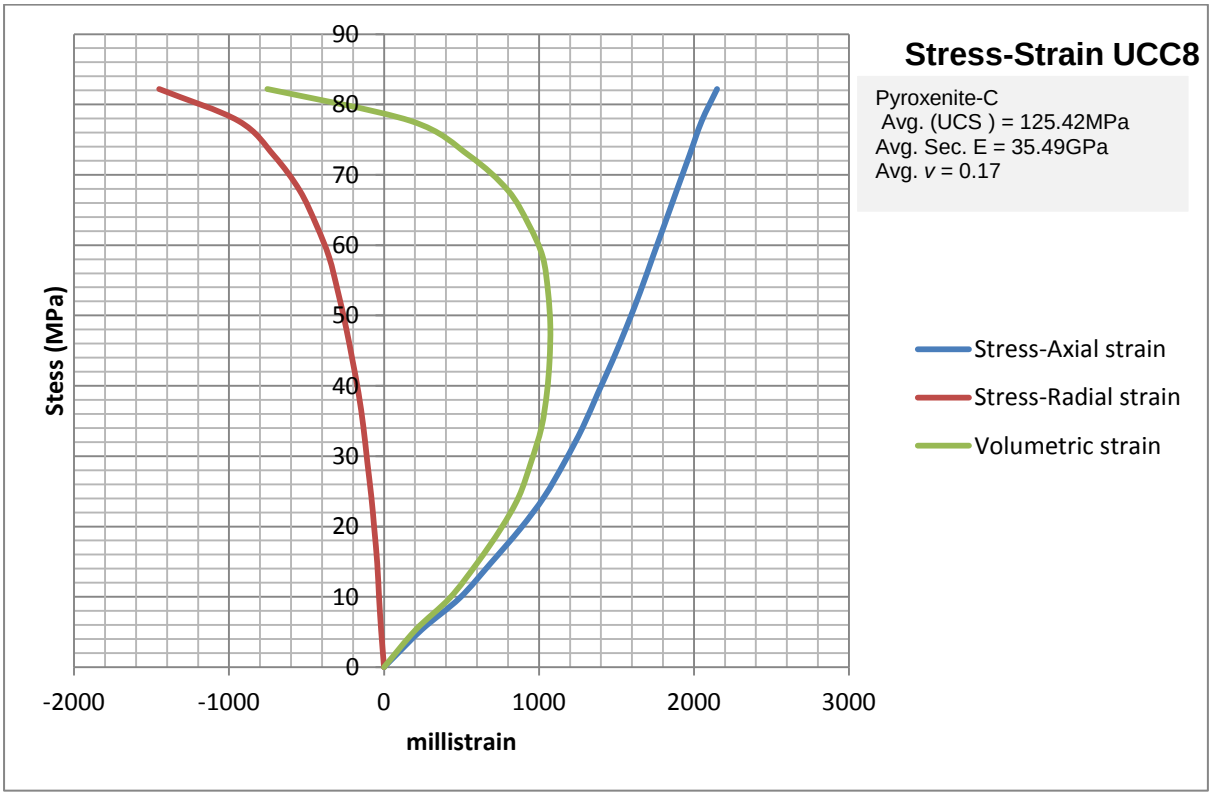


Figure B1-2: Stress-strain graph for pyroxenite (P.) rock type specimen UCC8

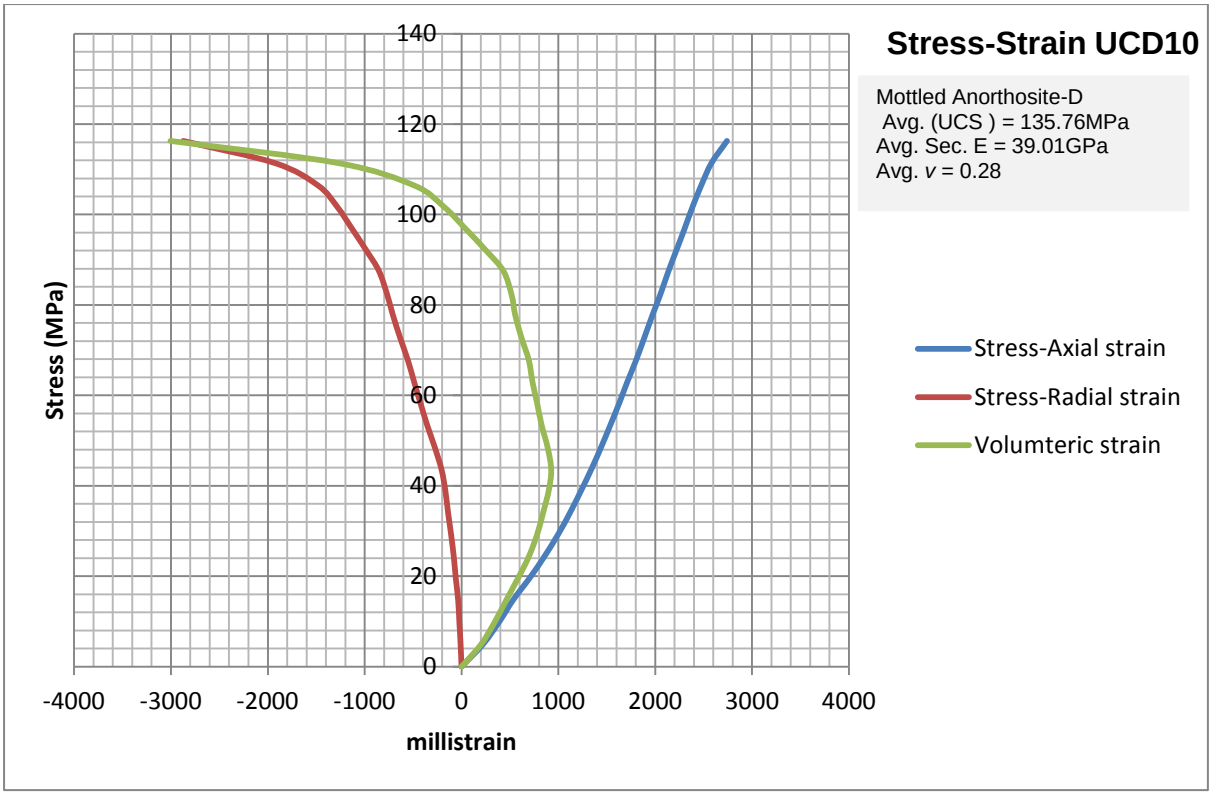


Figure B1-3: Stress-strain graph for mottled anorthosite (M.A.) rock type specimen UCD10

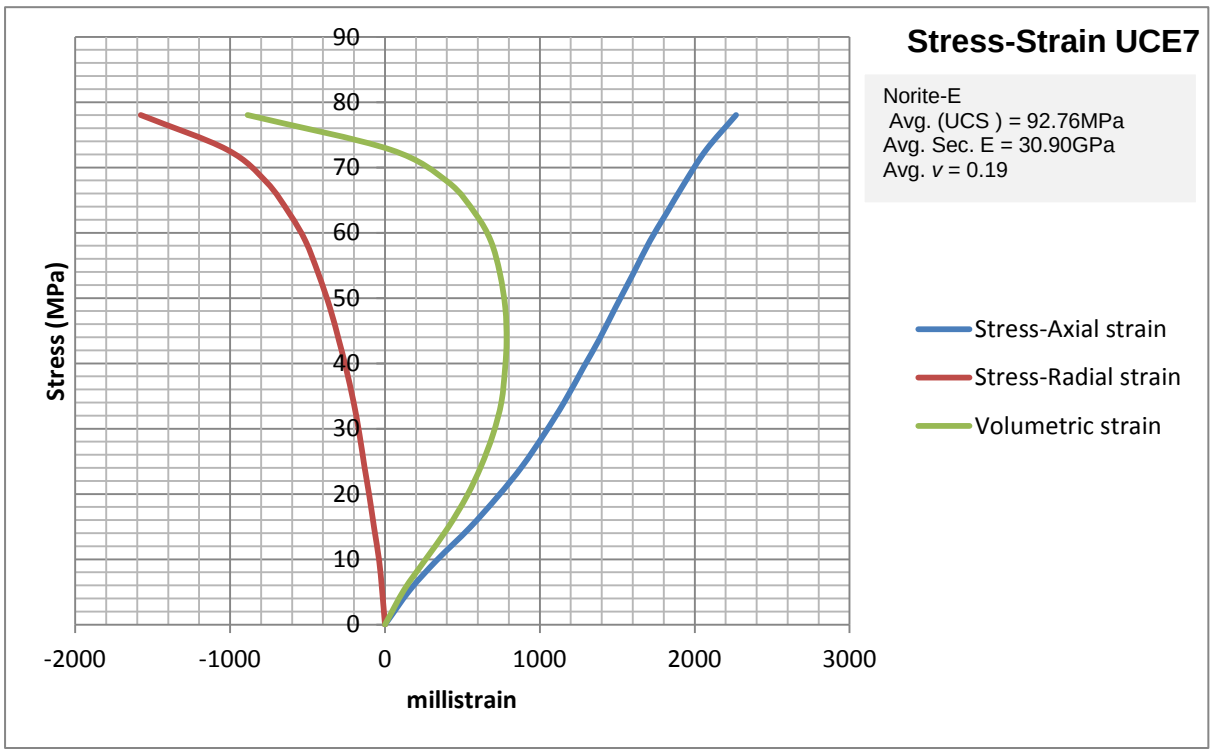


Figure B1-4: Stress-strain graph for norite (N.) rock type specimen UCE7

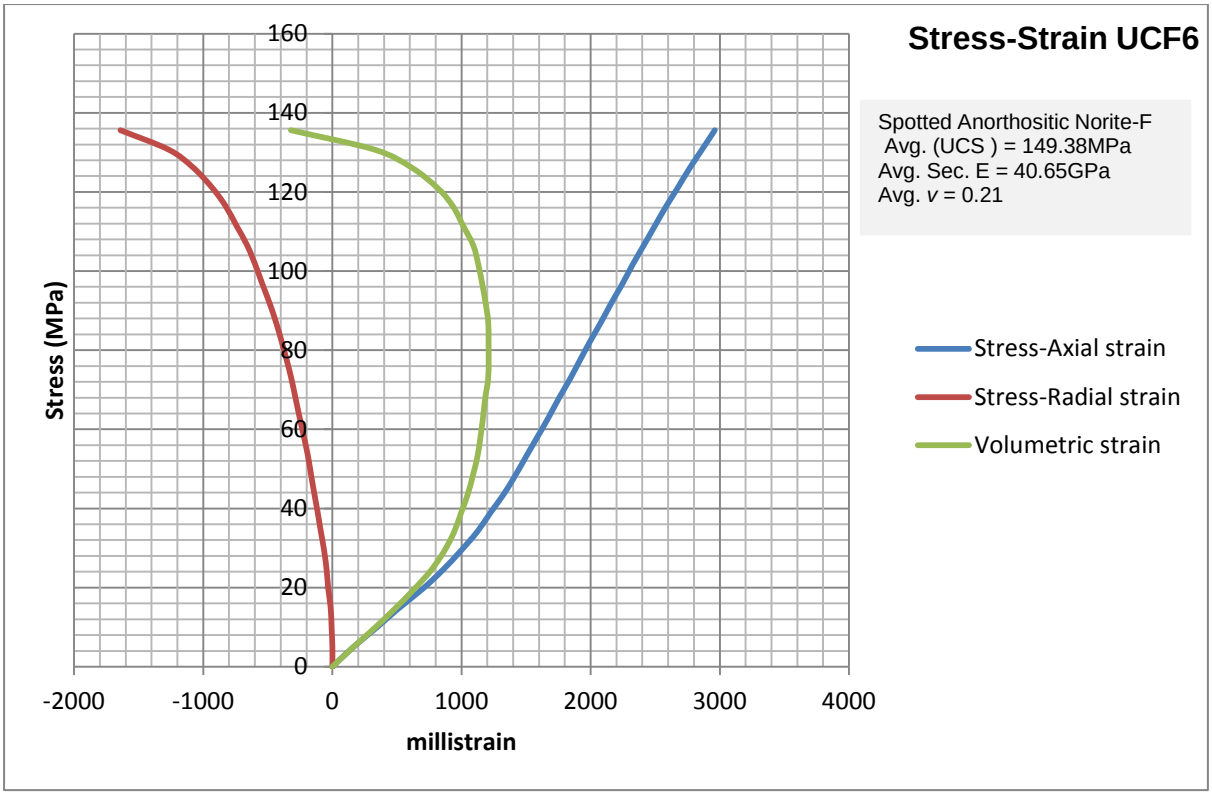


Figure B1-5: Stress-strain graph for spotted anorthositic norite (S.A.N.) rock type specimen UCF6

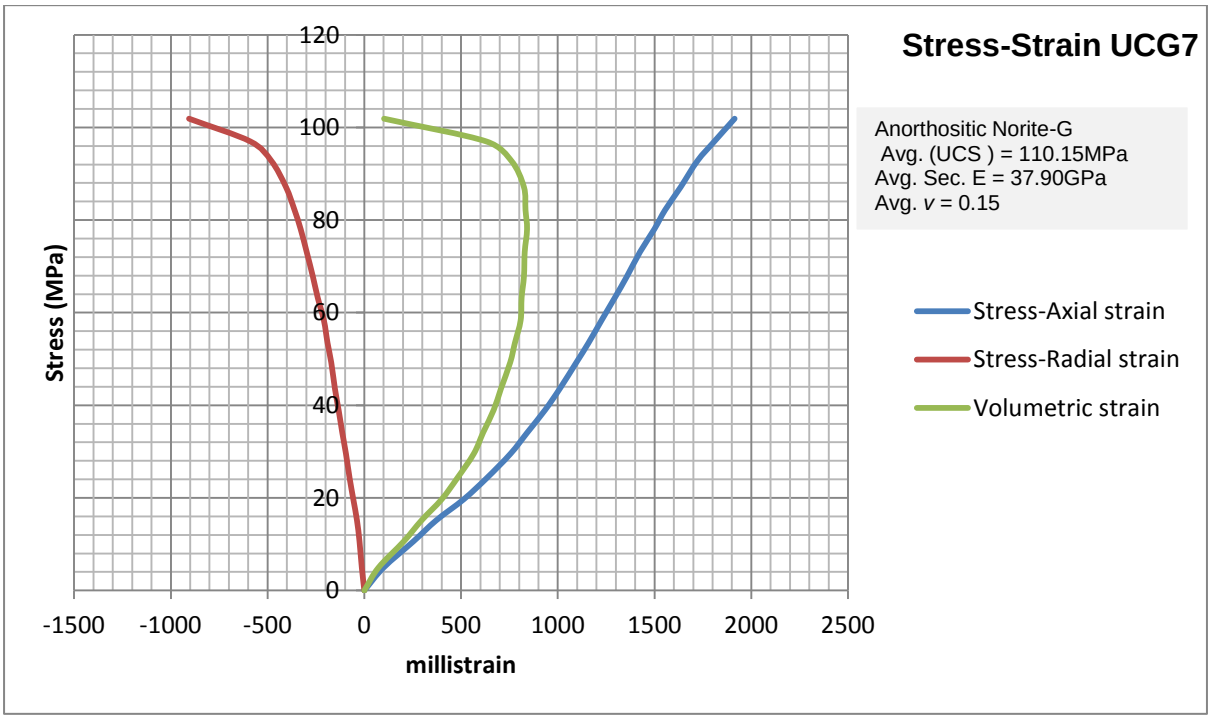


Figure B1-6: Stress-strain graph for anorthositic norite (A.N.) rock type specimen UCG7

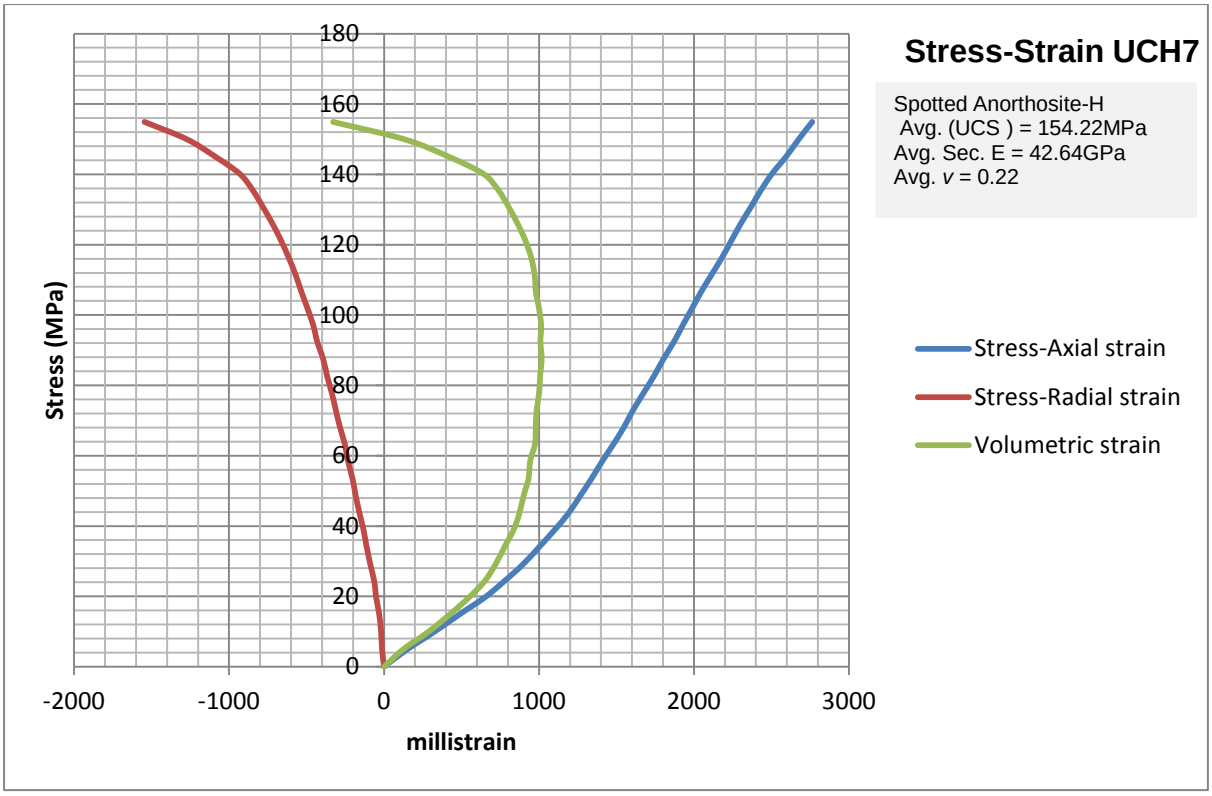


Figure B1-7: Stress-strain graph for spotted anorthosite (S.A.) rock type specimen UCH7

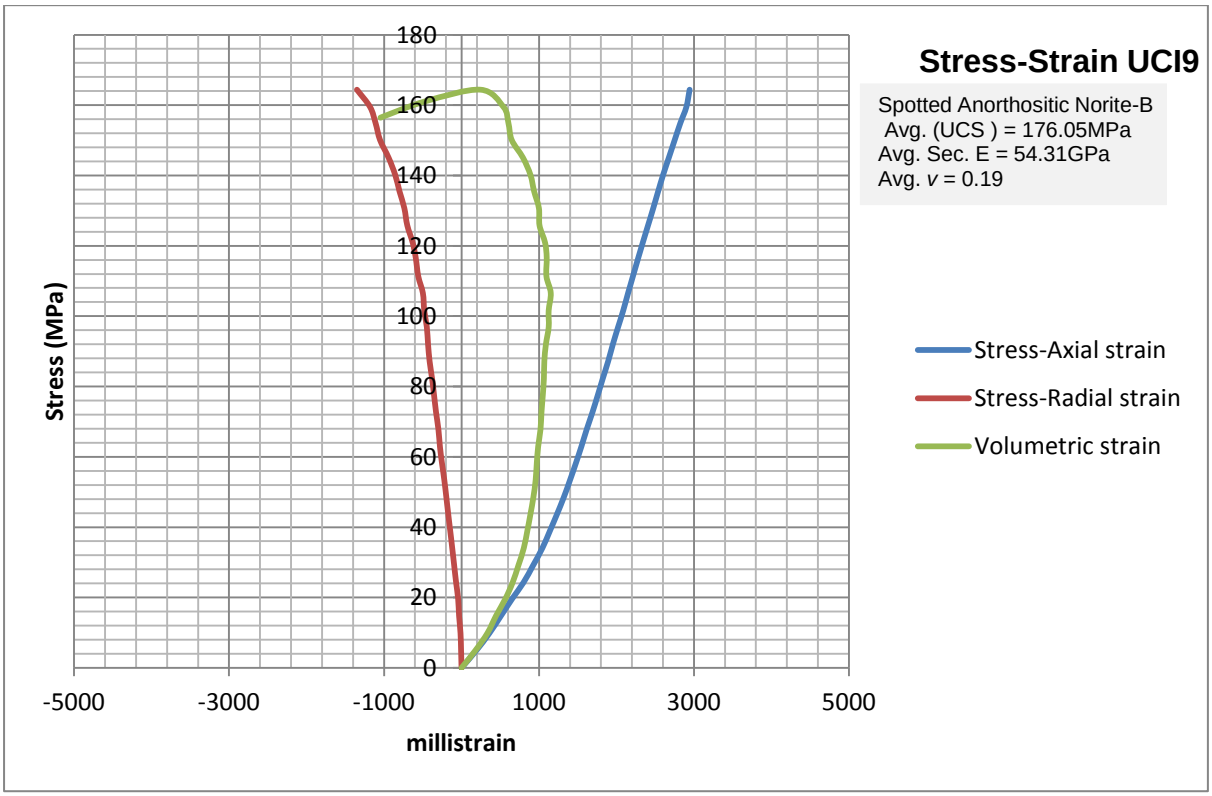


Figure B1-8: Stress-strain graph for mottled anorthosite (M.A.) rock type specimen UCI9

To assess the long term strength of the various BC rock types volumetric strain-stress plots were used following the analysis by Bieniawski (1967) discussed in Chapter 2 and illustrated in section 4-3-3. The point of inflection could not be read off easily from a casual inspection of the stress-strain plots shown in Figures B1-1 to B1-8 so the rate of change of volumetric strain with stress was used to determine the point where the plot crossed the horizontal stress axis. The determination of the long term strength is illustrated in Figures B1-9 to B1-16 through representative plots. A summary of the average values obtained here was presented in the UCS test results in Chapter 4 and in Table B1-1.

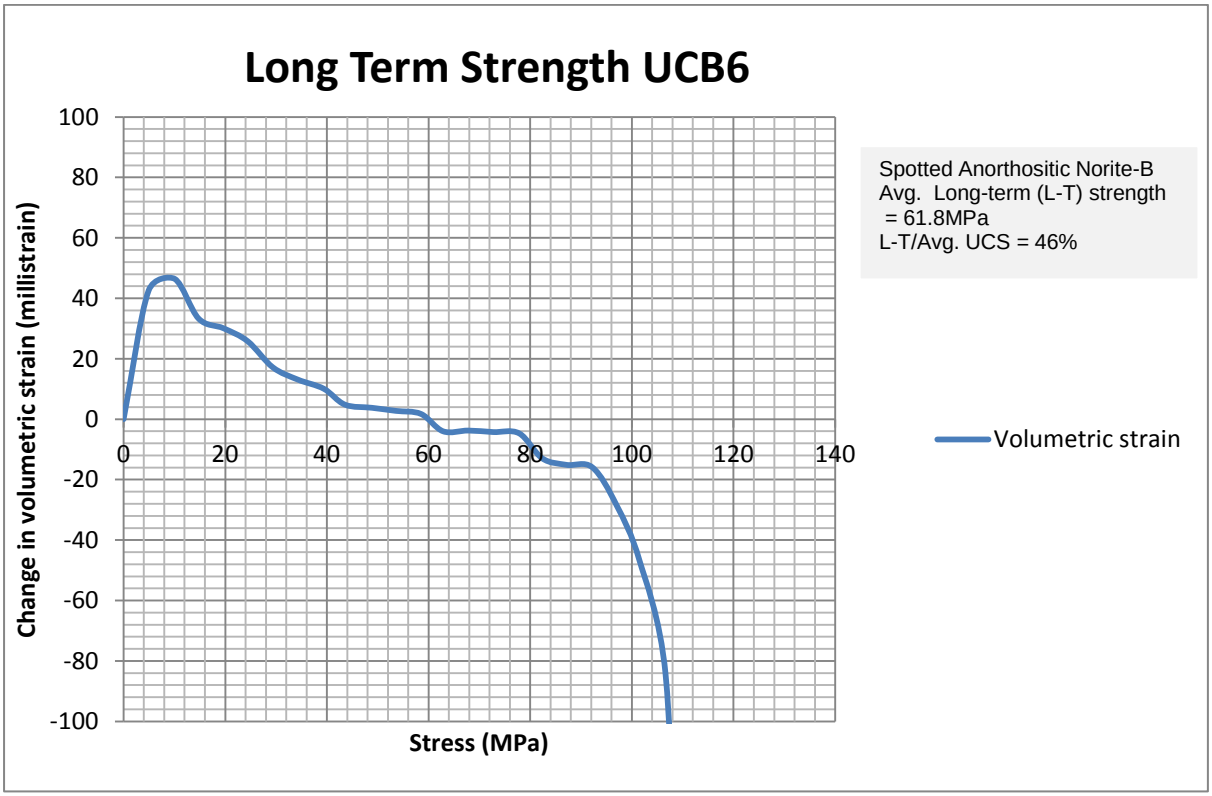


Figure B1-9: Rate of change of volumetric strain with respect to stress (UCB6)

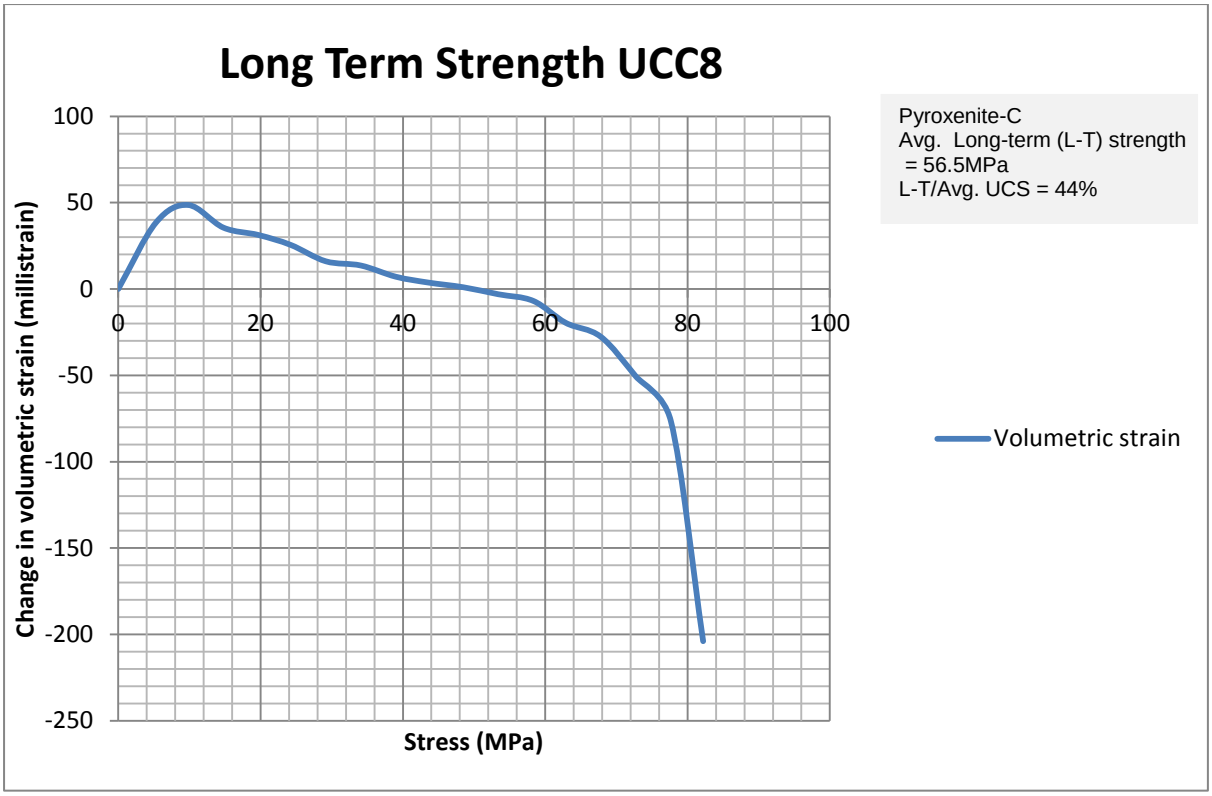


Figure B1-10: Rate of change of volumetric strain with respect to stress (UCC8)

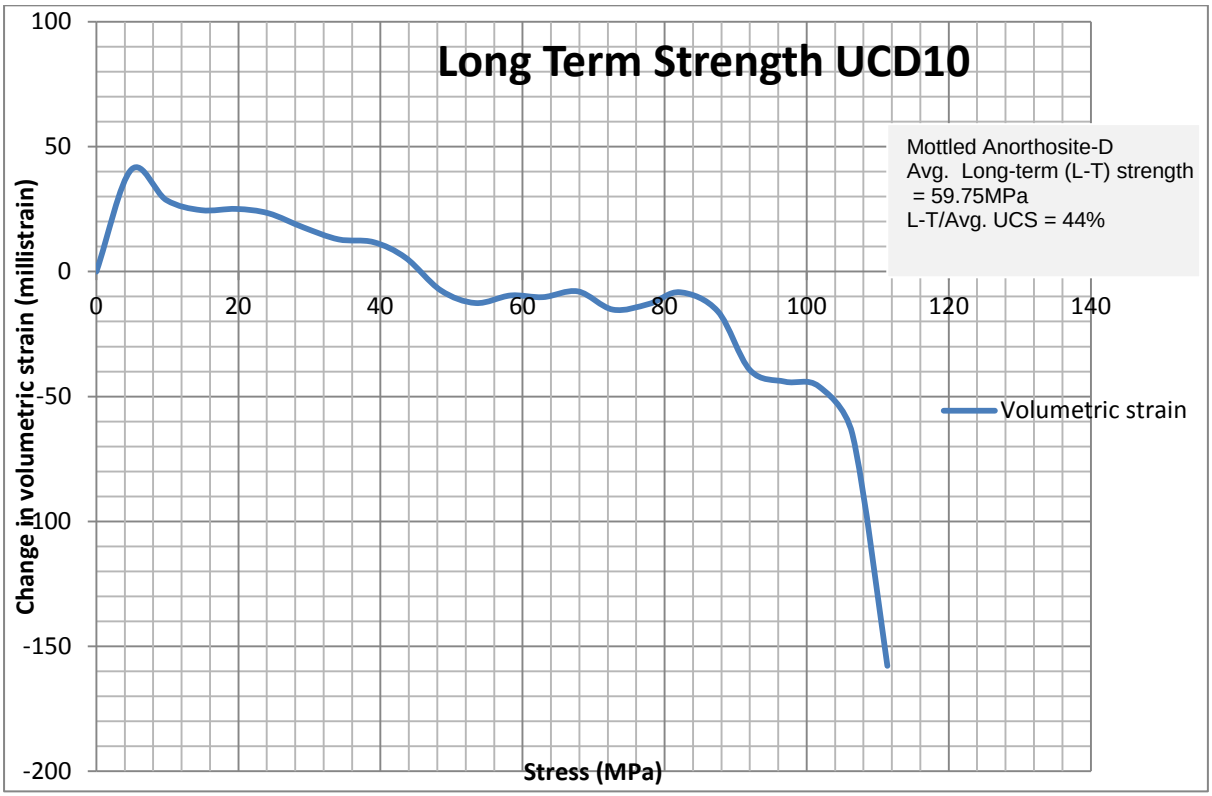


Figure B1-11: Rate of change of volumetric strain with respect to stress (UCD10)

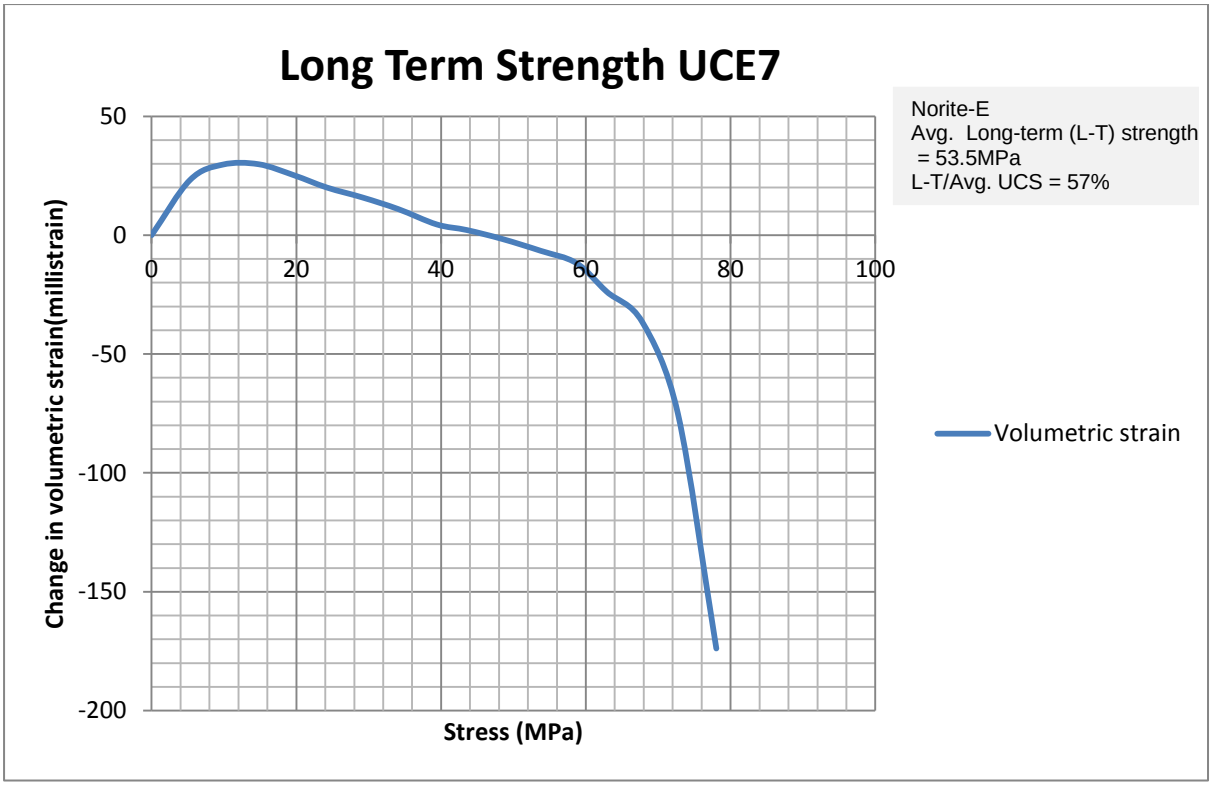


Figure B1-12: Rate of change of volumetric strain with respect to stress (UCE7)

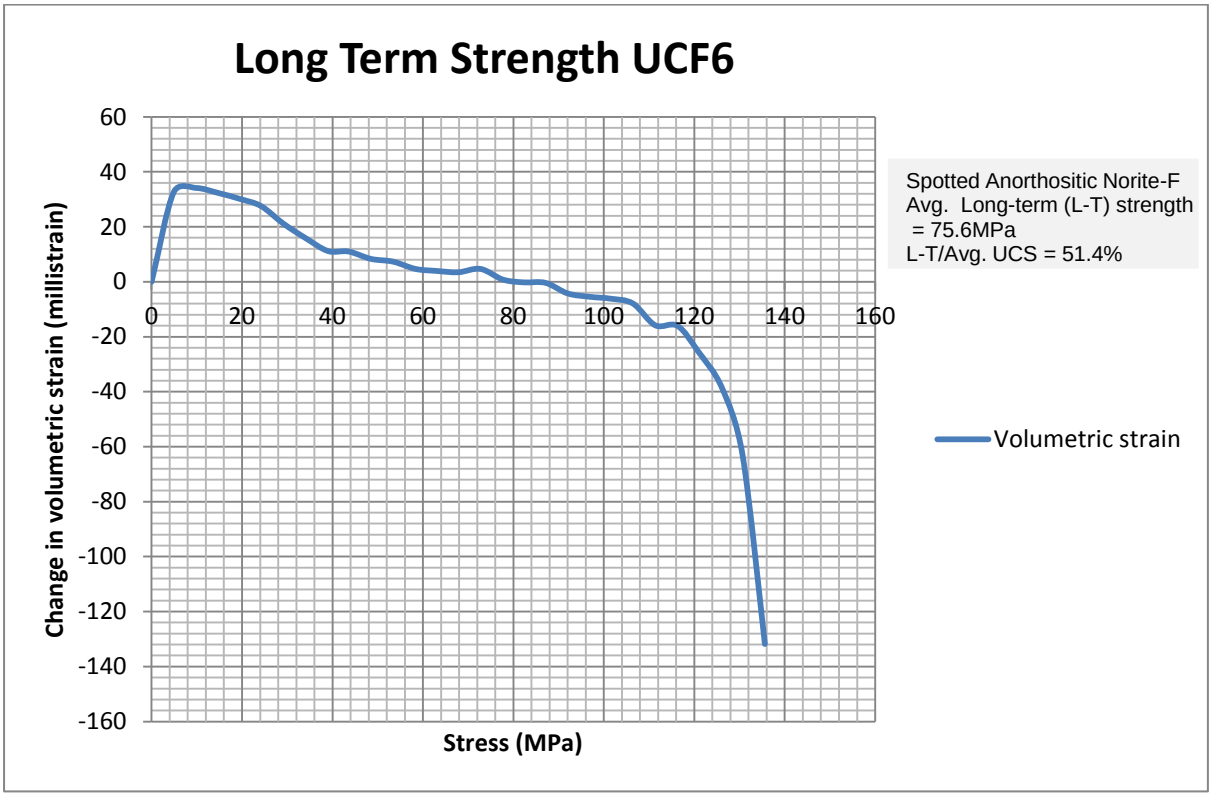


Figure B1-13: Rate of change of volumetric strain with respect to stress (UCF6)

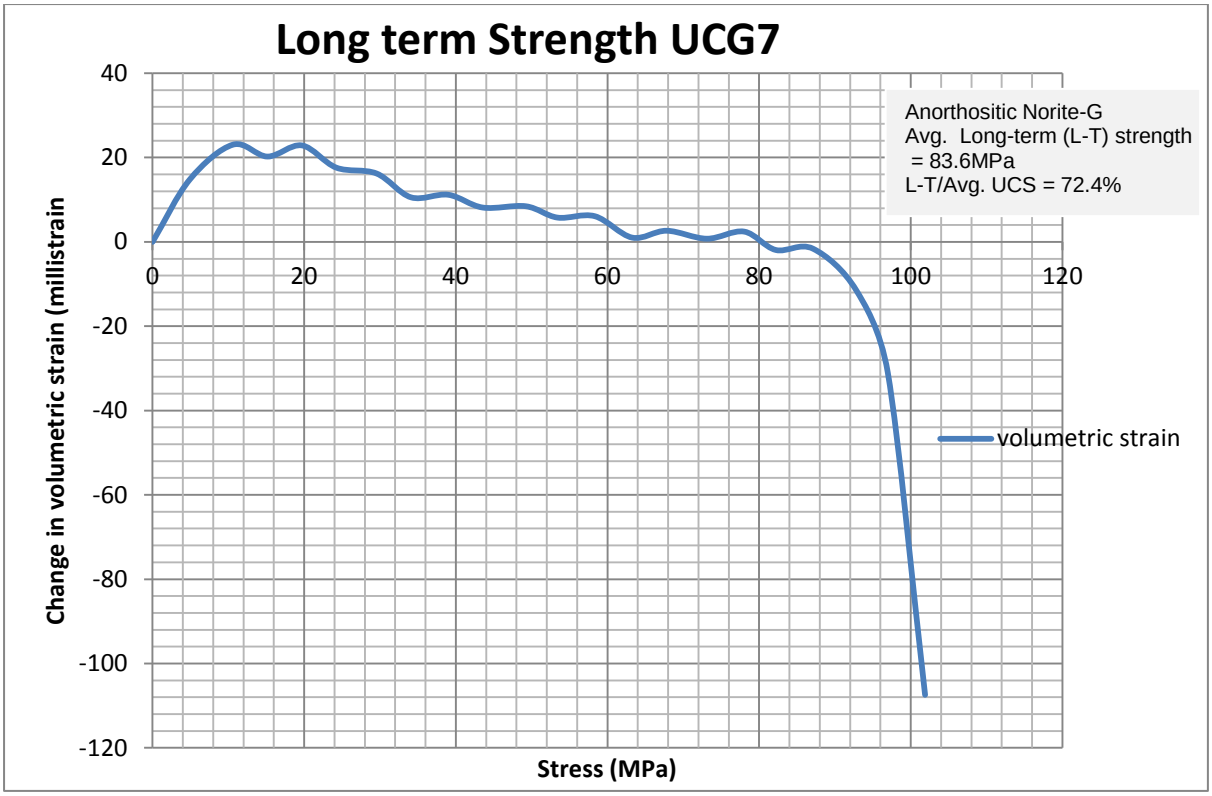


Figure B1-14: Rate of change of volumetric strain with respect to stress (UCG7)

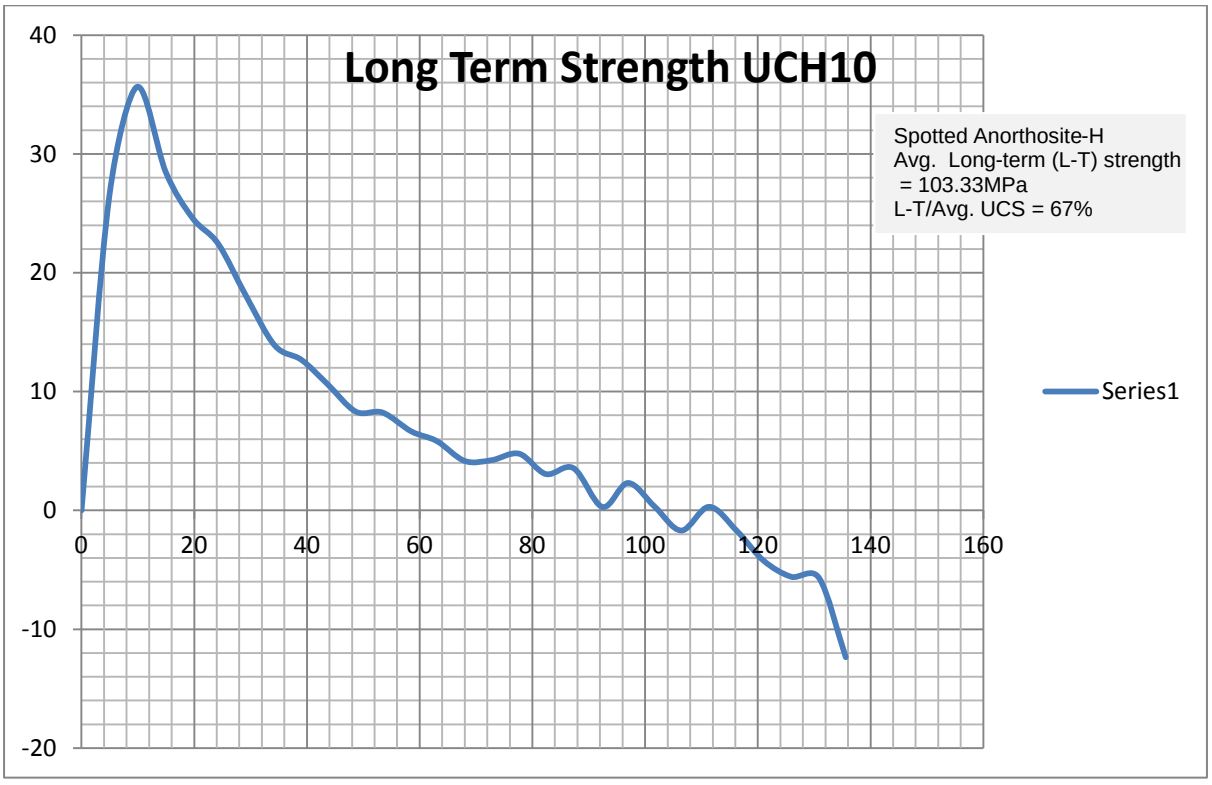
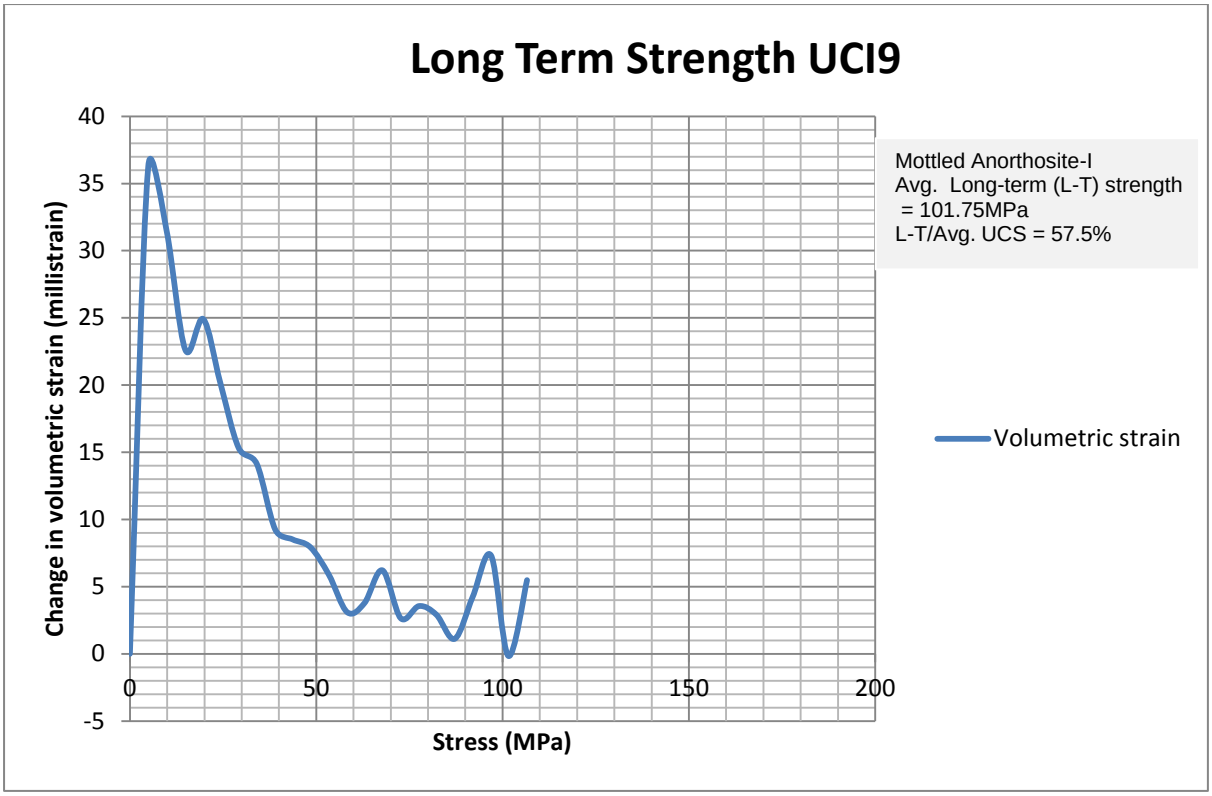


Figure B1-15: Rate of change of volumetric strain with respect to stress (UCH10)



B1-16: Rate of change of volumetric strain with respect to stress (UCI9)

Due to the noise in the data plots after the peak strength, the first intercept on the stress (horizontal) axis was recorded as the “long term strength” for the particular specimen.

B2 Normal Brazilian Indirect Tensile (BIT) strength test results

The full set of the normal BIT test results for all nine test categories is given in Table B2-1.

Table B2-2: Normal Brazilian Indirect Tensile (BIT) strength test results

Rock type	Sample ID	Sample diameter, D (mm)	Sample thickness, t (mm)	t/D ratio	Sample mass, M (g)	Load at failure, P (kN)	BIT, σ_t (MPa)	Time-to-failure (s)
Mottled	DBA1	36.30	18.80	0.52	53.20	7.90	7.37	286.28
Anorthosite A	DBA2	36.30	19.15	0.53	54.10	8.74	8.00	241.70
	DBA3	36.30	19.70	0.54	54.60	6.95	6.19	230.18
	DBA4	36.30	19.40	0.53	54.70	8.29	7.49	161.52
	DBA5	36.30	19.30	0.53	54.70	9.08	8.25	183.86
Average		**36.30**	**19.27**	**0.53**	**54.26**	**8.19**	**7.46**	**220.71**
Spotted	DBB1	36.30	18.20	0.50	51.90	7.10	6.84	265.70
Anorthositic	DBB2	36.30	18.00	0.50	52.00	5.95	5.80	207.68
Norite B	DBB3	36.30	19.00	0.52	56.10	6.31	5.82	176.91
	DBB4	36.30	19.00	0.54	57.90	7.63	6.86	180.41
	DBB5	36.30	19.50	0.54	57.00	7.07	6.36	181.27
	DBB6	36.30	19.00	0.52	56.70	6.90	6.37	191.20
	DBB7	36.30	18.75	0.52	55.70	6.78	6.34	196.58
	DBB8	36.30	19.10	0.53	56.40	7.00	6.43	246.00
Average		**36.30**	**18.88**	**0.52**	**55.46**	**6.84**	**6.35**	**205.72**
Pyroxenite C	DBC1	36.30	19.50	0.54	64.20	5.55	4.99	217.16
	DBC2	36.30	18.20	0.50	60.20	7.05	6.79	267.60
	DBC3	36.30	19.20	0.53	63.10	6.60	6.03	200.49
	DBC4	36.30	18.40	0.51	60.00	9.98	9.51	186.15
	DBC5	36.30	19.20	0.53	63.40	6.87	6.28	192.86
	DBC6	36.30	19.10	0.53	63.20	8.19	7.52	180.15
	DBC7	36.30	19.20	0.53	64.60	7.79	7.12	203.01
Average		**36.30**	**18.97**	**0.52**	**62.67**	**7.43**	**6.89**	**206.77**
Mottled	DBD1	36.30	18.80	0.52	54.70	6.20	5.78	155.90
Anorthosite D	DBD2	36.30	18.50	0.51	54.10	6.30	5.97	204.03
	DBD3	36.30	18.70	0.52	53.80	5.70	5.35	257.24
	DBD4	36.30	18.85	0.52	54.10	6.88	6.40	163.37
	DBD5	36.30	18.95	0.52	52.00	8.02	7.42	149.33
	DBD6	36.30	18.80	0.52	54.00	6.30	5.88	223.97
	DBD7	36.30	18.80	0.52	54.20	8.39	7.83	232.31
Average		**36.30**	**18.77**	**0.52**	**53.84**	**6.83**	**6.38**	**198.02**
Norite E	DBE1	36.30	18.40	0.51	58.60	8.25	7.86	156.52
	DBE2	36.30	18.50	0.51	55.00	5.54	5.25	161.19
	DBE3	36.30	18.55	0.51	56.40	9.55	9.03	152.58
	DBE4	36.30	17.60	0.48	55.10	6.43	6.41	184.56
	DBE5	36.30	18.30	0.50	57.40	7.62	7.30	155.54
	DBE6	36.30	19.25	0.53	64.00	4.82	4.39	155.54
	DBE7	36.30	17.95	0.49	57.20	6.25	6.11	156.52
Average		**36.30**	**18.36**	**0.50**	**57.67**	**6.92**	**6.62**	**160.35**
Spotted	DBF1	36.30	19.40	0.53	58.70	6.60	5.97	243.36
Anorthositic	DBF2	36.30	19.60	0.54	57.10	7.60	6.80	262.82
Norite F	DBF3	36.30	19.55	0.54	57.60	9.35	8.39	168.34
	DBF4	36.30	19.55	0.54	56.30	13.40	12.02	186.06
	DBF5	36.30	18.45	0.51	57.80	7.26	6.90	175.82
	DBF6	36.30	16.85	0.46	49.60	6.35	6.61	167.84
	DBF7	36.30	16.85	0.46	49.60	7.31	7.61	182.93
Average		**36.30**	**18.61**	**0.51**	**55.24**	**8.27**	**7.76**	**198.17**
Anorthositic	DBG1	36.30	19.70	0.54	63.10	9.00	8.01	313.71
Norite G	DBG2	36.30	19.40	0.53	61.70	7.50	6.78	262.23
	DBG3	36.30	17.30	0.48	55.20	9.33	9.46	182.63
	DBG4	36.30	17.65	0.49	57.00	9.07	9.01	200.68
	DBG5	36.30	16.45	0.45	53.00	7.81	8.33	160.33
	DBG6	36.30	16.20	0.45	52.30	7.26	7.86	154.93
	DBG7	36.30	16.00	0.44	48.90	4.45	4.88	157.16
	DBG8	36.30	18.50	0.51	59.30	7.23	6.85	199.13
Average		**36.30**	**17.65**	**0.49**	**56.31**	**7.71**	**7.65**	**203.85**
Spotted	DBH1	36.30	16.90	0.47	49.50	8.15	8.46	285.81
Anorthosite H	DBH2	36.30	18.60	0.51	53.70	7.30	6.88	247.40
	DBH3	36.30	18.50	0.51	53.60	8.20	7.77	197.19
	DBH4	36.30	18.00	0.50	53.00	6.26	6.10	166.34
	DBH5	36.30	16.80	0.46	49.30	6.70	6.99	179.97
	DBH6	36.30	17.25	0.48	50.40	6.16	6.26	178.97
	DBH7	36.30	17.05	0.47	49.50	7.03	7.23	283.13
Average		**36.30**	**17.59**	**0.48**	**51.29**	**7.11**	**7.10**	**219.83**
Mottled	DBI1	36.30	16.40	0.45	47.10	7.00	7.49	256.91
Anorthosite I	DBI2	36.30	18.00	0.50	51.40	6.60	6.43	234.56
	DBI3	36.30	17.20	0.47	48.90	6.18	6.30	192.33
	DBI4	36.30	16.25	0.45	47.40	8.61	9.29	213.95
	DBI5	36.30	18.00	0.50	51.50	6.94	6.76	201.07
	DBI6	36.30	16.45	0.45	47.10	6.14	6.55	187.16
	DBI7	36.30	17.10	0.47	49.10	6.29	6.45	212.13
Average		**36.30**	**17.06**	**0.47**	**48.93**	**6.82**	**7.04**	**214.02**

B3 Time-dependent Brazilian Indirect Tensile (BIT) Strength test results

The full set of the time-dependent test results is given in Table B3-1.

Table B3-3: Time-dependent Brazilian Indirect Tensile (BIT) strength test results

Sample ID	Sample diameter, D (mm)	Sample thickness, T (mm)	T/D ratio	Sample mass, M (g)	Percentage of Average tensile load, $X_{\%}$	Test load, kN	Time-to-failure, t (s)
SB90A1	36.30	18.90	0.52	53.40	90	7.37	27
SB90A2	36.30	19.00	0.52	53.70	90	7.37	38
SB90A3	36.30	19.10	0.53	53.90	90	7.37	1140
SB90A4	36.30	19.10	0.53	54.00	90	7.37	38
SB90A5	36.30	19.00	0.52	53.60	90	7.37	98
Average	**36.30**	**19.02**	**0.52**	**53.72**	**90**	**7.37**	**268**
SB85A1	36.30	18.90	0.52	53.30	85	6.98	2100
SB85A2	36.30	18.90	0.52	53.30	85	6.98	25
SB85A3	36.30	19.00	0.52	53.60	85	6.98	133
SB85A4	36.30	19.10	0.53	53.80	85	6.98	2240
SB85A5	36.30	19.00	0.52	53.70	85	6.98	364
Average	**36.30**	**18.98**	**0.52**	**53.54**	**85**	**6.98**	**972**
SB80A1	36.30	18.45	0.51	52.10	80	6.55	1943
SB80A2	36.30	19.00	0.52	53.40	80	6.55	6803
SB80A3	36.30	19.10	0.53	53.70	80	6.55	5680
SB80A4	36.30	18.90	0.52	53.20	80	6.55	30692
SB80A5	36.30	19.20	0.53	54.10	80	6.55	13174
Average	**36.30**	**18.93**	**0.52**	**53.30**	**80**	**6.55**	**11658**
SB75A1	36.30	19.05	0.52	53.80	75	6.14	126188
SB75A2	36.30	19.00	0.52	53.50	75	6.14	62122
SB75A3	36.30	18.70	0.52	53.30	75	6.14	125
SB75A4	36.30	19.10	0.53	53.90	75	6.14	199
SB75A5	36.30	18.90	0.52	53.20	75	6.14	10520
Average	**36.30**	**18.95**	**0.52**	**53.54**	**75**	**6.14**	**39831**
SB70A1	36.30	18.60	0.51	52.80	70	5.73	93616
SB70A2	36.30	18.95	0.52	52.20	70	5.73	258543
SB70A3	36.30	18.80	0.52	53.10	70	5.73	93481
SB70A4	36.30	19.10	0.53	53.90	70	5.73	280
Average	**36.30**	**18.86**	**0.52**	**53.00**	**70**	**5.73**	**111480**
SB90B1	36.30	18.20	0.50	51.70	90	6.16	1354
SB90B2	36.30	18.55	0.51	54.60	90	6.16	2130
SB90B3	36.30	18.40	0.51	52.60	90	6.16	3768
SB90B4	36.30	18.80	0.52	55.70	90	6.16	245
SB90B5	36.30	18.00	0.50	52.20	90	6.16	439
Average	**36.30**	**18.39**	**0.51**	**53.36**	**90**	**6.16**	**1587**
SB85B1	36.30	18.00	0.50	52.00	85	5.81	1516
SB85B2	36.30	18.20	0.50	51.90	85	5.81	2703
SB85B3	36.30	18.20	0.50	51.70	85	5.81	2858
SB85B4	36.30	18.55	0.51	54.60	85	5.81	1502
SB85B5	36.30	18.40	0.51	52.60	85	5.81	2422
Average	**36.30**	**18.27**	**0.50**	**52.56**	**85**	**5.81**	**2200**
SB80B1	36.30	18.80	0.52	55.70	80	5.47	16964
SB80B2	36.30	18.00	0.50	52.20	80	5.47	149
SB80B3	36.30	18.00	0.50	52.00	80	5.47	4805
SB80B4	36.30	18.20	0.50	51.90	80	5.47	140
SB80B5	36.30	18.70	0.52	55.30	80	5.47	832
Average	**36.30**	**18.34**	**0.51**	**53.42**	**80**	**5.47**	**4578**
SB75B1	36.30	18.40	0.51	52.60	75	5.13	73429
SB75B2	36.30	18.70	0.52	55.30	75	5.13	641
SB75B3	36.30	18.00	0.50	51.50	75	5.13	1886
SB75B4	36.30	18.40	0.51	52.55	75	5.13	5994
SB75B5	36.30	18.40	0.51	52.57	75	5.13	17234
Average	**36.30**	**18.38**	**0.51**	**52.90**	**75**	**5.13**	**19837**
SB70B1	36.30	18.20	0.50	51.90	70	4.79	58681
SB70B2	36.30	18.15	0.50	50.40	70	4.79	85504
SB70B3	36.30	18.18	0.50	50.40	70	4.79	19691
SB70B4	36.30	18.15	0.50	50.40	70	4.79	85027
Average	**36.30**	**18.17**	**0.50**	**50.78**	**70**	**4.79**	**62226**
SB90C1	36.30	18.20	0.50	60.20	90	6.69	1080

SB90C2	36.30	19.20	0.53	63.10	90	6.69	32580
SB85C1	36.30	19.20	0.53	62.00	85	6.32	71041
SB85C2	36.30	18.75	0.52	61.30	85	6.32	6349
Average	**36.30**	**18.98**	**0.52**	**61.65**	**85**	**6.32**	**38695**
SB80C1	36.30	18.90	0.52	62.20	80	5.94	33705
Average	**36.30**	**18.90**	**0.52**	**62.20**	**80**	**5.94**	**33705**
SB75C1	36.30	18.75	0.52	61.50	75	5.57	207423
Average	**36.30**	**18.75**	**0.52**	**61.50**	**75**	**5.57**	**207423**
SB70C1	36.30	19.05	0.52	62.60	70	5.20	3840
SB70C2	36.30	19.30	0.53	63.40	70	5.20	88441
SB70C4	36.30	19.05	0.52	62.60	70	5.20	2013
SB70C5	36.30	19.30	0.53	63.40	70	5.20	126
Average	**36.30**	**19.18**	**0.53**	**63.00**	**70**	**5.20**	**23605**
SB90D1	36.30	18.85	0.52	54.10	90	6.15	220
SB90D2	36.30	18.50	0.51	54.10	90	6.15	340
SB90D3	36.30	18.95	0.52	52.00	90	6.15	259
SB90D5	36.30	18.80	0.52	54.20	90	6.15	96
Average	**36.30**	**18.78**	**0.52**	**53.60**	**90**	**6.15**	**229**
SB85D1	36.30	18.77	0.52	54.10	85	5.81	1495
SB85D2	36.30	18.5	0.51	52.00	85	5.81	72424
SB85D3	36.30	18.95	0.52	54.00	85	5.81	1056
SB85D4	36.30	18.8	0.52	54.20	85	5.81	5358
SB85D5	36.30	18.8	0.52	54.20	85	5.81	146
SB85D6	36.30	18.8	0.52	55.20	85	5.81	17487
Average	**36.30**	**18.77**	**0.52**	**53.95**	**85**	**5.81**	**16328**
SB80D1	36.30	18.85	0.52	54.10	80	5.46	14525
SB80D2	36.30	18.5	0.51	54.10	80	5.46	6070
SB80D3	36.30	18.95	0.52	52.00	80	5.46	36173
SB80D4	36.30	18.8	0.52	54.00	80	5.46	85861
SB80D5	36.30	18.8	0.52	54.20	80	5.46	270873
Average	**36.30**	**18.78**	**0.52**	**53.68**	**80**	**5.46**	**82700**
SB75D1	36.30	18.85	0.52	54.10	75	5.12	6023
SB75D2	36.30	18.5	0.51	54.10	75	5.12	75876
SB75D3	36.30	18.95	0.52	52.00	75	5.12	20808
SB75D4	36.30	18.8	0.52	54.00	75	5.12	20878
SB75D5	36.30	18.8	0.52	54.20	75	5.12	76824
SB75D6	36.30	18.8	0.52	54.20	75	5.12	17429
Average	**36.30**		**0.52**	**53.77**	**75**	**5.12**	**36306**
SB70D1	36.30	18.85	0.52	54.10	70	4.78	232577
SB70D2	36.30	18.5	0.51	54.10	70	4.78	71201
Average	**36.30**	**18.68**	**0.51**	**54.10**	**70**	**4.78**	**151889**
SB90E1	36.30	18.40	0.51	58.60	90	6.23	2901
SB90E2	36.30	17.60	0.48	55.10	90	6.23	402
Average	**36.30**	**18.00**	**0.50**	**56.85**	**90**	**6.23**	**1652**
SB85E1	36.30	18.4	0.51	58.60	85	5.88	556
SB85E2	36.30	17.6	0.48	55.10	85	5.88	193
Average	**36.30**	**18.00**	**0.50**	**56.85**	**85**	**5.88**	**375**
SB80E1	36.30	18.4	0.51	58.60	80	5.54	1563
SB80E2	36.30	17.6	0.48	55.10	80	5.54	3529
SB80E3	36.30	18.3	0.50	57.40	80	5.54	25890
Average	**36.30**	**18.10**	**0.50**	**57.03**	**80**	**5.54**	**10327**
SB75E1	36.30	18.4	0.51	58.60	75	5.19	203
SB75E2	36.30	17.6	0.48	55.10	75	5.19	100
SB75E3	36.30	18.3	0.50	57.40	75	5.19	2933
SB75E4	36.30	19.25	0.53	64.00	75	5.19	5138
SB75E5	36.30	17.95	0.49	57.20	75	5.19	22
Average	**36.30**	**18.30**	**0.50**	**58.46**	**75**	**5.19**	**1679**
SB70E1	36.30	18.4	0.51	58.60	70	4.84	179689
SB70E2	36.30	17.6	0.48	55.10	70	4.84	2287
SB70E3	36.30	18.3	0.50	57.40	70	4.84	142
Average	36.30	18.10	0.50	57.03	70	4.84	60706
SB85F1	36.30	19.55	0.54	57.60	85	7.03	556
SB85F2	36.30	19.55	0.54	56.30	85	7.03	193
Average	**36.30**	**19.55**	**0.54**	**56.95**	**85**	**7.03**	**375**
SB80F1	36.30	19.55	0.54	57.60	80	6.62	1564
SB80F2	36.30	19.55	0.54	56.30	80	6.62	3529
SB80F3	36.30	18.45	0.51	57.80	80	6.62	21
Average	36.30	19.18	0.53	57.23	80	6.62	1705
SB75F1	36.30	19.55	0.54	57.60	75	6.20	2933
SB75F2	36.30	19.55	0.54	56.30	75	6.20	5138
SB75F3	36.30	18.45	0.51	57.80	75	6.20	22
Average	**36.30**	**19.18**	**0.53**	**57.23**	**75**	**6.20**	**2698**
SB70F1	36.30	19.55	0.54	57.60	70	5.79	179699

SB70F2	36.30	19.55	0.54	56.30	70	5.79	2287
SB70F3	36.30	18.45	0.51	57.80	70	5.79	142
Average	**36.30**	**19.18**	**0.53**	**57.23**	**70**	**5.79**	**60709**
SB90G1	36.30	17.3	0.48	55.20	90	6.94	643
Average	**36.30**	**17.30**	**0.48**	**55.20**	**90**	**6.94**	**643**
SB85G2	36.30	17.65	0.49	57.00	85	6.55	147
Average	**36.30**	**17.65**	**0.49**	**57.00**	**85**	**6.55**	**147**
SB75G5	36.30	18.00	0.50	53.00	75	5.78	2483
SB75G6	36.30	18.00	0.50	53.00	75	5.78	2483
Average	**36.30**	**18.00**	**0.50**	**53.00**	**75**	**5.78**	**2483**
SB70G1	36.30	17.25	0.48	53.20	90	5.40	795
SB70G2	36.30	17.05	0.47	55.20	90	5.40	1306
SB70G3	36.30	16.90	0.47	54.70	90	5.40	313
Average	**36.30**	**17.07**	**0.47**	**54.37**	**90**	**5.40**	**805**
SB90H1	36.30	18	0.50	53.00	90	6.40	7308
SB90H2	36.30	16.8	0.46	49.30	90	6.40	6256
SB90H3	36.30	17.25	0.48	50.40	90	6.40	5477
SB90H4	36.30	17.05	0.47	49.50	90	6.40	1232
SB90H5	36.30	16.9	0.47	49.50	90	6.40	796
Average	**36.30**	**17.20**	**0.47**	**50.34**	**90**	**6.40**	**4214**
SB85H1	36.30	18	0.50	53.00	85	6.04	28432
SB85H2	36.30	16.8	0.46	49.30	85	6.04	6949
SB85H3	36.30	17.25	0.48	50.40	85	6.04	1889
SB85H4	36.30	17.05	0.47	49.50	85	6.04	11895
Average	**36.30**	**17.28**	**0.48**	**50.55**	**85**	**6.04**	**12291**
SB80H1	36.30	18.85	0.52	54.10	80	5.69	94
SB80H2	36.30	18.5	0.51	54.10	80	5.69	29908
SB80H3	36.30	18.95	0.52	52.00	80	5.69	451
SB80H4	36.30	18.8	0.52	54.00	80	5.69	10996
SB80H5	36.30	18.8	0.52	54.20	80	5.69	1898
SB80H6	36.30	18.8	0.52	54.20	80	5.69	5662
Average	**36.30**	**18.78**	**0.52**	**53.77**	**80**	**5.69**	**8168**
SB75H1	36.30	18	0.50	53.00	75	5.33	7926
SB75H2	36.30	16.8	0.46	49.30	75	5.33	76443
SB75H3	36.30	17.25	0.48	50.40	75	5.33	1561
SB75H4	36.30	17.05	0.47	49.50	75	5.33	7942
SB75H5	36.30	16.9	0.47	49.50	75	5.33	241671
Average	**36.30**	**17.20**	**0.47**	**50.34**	**75**	**5.33**	**67109**
SB70H1	36.30	17.20	0.47	48.90	70	4.98	10092
SB70H2	36.30	16.25	0.45	47.40	70	4.98	4695
SB70H3	36.30	16.40	0.45	47.10	70	4.98	147976
SB70H4	36.30	16.45	0.45	47.10	70	4.98	9014
SB70H5	36.30	17.10	0.47	49.10	70	4.98	62350
SB70H6	36.30	17.10	0.47	49.10	70	4.98	13179
Average	**36.30**	**16.68**	**0.46**	**47.92**	**70**	**4.98**	**46825**
SB90I1	36.30	17.20	0.47	48.90	90	6.14	229
SB90I2	36.30	17.10	0.47	49.10	90	6.14	1370
SB90I3	36.30	16.45	0.45	47.10	90	6.14	417
SB90I4	36.30	16.50	0.45	47.90	90	6.14	27865
SB90I5	36.30	16.50	0.45	47.90	90	6.14	1183
Average	**36.30**	**16.75**	**0.46**	**48.18**	**90**	**6.14**	**6213**
SB85I1	36.30	17.20	0.47	48.90	85	5.80	56
SB85I2	36.30	17.10	0.47	49.10	85	5.80	67322
SB85I3	36.30	16.45	0.45	47.10	85	5.80	206
SB85I4	36.30	16.50	0.45	47.90	85	5.80	158217
SB85I5	36.30	16.50	0.45	47.900	85	5.80	154
Average	**36.30**	**16.75**	**0.46**	**48.18**	**85**	**5.80**	**45191**
SB80I1	36.30	17.20	0.47	48.90	80	5.46	26295
SB80I2	36.30	17.10	0.47	49.10	80	5.46	104174
SB80I3	36.30	16.45	0.45	47.10	80	5.46	1653
SB80I4	36.30	16.50	0.45	47.90	80	5.46	28
Average	**36.30**	**16.81**	**0.46**	**48.25**	**80**	**5.46**	**33038**
SB75I1	36.30	17.20	0.47	48.90	75	5.12	58565
SB75I2	36.30	17.10	0.47	49.10	75	5.12	11801
SB75I3	36.30	16.45	0.45	47.10	75	5.12	94169
SB75I4	36.30	16.50	0.45	47.90	75	5.12	8910
SB75I5	36.30	16.50	0.45	47.9	75	5.12	21521
Average	**36.30**	**16.75**	**0.46**	**48.18**	**75**	**5.12**	**38993**
SB70I1	36.30	17.20	0.47	48.90	70	4.77	40685
SB70I2	36.30	17.10	0.47	49.10	70	4.77	13602
SB70I3	36.30	16.45	0.45	47.10	70	4.77	139456
SB70I4	36.30	16.50	0.45	47.90	70	4.77	431
SB70I5	36.30	16.50	0.45	47.90	70	4.77	1583
Average	**36.30**	**16.75**	**0.46**	**48.18**	**70**	**4.77**	**39151**

Percentage tensile strength-time plots of the nine test categories are presented here. The results show huge variation that a logarithmic trend line is plotted here. The general trend shows a time-dependency with the short times to failure for test loads between 80 and 90% of the tensile strength and prolonged failure times for the tests loads below 80% of the tensile strength.

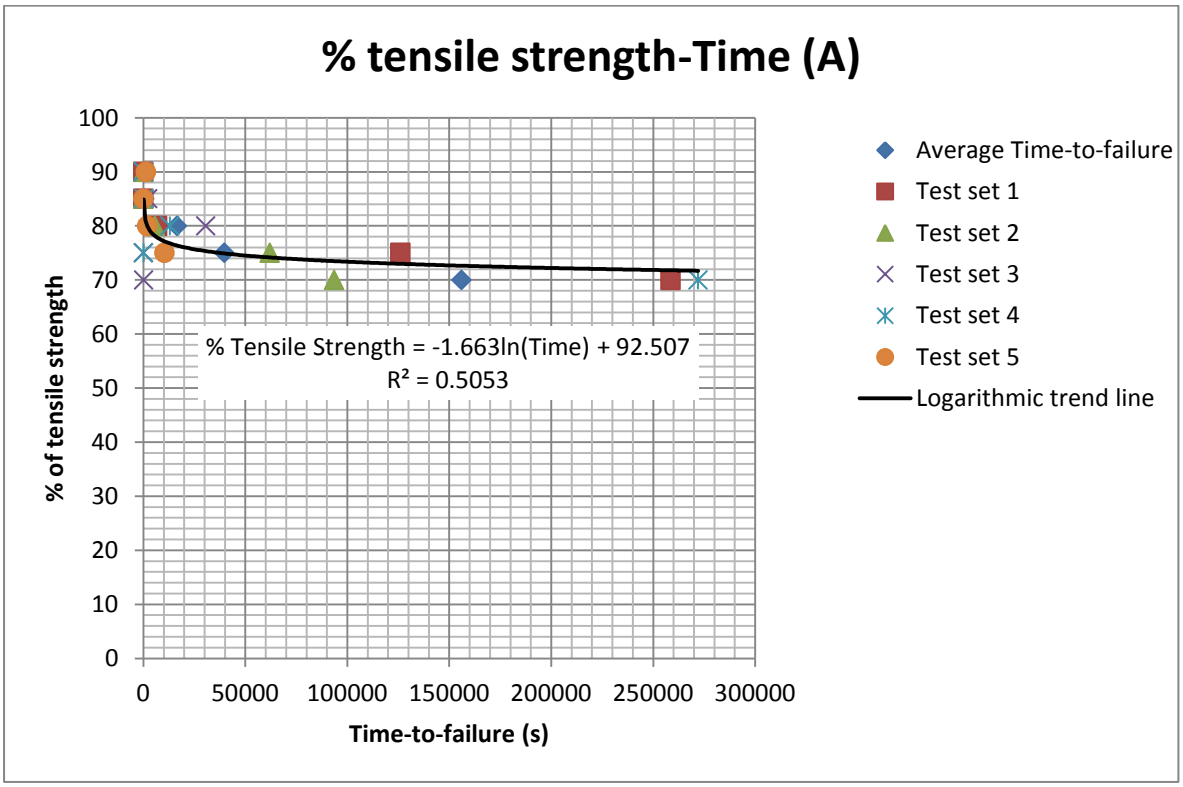


Figure B3-1: Time-to-failure plots: (mottled anorthosite)

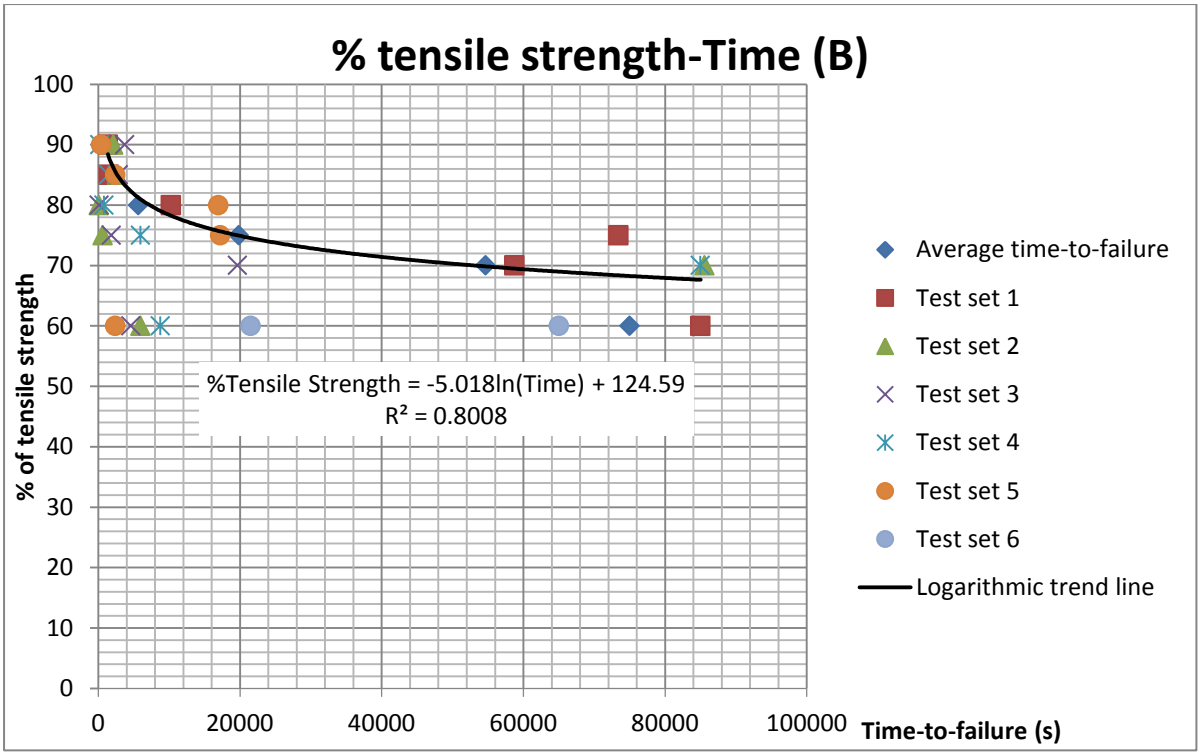


Figure B3-2: Time-to-failure plots: (spotted anorthositic norite)

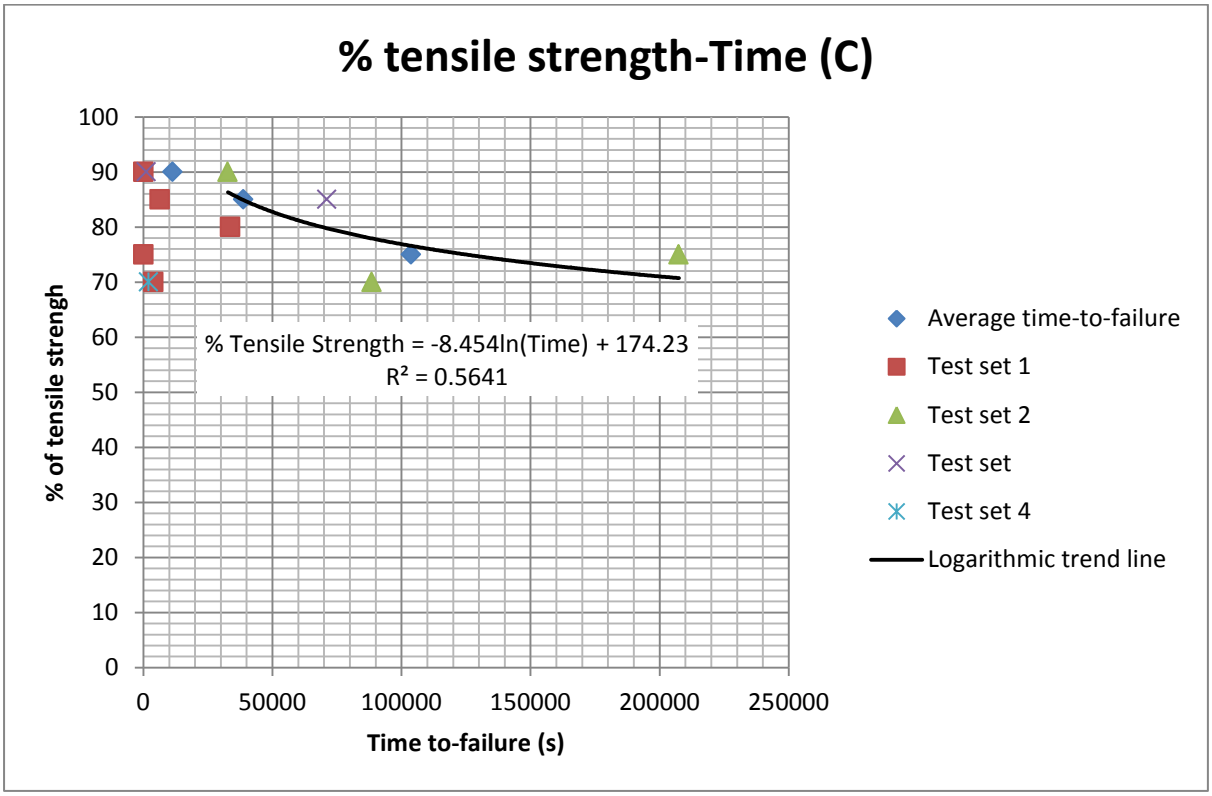


Figure B3-3: Time-to-failure plots: (pyroxenite)

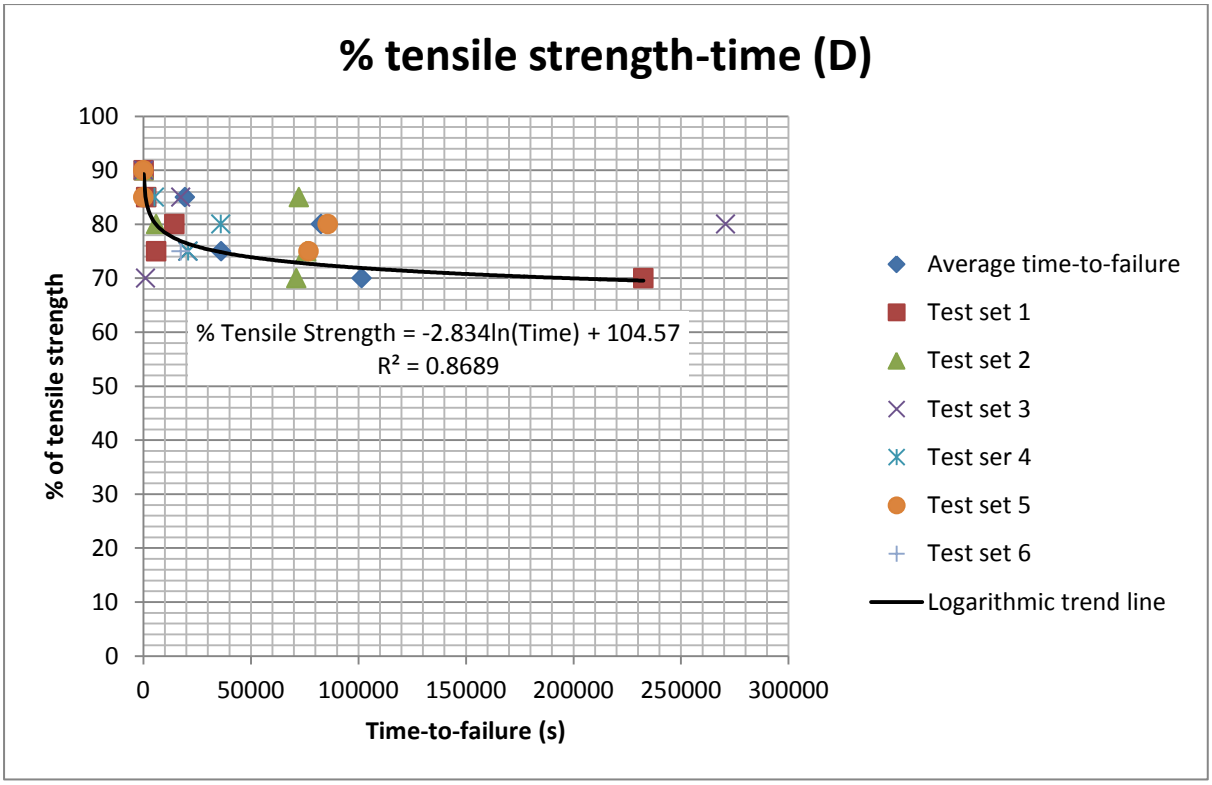


Figure B3-4: Time-to-failure plots: (mottled anorthosite)

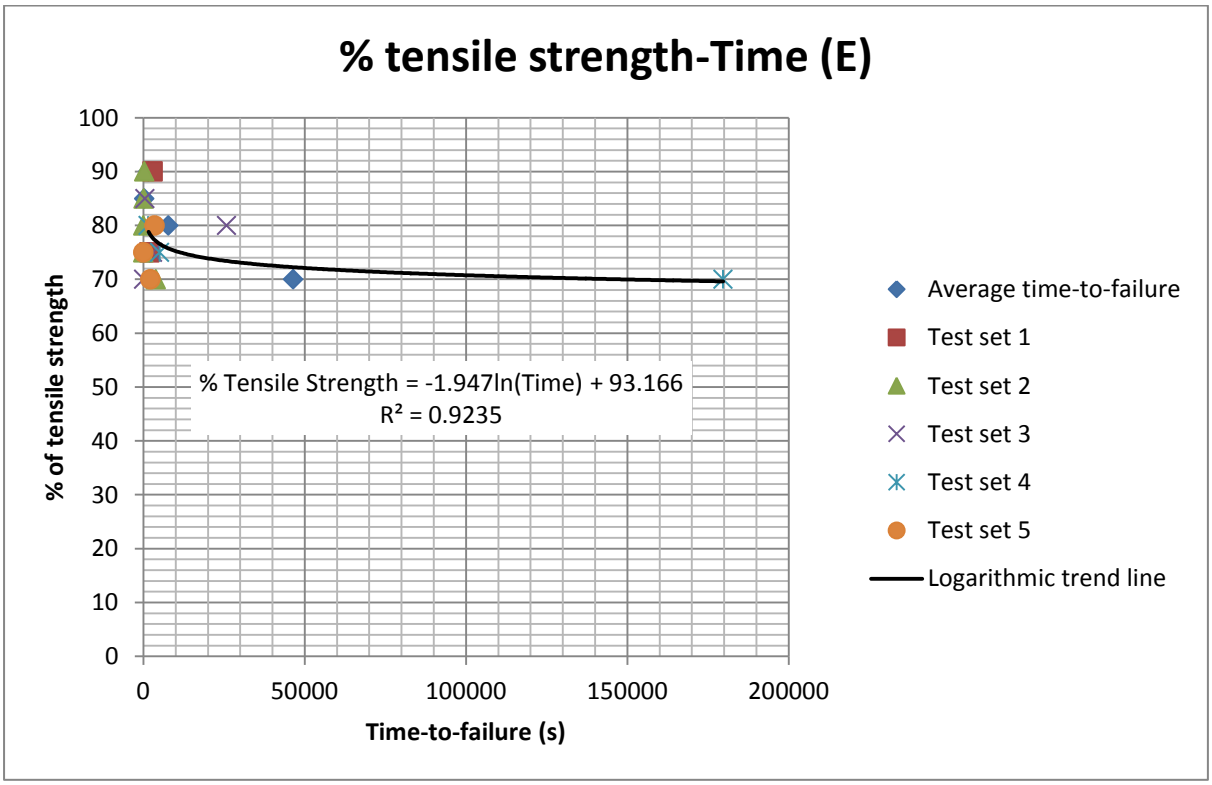


Figure B3-5: Time-to-failure plots: (norite)

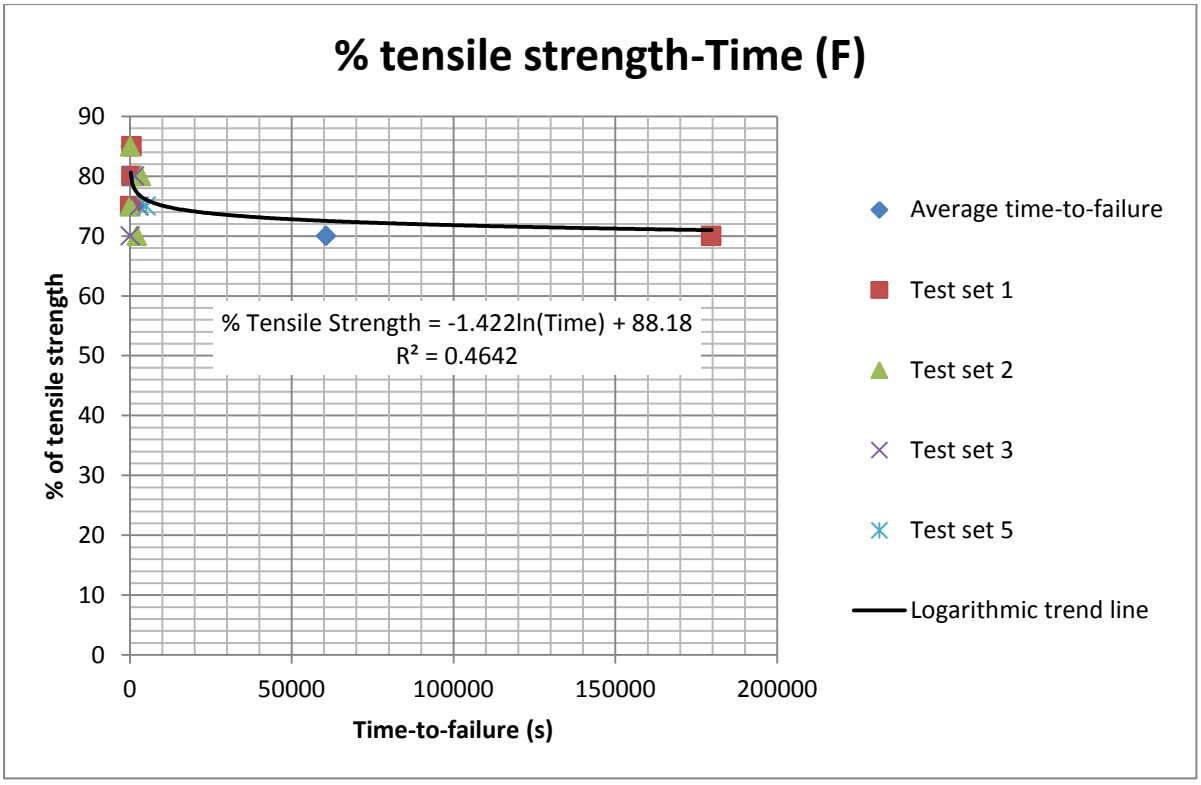


Figure B3-6: Time-to-failure plots: (spotted anorthositic norite)

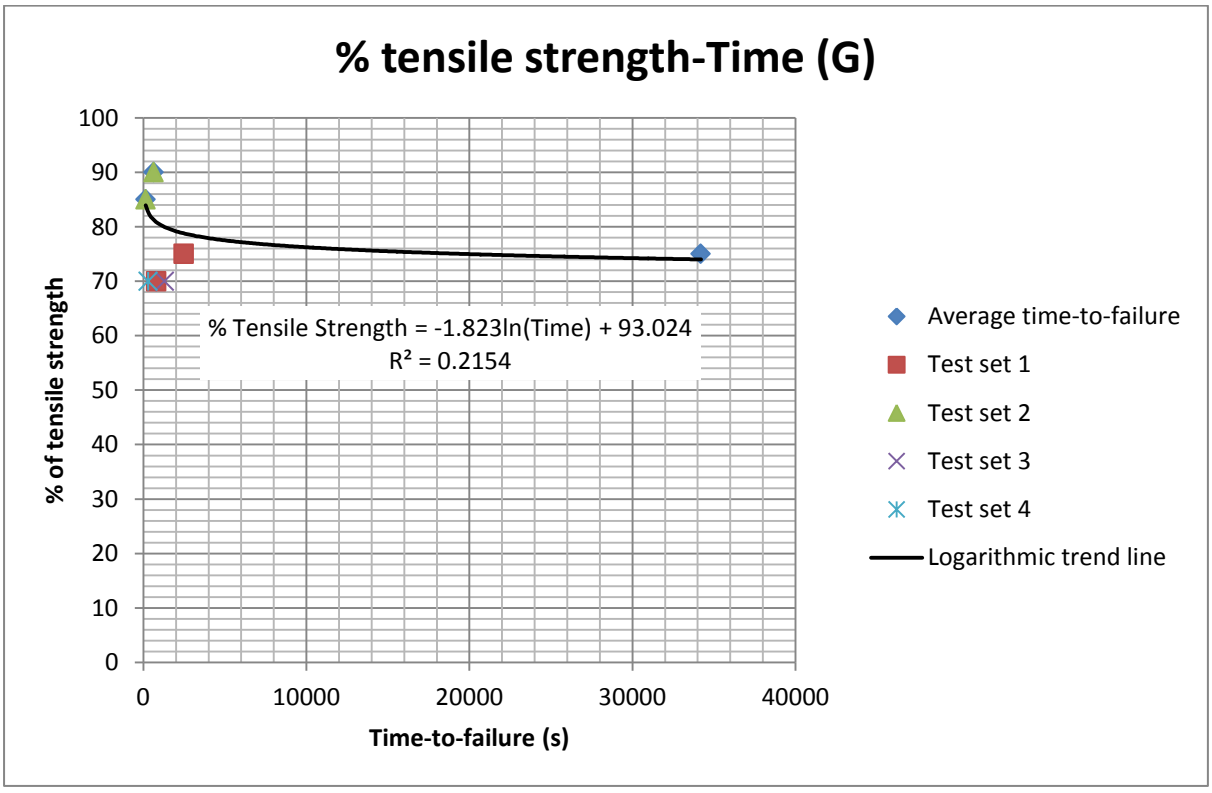


Figure B3-7: Time-to-failure plots: (anorthositic norite)

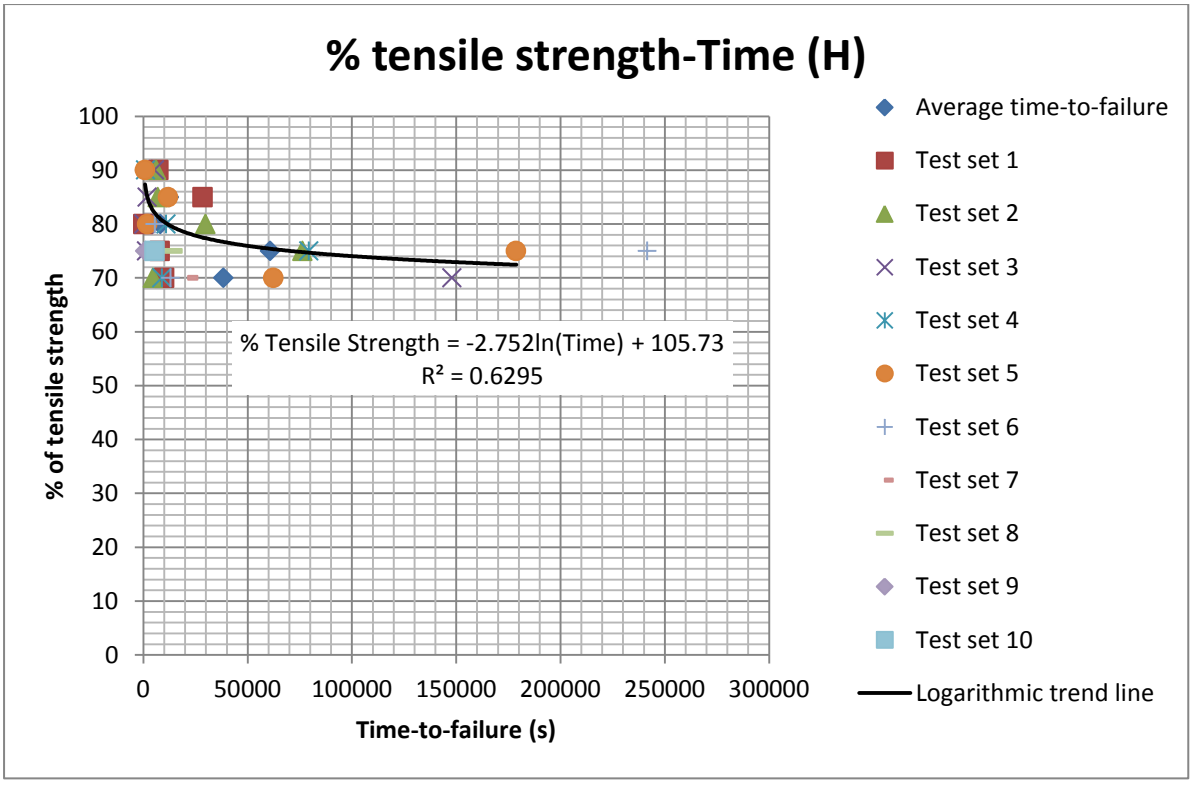


Figure B3-8: Time-to-failure plots: (spotted anorthosite)

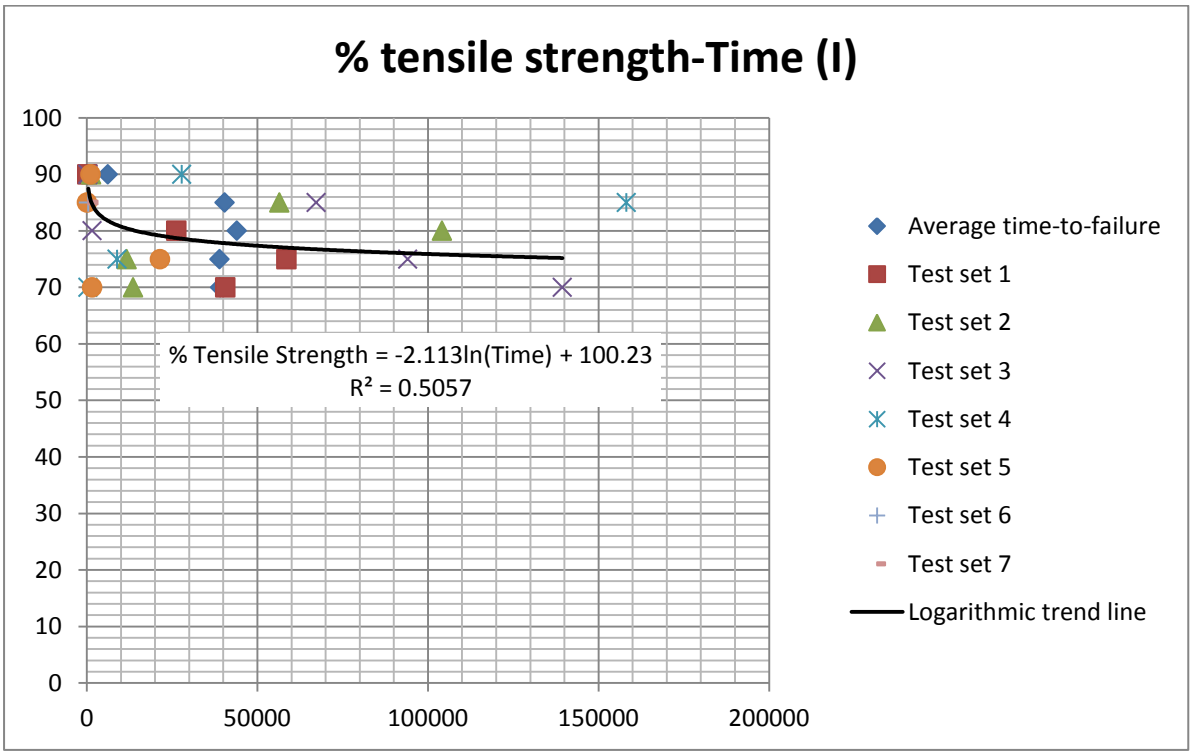


Figure B3-9: Time-to-failure plots: (mottled anorthosite)

Appendix C: Numerical modelling results (Stress and strain analysis)

C1 Stress and strain analysis: Incline shaft

Models of an incline shaft and a stope were analysed in a similar way to the in-stope pillar models. These models were run to validate the observations made in the in-stope pillar models presented in Chapter 3 with differently shaped models. Major Principal Stress contours for four different scenarios are shown in Figures C1-1 to 1-4.

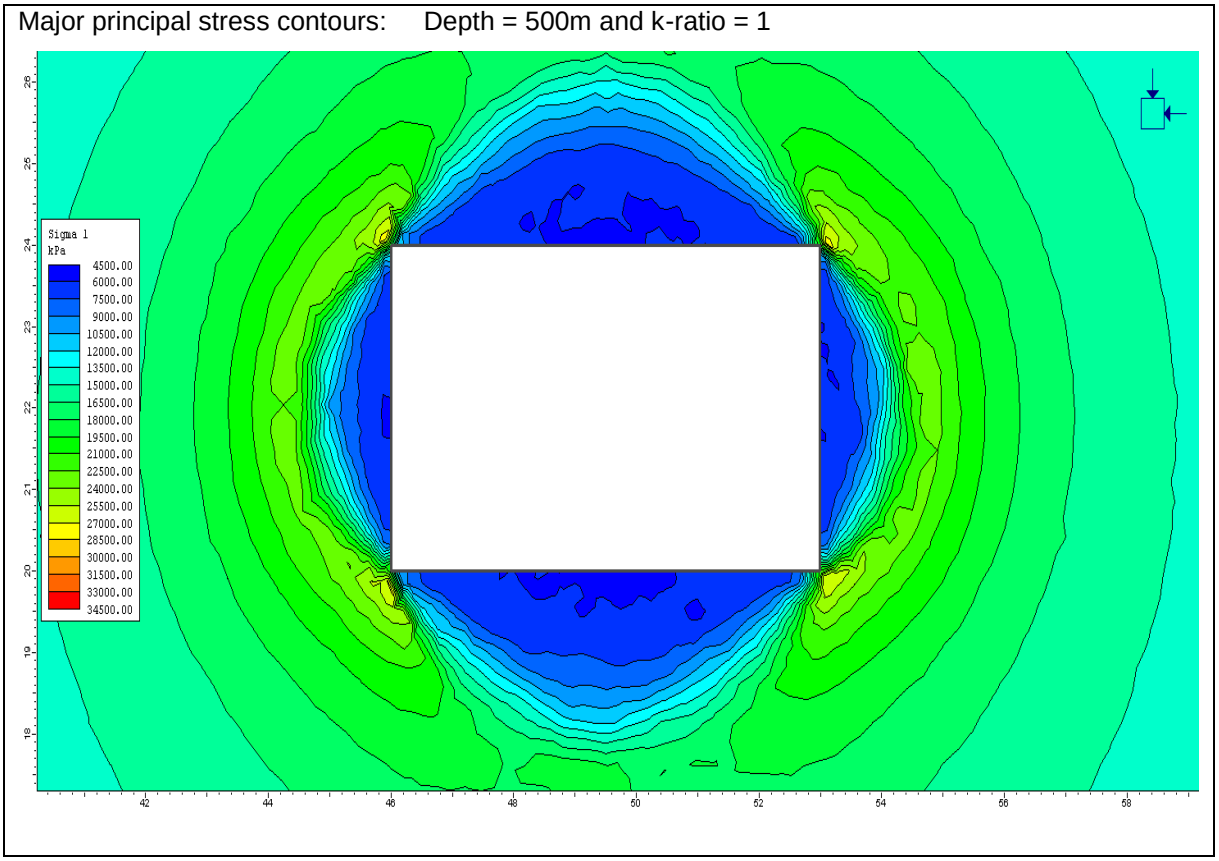


Figure C1-1: Major Principal Stress at a depth of 500m with k-ratio = 1

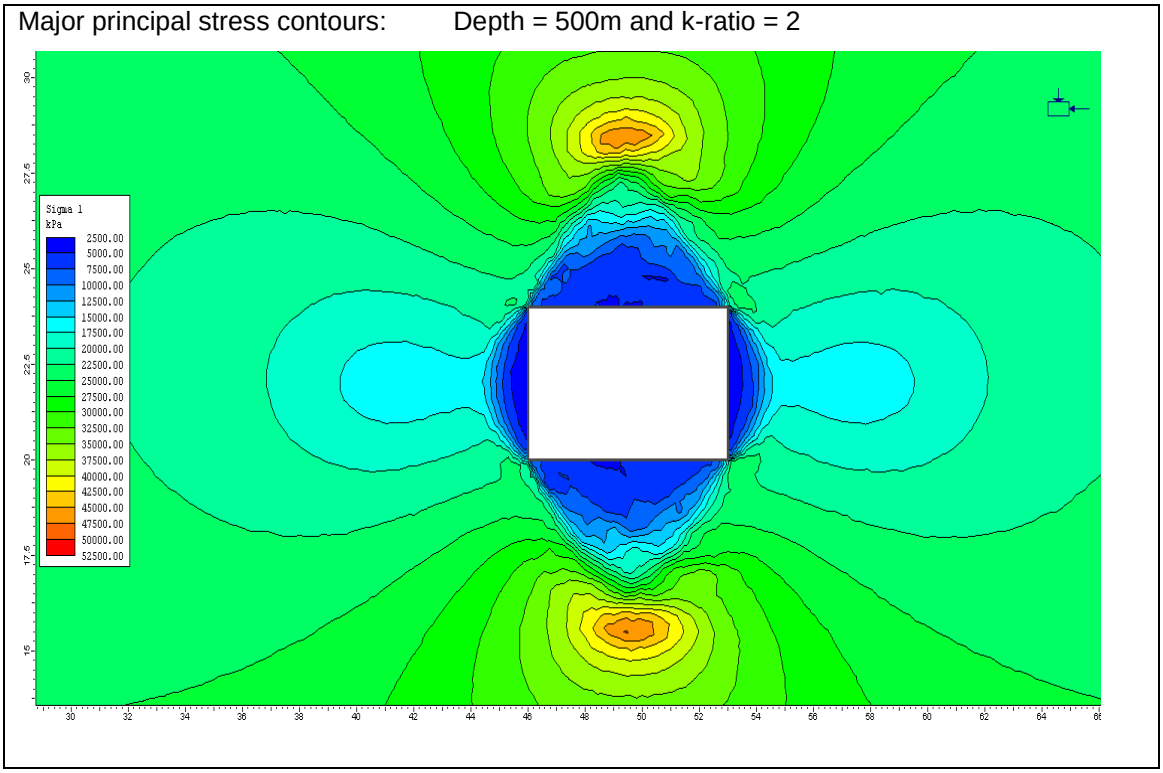


Figure C1-2: Major Principal Stress at a depth of 500m with k-ratio = 2

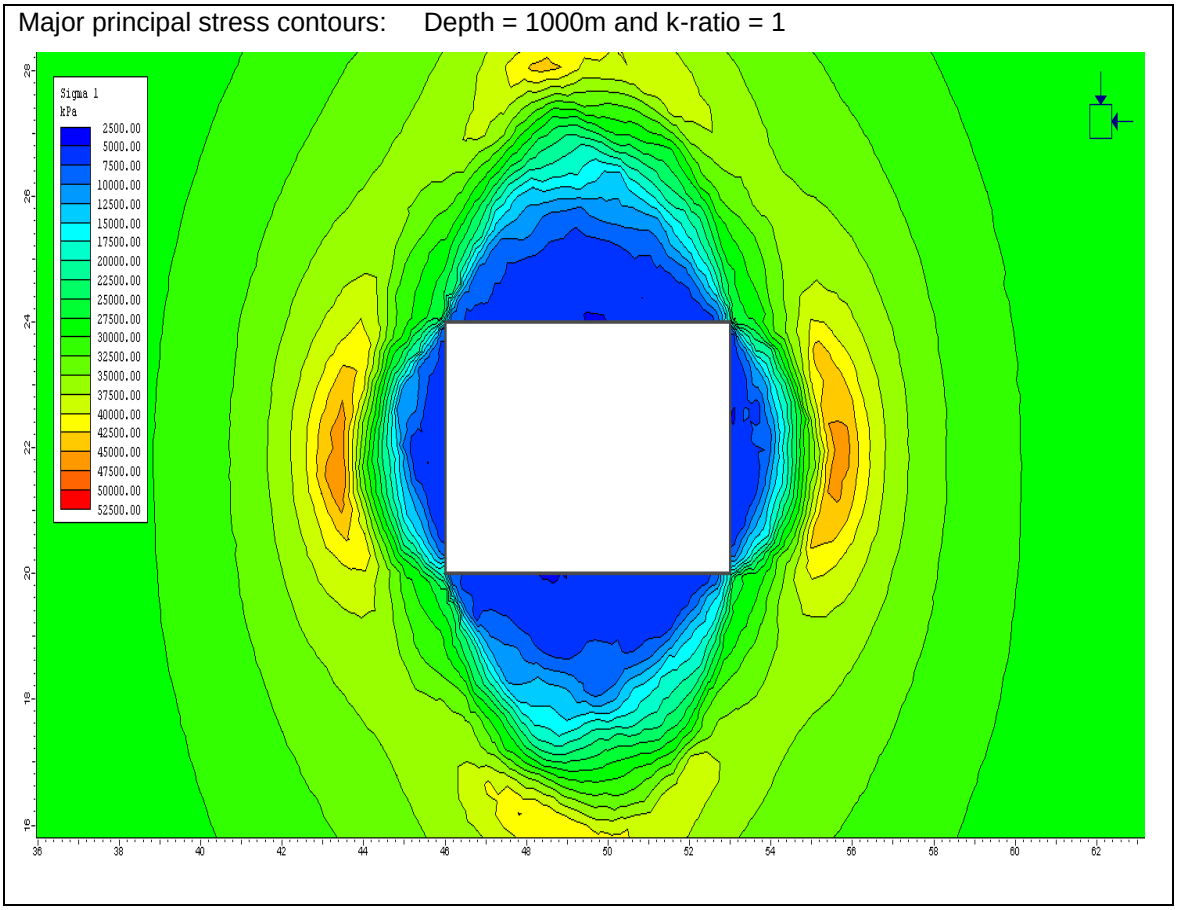


Figure C1-3: Major Principal Stress at a depth of 1000m with k-ratio = 1

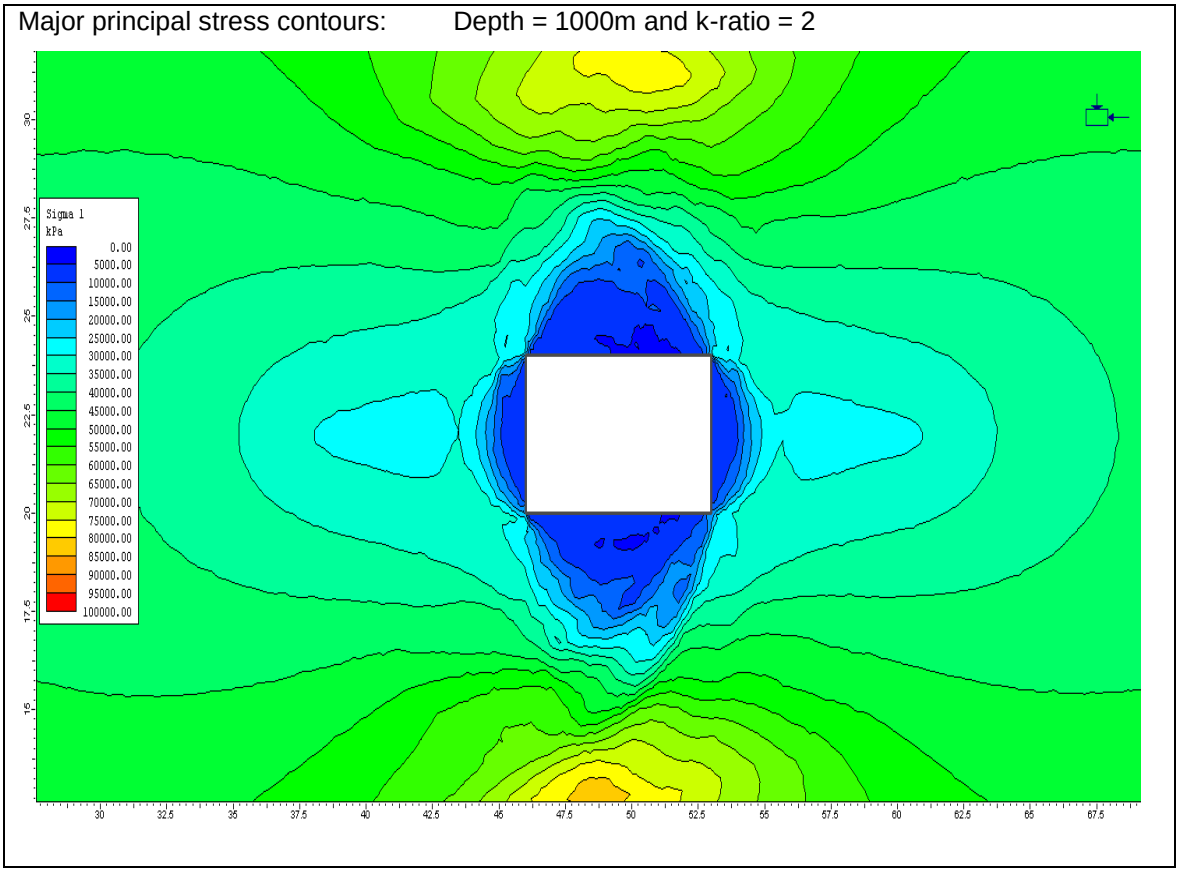


Figure C1-4: Major Principal Stress at a depth of 1000m with k-ratio = 2

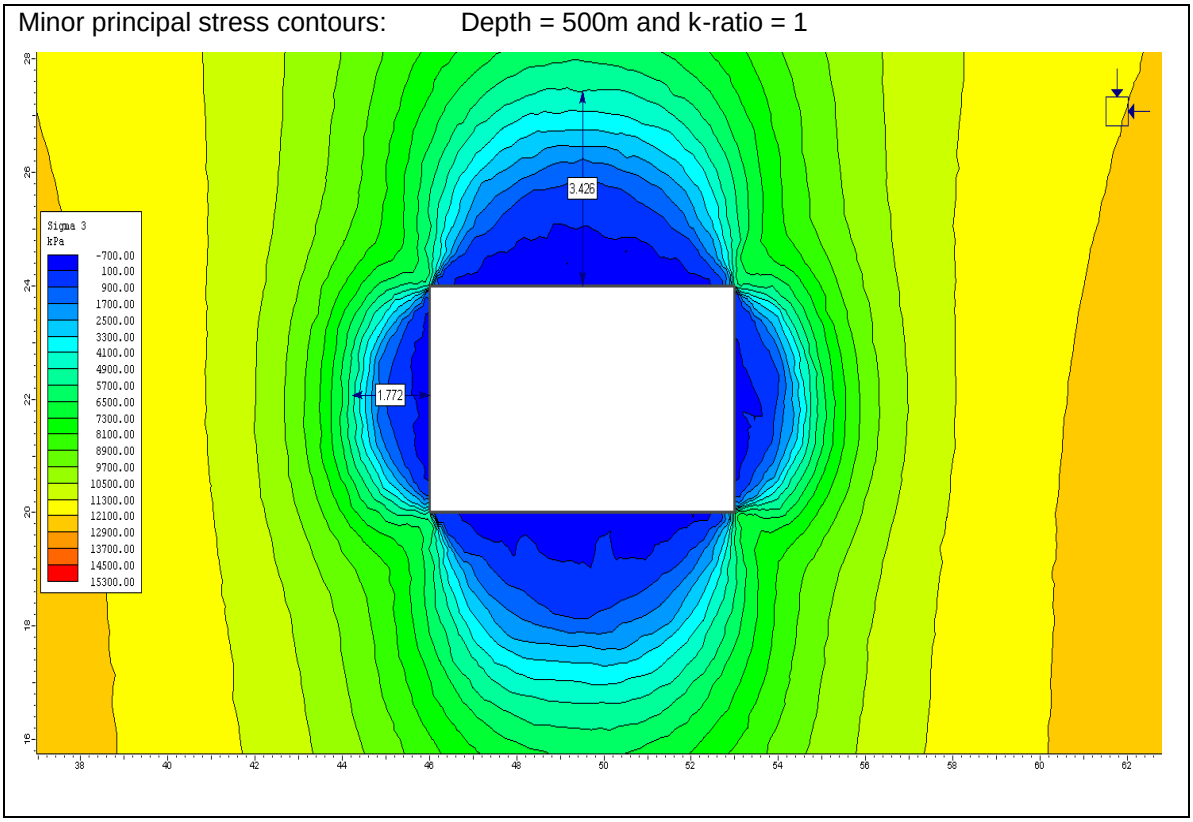


Figure C1-5: Minor Principal Stress at a depth of 500m with k-ratio = 1

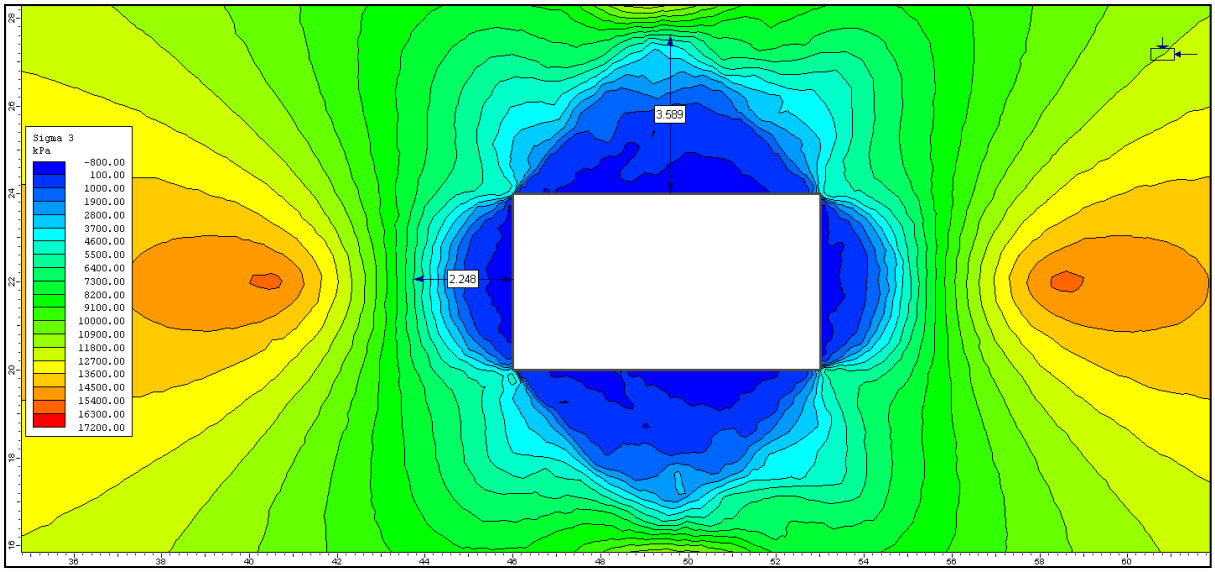


Figure C1-6: Minor Principal Stress at a depth of 500m with k-ratio = 2. The depth of influence of low compressive and tensile stresses is indicated

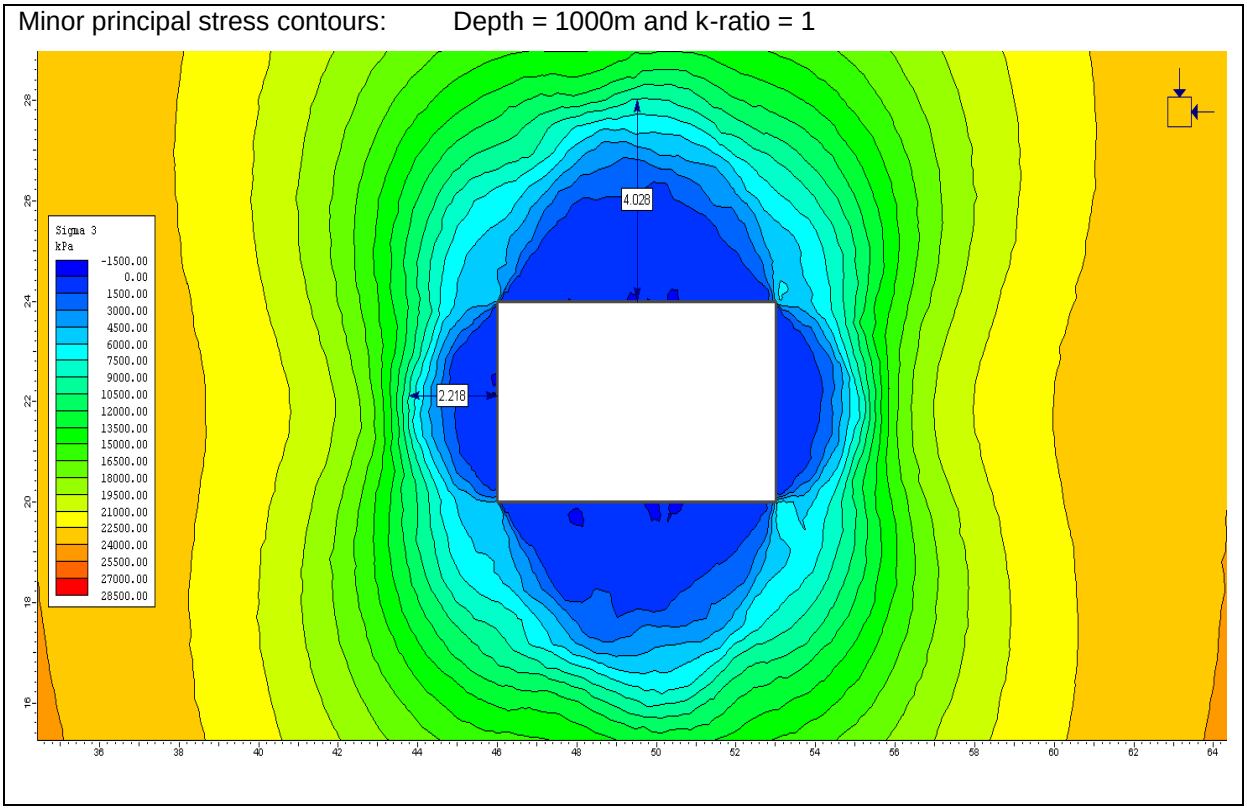


Figure C1-7: Minor Principal Stress at a depth of 1000m with k-ratio = 1

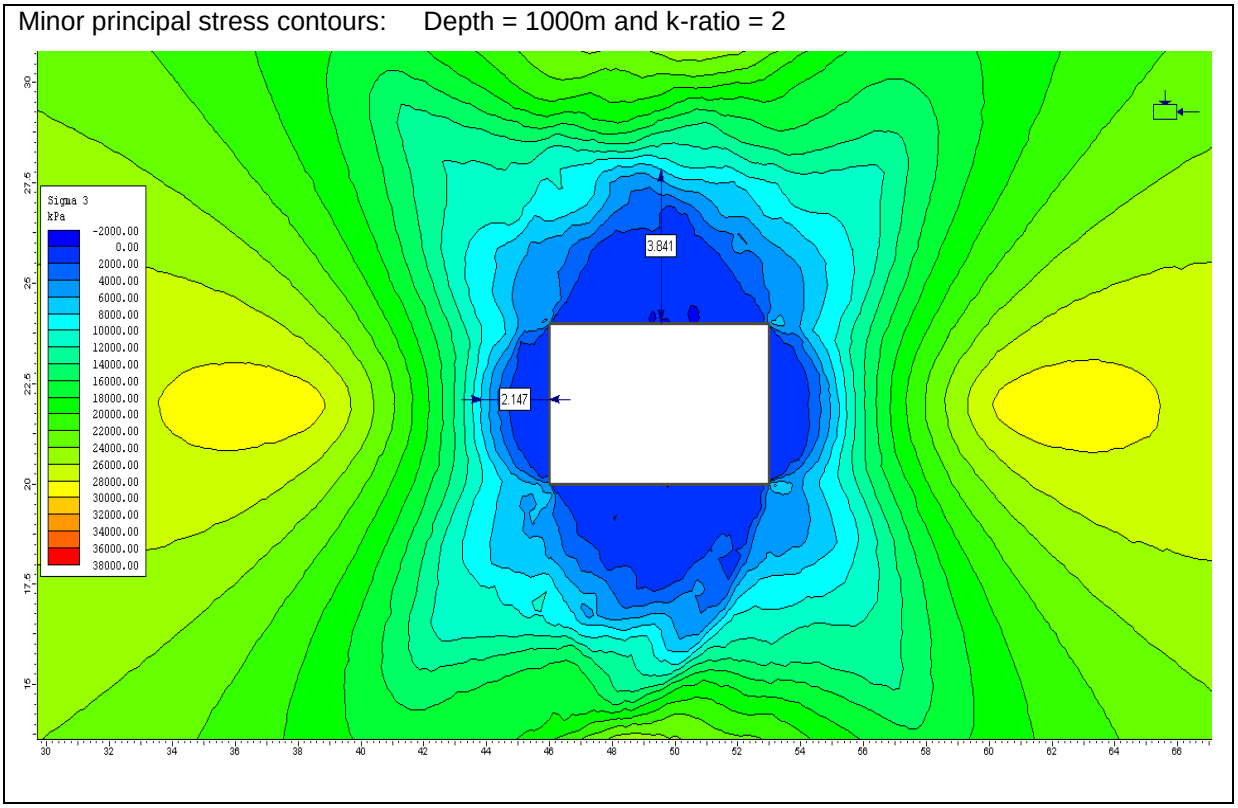


Figure C1-8: Minor Principal Stress at a depth of 1000m with k-ratio = 2

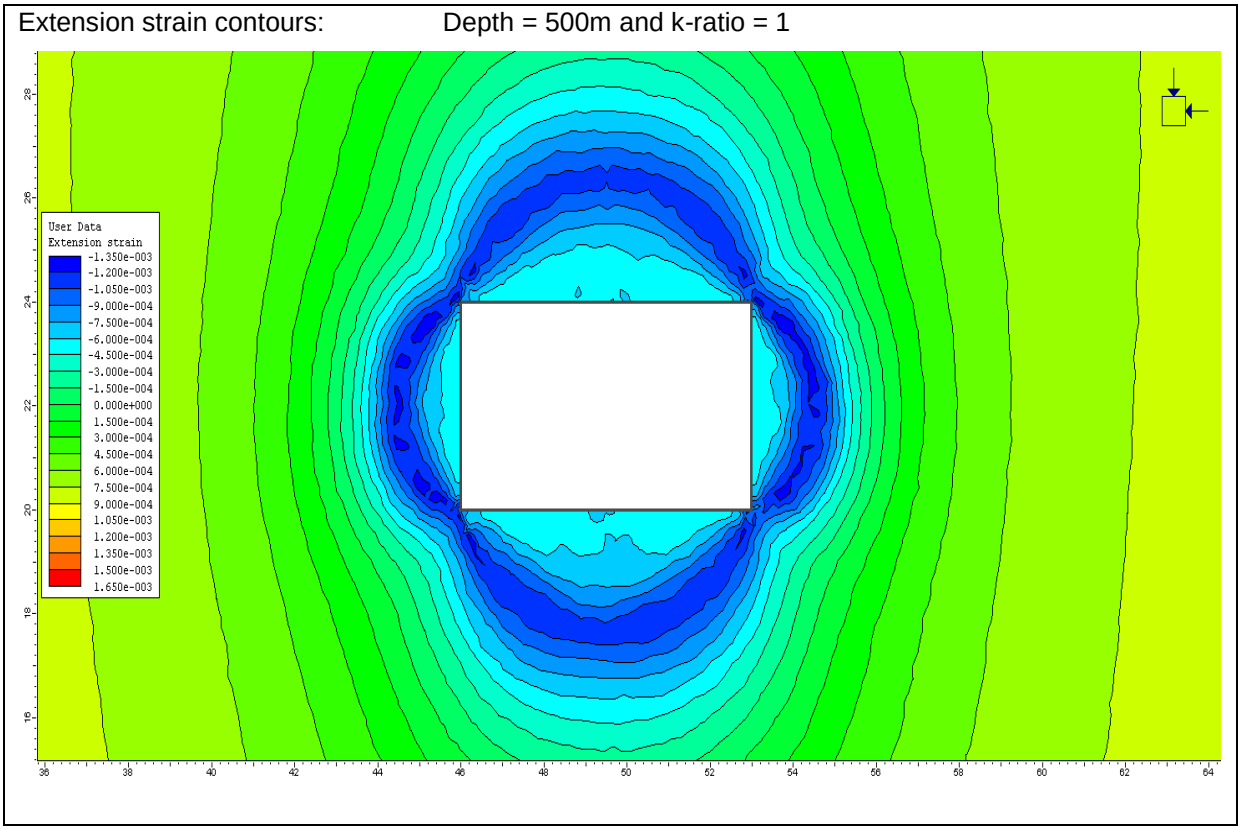


Figure C1-9: Extension strain at a depth of 500m with k-ratio = 1

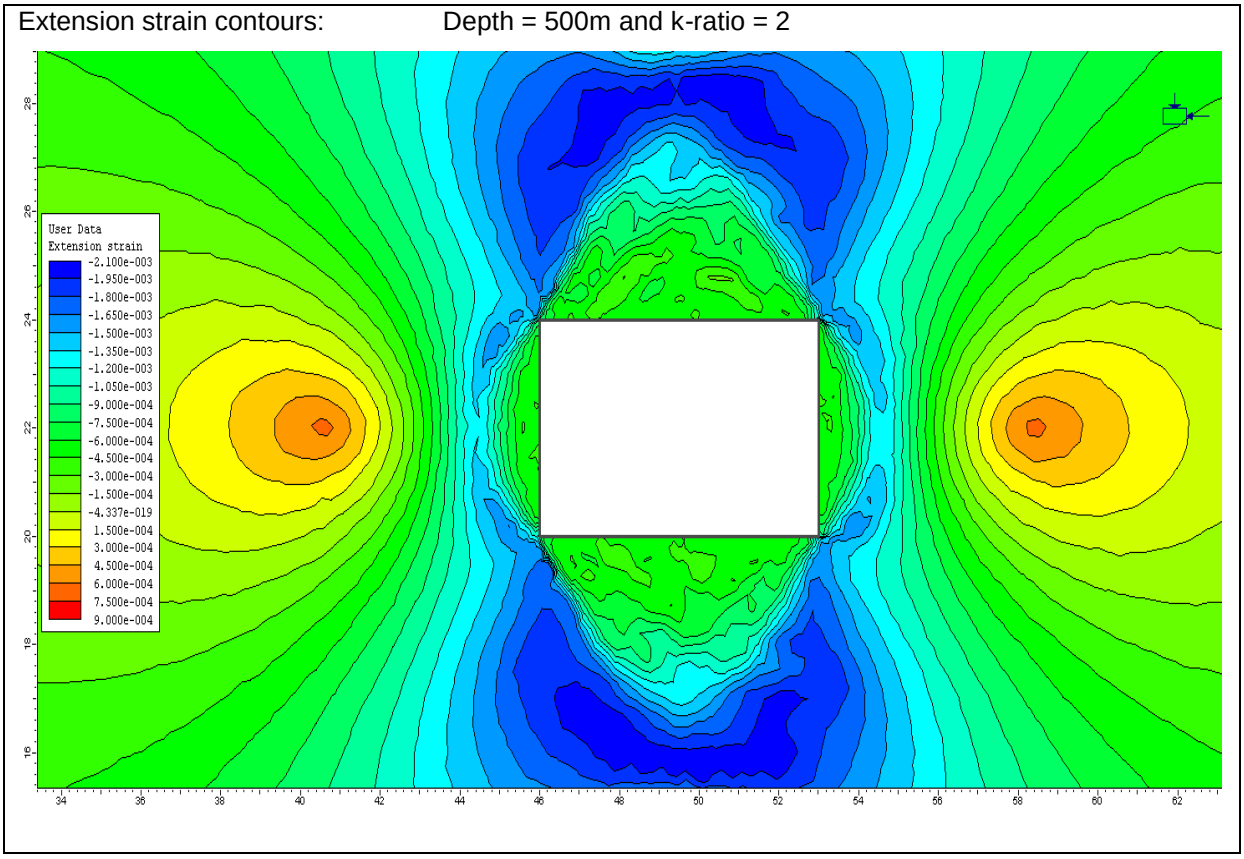


Figure C1-10: Extension strain at a depth of 500m with k-ratio = 2

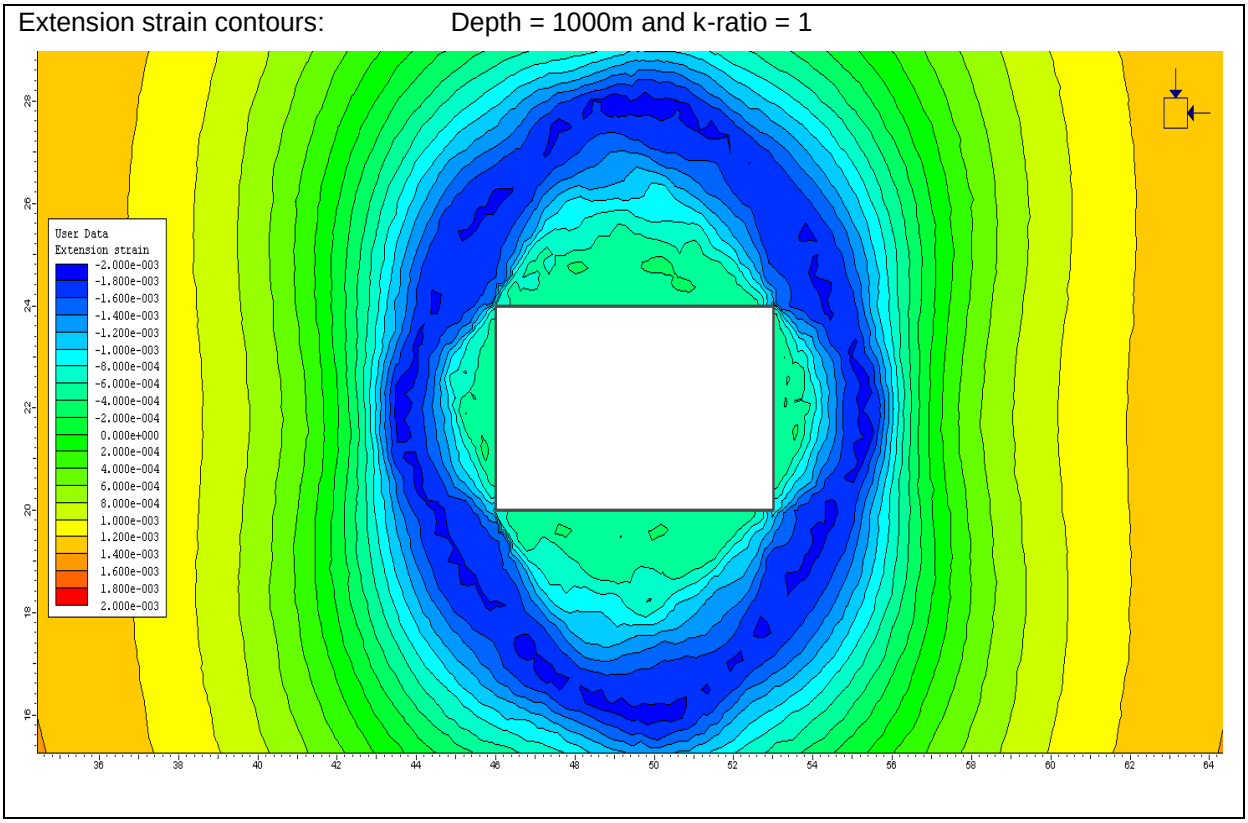


Figure C1-11: Extension strain at a depth of 1000m with k-ratio = 1

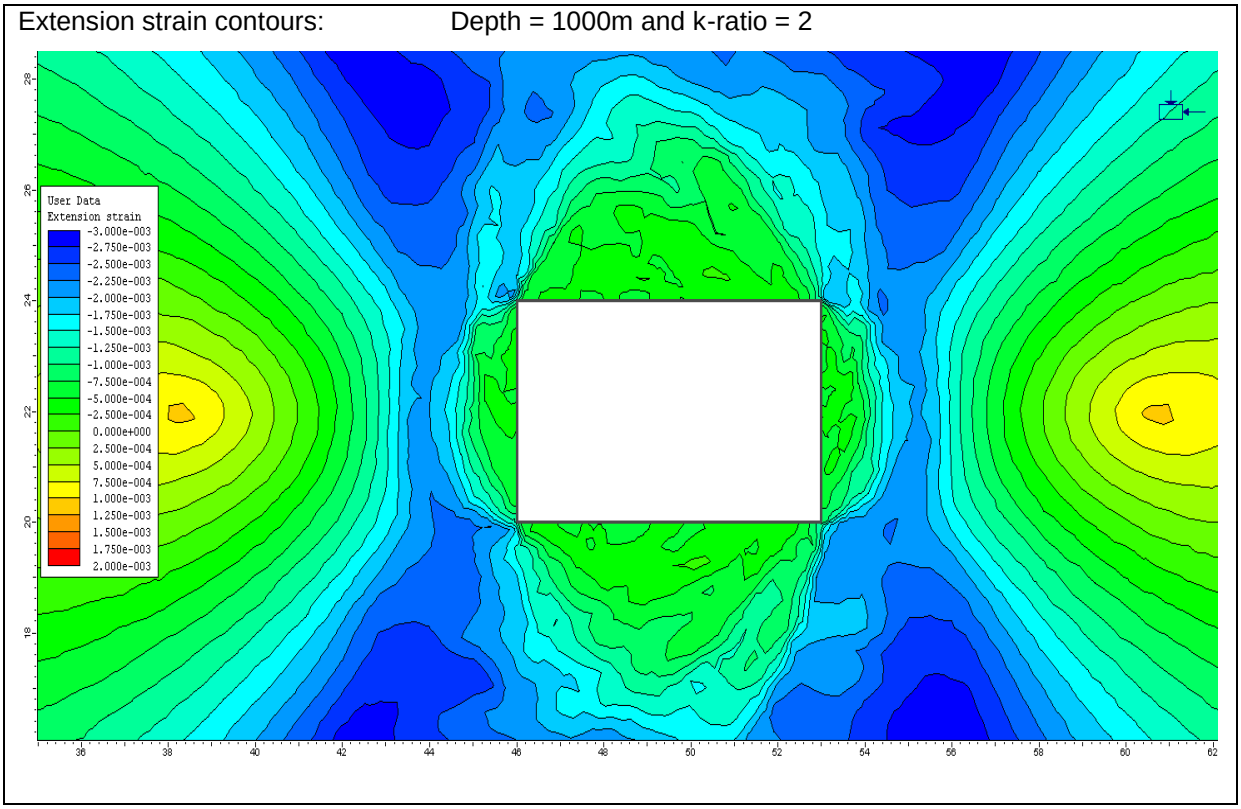


Figure C1-12: Extension strain at a depth of 1000m with k-ratio = 2

Figures C1-5 to C1-8 show the excavation walls under stress conditions ranging from tensile (-2 MPa) to very low compressive stress (maximum 5.7 MPa) at a depth of 500m and k = 1. Similar low compressive stress trends were shown for the other loading conditions with the deepest low compression influence being 3.589 m into the hanging wall. The extension strain contours are shown in Figures C1-9 to C1-12. The immediate walls of the excavation were observed to experience negative extension strain implying the probability of fracture initiation in these walls. Very low confinement is experienced in the walls of the excavation, conditions conducive for spalling of the wall rock. In the BC mine excavations confinement is often provided by installed area cover support, curbing the spalling in life of mine excavations. Analysis of stress-strain in a mining stope follows in appendix C2.

C2 Stress and strain analysis: mining stope

Results of stress-strain analysis of a mining stope are presented in Figures C2-1 to C2-4.

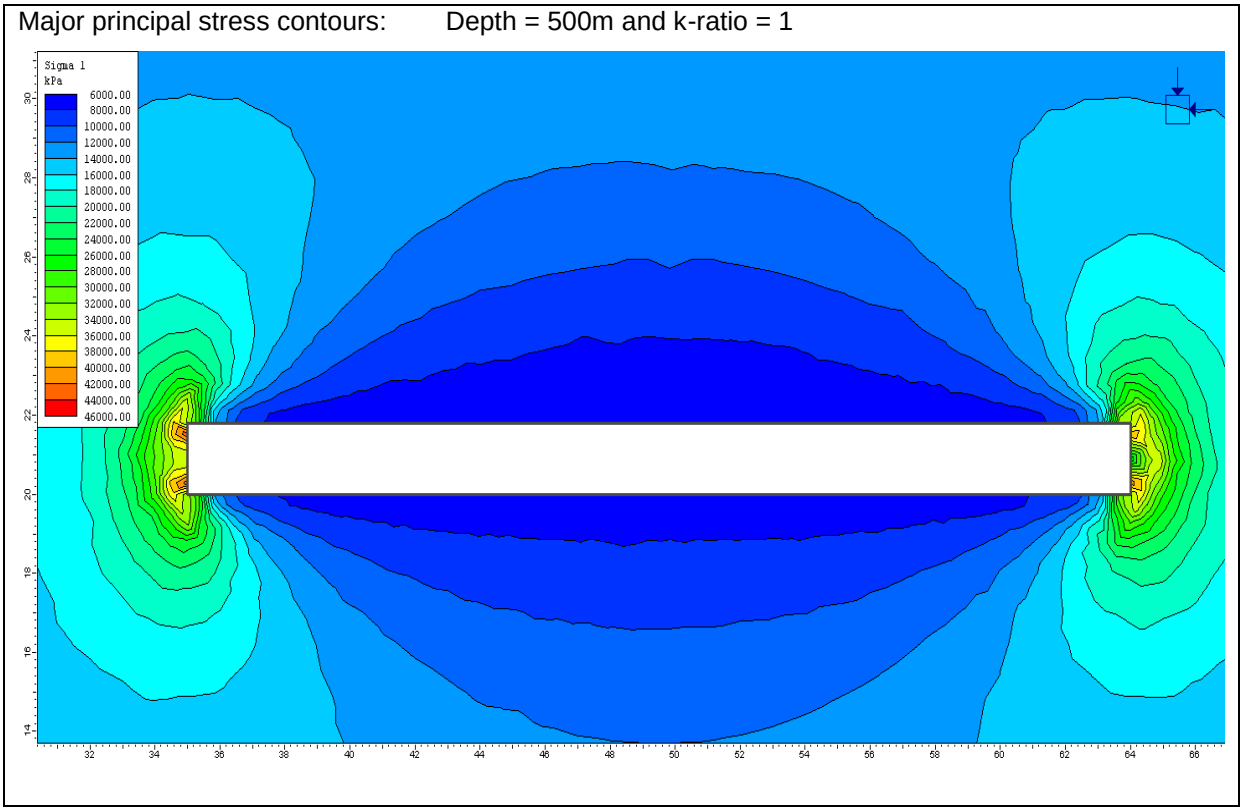


Figure C2-1: Major Principal Stress at a depth of 500m with k-ratio = 1

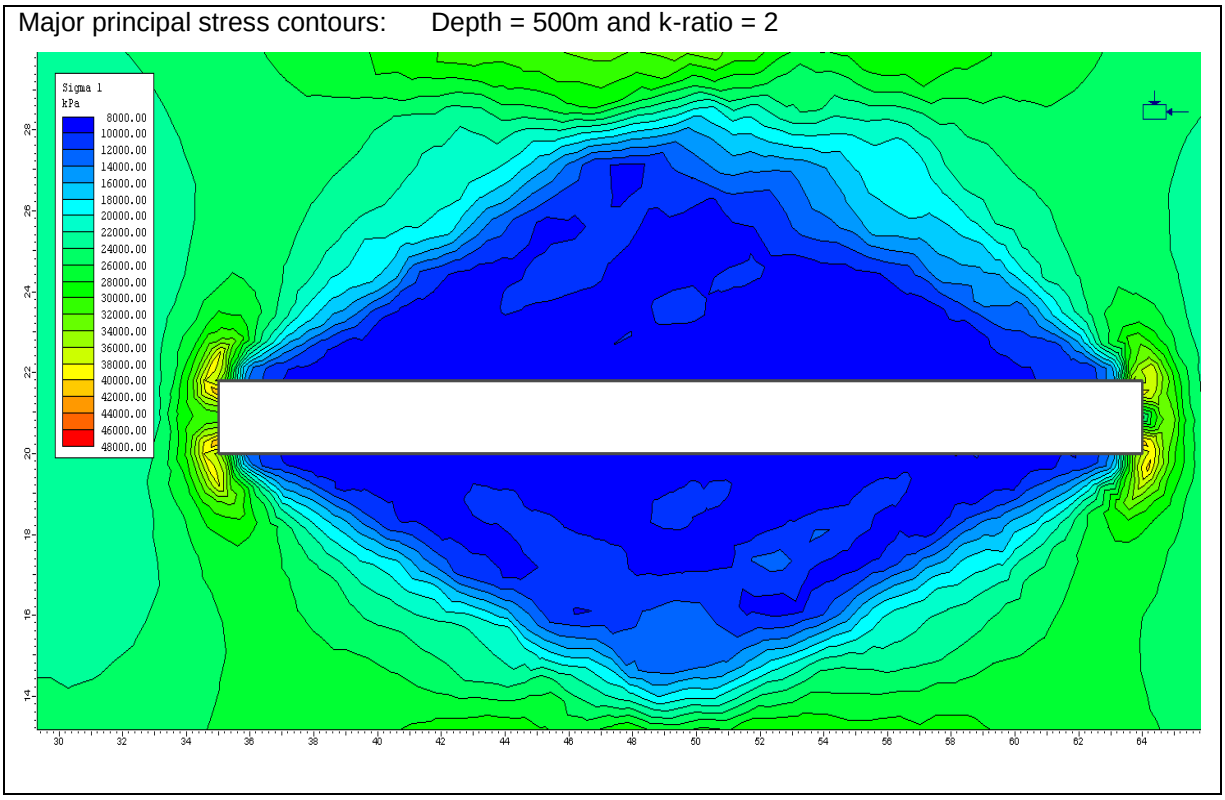


Figure C2-2: Major Principal Stress at a depth of 500m with k-ratio = 2

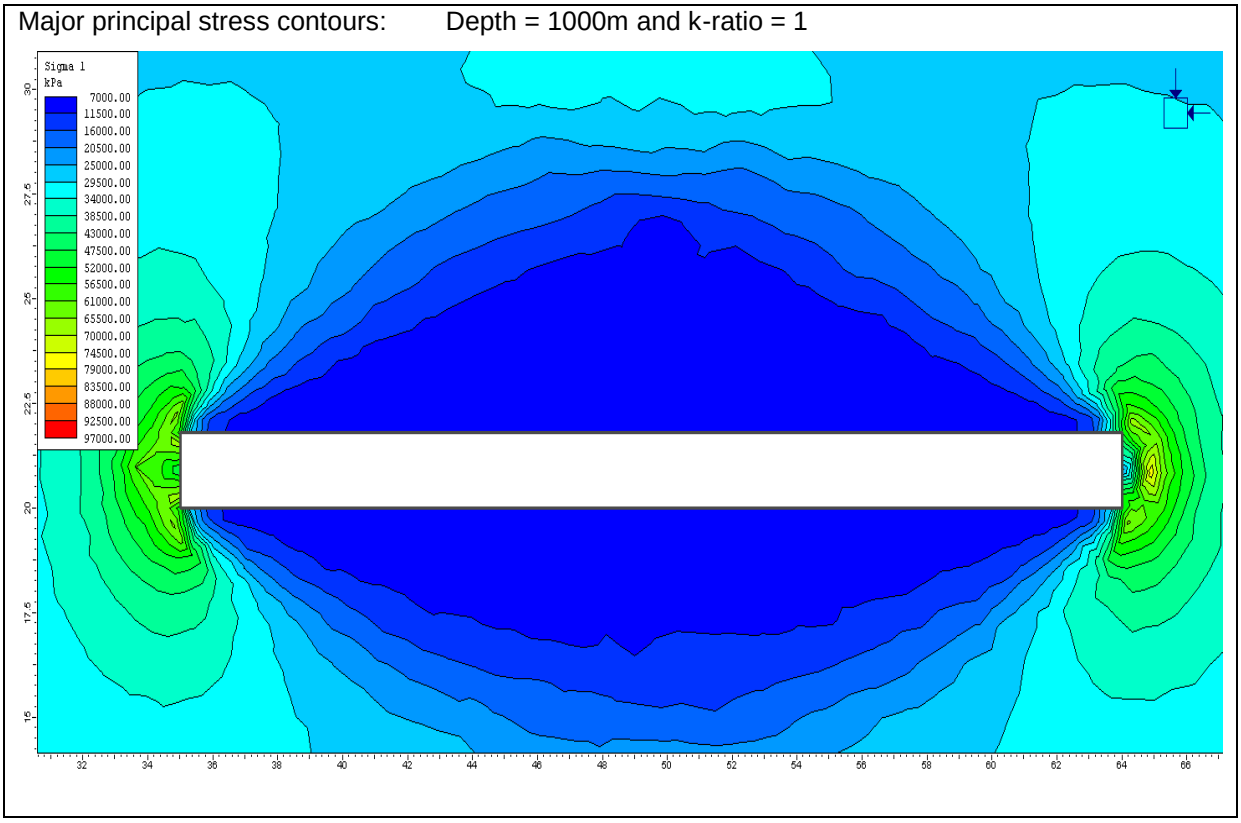


Figure C2-3: Major Principal Stress at a depth of 1000m with k-ratio = 1

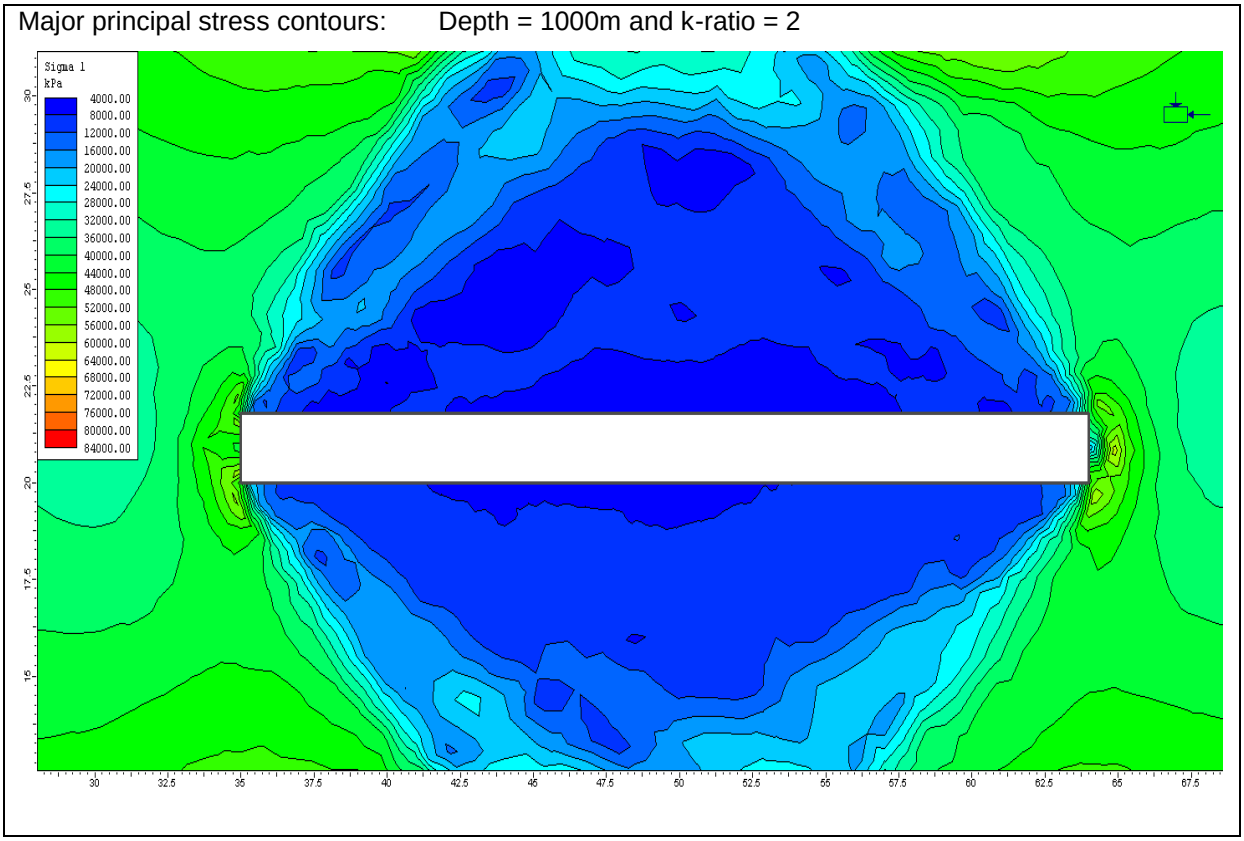


Figure C2-4: Major Principal Stress at a depth of 1000m with k-ratio = 2

Notice the similarity in the pictures of contour plots with the in-stope pillar models already presented in chapter 3. It is observed here that the excavation walls are under very low compressive stress, similar to the observations made in the in-stope pillar and incline shaft models. Minor principal stress contours are shown in Figures C2-5 to C2-8.

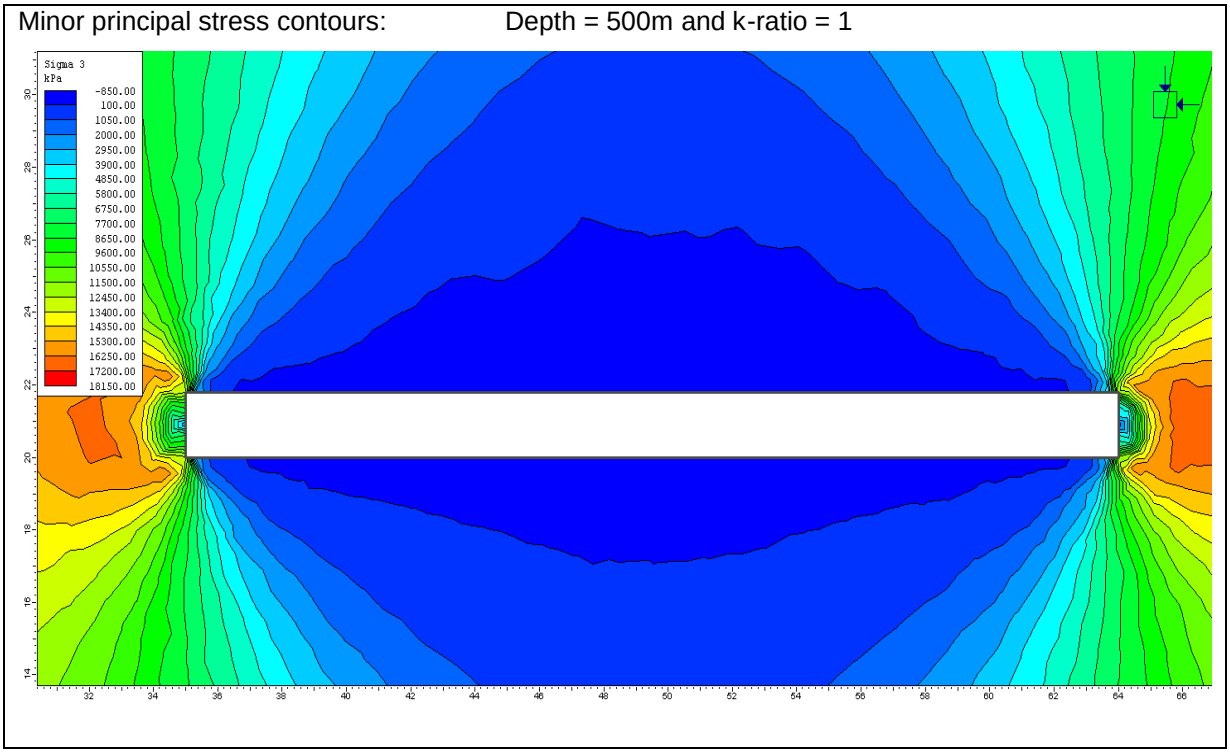


Figure C2-5: Minor Principal Stress at a depth of 500m with k-ratio = 1

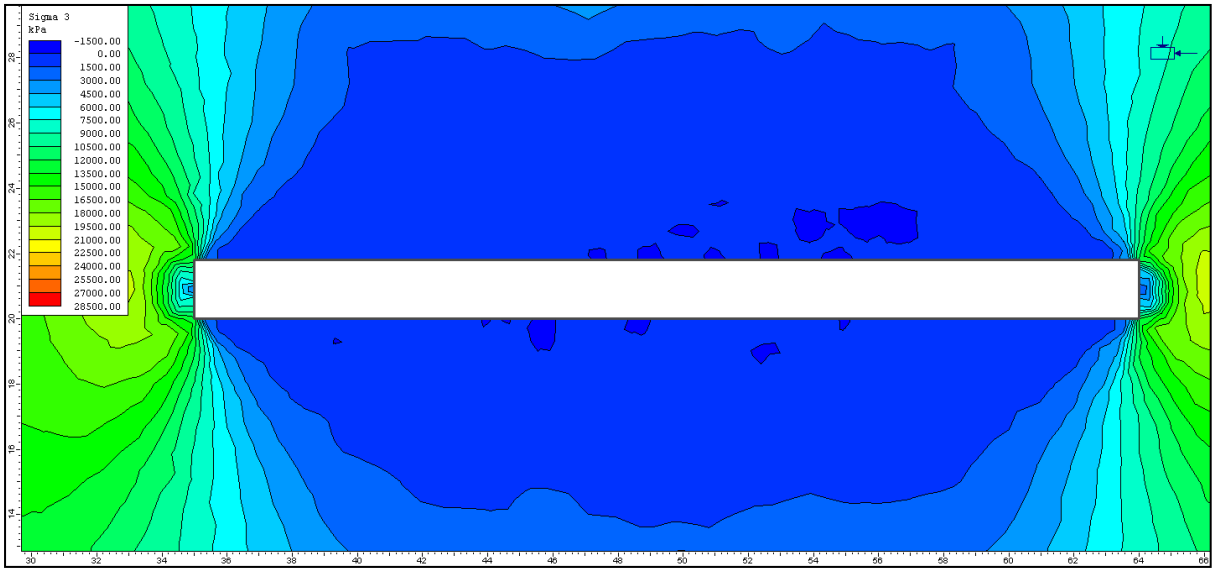


Figure C2-6: Minor Principal Stress at a depth of 500m with k-ratio = 2

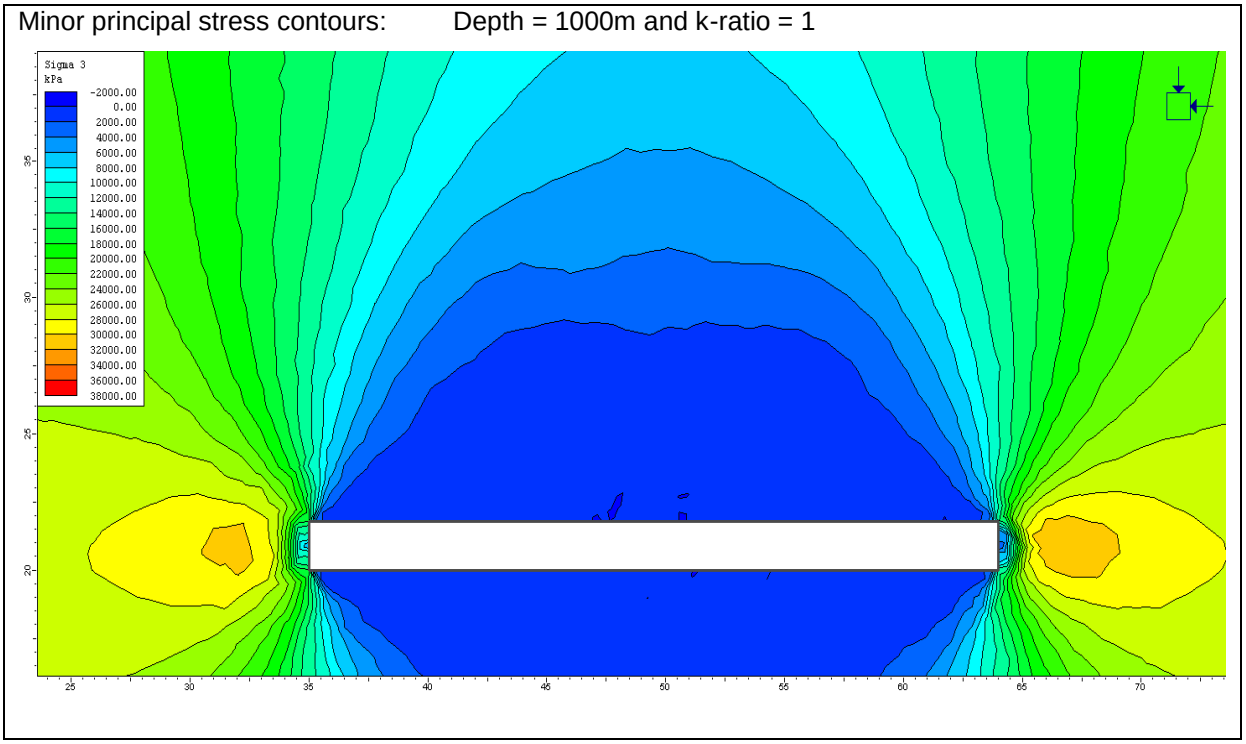


Figure C2-7: Minor Principal Stress at a depth of 1000m with k-ratio = 1

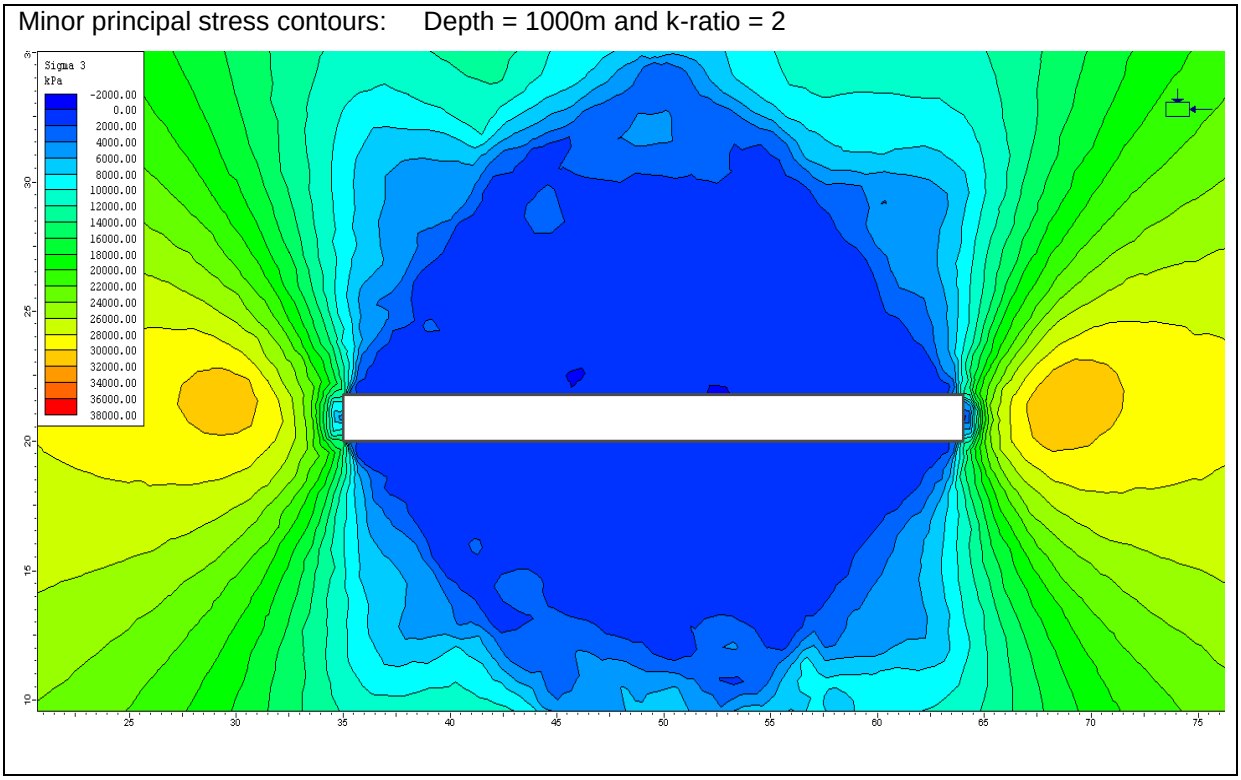


Figure C2-8: Minor Principal Stress at a depth of 1000m with k-ratio = 2

Notice how the periphery of the stope is largely under very low compressive stress and in some instances tensile stress.

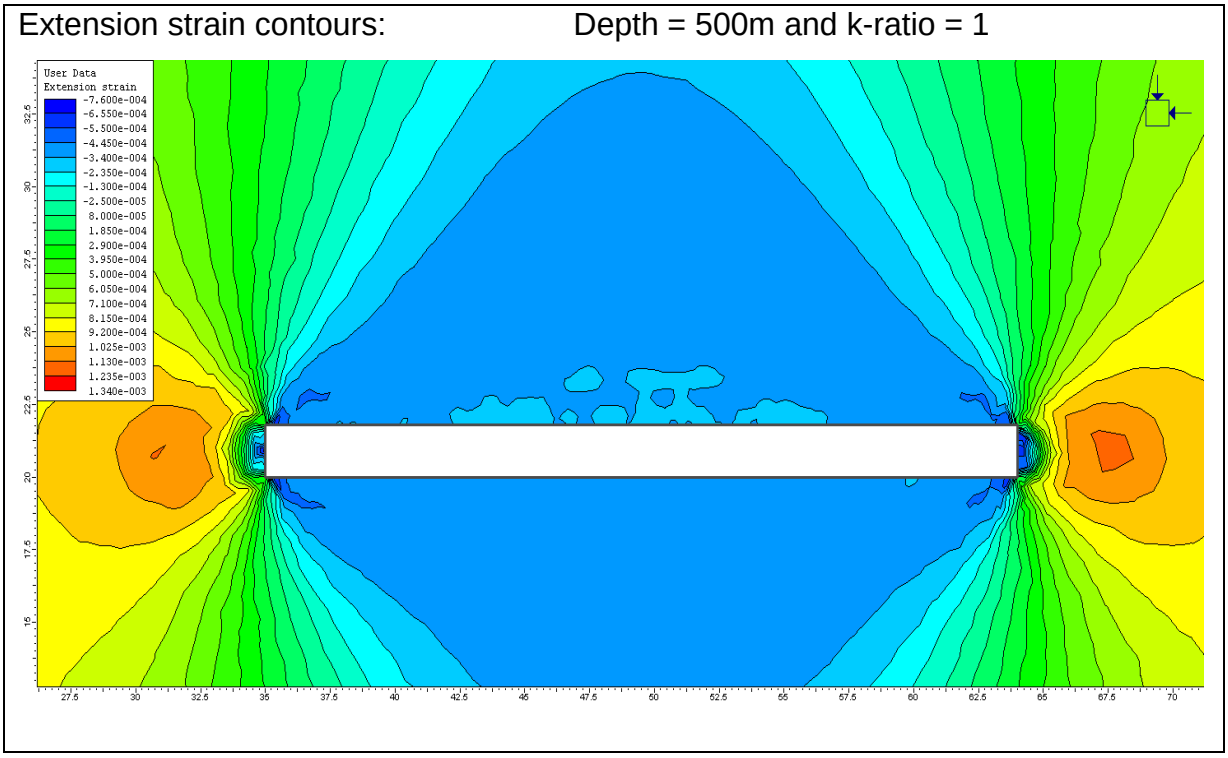


Figure C2-9: Extension strain at a depth of 500m with k-ratio = 1

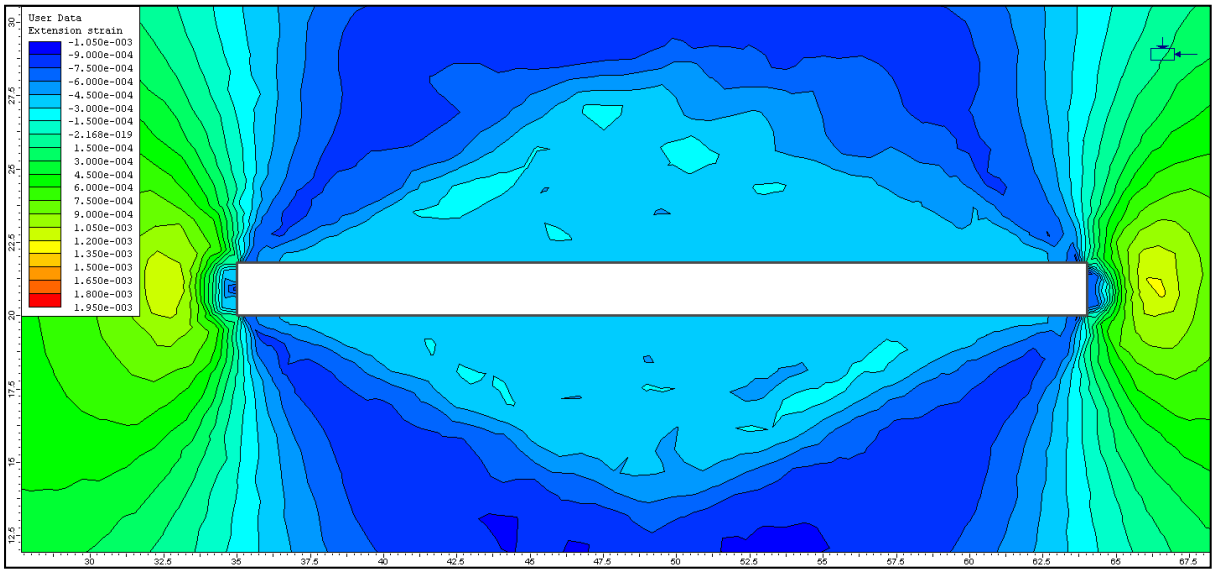


Figure C2-10: Extension strain at a depth of 500m with k-ratio = 2

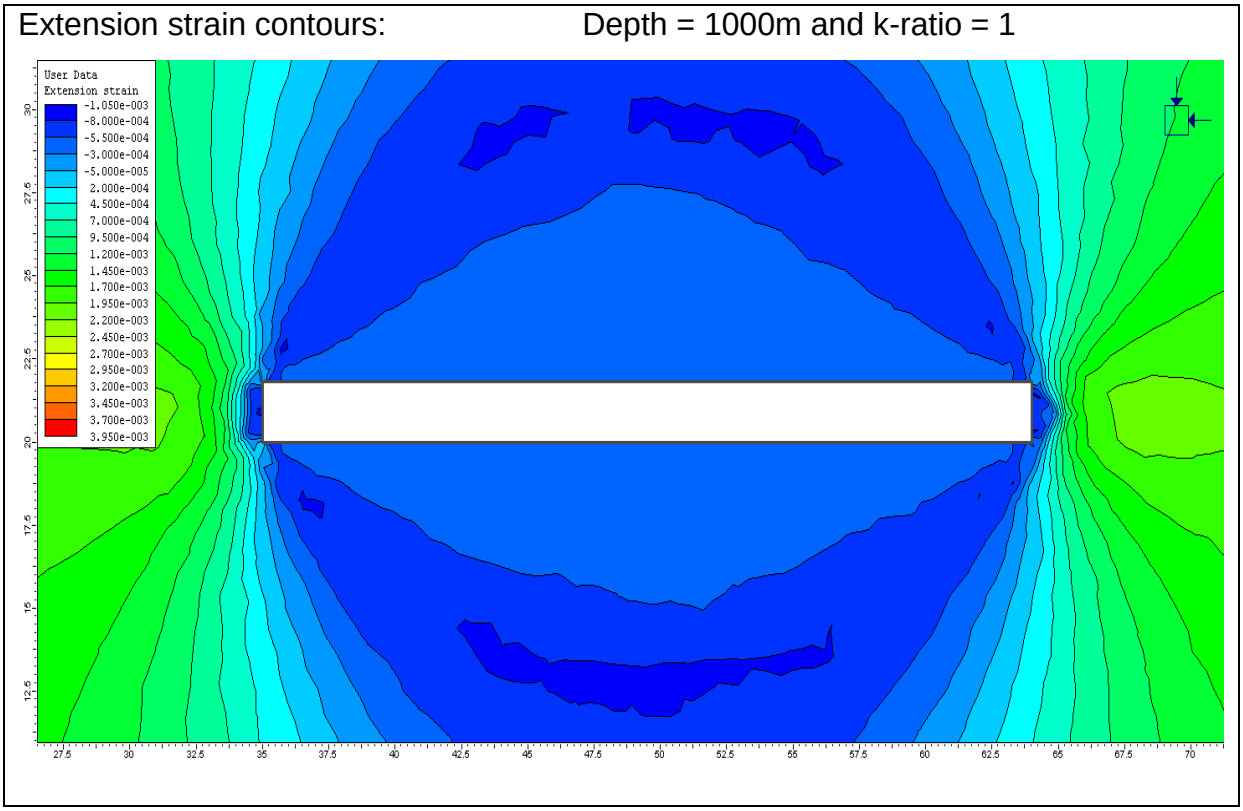


Figure C2-11: Extension strain at a depth of 1000m with k-ratio = 1

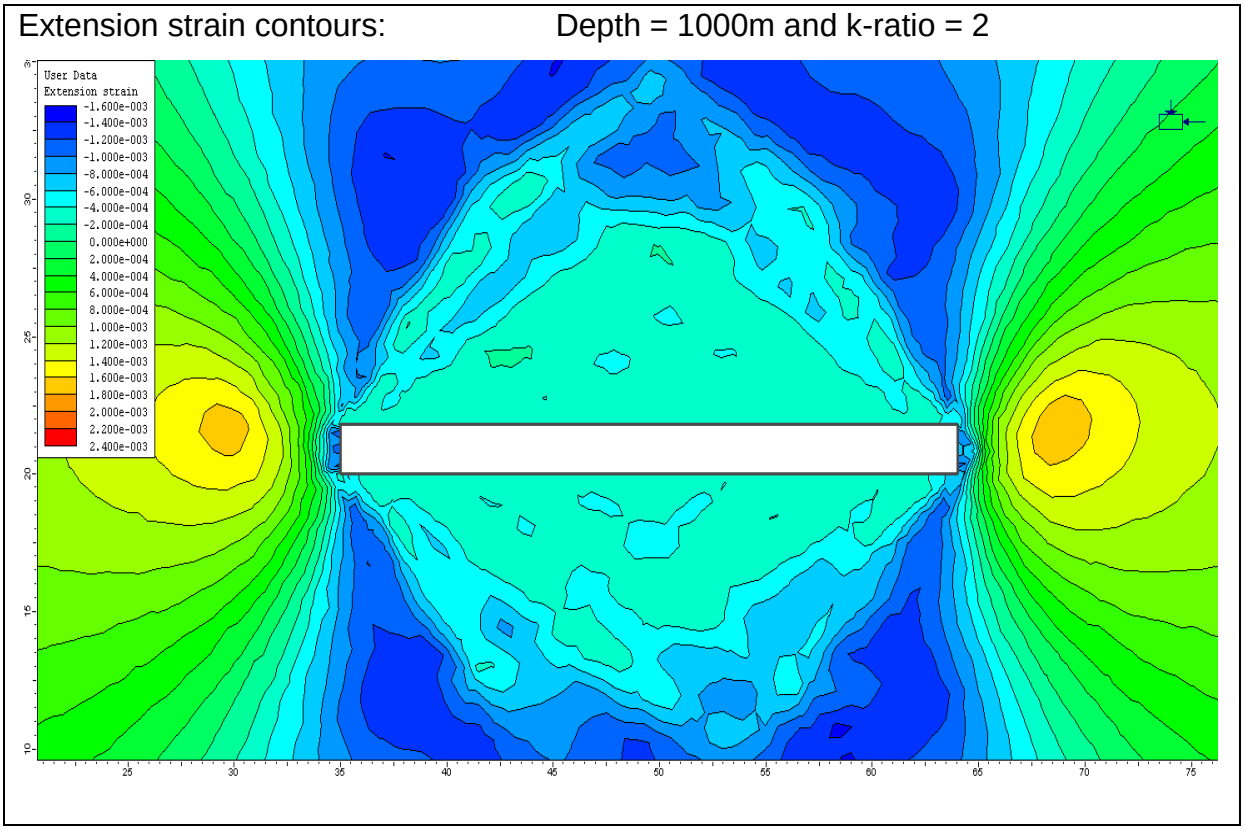


Figure C2-12: Extension strain at a depth of 1000m with k-ratio = 2

Notice how the extension strain contours take a sub-horizontal direction in the hanging wall in line with the expected principal stresses existing in the shallow Bushveld Complex mines.